

# VU Research Portal

## **Weathering the Storm: tropical cyclone risk under climate change**

Bloemendaal, Nadia

2021

### **document version**

Publisher's PDF, also known as Version of record

[Link to publication in VU Research Portal](#)

### **citation for published version (APA)**

Bloemendaal, N. (2021). *Weathering the Storm: tropical cyclone risk under climate change*. Gildeprint.

### **General rights**

Copyright and moral rights for the publications made accessible in the public portal are retained by the authors and/or other copyright owners and it is a condition of accessing publications that users recognise and abide by the legal requirements associated with these rights.

- Users may download and print one copy of any publication from the public portal for the purpose of private study or research.
- You may not further distribute the material or use it for any profit-making activity or commercial gain
- You may freely distribute the URL identifying the publication in the public portal ?

### **Take down policy**

If you believe that this document breaches copyright please contact us providing details, and we will remove access to the work immediately and investigate your claim.

### **E-mail address:**

[vuresearchportal.ub@vu.nl](mailto:vuresearchportal.ub@vu.nl)

# **WEATHERING THE STORM**

Tropical cyclone risk under climate change

Nadia Bloemendaal

Reading committee:

prof.dr. Suzana Camargo  
prof.dr. James Done  
prof.dr. Bart van den Hurk  
prof.dr. Roshanka Ranasinghe  
dr.ir. Kees Boersma

Artwork: Julieta Matos Castaño

Printed by: Gildeprint ([www.gildeprint.nl](http://www.gildeprint.nl))

**Weathering the Storm: tropical cyclone risk under climate change**

PhD thesis, Vrije Universiteit Amsterdam, The Netherlands

ISBN: 978-94-641-9322-0

Nadia Bloemendaal, Amsterdam, November 2021

This research was conducted under the auspices of the Graduate School for Socio-Economic and Natural Sciences of the Environment (SENSE). The research for this thesis was carried out at the Institute for Environmental Studies (IVM), Vrije Universiteit Amsterdam.

VRIJE UNIVERSITEIT

**WEATHERING THE STORM:  
TROPICAL CYCLONE RISK UNDER CLIMATE CHANGE**

ACADEMISCH PROEFSCHRIFT

ter verkrijging van de graad Doctor aan  
de Vrije Universiteit Amsterdam,  
op gezag van de rector magnificus  
prof.dr. C.M. van Praag,  
in het openbaar te verdedigen  
ten overstaan van de promotiecommissie  
van de Faculteit der Bètawetenschappen  
op woensdag 3 november 2021 om 15.45 uur  
in een bijeenkomst van de universiteit,  
De Boelelaan 1105

door

Nadia Bloemendaal

geboren te Arnhem



promotor:

prof.dr. J.C.J.H. Aerts

copromotoren:

dr. H. de Moel

dr. S. Muis

*Mathematical science shows what it is. It is the language of unseen relations between things. But to use and apply that language, we must be able to fully appreciate, to feel, to seize the unseen, the unconscious.*

- Ada Lovelace

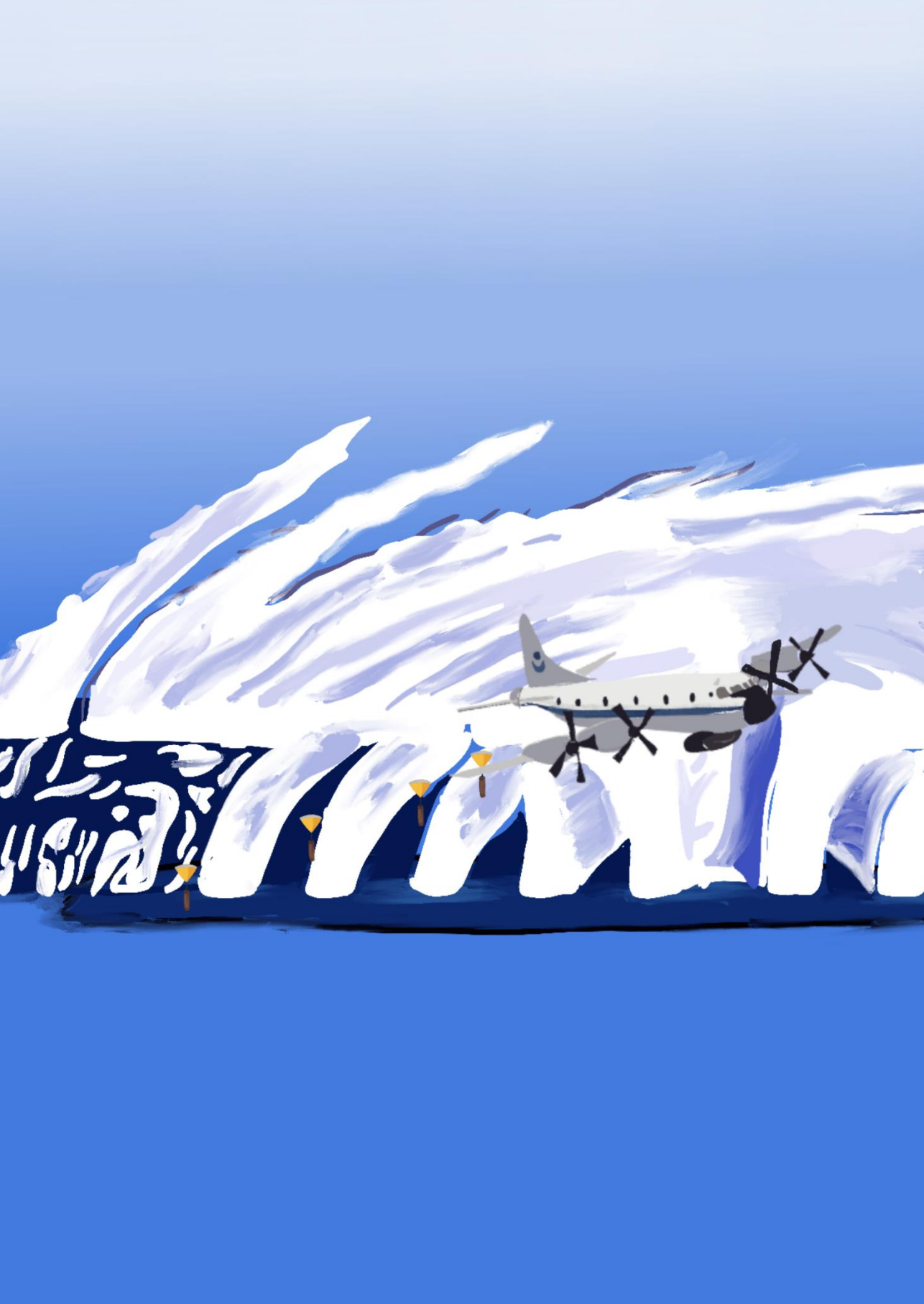


# Table of Contents

Summary	11
Samenvatting	17
1 Introduction	23
1.1 Tropical cyclones	24
1.2 Research challenges	26
1.3 Main goal and research questions	31
2 The influence of spatial model resolution on tropical cyclone storm surges	35
2.1 Introduction	36
2.2 Methods	38
2.3 Results and discussion	43
2.4 Concluding remarks	50
3 The Synthetic Tropical cyclOne geneRation Model	53
3.1 Introduction	54
3.2 Methods	55
3.3 Technical validation	65
3.4 Usage notes	69
4 Low-probability tropical cyclone events in the present climate	73
4.1 Introduction	74
4.2 Methods	75
4.3 Results and discussion	78
4.4 Concluding remarks	88
5 Low-probability tropical cyclone events under climate change	91
5.1 Introduction	92
5.2 Methods	93
5.3 Results and discussion	99
5.4 Concluding remarks	107
6 The Tropical Cyclone Severity Scale	111
6.1 Introduction	112
6.2 Methods	117

6.3	Results and discussion	122
6.4	Concluding remarks	126
7	Synthesis	129
7.1	Introduction	130
7.2	Overview of the main findings	130
7.3	Directions for future research	134
7.4	Implications for tropical cyclone risk research and mitigation strategies	138
	Appendices	141
	References	171
	About the author	183
	List of publications	185
	Acknowledgments	187





# Summary



---

Tropical cyclones (TCs), locally known as hurricanes or typhoons, are one of the deadliest and costliest natural hazards, causing widespread havoc in coastal areas when they make landfall. Their primary hazards include high wind speeds, storm surge, and precipitation, but these can, in turn, trigger other hazards, such as landslides or the spread of water-borne diseases. The 2017 Atlantic Hurricane Season has been the costliest to date, with Hurricanes Harvey, Irma, and Maria's combined overall losses estimated around US\$ 220 billion. To protect coastal communities from these powerful storms and to reduce the future loss of life and property, it is crucial to support risk mitigation efforts with reliable TC risk assessments. Achieving this goal, however, requires adequate understanding of the characteristics of TCs (e.g., intensity, frequency, etc.) and of how these characteristics change under (near-) future climate change. The goal of this thesis is therefore to develop a novel method to derive and assess global-scale TC activity and wind speed probabilities, now and under climate change.

The first step in improving the understanding of TC hazards is ensuring that the meteorological data used to study TCs sufficiently capture the high wind speeds and low atmospheric pressure characteristic of TCs. This knowledge is crucial for risk assessments because a poor representation of these features may lead to an over- or underestimation of hazards, impacts, and risk further down the model chain. To answer this question, this thesis first assesses the effect of horizontal model resolution of meteorological data on simulating TC storm surges for eight case studies. Results show that, in general, a spatial resolution of around 25 x 25 km is sufficient to adequately capture the large-scale spatial patterns of the maximum storm surge heights. In addition, the use of coarser-resolution models generally results in lower storm surge estimates, predominantly in regions prone to high surges.

Next, understanding TC risk requires understanding the full range of the possible TC events in a location, particularly the most extreme events – that is, events that have a low probability of occurrence/high return period (RP). It can, however, be challenging to properly estimate this range using solely historical data. Historical data on TC events is sparse because TCs are relatively rare events, with around 90 ( $\pm$  10) formations per year globally. From these formations, on average only 16 TCs make landfall as a Category-1 TC or stronger. Furthermore, landfalling TCs generally affect a relatively small (< 500 km) stretch of coastline. Moreover, reliable global-scale TC datasets are only available from the start of the satellite era, in 1980 onwards; as a result, some coastal regions do not even have a single landfalling TC event in the available datasets.

Many regions thus lack information on the full range of possible TCs, particularly for the most extreme events. To overcome this obstacle, this thesis presents the Synthetic Tropical cyclOne geneRation Model (STORM). STORM takes historical TC data as input and statistically resamples this data to a TC event set equivalent to 10,000 years under the same climate conditions. The resulting synthetic STORM dataset contains

the full range of possible TC events (including events exceeding the 1-in-1,000yr RP, equivalent to a 0.1% probability of occurring in any given year) in TC-prone regions under present climate conditions. Therefore, this dataset can be used to study extreme events likely not captured by historical data. To demonstrate the use of the STORM dataset, its synthetic tracks are coupled with a parametric wind field model to generate the present-climate wind speed RPs at 10-km resolution for every TC-prone location. Validation against other studies shows that these RPs are in strong agreement, with the majority of wind speeds being within 5 m/s of each other for a given RP. These datasets are particularly beneficial to use as hazard layers in, for instance, catastrophe models, which are often used in the (re)insurance industry.

To understand how these RPs are changing under climate change, information from four global climate models (GCMs) is used as input for STORM. This thesis presents a novel methodology (based on the concept of “the delta approach”) for such future-climate simulations. First, the delta, defined as the difference between present and future climate data, is extracted for the various TC input variables from each of the four GCMs. Second, this delta is added to the variables derived from the historical data used previously for the construction of the present-climate STORM dataset. Applying this delta approach results in a future-climate version of the historical data that omits the first-order model bias, such as the GCMs containing TC intensities that are too low. STORM is then used to generate 10,000 years of synthetic TC tracks and high-resolution wind speed maps for fixed RPs for each of the four GCMs. The use of these four GCMs enables the assessment of the intra-model spread in projected changes in TC wind speed hazard. The data show that most TC-prone regions will face an increase in TC wind speed hazard under future climate change, with the largest changes being in the South Pacific and the Hong Kong region. Furthermore, results indicate that predominantly developing countries, such as Cambodia, are facing the largest changes in exposed population with regard to the difference between the present and near-future climate.

Lastly, a crucial aspect in short-term TC risk mitigation strategies is adequate risk communication, which serves to warn and prepare coastal communities for an imminent storm. A common practice in this context is classifying a TC on the Saffir-Simpson Hurricane Wind Scale (SSHWS), which categorizes a TC’s wind speed on a scale from 1 to 5. Past events, however, have demonstrated that the largest TC impacts often come from flooding, caused by a TC’s storm surge and extreme precipitation totals, rather than wind alone. As such, the SSHWS category does not fully reflect the potential severity of a TC. To overcome this limitation, this thesis presents the Tropical Cyclone Severity Scale (TCSS), which also includes storm surges and precipitation totals (in addition to wind speeds). Similar to the SSHWS, the TCSS uses a Category 0–5 system to maintain familiarity amongst the general public. In addition, the TCSS is extended with a Category 6 in order to support communication about the most extreme TCs that threaten in multiple ways. Applied to past extreme events, the TCSS would have classified Hurricane Katrina (Category 3 on the

---

SSHWS, but the costliest US TC on record) as a Category-5, for example. The scale can easily be coupled to meteorological and hydrodynamical forecasts to generate local-scale categorization maps, which can then be communicated to the public, thereby allowing for enhanced storm preparation and ultimately saving more lives.

The research presented in this thesis contributes to ongoing efforts to better understand and mitigate TC risk on a global scale. The STORM present- and future-climate datasets can help identify hotspot regions most prone to TCs both now and under future warming scenarios. Such scenarios can then be subject to additional local-scale and in-depth research. Furthermore, STORM provides valuable insights into the magnitude of the risk for those regions infrequently hit by TCs. STORM can also form the basis for studying the other main TC hazards. TC storm surges can be studied by coupling the STORM synthetic tracks to a hydrodynamical model. Studying precipitation risk first requires the development of a parametric rain field model, which can then be coupled with the STORM synthetic tracks. Such a full set of TC hazards provides an important missing piece in the puzzle to assess the full scope of TC risk. Additionally, this full set also opens up a wealth of new research opportunities, such as inland and compound flooding risk assessments.





# Samenvatting

---

Tropische cyclonen, ook wel orkanen of tyfoons genoemd, veroorzaken vaak grootschalige verwoesting wanneer ze aan land komen, en behoren hiermee tot de gevaarlijkste natuurrampen op aarde. De grootste bedreigingen van een tropische cycloon zijn de hoge windsnelheden, stormvloed en neerslag, maar deze kunnen tevens weer andere gevaarlijke situaties veroorzaken, zoals watervervuiling of aardverschuivingen. In 2017 zorgden de orkanen Harvey, Irma en Maria gezamenlijk voor US\$ 220 miljard aan schade, waarmee dat seizoen het duurste orkaanseizoen ooit werd. Betrouwbare risicoanalyses zijn cruciaal voor het verbeteren van risicobeperkende maatregelen, als we kustgebieden in de toekomst beter willen beschermen tegen deze krachtige stormen. Om dit te bereiken hebben we echter goed inzicht nodig in de karakteristieken van een tropische cycloon (waaronder de intensiteit en frequentie) en hoe deze veranderen onder toekomstige klimaatverandering. Het doel van dit proefschrift is om een nieuwe methode te ontwikkelen om wereldwijde tropische cyclonen-activiteit en bijbehorende kansen te berekenen, voor zowel het huidige als toekomstige klimaat.

De eerste stap in het verkrijgen van meer inzicht in de karakteristieken van tropische cyclonen betreft de meteorologische data: we moeten er zeker van zijn dat de data die we gebruiken om tropische cyclonen te analyseren, de karakteristieke hoge windsnelheden en lage luchtdrukvelen goed kan weergeven. Dit is cruciaal voor risicoanalyses, omdat een slechte weerspiegeling van deze kenmerken voor een over- of onderschatting van het gevaar, de impact, en het risico in de modelketen kan zorgen. Om dit te onderzoeken wordt als eerste het effect van de horizontale modelresolutie van de meteorologische data op de stormvloed van tropische cyclonen bestudeerd. De modelresultaten laten zien dat een resolutie van 25 x 25 km over het algemeen voldoende is om de grootschalige ruimtelijke patronen van maximale stormvloedhoogtes goed te simuleren. Daarnaast leidt het gebruik van een grovere resolutie doorgaans tot lagere stormvloeden, wat voornamelijk tot uiting komt in regio's waar hoge stormvloeden voorkomen.

Vervolgens behoeft het begrijpen van de risico's van tropische cyclonen een duidelijk beeld van alle mogelijke tropische cyclonen op een bepaalde locatie, in het bijzonder van de meest extreme stormen (dat wil zeggen: een lage kans van voorkomen, ofwel een hoge terugkeertijd). Het is echter soms lastig om een goede schatting te maken van al deze mogelijkheden wanneer men alleen naar historische gebeurtenissen kijkt. Historische data is hierin namelijk beperkt omdat tropische cyclonen relatief zeldzaam zijn: er ontstaan wereldwijd ongeveer 90 ( $\pm 10$ ) stormen per jaar, waarvan er gemiddeld 16 aan land komen met orkaankracht. Daarbij komt nog dat de tropische cyclonen die aan land komen, meestal in een relatief klein (<500 km) kustgebied daadwerkelijk impact hebben. Bovendien zijn goede wereldwijde tropische cyclonen datasets pas vanaf de start van het satelliettijdperk, in 1980, beschikbaar. Dit betekent dat er in deze datasets kustgebieden zullen zijn waar geen tropische cyclonen aan land gekomen zijn, en waar dus ook geen informatie beschikbaar is over mogelijke kansverdelingen of impacts.

Voor veel regio's bestaat dus geen informatie over alle mogelijke tropische cyclonen die dat gebied zouden kunnen raken, in het bijzonder voor de meest extreme stormen. Om dit inzicht toch te verkrijgen presenteert dit proefschrift de Synthetic Tropical cyclOne geneRation Model (STORM). STORM gebruikt historische informatie van tropische cyclonen als input, en past vervolgens statistische methodes toe om zo een dataset van tropische cyclonen te maken die equivalent is aan 10.000 jaar onder dezelfde klimaatcondities. De resulterende STORM dataset bevat een volledig overzicht van alle (theoretisch) mogelijke tropische cyclonen in het huidige klimaat, inclusief extreme tropische cyclonen met een terugkeertijd van meer dan 1.000 jaar, ofwel een jaarlijkse kans van voorkomen van 0,1%. De STORM dataset kan dan ook gebruikt worden om extreme gebeurtenissen te analyseren die doorgaans niet in de historische data voorkomen. Om het gebruik van de STORM dataset te demonstreren zijn de synthetische tracks gekoppeld aan een parametrisch windveld model om zo de terugkeertijden van windsnelheden op 10 km resolutie in het huidig klimaat te berekenen. Vergelijking met andere onderzoeken laat zien dat deze terugkeertijden goed met elkaar overeenkomen, met in de meeste gevallen een verschil in windsnelheid van minder dan 5 m/s voor een gegeven terugkeertijd. Deze datasets zijn bijzonder handig om als invoer (zogenaamde *hazard layers*) te gebruiken in het modelleren van catastroferisico's, wat vaak gedaan wordt door (her)verzekeraars.

Om inzicht te krijgen in de manier waarop deze terugkeertijden veranderen onder klimaatverandering, zijn vier mondiale klimaatmodellen (*global climate models*; GCMs) gebruikt als input voor STORM. In dit proefschrift wordt een nieuwe methode gepresenteerd (gebaseerd op de "delta approach") voor zulke toekomstig-klimaat-simulaties. Als eerste wordt het klimaatsignaal, gedefinieerd als het verschil tussen de huidig en toekomstig-klimaat data, voor de verschillende tropische cyclonen input variabelen en voor elk model herleid. Hierna wordt dit klimaatsignaal opgeteld bij de variabelen uit de historische data, die eerder gebruikt werd om de huidig-klimaat STORM dataset te genereren. Op deze manier wordt een toekomstig-klimaat versie van de historische data gecreëerd, en hiermee wordt de eerste-orde modelafwijking voorkomen, zoals te zwakke tropische cyclonen in de GCMs. STORM wordt vervolgens gebruikt om 10.000 jaar aan synthetische tropische cyclonen tracks en hoge-resolutie windkaarten voor vaste terugkeertijden te berekenen. Het gebruik van deze vier GCMs zorgt ervoor dat de spreiding in verwachte veranderingen in tropische cyclonen windsnelheden bepaald kan worden. De data laten zien dat in de meeste regio's waar tropische cyclonen voorkomen, de kansen op hogere windsnelheden zullen toenemen, met de grootste toenames in de Zuidelijke Stille Oceaan en de regio van Hong Kong. Bovendien laten de resultaten zien dat mensen in ontwikkelingslanden, zoals Cambodja, de grootste toename in het gevaar van tropische cyclonen zullen doormaken.

Als laatste vormt goede risicocommunicatie een cruciaal onderdeel van de risicobeperkende maatregelen die op de kortere termijn genomen kunnen worden, want hiermee kunnen kustgemeentes gewaarschuwd en voorbereid worden op een



---

naderende storm. Hiervoor wordt doorgaans een tropische cycloon geclassificeerd op de schaal van Saffir-Simpson, die de maximale windsnelheid van een tropische cycloon categoriseert op een schaal van 1 tot 5. Historische tropische cyclonen hebben echter laten zien dat de voornaamste impacts van een cycloon niet door de wind, maar door overstromingen komen, veroorzaakt door de stormvloed en extreme neerslaghoeveelheden. Dit betekent dus dat de schaal van Saffir-Simpson het totale gevaar van een tropische cycloon onvoldoende weergeeft. Om deze reden wordt in dit proefschrift de Tropical Cyclone Severity Scale (TCSS) ontworpen, waarin ook stormvloed en neerslag meegenomen worden in de categorisering. Net zoals de schaal van Saffir-Simpson gebruikt de TCSS een categorisering van 0-5, omdat het algemene publiek hier al bekend mee is. Hiernaast is de TCSS uitgebreid met een categorie 6, om zo communicatie over de meest extreme tropische cyclonen te ondersteunen. Toepassing van de schaal laat zien dat historische extreme gebeurtenissen zoals orkaan Katrina (categorie 3, maar de duurste Amerikaanse orkaan ooit) geclassificeerd zou zijn als een categorie 5 op de TCSS. De nieuwe schaal kan gemakkelijk gekoppeld worden aan meteorologische en hydrodynamische verwachtingen om zo categorisering op lokale schaal te bewerkstelligen. Deze informatie kan vervolgens gecommuniceerd worden met het algemene publiek, waarmee betere voorbereidingen getroffen kunnen worden, en zo uiteindelijk meer levens gered kunnen worden.

Het onderzoek uit dit proefschrift draagt bij aan de doorlopende inspanningen om de wereldwijde risico's van tropische cyclonen beter te begrijpen en te beperken. De STORM huidig en toekomstig-klimaat datasets helpen om *hotspot* gebieden te definiëren; regio's kwetsbaar voor tropische cyclonen nu en in de toekomst, waar dan aanvullend grondig, en op lokale schaal, onderzoek gedaan kan worden. Hiernaast verschaft STORM waardevol inzicht in de omvang van het risico voor gebieden waar deze stormen weinig voorkomen. STORM kan ook de basis vormen voor onderzoek naar de andere gevaren van tropische cyclonen. De stormvloed kan bestudeerd worden door de synthetische tracks van STORM te koppelen met een hydrodynamisch model. Om onderzoek te doen naar neerslagrisico's moet eerst een parametrisch regenveld model ontwikkeld worden, die vervolgens gekoppeld kan worden met de STORM datasets. Zo'n volledige verzameling van gevaren van tropische cyclonen zal een belangrijk puzzelstuk vormen om de volledige omvang van risico's te bepalen. Daarnaast zal dit ook voor veel nieuwe onderzoeksmogelijkheden zorgen, zoals risicoanalyses naar binnenlandse en samengestelde overstromingen.





HURRICANE  
SEASON

# 1 Introduction

## 1.1 Tropical cyclones

Tropical cyclones (TCs) are one of the deadliest and most devastating natural hazards and are characterized by their strong winds, heavy precipitation, and high storm surges and waves. These storms form in tropical and subtropical regions (Figure 1.1), and depending on the genesis location, they are locally known as hurricanes (Eastern Pacific and North Atlantic) or typhoons (Western Pacific). Mature TCs have a closed surface wind circulation with a well-defined center, called the eye. This center is also where the lowest atmospheric pressure is found. The band of clouds surrounding the eye is called the eyewall, and typically forms the region of the TC with the highest wind speeds. In a mature system, these wind speeds can exceed 120 km/h. In fact, the most intense TC that ever occurred was Hurricane Patricia (2015), with sustained wind speeds of 345 km/h and a minimum pressure of 872 hPa. TCs can reach sizes of 100–2000 km in diameter and can last for days to weeks.

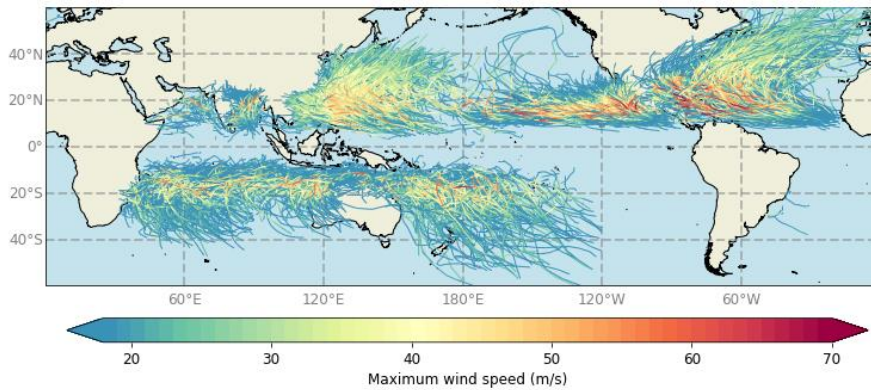


**Figure 1.1** Historical tropical cyclone tracks from International Best Track Archive for Climate Stewardship (IBTrACS, Knapp et al., 2010)

The best-known scale for the classification of TC intensity is the Saffir-Simpson Hurricane Wind Scale (SSHWS), which categorizes a TC on a scale from 1 to 5 based on its maximum sustained wind speed. A Category-1 TC has a maximum wind speed exceeding 33 m/s (approximately 120 km/h), whereas the threshold for a Category-5 TC lies at 70 m/s (approximately 250 km/h). The classifications “Tropical Storm” or “Tropical Depression” are used for TCs with maximum wind speeds below 33 m/s.

Wind is one of the major hazards associated with TCs, and it can do substantial damage to housing, infrastructure, and ecosystems both in coastal regions and far inland (Kruk et al., 2010). Moreover, the magnitude of other TC-induced hazards, such as storm surges, waves, and precipitation depends on the strength of the wind (Cerveny and Newman, 2000; Phadke et al., 2003). Historical TC events exemplify the havoc these storms can cause. The deadliest TC to date is the Great Bhola Cyclone (1970), which hit the low-lying shores of the Bay of Bengal and caused approximately

500,000 fatalities (Cervený et al., 2017). In 2005, Hurricane Katrina's storm surges were 8.6 m high and caused widespread levee failure in New Orleans (USA), making this hurricane the costliest ever, with damages totaling US\$ 160 billion (NOAA, 2020a). TC impacts can be further enhanced when two storms affect the same area within a short time span (a so-called consecutive event). Such an event happened, for example, in Southeast Africa in 2019, where TCs Idai and Kenneth both made landfall in Mozambique. TC Idai caused around 1,000 fatalities and displaced around 3 million people, and humanitarian aid was still ongoing when TC Kenneth struck the same region only six weeks later (OCHA, 2019). Climate change is expected to further amplify the disruptive impacts of TCs; TCs are projected to become more intense because of increasing sea-surface temperatures, and warm ocean waters function as fuel for a TC (Knutson et al., 2020). At the same time, it is uncertain how TC frequency will change and how this change will be distributed over the different ocean basins. In addition, some models project a poleward shift in TC tracks, meaning that regions currently not under direct threat of TCs might be facing TC impacts in the future (Altman et al., 2018; Haarsma et al., 2013; Kossin et al., 2014a). Socio-economic trends, such as population growth and the increase in wealth in coastal areas, will further increase exposure to and risk from TCs (Jongman et al., 2015; Peduzzi et al., 2012).

To combat this increasing trend, it is crucial to protect coastal communities, economies, and ecosystems from these powerful storms by implementing adequate disaster risk reduction (DRR) strategies. These strategies operate on different timescales (long term versus short term) and on different organizational levels (policy-makers versus homeowners). Examples of long-term strategies by policy makers include the construction of dykes or mangrove forests to reduce storm surge impacts or imposing building regulations for coastal zones (Aerts, 2018). In addition, homeowners in the United States, for instance, can increase their resilience through insurance, which is used to compensate households after they have experienced losses but which can also be used to incentivize the adoption of risk-reduction measures through reductions in insurance costs. Examples of short-term mitigation strategies include (mandatory) evacuations and the installation of sand bags in flood-prone regions.

Designing such (long-term) DRR strategies requires detailed and accurate information on TC events in the location of interest, particularly for the most extreme events – that is, events that have a low probability of occurrence/high return period (RP) - and how these events change under climate change. Such information has been derived for e.g. New York City (Aerts et al., 2014; Aerts et al., 2013; Lin et al., 2010; Lin et al., 2016) and Miami-Dade County (Klima et al., 2012). However, insights into how the probabilities of such extreme events are going to change under climate change for any location on earth are still missing. Improving short-term DRR strategies can be achieved through improving people's risk perception. As a result,

communities living in the path of an imminent storm can respond in a timely and appropriate way, thereby reducing the TC's impact.

## 1.2 Research challenges

Under a warming climate, TCs are likely to become more intense (Knutson et al., 2020), thus increasing wind speeds and the associated risks. As such, it is vital to understand and accurately map TC occurrences and impacts—particularly regarding extreme events (high RPs) and how their impacts might change under climate change. Such knowledge will ensure that coastal communities are protected from future loss of life and from damage to property and insurance.

Several models and datasets are needed to assess current and future TC risk. The meteorological data, extracted either from global climate models (GCMs), observational data, or forecasting systems, form the basis of the model chain and serve as input for various models that simulate TC hazards and impacts. Observational datasets, such as IBTrACS, are beneficial for present-climate studies, which generally contain accurate information on historical TC tracks and intensities (Knapp et al., 2010). Future-climate TCs, in turn, are often simulated using GCMs (Walsh et al., 2016), or by coupling environmental conditions from such GCMs to a TC simulation model (Emanuel, 2021; Emanuel et al., 2008). Using such meteorological data, however, poses some challenges. First of all, TCs are characterized by small-scale wind and pressure gradients, which are underrepresented in coarse(r) resolution datasets, leading to an underestimation in TC intensity (Camargo, 2013; Murakami and Sugi, 2010). This poor representation of TC intensity can lead to an over- or underestimation of hazards, impacts, and risk further down the model chain. Second, the temporal scale of meteorological data is too short to capture the full range of possible TC events for all coastal areas in TC-prone regions (Lin and Emanuel, 2016). This limitation is due to TCs' relative rarity, with around 90 ( $\pm 10$ ) formations per year (Emanuel, 2008), of which approximately 16 make landfall as a Category 1 or stronger (Weinkle et al., 2012). Moreover, when making landfall, TCs generally affect a relatively small stretch of coastline (<500 km; Pugh and Woodworth, 2014). As a result, the number of TCs in GCM simulations, which typically have a duration of 30 years, is too small to reliably estimate probabilities. The same limitations apply to reliable global-scale observations, which are only available from 1980 onwards, meaning that for many coastal regions, there may not even be a single landfalling TC event in the available datasets. So, for many coastal regions, it is impossible to give a reliable estimation of the intensity of low-probability (high RP) events based on solely meteorological data. Therefore, to perform adequate TC risk assessments, we need to overcome these complicating factors.

Besides improving the quantification of TC risk, another important component in building more resilient societies is improving people's risk perception. With such knowledge, communities living in the path of an imminent storm can respond in a

timely and appropriate way, thereby reducing the TC's impact. As explained above, the Saffir-Simpson Hurricane Wind Scale (SSHWS) is commonly used for categorizing TCs— more specifically, those that form in the Eastern Pacific and North Atlantic. This scale, however, only considers wind speed, whereas a TC can also cause flooding through high storm surges and extreme rainfall. For example, Hurricane Harvey (2017), despite being classified a Tropical Storm, caused widespread flooding in the Houston (USA) area, with precipitation totals exceeding 1.5 m. Because the SSHWS does not include storm surge and rainfall information, adequate risk communication can be challenging, as the public can (mistakenly) perceive a low-category TC as a low-risk TC.

### 1.2.1 Spatial model resolution

GCMs are often run at the global scale to assess present-day climate conditions and to evaluate changes for future climate scenarios. There are, however, several challenges associated with the use of GCMs. One major limitation in using GCMs is the spatial resolution, which is often too coarse for solving TC dynamics. Previous generations of GCMs had horizontal resolutions of  $0.45^\circ$  to  $1.8^\circ$  (ca. 50–200 km at the equator) (Saha et al., 2006; Yukimoto et al., 2006), which is insufficient to fully resolve TC intensity, size, and track (Murakami and Sugi, 2010; Schenkel and Hart, 2012; Walsh et al., 2007), and which are especially problematic for weak TCs (Hodges et al., 2017; Murakami, 2014).

Nowadays, there are higher-resolution GCMs available, offering improved TC representations. One such high-resolution GCM is EC-Earth, which consists of model components from the European Centre for Medium-Range Weather Forecasting (ECMWF) Integrated Forecasting System (IFS) (Doblas-Reyes et al., 2018). In addition to being an operational weather forecasting model, IFS has been used for producing reanalysis products, such as ERA5 and ERA-Interim (Dee et al., 2011; ECMWF, 2017c). In ERA-Interim, the average number of TCs per year is simulated well (Strachan et al., 2013), but modeled tracks differ from observed ones, and the intensity and size are underestimated (Murakami and Sugi, 2010; Schenkel and Hart, 2012). The underestimation of intensity is usually driven by resolution effects and poor physical schemes (Flato et al., 2013; Walsh et al., 2007). Previous updates in tropical atmospheric conditions in ECMWF IFS have improved tropospheric wind and convection representation compared to observations (Fiorino, 2008) and the model's spatial resolution was increased from  $\pm 0.225^\circ$  at the equator in 2006 to its current resolution of  $\pm 0.08^\circ$  (ECMWF, 2017a). These updates have significantly contributed to the improvement of the IFS TC track ensemble forecasts. An example of this improved performance is the IFS ensemble forecast for Hurricane Sandy's track, which predicted Sandy's landfall up to seven days in advance (Bassill, 2014; Magnusson et al., 2014). Apart from track ensemble forecasts, TC intensity forecasts have also improved in the recent IFS model updates (ECMWF, 2017a).



Hydrodynamic models are one type of hazard model using meteorological data (wind, pressure) as input. These models can be used to simulate storm surges, both for operational applications and risk assessments. Storm surge is often the main driver of TC-related impacts: research has shown that most TC-related fatalities in the United States are caused by storm surges (49%), as opposed to wind (8%) and rainfall (27%) (Rappaport, 2014). Hence, a correct representation of TC intensity in the meteorological input dataset (also referred to as forcing) is crucial to better understand impacts and risks. Despite research focusing on methods to test how sensitive simulated storm surges are to TC wind fields (Cardone and Cox, 2009), few studies have analyzed the effects of the resolution of meteorological forcing on simulated storm surges. Wakelin and Proctor (2002) used three meteorological operational analysis datasets to analyze two storm surge events in the Adriatic Sea. They concluded that their model works best with meteorological forcing with the highest spatial and temporal resolution, which were observational data at 43 meteorological stations. Muis et al. (2016) demonstrated the implications of using coarse-resolution meteorological forcing for global storm surge modeling. They generated time series of storm surges on a global scale using the six-hourly 0.75° ERA-Interim dataset (Dee et al., 2011; ECMWF, 2016) and found that extreme sea levels induced by TCs are underestimated because of the coarse resolution of meteorological datasets. However, the field still lacks a global-scale study addressing what resolution of meteorological forcing is needed to adequately simulate TC-induced storm surges.

### 1.2.2 Analyzing low-probability tropical cyclones: Extending the temporal extent of the meteorological data

To enhance our understanding of TC risk at the global scale, it is essential to analyze TC characteristics, such as wind speed probabilities, in TC-prone regions. Risk is commonly calculated as the integrated value of expected damages over all exceedance probabilities—the inverse of these probabilities being RPs (Ward et al., 2011). As such, to compute the full envelope of risk for a location requires the calculation of RPs for a wide range of events, which, in turn, are derived from a set of TC tracks.

An early attempt to calculate TC wind speed RPs was done by Simpson and Lawrence (1971), who used historical TCs to empirically estimate TC RPs along 80-km-long coastal segments of the US coastline. However, some coastal segments had not been hit by a TC in the 85 years of observations, and therefore no RP could be calculated. Moreover, because of the short duration of the observational record, there was a large uncertainty in the estimation of the RPs, especially for those RPs outside of the observational record. This example exposes the shortcomings of observational records and other climatological datasets as input datasets for such RP and risk

analyses: Their spatial and temporal extent is too short for RP calculation, especially at higher spatial scales.

One way to overcome the data scarcity for low-probability TCs is to extend the historical record. For example, paleoclimate records from coastal sediments can be used to reveal periods of past coastal floods driven by TCs, an approach known as paleotempestology (Lin et al., 2014; Nott and Hayne, 2001). Such records can extend back thousands of years and can present a wealth of information on TCs that have affected a given region. These records, however, are only available for small coastal stretches, and this method of collecting coastal sediment records cannot realistically be used at a global scale.

Another method that has been widely explored is the generation of synthetic TC tracks (Emanuel et al., 2006; Powell et al., 2005; Vickery et al., 2000). In such an approach, TC tracks and intensities are statistically resampled and modeled from an underlying dataset—either historical TC tracks (Casson and Coles, 2000; Emanuel et al., 2006; Haigh et al., 2014) or meteorological datasets from GCMs (Lin et al., 2012). This approach makes it possible to generate thousands of years of TC activity, including TCs with high RPs, that have statistical properties similar to the underlying dataset. This sampling method can be repeated for many years, thereby creating a large TC dataset that includes TCs with high RPs. There are two main methods for doing so: (i) a coupled statistical-dynamical model and (ii) a fully statistical model. Coupled statistical-dynamical models use autoregressive functions to, for example, generate the TC track, whilst intensity is simulated using a dynamical model. Examples of such models include the models developed by Emanuel et al. (2006) and Lee et al. (2018). Both models are run on a global scale; however, they are computationally intensive and require a substantial number of input variables. Fully statistical models use Markov Chains (Kolmogorov, 1937) for both the track generation and intensity simulation. These models generally require a limited number of input variables and are less computationally intensive, making them easily applicable. This method has previously been used by for instance Haigh et al. (2014), Vickery et al. (2000), Hardy et al. (2003) and James and Mason (2005), but only on local and country scales. A, fully statistical, global-scale model has thus far not been developed.

### 1.2.3 Low-probability tropical cyclone events under climate change

Enhancing our understanding of low-probability TC events in the present climate is already a challenge in itself, so studying the change in these events under climate change inserts a whole new level of complexity. GCMs are commonly used to analyze changes in global-scale climate patterns under different forcing scenarios. There is, however, still no general consensus amongst these models regarding how much TC intensity, frequency, and tracks will change in the future as a result of climate change

and how these changes will manifest on the local and continental scales. Knutson et al. (2020) summarizes that there exists low confidence for how much the total TC frequency, as well as the frequency of very intense (Category 4-5) TCs will change under climate change. This lack of consensus has partly arisen because historically, the lower spatial and temporal resolution of GCMs has not been able to adequately resolve TC intensity, size, and track (Murakami and Sugi 2010). Substantial progress has been made in recent years by for example by e.g. the PRIMAVERA-HighResMIP consortium, where higher-resolution models have been developed and analyzed for a wide variety of subjects (Haarsma et al., 2016). However, even within these models, higher-intensity TCs are still poorly captured (Roberts et al., 2020b). Furthermore, efforts to compare historical and future changes in TC activity are hindered by the fact that TCs are rare and that there is only a small sample of events in multi-decadal to centennial time-scales, further limiting accurate estimation of the probability of future extreme events.

Synthetic models are particularly beneficial to overcome the limitations imposed by GCMs because they can be run for a large number of years, and can thereby better capture the low-probability events likely underrepresented in the GCMs. Furthermore, because of the large sample, information from such synthetic tracks does not need to be aggregated over larger spatial scales to obtain information about RPs (e.g., for coastal sections). Lee et al. (2020) used CMIP5 models as input for the CHAZ statistical-dynamical model to calculate wind speed return periods of Category 4–5 TCs at  $3.6^\circ \times 1.8^\circ$  grid boxes. This resolution, however, is still too coarse to capture local-scale changes in wind speed RPs. As such, additional research is needed to compute wind speed RPs at high resolution, so that the full spatial heterogeneity of such distributions can be captured.

### 1.2.4 Tropical cyclone risk communication to the general public

Besides overcoming the limitations imposed by the use of GCMs (and thereby improving our understanding the physical aspects of TC risk), another important aspect in mitigating the effects of TCs is risk communication. In order to communicate the potential threat of a TC, TCs are commonly classified based on their maximum wind speeds following the Saffir-Simpson Hurricane Wind Scale (SSHWS; Simpson and Saffir, 1974). However, wind is not always the main driver of TC impacts (Rappaport, 2014). For instance, Hurricane Katrina (2005) was classified as a Category 3 at landfall, with wind speeds of around 55 m/s, but its 8.6 m storm surge caused widespread levee failure around New Orleans (USA). This caused over 1,800 casualties and US\$ 125 billion in damage, making it the costliest US TC to date (NOAA, 2020a). Another example is Hurricane Harvey (2017), which weakened to a tropical storm after landfall in Texas; nevertheless, it stalled over land, leading to the highest precipitation event in recorded history, with precipitation totals exceeding 1.5 m in the greater Houston area (Blake and Zelinsky, 2018). These

examples demonstrate that a classification method solely based on wind speed, such as the SSHWS, often fails to capture the full severity of a TC. Various alternative methods of TC classification and indexation have been proposed (Hebert et al., 2010; Irish and Resio, 2010; Kantha, 2006, 2008; Powell and Reinhold, 2007; Senkbeil and Sheridan, 2006; Song et al., 2020). Almost all these methods are applied on a pre-empt basis, in that they use forecast information to classify a TC hazard. Basing the classification on forecasts is, of course, important given the function of such classifications being to warn and prepare. However, most classification methods assess either the wind or storm surge hazard but rarely combine them. Moreover, most of the methods leave out precipitation altogether. The Hurricane Classification System by Senkbeil and Sheridan (2006) is the only method that includes all three TC hazards. However, their Hurricane Classification System is computed post-landfall, so its usefulness is limited relative to warning and preparation. An easy-to-use TC classification method incorporating all three hazards and allowing for pre-landfall usage has not been developed yet.

### 1.3 Main goal and research questions









The previous section summarizes how we can improve society's resilience against TCs by addressing a series of research challenges. First, we need to better understand how the resolution of meteorological forcing affects hazard modeling. Second, synthetic modeling approaches need to be further developed to overcome the spatial and temporal limitations of GCMs and historical data. Third, there is a need to understand the distribution of RPs at the global scale, especially for low-probability TCs. Fourth, with the aforementioned synthetic approach, the influence of climate change has to be incorporated, to understand how these probabilities are going to change in the future. Finally, we need to diverge from the SSHWS and design a new scale, to improve societies' resilience through improved risk communication. Following these challenges, we set the following goal and research questions:

**Goal:** to improve our understanding of tropical cyclone risk by developing a global statistical synthetic model to assess return periods of TCs in the current and future climate, including low-probability events, and by improving TC risk communication strategies.

This goal is addressed through the following research questions:

1. Which climate model resolution is sufficient to adequately represent TCs for storm surge modeling?
2. Can we build a global-scale, fully statistical synthetic TC model to simulate TC activity over longer temporal time scales?
3. What is the global distribution of TC wind speeds for extreme (low-probability) events, and how do these compare to observed TC activity?
4. What is the influence of climate change on the spatial distribution of TC wind speed probabilities, especially for low-probability events?

5. Can the Saffir-Simpson Hurricane Wind Scale be improved by accounting for the combination of wind, storm surge, and precipitation?

	Spatial model resolution of input data	Temporal extent of the hazard data	Climate change	TC risk communication
Chapter 2: Model resolution				
Chapter 3: STORM methodology				
Chapter 4: STORM return periods				
Chapter 5: STORM climate change				
Chapter 6: TC risk perception				

**Figure 1.2** Overview of research challenges covered per chapter in this thesis.

These research questions are addressed in the chapters of this thesis. The individual chapters cover the following topics (see also Figure 1.2).

- In Chapter 2 we assess the influence of spatial model resolution on storm surge heights for eight case studies.
- In Chapter 3, we overcome the spatial and temporal limitations imposed by meteorological datasets by building the global-scale, fully statistical synthetic TC model STORM (Synthetic Tropical cyclOne geneRation Model). The resulting STORM dataset spans 10,000 years of TC activity under present-climate conditions, preserving the TC statistics from the input dataset.
- In Chapter 4, we apply the STORM dataset to derive TC return periods up to 10,000 years, both for a selection of coastal cities and islands, as well as at 10 km resolution.
- In Chapter 5, we develop a novel method to use the climate change signal from GCMs as input for STORM, to simulate 10.000 years of TC activity under climate change and identify regions most at risk from a change in TC activity.
- In Chapter 6, we improve the SSHWS by including separate categories for storm surge and precipitation. The new Tropical Cyclone Severity Scale

reflects on the total severity of the TC, hereby allowing for enhanced storm preparations and ultimately saving more lives.



## 2 The influence of spatial model resolution on tropical cyclone storm surges

**This chapter is published as**

Bloemendaal, N., Muis, S., Haarsma, R.J., Verlaan, M., Irazoqui Apecechea, M., de Moel, H., Ward, P.J. & Aerts, J.C.J.H. Global modeling of tropical cyclone storm surges using high-resolution forecasts. *Climate Dynamics* **52**, 5031-5044 (2019).  
<https://doi.org/10.1007/s00382-018-4430-x>



## Abstract

We assess the suitability of ECMWF Integrated Forecasting System (IFS) data for the global modeling of tropical cyclone (TC) storm surges. We extract meteorological forcing from the IFS at a  $0.225^\circ$  horizontal resolution for eight historical TCs and simulate the corresponding surges using the Global Tide and Surge Model. Maximum surge heights for Hurricanes Irma and Sandy are compared with tide gauge observations, with  $R^2$ -values of 0.86 and 0.74 respectively. Maximum surge heights for the other TCs are in line with literature. Our case studies demonstrate that a horizontal resolution of  $0.225^\circ$  is sufficient for the large-scale modeling of TC surges.

By upscaling the meteorological forcing to coarser resolutions as low as  $1.0^\circ$ , we assess the effects of horizontal resolution on the performance of surge modeling. We demonstrate that coarser resolutions result in lower-modeled surges for all case studies, with modeled surges up to 1 m lower for Irma and Nargis. The largest differences in surges between the different resolutions are found for the TCs with the highest surges. We discuss possible drivers of maximum surge heights (TC size, intensity, and coastal slope and complexity), and find that coastal complexity and slope play a more profound role than TC size and intensity alone. The highest surges are found in areas with complex coastlines (fractal dimension  $> 1.10$ ) and, in general, shallow coastlines. Our findings show that using high-resolution meteorological forcing is particularly beneficial for areas prone to high TC surges, since these surges are reduced the most in coarse-resolution datasets.

## 2.1 Introduction

The strong winds and low pressures of tropical cyclones (TCs) often induce highly damaging storm surges, affecting people and economies over large coastal areas. In 2017, U.S. hurricane damage totals exceeded US\$ 265 billion, with Hurricanes Harvey, Irma, and Maria entering the top five of costliest hurricanes in recorded history (NOAA National Centers for Environmental Information, 2021). Storm surges are influenced by TC intensity, size, and track and can be amplified by shallow coastal bathymetry or local geometry (Mori et al., 2014). Hence, even relatively weak TCs can induce high storm surges under certain conditions.

Hydrodynamic models are used to simulate storm surges, both for operational applications and risk assessments. These hydrodynamic models use wind speed and mean sea-level pressure (MSLP) as forcing, which is usually derived from general circulation models (GCMs). Until recently, these GCMs had horizontal resolutions of  $0.45^\circ$  to  $1.8^\circ$  (ca. 50-200 km at the equator) (Saha et al., 2006; Yukimoto et al., 2006). Currently, all available climate reanalysis products have horizontal resolutions of up to  $0.75^\circ$ , including ERA-Interim (Dee et al., 2011) and NCEP/NCAR Reanalysis 1 (Kalnay et al., 1996). Such resolutions are insufficient to fully resolve TC intensity, size, and track (Murakami and Sugi, 2010; Schenkel and Hart, 2012; Walsh et al., 2007), and are especially problematic for weak TCs (Hodges et al., 2017; Murakami,

2014). At the local scale, many studies have employed parametric models (Haigh et al., 2014; Harper and Holland, 1999; Holland, 1980; Lin and Chavas, 2012; Lin et al., 2010) to obtain high-resolution wind and pressure fields. Such models fit MSLP and 10 m wind speeds (U10) to radial profiles with an exponential decay away from the eye. Limitations of such parametric models include the fact that they do not fully capture asymmetric cyclones (Harper and Holland, 1999) and do not include dissipation effects over land (Jakobsen and Madsen, 2004). Other studies have used high-resolution (down to 50 m) hindcasts to simulate TC characteristics and surge heights (Bunya et al., 2010; Dietrich et al., 2010). These hindcasts are based on regional downscaling and/or regional climate models, and consequently, hindcasts are not applicable in regions with sparse observational data (Nikulin et al., 2012).

A limited set of GCMs is run at horizontal resolutions of 10 to 30 km (0.09°-0.27°), a scale at which TCs can be resolved (Bacmeister et al., 2016; Mizuta et al., 2012). With the launch of ERA5 (0.25°) in 2017, reanalysis products are now also available at these horizontal resolutions. One high-resolution GCM is the European Centre for Medium-Range Weather Forecasting (ECMWF) Integrated Forecasting System (IFS). In addition to being an operational weather forecasting model, IFS has been used for producing reanalysis products such as ERA5 and ERA-Interim (Dee et al., 2011; ECMWF, 2017c). In ERA-Interim, the average number of TCs per year is simulated well (Strachan et al., 2013), but modeled tracks differ from observed ones, and the intensity and size are underestimated (Murakami and Sugi, 2010; Schenkel and Hart, 2012). The underestimation of intensity is usually driven by resolution effects and poor physical schemes (Flato et al., 2013; Walsh et al., 2007). Previous updates in the ECMWF IFS tropical atmospheric conditions have improved tropospheric wind and convection compared to observations, (Fiorino, 2008) and the model's spatial resolution was increased from  $\pm 0.225^\circ$  at the equator in 2006 to its current resolution of  $\pm 0.08^\circ$  (ECMWF, 2017a). These updates have significantly contributed to the improvement of the IFS TC track ensemble forecasts. A recent example of the improved performance is the IFS ensemble forecast for Hurricane Sandy's track, which predicted Sandy's landfall up to seven days in advance (Bassill, 2014; Magnusson et al., 2014).

Apart from track ensemble forecasts, TC intensity forecasts have also improved in the latest model updates (ECMWF, 2017a). Together with the emergence of global hydrodynamic models (Carrère and Lyard, 2003; Jagers et al., 2014; Verlaan et al., 2015; Vitousek et al., 2017), it is possible to simulate TC surges at local to global scales using direct output from GCMs. These simulations are already carried out operationally, such as for the Atlantic Ocean using the NHC TC advisories, a parametric wind model and SLOSH model (Byrne et al., 2017; Jelesnianski et al., 1984). However, no research has been conducted on the use of ECMWF IFS meteorological forcing for high-resolution storm surge modeling. In addition, despite research focusing on methods to test the sensitivity of simulated storm surges to TC wind fields (Cardone and Cox, 2009), few studies have analyzed the effects of the

resolution of meteorological forcing on simulated storm surges. Wakelin and Proctor (2002) used three meteorological operational analysis datasets to analyze two storm surge events in the Adriatic Sea and concluded that their model works best using meteorological forcing with the highest spatial and temporal resolution. Recent research by Muis et al. (2016) has demonstrated the implications of using coarse-resolution meteorological forcing for global storm surge modeling. They generated time series of storm surges on a global scale using the six-hourly  $0.75^\circ$  ERA-Interim dataset (Dee et al., 2011; ECMWF, 2016) and found that extreme sea levels induced by TCs are underestimated due to the coarse resolution of meteorological datasets. This raises the question: what resolution of meteorological forcing is needed to adequately simulate TC-induced storm surges?

In this chapter, we test the suitability of ECMWF IFS as meteorological forcing for high-resolution global storm surge modeling. In addition, we analyze the effect of the horizontal resolution of meteorological forcing on maximum storm surge heights. We explore and discuss possible drivers of maximum surge heights.

## 2.2 Methods

The overall methodology is illustrated in Figure 2.1. The U10 and MSLP are derived from the ECMWF IFS and aggregated from their original resolution to T799 resolution ( $\pm 0.225^\circ$  at the equator) and to various coarser resolutions between  $0.25^\circ$  and  $1.0^\circ$  (Section 2.2.1). Relevant meteorological parameters for the analysis (maximum U10, minimum MSLP, TC size) are derived by tracking each TC (Section 2.2.2). The U10 and MSLP fields are then used to model the associated surge heights using the Global Tide and Surge Model (GTSM) (Section 2.2.3). Storm surges modeled at T799-resolution forcing are compared with observations (Section 2.2.4). Lastly, the effects of different horizontal resolutions of meteorological forcing on maximum surge heights are explained through TC size and intensity, and coastline complexity and slope (Section 2.2.5).

We focus on eight case studies of historical TCs (Figure 2.2), one in each TC basin. We only consider landfalling TC events occurring after 5 June 2007 0 UTC, to allow for use of the new 4D-VAR data assimilation scheme, which considerably improved clouds and convection in IFS and thereby tropical troposphere forecasts (ECMWF, 2017a). In the November 2007 update, lower tropospheric winds in the tropics are also improved.

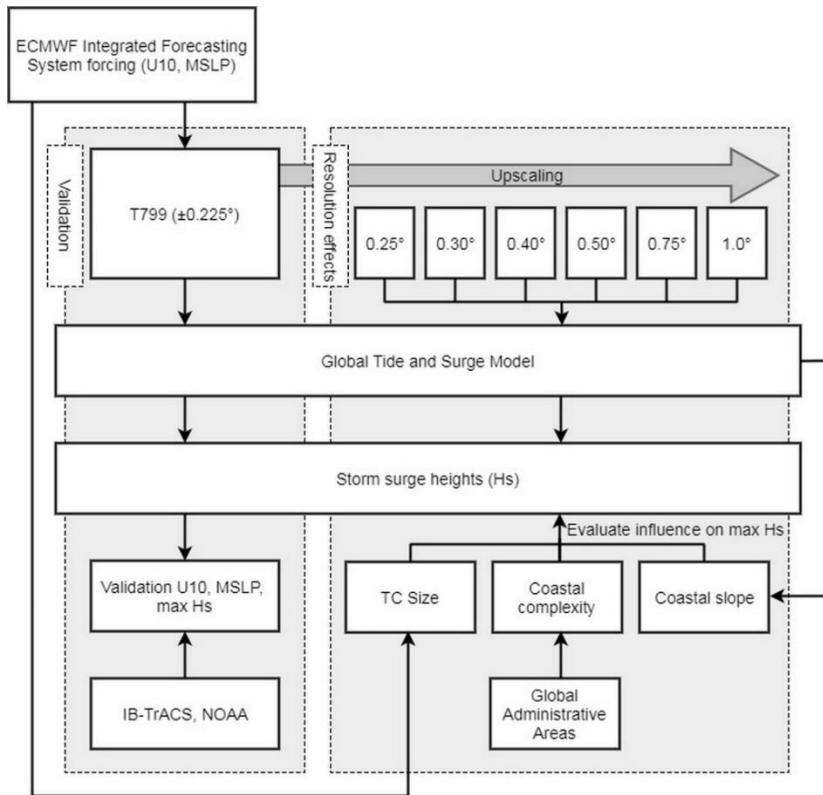


**Figure 2.1** Schematic overview of the approach followed in this study. Meteorological forcing is extracted from the ECMWF Integrated Forecasting (IFS) at the native grid resolution (T799,  $\pm 0.225^\circ$ ). Comparison to observations is performed for the 10 m wind speed (U10), mean sea-level pressure (MSLP) and maximum surge height (Hs). Land maps to derive coastal complexity are taken from the Global Administrative Areas (GADM).

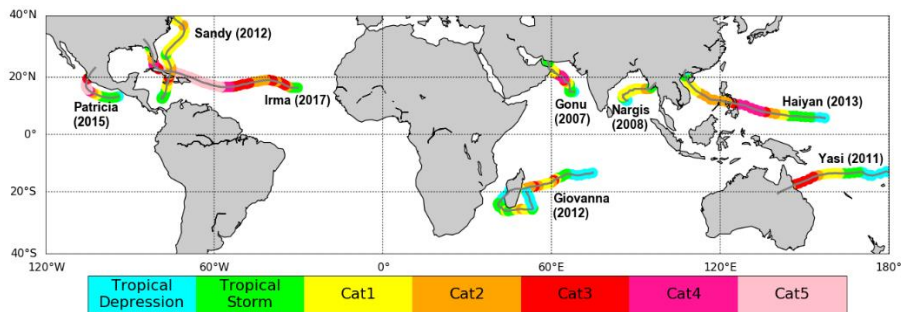


**Figure 2.2** Overview of the eight selected case studies. Colors indicate the TC intensity on the Saffir-Simpson scale.

### 2.2.1 ECMWF IFS forcing

For each case study, U10 and MSLP data are extracted from the ECMWF IFS (ECMWF, 2017a). The ECMWF general circulation model is used for numerical weather predictions and consists of a dynamical, physical, and coupled ocean wave component (Persson and Grazzini, 2005). The temporal resolution is three hours. Because of continuous updates in IFS resolution (ECMWF, 2017a), original model resolution varies between the different TCs. Therefore, we homogenize the horizontal resolution of all cases to T799 resolution. We use the 0 and 12 UTC runs and their +3h, +6h and +9h forecast runs. Upscaling is achieved by averaging over neighboring grid cells (first-order conservative remapping on all spatial variables in the dataset; Jones, 1999). This process is likely to produce lower differences in wind and pressure intensities between the different resolutions than re-running the global atmospheric model on a coarser resolution would, because small coherent features are typically poorly resolved in numerical models at coarser resolution, but they can still be included when upscaling from a high-resolution to a lower-resolution grid (Boer and Denis, 1997).

### 2.2.2 TC Tracking algorithm

To capture the TC characteristics at every time step and to enable comparison with the IBTrACS dataset (v03r10), we track the eight TCs and their characteristics throughout their lifetimes. We use IBTrACS because it is considered the most complete best-track dataset of global historical TC activity (Knapp et al., 2010). The cyclone's position as given in IBTrACS is taken as the initial position of the eye in the tracking algorithm. The spatial resolution in IBTrACS is generally listed at  $0.1^\circ$ , whereas the spatial resolution in ECMWF IFS is approximately  $0.225^\circ$  at the equator. Because of this difference, we apply the tracking algorithm from Baatsen et al. (2015) to ensure we are looking at the 'true' position of the eye in ECMWF IFS. Following this tracking algorithm, we determine the location with the maximum relative vorticity (a measure of the rotation of the horizontal velocity field) is in a surrounding  $5^\circ \times 5^\circ$  box from the initial position of the eye. If this location corresponds to a lower MSLP than the initial position, the position of the eye is updated. We then set the location with the minimum MSLP in a surrounding  $2.5^\circ \times 2.5^\circ$  box as the final position of the eye. Using the tracking algorithm from Schenkel and Hart (2012), we extract the maximum U10 and minimum MSLP at every time step within a  $7^\circ$  radius of the final position of the eye. Using this  $7^\circ$  radius, we ensure that these two TC characteristics are captured inside the domain. Following Chavas et al. (2016), we determine TC size by using the radius of vanishing winds  $r_0$ , defined as the average distance outside of the eye where  $U10 < 12$  m/s.

### 2.2.3 Storm surge modelling

For each TC, storm surges are simulated by forcing GTSM with meteorological data (U10 and MSLP) from the ECMWF IFS. GTSM is a global hydrodynamic model implemented with unstructured grids, based on the Delft3D FM software developed

by Deltares (Kernkamp et al., 2011). GTSM has a spherical grid with thinning at high latitudes, with cell size dependent on the bathymetry (also known as courant grid refinement) (Irazoqui Apecechea et al., 2017). Additional refinement is applied in areas with steep slopes, such as mid-oceanic ridges, to improve the representation of the internal tides. This allows for high computational efficiency with high resolution (lower than 7.5 km, and on average 5 km) near coasts and coarser resolutions (up to 50 km) in the deep ocean. The General Bathymetric Chart of Oceans (GEBCO) 2014 dataset ([https://www.gebco.net/data\\_and\\_products/gridded\\_bathymetry\\_data/](https://www.gebco.net/data_and_products/gridded_bathymetry_data/)), defined in a 30'' grid, is used for bathymetry. The computational time step is 150 s. GTSM and the output dataset GTSR (Muis et al., 2016) are used in many recent research, including Hiroaki et al. (2017), Irazoqui Apecechea et al. (2017), Muis et al. (2017), Vousdoukas et al. (2018) and Williams et al. (2018).

Muis et al. (2016) used 6-hourly ERA-Interim data (at 0.75°) as meteorological forcing in GTSM to obtain a global reanalysis of storm surges (1979-2014). They validate modeled sea levels against observed sea levels using a global set of 472 tide gauges stations from the University of Hawaii Sea Level Center (available at <https://uhslc.soest.hawaii.edu/>). A validation of the surge levels shows that 95% of all stations have a root-mean-square error (RMSE) lower than 0.2 m, with the average RMSE being 0.11 m (standard deviation 0.05 m). Extratropical storm surges are modeled relatively well, whereas TC storm surges are substantially underestimated. This is shown by the average correlation coefficient in tropical regions of 0.77 being significantly lower than the average correlation coefficient of 0.87 in extratropical regions. This underestimation is driven by the relatively coarse resolution of the meteorological forcing, which is unable to fully capture the strong wind and pressure gradients in the TCs in both space and time.

A storm surge is a rise of the sea level as a result of changes in atmospheric pressure and wind drag on the sea surface. The influence of atmospheric pressure is given by the inverse barometer effect (Ross, 1854): every 1 hPa drop in atmospheric pressure is accompanied by a roughly 0.01 m increase in sea-level height. In addition, in shallow water there is an additional wind set up that can be approximated roughly as:

$$g \frac{\partial h}{\partial x} = C_d \frac{U^2}{H} \quad (2.1)$$

where  $g$  is the gravitational constant ( $\text{m/s}^2$ ),  $h$  the surface level above the reference height (m),  $x$  the horizontal distance (m),  $C_d$  the drag coefficient (-),  $U$  the average wind speed at 10 m perpendicular to the coast (m/s) and  $H$  the total water depth (m) (Weenink, 1958). From Equation 2.1 it follows that the largest surges occur in shallow water with a wide coastal shelf.

Hourly output data are extracted from the GTSM coastal grid points. For each TC, we consider an area of  $15^\circ \times 15^\circ$  around the landfall location and a time period of three days on either side of the moment of landfall. In this time period, we then select all coastal points in the T799-resolution forcing at which the maximum surge height is at

least 50% of the overall maximum surge height, with a minimum height of 15 cm. This way, only coastal points with high storm surges are included in the statistical analysis. For the other resolutions, the same set of coastal grid points in GTSM is used, to ensure a direct comparison in storm surge heights at coarser resolutions.

## 2.2.4 Comparison of results

We compare the minimum MSLP and maximum U10 in the T799-resolution forcing against IBTrACS. The MSLP is given as an instantaneous value in both datasets. The U10 is given as a 7.5-minute average in the T799-resolution forcing, and the observed U10 is the 10-minute average wind speed in 3- or 6-hourly intervals. Since the conversion factor between these two averages is approximately 1 (Harper et al., 2008), we directly compare the two variables throughout this chapter.

Before analyzing surge heights at coarser resolutions, we first need to demonstrate that our IFS-GTSM model setup is sufficient in simulating maximum surge heights. To do so, we analyze the performance of the model setup at the T799-resolution forcing by comparing the maximum surge heights modeled with the T799-resolution forcing to observed maximum heights. Because of the dense tide gauge network on the U.S. mainland, it is possible to compare modeled and observed storm surge heights for Irma and Sandy at multiple locations along the coastline. For this, we take tide gauge stations within 250 km of the TC track and subtract the daily maxima of tides from the daily maxima of the observed sea levels to calculate skew surge (NOAA, 2017). Since these sea levels are referenced above the mean sea level, we correct for mean sea-level trends by removing the monthly mean sea level. We compare the tide gauge measurements to neighboring GTSM coastal grid points. For the other TCs, the observed maxima and any applied corrections are taken from the available literature.

## 2.2.5 Coastal slope and complexity

Apart from being driven by meteorological factors such as U10 and MSLP, storm surge heights can be further amplified when the surge is interacting with shallow coastal bathymetry and coastal complexity (Mori et al., 2014). For this reason, we will also look at coastal slope and coastal complexity as drivers for changes in storm surge heights between different resolutions.

The coastal slope is derived from GEBCO, and calculated as the average slope between the coastline and the bed level 100 km off the coast, perpendicular to the coastline. Coastal complexity is assessed by calculating the fractal dimension  $D$  of the coastline around the landfall location (Mandelbrot, 1967). A fractal dimension is the ratio of change between pattern details and measuring scales, calculated using different length scales to measure the length of the outline of an object, such as a coastline. The values of  $D$  lie between 1 and 2 for coastlines, where a high  $D$  implies a more complex coastline. To calculate  $D$ , we use high-resolution country maps (30 m) from the database of Global Administrative Areas (GADM, 2017) and length

scales between 1 and 100 km. The algorithm for calculating the coastline complexity is based on Hijmans (2016).

## 2.3 Results and discussion

### 2.3.1 IFS-GTSM model performance at T799-resolution forcing

#### *Comparison of U10 and MSLP*

The modeled and observed U10 and MSLP for all TCs are listed in Table 2.1. Spatial plots of U10 and MSLP at landfall can be found in Figures A.1 – A.4. We see that the modeled MSLP and U10 intensities are generally underestimated in the T799-resolution forcing as compared to the observed values. The modeled MSLP values are up to 60 to 70 hPa higher than the observed values (Hurricane Patricia and Typhoon Haiyan). Conversely, Cyclone Gonu has a lower modeled MSLP as opposed to the observed value (15 hPa). Although in most cases, the underestimation of U10 is between 10 and 30 m/s, Patricia’s U10 is underestimated by almost 50 m/s. These intensity underestimations for Patricia and Haiyan are likely related to the failure of the data resolution to fully capture their small eyes. The T799-resolution forcing is known to cause considerable intensity underestimations for relatively small TCs with a small eye (ECMWF, 2017b), as was the case for Patricia and Haiyan, which had eyes of 13 and 15 km in diameter, respectively.

#### *Comparison of maximum surge heights*

For Irma and Sandy, tide gauge records can be used to analyze the modeled maximum surge heights. The results are shown in Figure 2.3. The  $R^2$ -values are 0.86 for Irma and 0.74 for Sandy, demonstrating a good fit between the modeled and observed surge heights. These results show that GTSM is capable of capturing the spatial variability in surge heights in both cases, as is also shown in panels c and d of Figure 2.3. However, when zooming in to the local level, we notice some deviations from observed values. Underestimations in modeled storm surges can be caused by various factors. One of these factors is that bays and estuaries are in general not captured by GTSM’s grid resolution (approximately 5 km near the coastline). In addition, uncertainties imposed by the meteorological forcing can also cause lower modeled storm surges. Overestimations in the modeled storm surges may be caused by differences in the locations of the coastal points and the tide gauges, such as a GTSM grid point at the coast versus a tide gauge located in a harbor or a semi-open inlet.

Because we compare the tide gauge locations to nearby GTSM coastal grid points, Irma’s maximum modeled surge height of 2.6 m near Everglades City (Table 2.1) is not included in the scatter plot (Figure 2.3a). The nearest tide gauge station was located at Fort Myers, approximately 100 km north of Everglades City, so that a GTSM coastal point closer by was selected.



**Table 2.1** Overview of modeled (Mod) and observed (Obs) variable values at landfall for the T799-resolution forcing. Observed values are extracted from IBTrACS (Knapp et al., 2010)

	Landfall location	Time and date of landfall	Min MSLP (hPa)			Max U10 (m/s)			Max surge height (m)		Source for observed maximum surge height	Remarks on observed surge height
			Mod	Obs	R <sup>2</sup>	Mod	Obs	R <sup>2</sup>	Mod	Obs		
<b>Irma (2017)</b>	Marco Island, Florida, United States.	10 Sep 2017 19:30 UTC	942	928	0.80	39.9	59.1	0.62	2.59	1.5-3.0	Cangialosi et al. (2018)	Based on high water marks and storm surge estimations in Everglades City, FL.
<b>Patricia (2015)</b>	Cuixmala Mexico	23 Oct 2015 23:00 UTC	993	932	0.93	18.5	66.9	0.62	0.18	-	Kimberlian et al. (2016)	Official tropical cyclone report does not mention occurrence of storm surge
<b>Haiyan (2013)</b>	Tacloban City, Philippines	7 Nov 2013 20:40 UTC	966	895	0.64	34.1	64.3	0.77	0.81	2-3 <sup>a</sup>	Mori et al. (2014)	Surge height estimates in San Pablo Bay
<b>Sandy (2012)</b>	New Jersey, United States	29 Oct 2012 23:30 UTC	993	945	0.80	15.6	36	0.61	2.22	2.6 <sup>b</sup>	Blake et al. (2013)	Tide gauge at Sandy Hook ( $\pm 25$ km east)
<b>Giovanna (2012)</b>	Andovoranto, Madagascar	14 Feb 2012 0:00 UTC	952	945	0.64	35.5	43.7	0.66	0.54	0.5 <sup>c</sup>	Probst et al. (2012)	Eyewitnesses report a sea level increase no more than 0.5 m
<b>Yasi (2011)</b>	Mission Beach, Australia	2 Feb 2011 14:30 UTC	972	929	0.67	25.7	56.5	0.93	1.74	2.3 <sup>b</sup>	Bureau of Meteorology (2017)	Tide gauge at Cardwell ( $\pm 60$ km north)
<b>Nargis (2008)</b>	Irrawaddy Delta, Myanmar	2 May 2008 10:00 UTC	965	962	0.63	33.1	46.3	0.73	2.10	1-2 <sup>a</sup>	Tasnim et al. (2015)	Derived from spatial plot
<b>Gonu (2007)</b>	Ras al-Hadd, Oman	5 June 2007 21:00 UTC	955	970	0.13	30.6	39.6	0.20	0.51	0.5-1.0 <sup>a</sup>	Fritz et al. (2010)	Numerically modeled based on high water marks in coastal regions in Oman

<sup>a</sup> Simulated based on surveys & high water marks<sup>b</sup> Nearest tide gauge measurement<sup>c</sup> Eyewitness reports/evidence of a storm surge

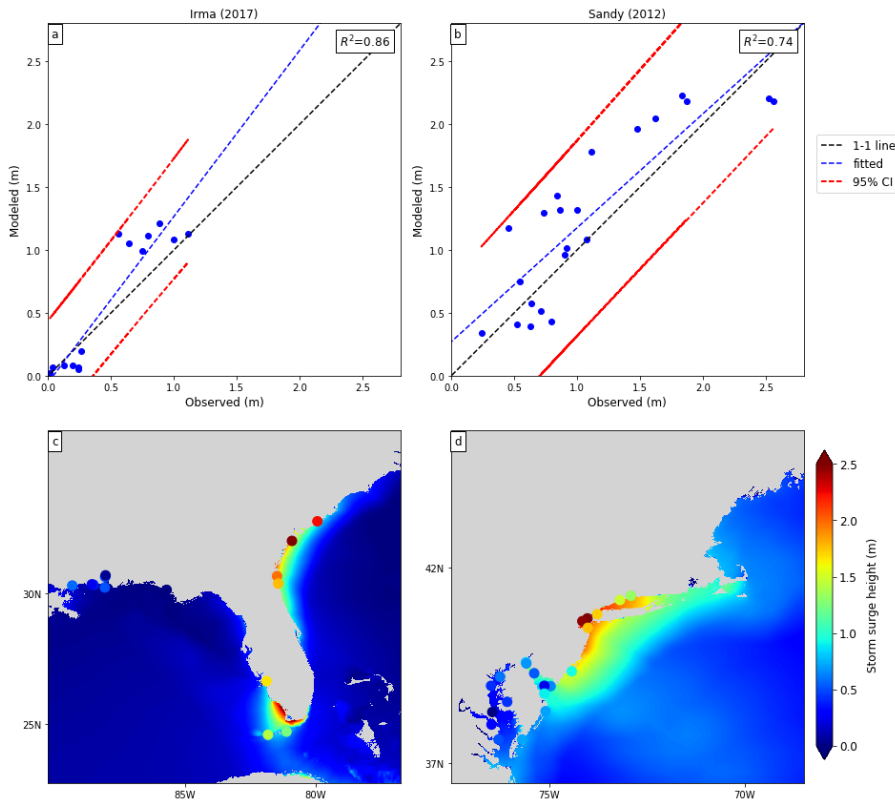


**Figure 2.3** Upper panels show scatter plots of the modeled and observed maximum storm surge heights for Irma (a) and Sandy (b). Lower panels show the modeled and observed (dots) maximum storm surge heights for Irma (c) and Sandy (d). Observations are taken from NOAA tide gauge stations (14 stations for Irma, 22 stations for Sandy)

From Table 2.1, we see that Sandy’s modeled maximum U10 is more than 50% lower than observed. From the quadratic relation between wind and surge (see Equation 2.1, we would expect a 75% lower surge, but this is not seen in the simulations (Figure 2.3). This is likely due to the fact that resolution effects of the climate model do not only lead to an underestimation of wind intensity and the pressure drop, but can also lead to an overestimation of the storm size (known as numerical diffusion). The relatively large wind field increases the storm surge, which compensates for the TC intensity underestimation. For the other case studies, we refer to the maximum surge heights around the landfall location listed in the literature (see Table 2.1). The differences between the modeled and observed maximum surge heights are lower than 0.5 m for five TCs: Hurricanes Irma and Sandy and Cyclones Giovanna, Nargis, and Gonu. For Patricia, the modeled maximum surge height is approximately 0.2 m. However, there is no mention of a storm surge in the official tropical cyclone report

(Kimberlian et al., 2016), from which we conclude that any possible storm surge would have been low. This conclusion is in line with our model results.

Larger differences between the modeled and observed maximum surge heights are seen for Haiyan and Yasi. In both cases, the maximum surge height was recorded in an inlet. Because of GTSM's resolution of approximately 5 km near coastlines, these inlets are not (fully) captured by the model. For Haiyan, it is likely that the strong intensity underestimation adds to the underestimation of the storm surge.

Based on the performance, we conclude that the IFS-GTSM model setup at the T799-resolution framework is capable of capturing large-scale spatial patterns of maximum surge height sufficiently well for the analysis on the effect of using lower-resolution meteorological forcing.

### 2.3.2 Horizontal resolution effects

Our results confirm that storm surge simulations using coarse-resolution meteorological forcing generally result in lower storm surge heights (Wakelin and Proctor, 2002). These reductions are shown in Figure 2.4, where the gradual decrease in slope for the different scatter plots shows that the maximum surge heights at GTSM coastal points decrease with decreasing horizontal resolution. Scatterplots for the other TCs are shown in Figure A.5.

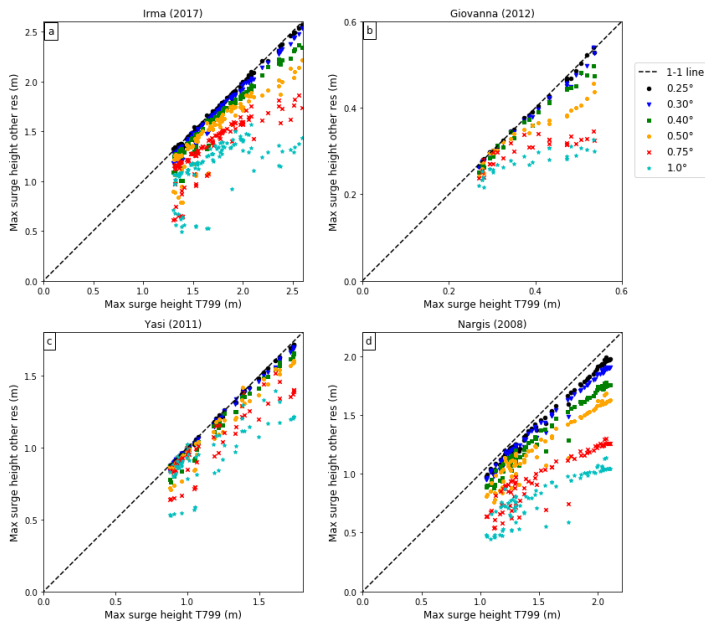


**Figure 2.4** Scatterplot of maximum surge height at the T799-resolution forcing vs. other resolutions for (a) Hurricane Irma (Florida), (b) Cyclone Giovanna (Madagascar), (c) Cyclone Yasi (Australia) and (d) Cyclone Nargis (Myanmar)

The differences in surge heights are illustrated in Figure 2.5, which displays surge heights during the storm’s lifetime for Irma, Giovanna, Yasi, and Nargis at T799 (left) and 1.0° (center) resolutions, and their difference (right). Differences in surge heights for the other TCs can be found in Figures A.6-A.9. We calculate the relative difference in maximum surge heights at all selected GTSM coastal points (black dots in Figure 2.5) to illustrate the resolution effects for the different TCs (see also Table A.3). For both Giovanna and Irma, relative differences in the average maximum surge height between T799- and 1.0°-resolution forcing amount to 39%. Patricia, Sandy, Yasi, and Gonu each have relative differences smaller than 20%, and the largest relative difference is found for Nargis with 47%.

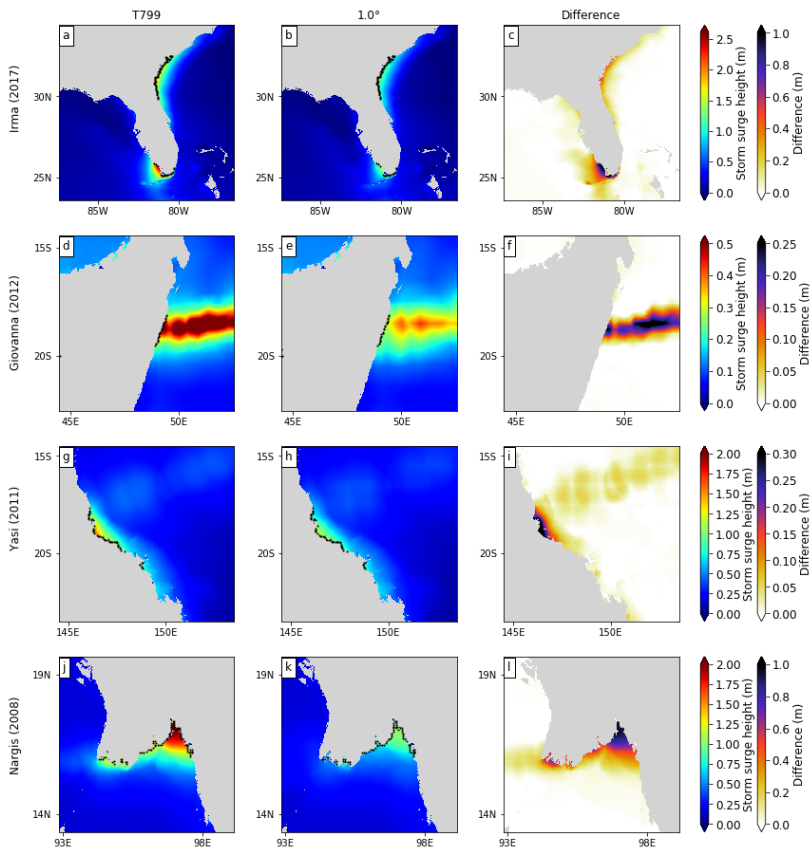


**Figure 2.5** Maximum surge heights at T799- and 1.0°-resolution forcing and difference in maximum surge heights during the storm’s lifetime between T799- and 1.0°-resolution forcing for (a-c) Hurricane Irma (Florida), (d-f) Cyclone Giovanna (Madagascar), (g-i) Cyclone Yasi (Australia) and (j-k) Cyclone Nargis (Myanmar). Black dots represent GTSM coastal points used in the statistical analysis.

For the remainder, we focus on the absolute differences in the average maximum surge heights. These absolute differences can directly affect inundation depths and flood

risk estimates (De Moel et al., 2012). Comparing the average maximum surge heights for simulations using different resolutions, Table 2.2 shows that there are four TCs for which the absolute difference is approximately or less than 0.2 m for all resolutions: Patricia, Haiyan, Giovanna and Gonu. For Sandy and Yasi, the maximum differences are approximately 0.35 m. The largest differences are found for Irma and Nargis, with maximum surge heights around 1 m lower in the  $1.0^\circ$ -resolution forcing. These results show that six out of the eight TCs can still be modeled relatively well at low resolutions, with maximum storm surge underestimations lower than 0.5 m, whereas for Irma and Nargis, meteorological forcing resolutions lower than  $0.75^\circ$  result in storm surge underestimations of around 0.8 m. Underestimations of this magnitude have a considerable effect on impact calculations (De Moel et al., 2012).

From Table 2.2 it follows that the difference in simulated maximum surge heights between different model resolutions is larger for higher storm surges. The height of a storm surge is driven by a combination of factors, which can broadly be classified into TC characteristics and geographical characteristics. The TC characteristics include intensity (measured via maximum U10 and minimum MSLP) and TC size (Irish et al., 2008). In addition, storm surges can be amplified by certain geographical characteristics, most importantly coastal slope and coastal complexity (Mori et al., 2014). We represent coastal complexity here as a fractal dimension  $D$ , where higher values of  $D$  imply a more complex coastline.

Table 2.3 shows the TC and geographical characteristics for our eight case studies at landfall. We see that intensity (U10 and MSLP) alone cannot explain the maximum storm surge heights. This insight corresponds with the results of Irish et al. (2008), who have shown that TC size also has a large effect on the storm surge, though we use the radius of vanishing winds (Chavas et al., 2016), where they use the radius to maximum winds as a proxy for TC size. In our cases, the effect of TC size is apparent with the storms Sandy and Yasi, which resulted in large storm surges, despite their relatively low maximum wind speed and high pressure. However, TC size alone is not enough to explain storm surge magnitudes, as some small storms (such as Nargis) still result in high storm surges.

Geographical characteristics also influence storm surges. Storms that make landfall on coasts with a low complexity and steep slopes generally result in low surges (e.g., Giovanna, Gonu, Patricia), while storms that make landfall on complex and shallow coastlines are associated with larger storm surges. Overall, both TC and geographical characteristics influence the size of the storm surge and, correspondingly, the underestimation that occurs when a coarse-resolution meteorological forcing is used.

**Table 2.2** Average maximum surge heights at the GTSM coastal points for the different TCs. Values between brackets indicate the maximum surge height. TCs are ordered from highest to lowest storm surge

	<b>Irma</b>	<b>Sandy</b>	<b>Nargis</b>	<b>Yasi</b>	<b>Haiyan</b>	<b>Giovanna</b>	<b>Gonu</b>	<b>Patricia</b>
<b>T799</b>	1.72 (2.59)	1.62 (2.22)	1.54 (2.10)	1.17 (1.74)	0.52 (0.81)	0.38 (0.54)	0.31 (0.51)	0.17 (0.18)
<b>0.25°</b>	1.70 (2.57)	1.61 (2.20)	1.46 (1.99)	1.16 (1.72)	0.52 (0.83)	0.38 (0.54)	0.31 (0.50)	0.17 (0.18)
<b>0.30°</b>	1.66 (2.54)	1.59 (2.15)	1.42 (1.90)	1.16 (1.70)	0.51 (0.74)	0.38 (0.54)	0.31 (0.49)	0.17 (0.18)
<b>0.40°</b>	1.59 (2.37)	1.55 (2.09)	1.33 (1.77)	1.12 (1.66)	0.48 (0.73)	0.36 (0.50)	0.30 (0.47)	0.17 (0.18)
<b>0.50°</b>	1.49 (2.22)	1.53 (2.09)	1.24 (1.69)	1.10 (1.60)	0.46 (0.61)	0.34 (0.46)	0.29 (0.44)	0.17 (0.18)
<b>0.75°</b>	1.33 (1.86)	1.46 (2.01)	0.96 (1.30)	1.03 (1.51)	0.42 (0.60)	0.30 (0.35)	0.28 (0.39)	0.17 (0.19)
<b>1.0°</b>	1.15 (1.57)	1.37 (1.90)	0.81 (1.14)	0.95 (1.39)	0.38 (0.61)	0.27 (0.33)	0.26 (0.41)	0.16 (0.17)
<b>Difference T799-1.0°</b>	0.57 (1.03)	0.25 (0.33)	0.73 (0.96)	0.22 (0.35)	0.15 (0.19)	0.11 (0.21)	0.05 (0.10)	0.02 (0.02)

**Table 2.3** TC (upper three rows) and geographical (bottom two rows) characteristics at landfall. All values are modeled values. TCs are ordered from highest to owest storm surge (left to right)

	<b>Correlation</b>	<b>Irma</b>	<b>Sandy</b>	<b>Nargis</b>	<b>Yasi</b>	<b>Haiyan</b>	<b>Giovanna</b>	<b>Gonu</b>	<b>Patricia</b>
<b>Max surge (T799) (m)</b>		<b>2.59</b>	<b>2.22</b>	<b>2.10</b>	<b>1.74</b>	<b>0.81</b>	<b>0.54</b>	<b>0.51</b>	<b>0.18</b>
<b>Max U10 (m/s)</b>	0.12	39.9	15.6	33.1	25.7	34.1	35.5	30.6	18.5
<b>Min MSLP (hPa)</b>	-0.13	942	993	965	972	966	952	955	993
<b>r<sub>0</sub> (km)</b>	0.41	314	612	254	419	411	332	289	213
<b>D</b>	0.90	1.22	1.20	1.27	1.19	1.13	1.03	1.03	1.07
<b>Coastal slope (°)</b>	-0.58	0.000002	0.003	0.04	0.003	0.01	0.02	0.06	0.28

## 2.4 Concluding remarks

In this research, we have assessed the suitability of the ECMWF IFS as meteorological forcing for high-resolution storm surge modeling with GTSM. For this, we compared the modeled maximum surge heights of Hurricanes Irma (2017) and Sandy (2012) with observations from tide gauge stations. We found  $R^2$ -values of 0.86 and 0.74 for Irma and Sandy, respectively, demonstrating that maximum surge heights and their spatial distributions are captured sufficiently well in our IFS-GTSM model setup to simulate historical TC storm surge events. For the other case studies, we compared the modeled maximum surge heights to observations and/or estimates from the literature. We found that modeled surge heights are generally lower than observed heights. For most case studies, the difference between the observed and modeled surge heights is less than 0.5 m, from which we conclude that the IFS-GTSM model setup at T799-resolution framework is capable of capturing the large-scale spatial patterns of the maximum surge heights sufficiently well.

In addition, we analyzed the effects of different horizontal resolutions of meteorological forcing data on the simulated maximum surge heights by upscaling the meteorological forcing of the eight selected TC case studies to various coarser resolutions between  $0.25^\circ$  to  $1.0^\circ$ . We found that simulated TC storm surges are lower using coarser resolution datasets, with differences between the highest-resolution and  $1.0^\circ$ -resolution forcing ranging between 0.01 m for Patricia and 1.02 m for Irma. Similar conclusions were reached by Appendini et al. (2013), who forced a wave model with three different atmospheric reanalyses datasets to model significant wave heights. Despite differences in the atmospheric models, they show that wave modeling is improved in finer spatial resolution datasets compared to coarser resolution forcings.

We also observed that the storms with the highest storm surges also generate the largest differences in storm surge heights between the different resolutions. Hence, TCs with high storm surges require high-resolution meteorological forcing for accurate storm surge and impact modeling. Apart from the atmospheric forcing, mesh resolution and bathymetry representation in the hydrodynamic model are also critical in storm surge modeling (Kerr et al., 2013), but the effects of these two elements were not explored here. Therefore, our results should be taken with some caution, as they only serve as a way of assessing the atmospheric resolution effects, rather than a way of validating the hydrodynamic model and providing accurate storm surge height estimates in a particular area.

Furthermore, we examined the relationship between storm surge heights and geographical characteristics known to influence them (Irish et al., 2008; Mori et al., 2014): intensity, TC size, coastal complexity, and coastal slope. It appears that storm surge height is a combination of all these factors. However, in the eight case studies examined in this study, it seems that the geographical characteristics have a larger effect than the TC characteristics: the highest storm surges are found in regions with

high coastal complexity and, in general, a small slope. At a local scale, the orientation of the coastline can play a more dominant role in storm surge enhancements: this can be seen for small islands where on one side the surge is positive and negative on the other, both with the same complex coastline.

Despite the limited dataset, there are indications that coastal complexity is an important driver for maximum surge heights and, in turn, the decrease in maximum surge heights in coarser-resolution meteorological forcing datasets. To further test the relationship between coastal complexity and horizontal resolution effects, we propose the use of a hydrodynamic model in which coastal slope and complexity can be (independently) adjusted for the same TC case study. Since coastal topography (e.g., mountainous regions) can also affect wind fields (Raderschall et al., 2008), the coastal complexity should be adjusted simultaneously in the global atmospheric circulation model.

Our findings show that the use of high-resolution meteorological forcing is particularly beneficial for areas prone to high (several meters) TC storm surges, since these high storm surges are reduced most when using coarser-resolution datasets. For TC case studies with surges below 0.5 m, our results suggest that coarser-resolution datasets can be used with limited effects on maximum surge heights.

## Acknowledgments

We thank ECMWF for the use of the ECMWF IFS dataset. Access to IFS data was granted by the national meteorological services of ECMWF Member and Co-operating States. All other users can gain access to ECMWF forecast product under various license agreement types, see <https://www.ecmwf.int/en/forecasts/accessing-forecasts/order-historical-datasets>. We thank Jan Barkmeijer for sharing his expertise on ECMWF IFS. We also thank the participants of the 6<sup>th</sup> International Summit on Hurricanes and Climate Change: from Hazard to Impact for the fruitful discussions on this topic. We thank SURFsara ([www.surfsara.nl](http://www.surfsara.nl)) for the support in using the Lisa Computer Cluster.

NB, SM and JCJHA are funded by a VICI grant from the Netherlands Organisation for Scientific Research (NWO) (grant number 453-13-006). RJH is funded by the PRIMAVERA project in the European Commission's Horizon 2020 research programme (grant number 641727). MV and MIA are funded by the European Union's Horizon 2020 research and innovation programme (grant number 687323). PJW is funded by a VIDI grant from the Netherlands Organisation for Scientific Research (NWO) (grant number 016.161.324).





# 3 The Synthetic Tropical cyclOne geneRation Model

**This chapter is published as**

Bloemendaal, N., Haigh, I.D, de Moel, H., Muis, S., Haarsma, R.J. & Aerts, J.C.J.H.  
Generation of a global synthetic tropical cyclone hazard dataset using STORM.  
*Nature Scientific Data* **7**, 40 (2020). <https://doi.org/10.1038/s41597-020-0381-2>

## Abstract

Over the past few decades, the world has seen substantial tropical cyclone (TC) damages, with the 2017 Hurricanes Harvey, Irma and Maria entering the top-5 costliest Atlantic hurricanes ever. Calculating TC risk at a global scale, however, has proven difficult given the limited temporal and spatial information on TCs across much of the global coastline. Here, we present a novel database on TC characteristics on a global scale using a newly developed synthetic resampling algorithm we call STORM (Synthetic Tropical cyclOne geneRation Model). STORM can be applied to any meteorological dataset to statistically resample and model TC tracks and intensities. We apply STORM to extracted TCs from 38 years of historical data from IBTrACS to statistically extend this dataset to 10,000 years of TC activity. We show that STORM preserves the TC statistics as found in the original dataset. The STORM dataset can be used for TC hazard assessments and risk modeling in TC-prone regions.

## 3.1 Introduction

Tropical cyclones (TCs), also referred to as hurricanes or typhoons, are one of the deadliest natural disasters, significantly impacting people, economies and the environment in coastal areas when they make landfall. The 2017 Atlantic Hurricane season became the costliest season ever with Hurricanes Harvey, Irma and Maria's combined overall losses estimated around US\$ 220 billion (Munich Re, 2017). It is therefore crucial to support risk mitigation efforts with reliable TC risk assessments. Performing such risk assessments can, however, be challenging. This is because TCs are relatively rare, with around 90 ( $\pm 10$ ) formations per year globally (Emanuel, 2008), of which on average 16 TCs make landfall with wind speeds greater than 33 m/s (Weinkle et al., 2012). Moreover, when making landfall, TCs generally affect a relatively small stretch of coastline ( $< 500$  km; Pugh and Woodworth, 2014), and impacts are higher in urbanized areas compared to rural or uninhabited regions of the world. In addition, reliable TC datasets are only available from 1980 onwards, meaning that for many coastal regions there may not even be a single landfalling TC event in available datasets. Correspondingly, many regions lack information about potential magnitudes and probabilities of TCs, particularly for extreme TCs (i.e. high return periods, low probabilities). This complicates reliable TC risk assessments and corresponding TC risk management.

One way to overcome both temporal and spatial data scarcity for low probability TCs is to extend the historical record. One such approach is by using paleo climate records from coastal sediments which can reveal periods of past coastal floods driven by TCs (Lin et al., 2014; Nott and Hayne, 2001). These records, however, are only available for small coastal stretches, and this method of collecting coastal sediment records is not feasible for upscaling at the global scale. Another method that has been widely explored in the past decades is the generation of synthetic TC tracks (Emanuel et al., 2006; Powell et al., 2005; Vickery et al., 2000). In such an approach, TC tracks and intensities are statistically resampled and modeled from an underlying dataset, which

can be either historical TC tracks (Casson and Coles, 2000; Emanuel et al., 2006; Haigh et al., 2014) or meteorological datasets from climate models (Lin et al., 2012). This creates a new TC, having similar characteristics as the ones in the underlying dataset. This sampling method can be repeated for a large number of years, hereby creating a larger TC dataset including TCs with high return periods.

There are two main synthetic model approaches, namely: (i) a coupled statistical-dynamical model; (ii) and a fully statistical model. Coupled statistical-dynamical models use autoregressive functions for certain parts of the simulation (e.g. only the track (Emanuel et al., 2006)), whilst the rest is simulated using a dynamical model. Examples of such models include the models developed by Emanuel et al. (2006) and Lee et al. (2018). Both models are run on the global scale, however they require a substantial number of input variables and are computationally intensive. Fully statistical models use Markov Chains (Kolmogorov, 1937) for both the track generation and intensity simulation. These models generally require a limited number of input variables, and are less computationally intensive, making them easily applicable. This method has been used by for instance Haigh et al. (2014), Vickery et al. (2000), Hardy et al. (2003) and James and Mason (2005), but only on local to regional scales.

In this chapter, we present the synthetic algorithm Synthetic Tropical cyclOne geneRation Model (STORM), and apply it to develop a global dataset representative of 10,000 years of TC activity under present climate conditions. STORM applies a fully statistical approach based on a modified version of the methodology set out in James and Mason (2005) and Haigh et al. (2014). STORM includes information on TC track, intensity, and size, which can be used to assess TC hazards such as wind, waves, and storm surge. Moreover, STORM requires a minimum number of input variables and is designed in a way that it can be applied to any meteorological dataset to statistically resample and model TC tracks and intensities. Here, we demonstrate STORM using best-track historical data from the International Best Track Archive for Climate Stewardship (IBTrACS) (Knapp et al., 2010). The length of the resulting dataset (i.e. 10,000 years under the same climate conditions) enables proper statistical analysis of return periods of various landfalling TCs. The dataset is particularly useful for TC risk assessments as it can serve as input for storm surge and wave impact modeling, and has characteristics important for wind damage assessments (maximum 10-meter wind speed).

### 3.2 Methods

To create 10,000 years of synthetic TC data, there are three main stages, as follows:

1. **Data preparation and input:** Extract TCs from the source dataset IBTrACS (see Figure 3.1 and Figure 3.2, blue column) and this forms the input for the STORM model.

2. **Fitting distributions and relationships:** The characteristics of the extracted storms are identified and pre-processed to create various distributions and relationships (see Figure 3.2, red column); and
3. **Creating the synthetic TCs:** The distributions and relationships are used to create 10,000 years of TCs, with their corresponding characteristics (see Figure 3.2, green column, and Figure 3.3).

These three stages are explained in more detail below.

### 3.2.1 Input datasets

The first stage is data preparation and input, which involves two steps. In step 1.1, as input data for STORM, we extract TCs from the global historical dataset IBTrACS (Knapp et al., 2010) for the time period 1980-2017 (38 years of data). We use data from 1980 onwards to comply with the modern era of satellite observations. IBTrACS is the unified dataset of the postseason best-track data produced by the tropical warning centers, for all the TC basins. Here, we use all basins except the South Atlantic. The basin domains are adapted from the basin domains used in the IBTrACS dataset (Table 3.1). The South Atlantic has been left out as there are too few TC formations in this basin for adequate distribution and relationships fitting.

**Table 3.1** Definition of the basin domains (Knapp, et al., 2010) and tropical cyclone (TC) seasons (World Meteorological Organization, 2018) used in this study. The basin domains are based on the basin domains used in the IBTrACS dataset

Basin name	Abbreviation	Basin domain	TC season
Eastern Pacific	EP	5°-60°N 180°-coastline of North America on the North Atlantic	1 June – 30 November
North Atlantic	NA	5°-60°N coastline of North America on the Eastern Pacific - 360°	1 June – 30 November
North Indian	NI	5°-60°N 30°-100°E	1 April – 30 June 1 September – 30 November
South Indian	SI	5-60°S 10°-135°E	1 November – 30 April
South Pacific	SP	5-60°S 135°-240°E	1 November – 30 April
Western Pacific	WP	5-60°N 100°-180°E	1 May – 30 November

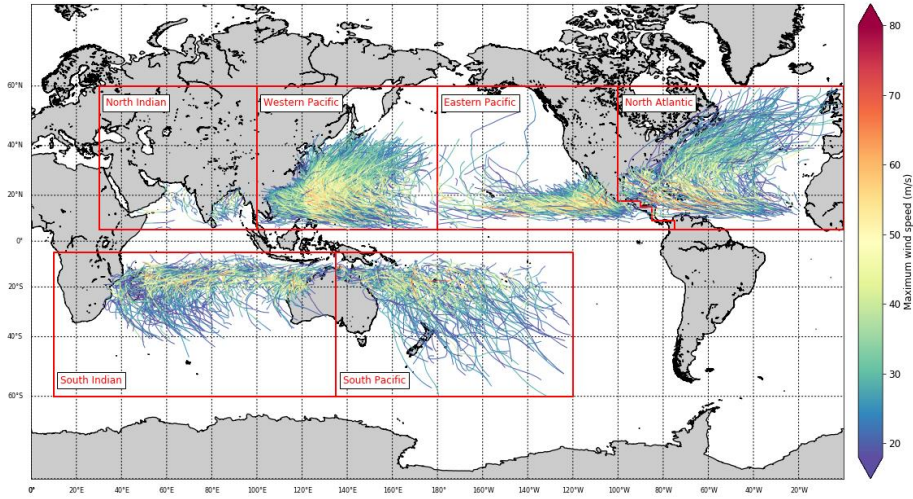


**Figure 3.1** Overview of the different basins (red boxes; see also Table 3.1) and the tracks and intensities of the tropical cyclones in the IBTrACS dataset

Prior to extracting the storms, we first unify the reported wind speeds to 10-minute average sustained wind speeds (U10; in m/s). This is done because the definition of these reported wind speeds differ per tropical warning center: 4 centers use either 1-minute or 3-minute averaging periods (Knapp et al., 2010). These wind speeds are multiplied by a factor of 0.88 to convert them to U10 (Harper et al., 2008). Next, for each basin, we extract the storms at all consecutive time steps where the U10 is greater than 18 m/s, or where the TC has not reached an extratropical cyclone-classification in the IBTrACS dataset. We selected the 18 m/s-threshold to comply with the tropical storm-classification on the Saffir-Simpson hurricane scale (Simpson and Saffir, 1974). For convenience, we refer to this subset of storms as tropical cyclones (TCs) hereafter. We linearly interpolate all extracted data to 3-hourly values. The extracted tracks are shown in Figure 3.1; an overview of all the extracted elements of the IBTrACS dataset is listed in Figure 3.2 (blue column).

The modeling of synthetic tracks also requires information on environmental conditions such as monthly mean MSLP and sea-surface temperatures (SST). Therefore, in stage 1, we extract MSLP and SST fields from the European Centre for Medium-Range Weather Forecasting (ECMWF)’s fifth generation climate reanalysis dataset ERA-5 (Hersbach et al., 2019). The spatial and temporal resolution of this dataset is  $0.25^\circ \times 0.25^\circ$  and 1-hourly. For both variables, we calculate the monthly mean values during the TC seasons, as defined in Table 3.1.

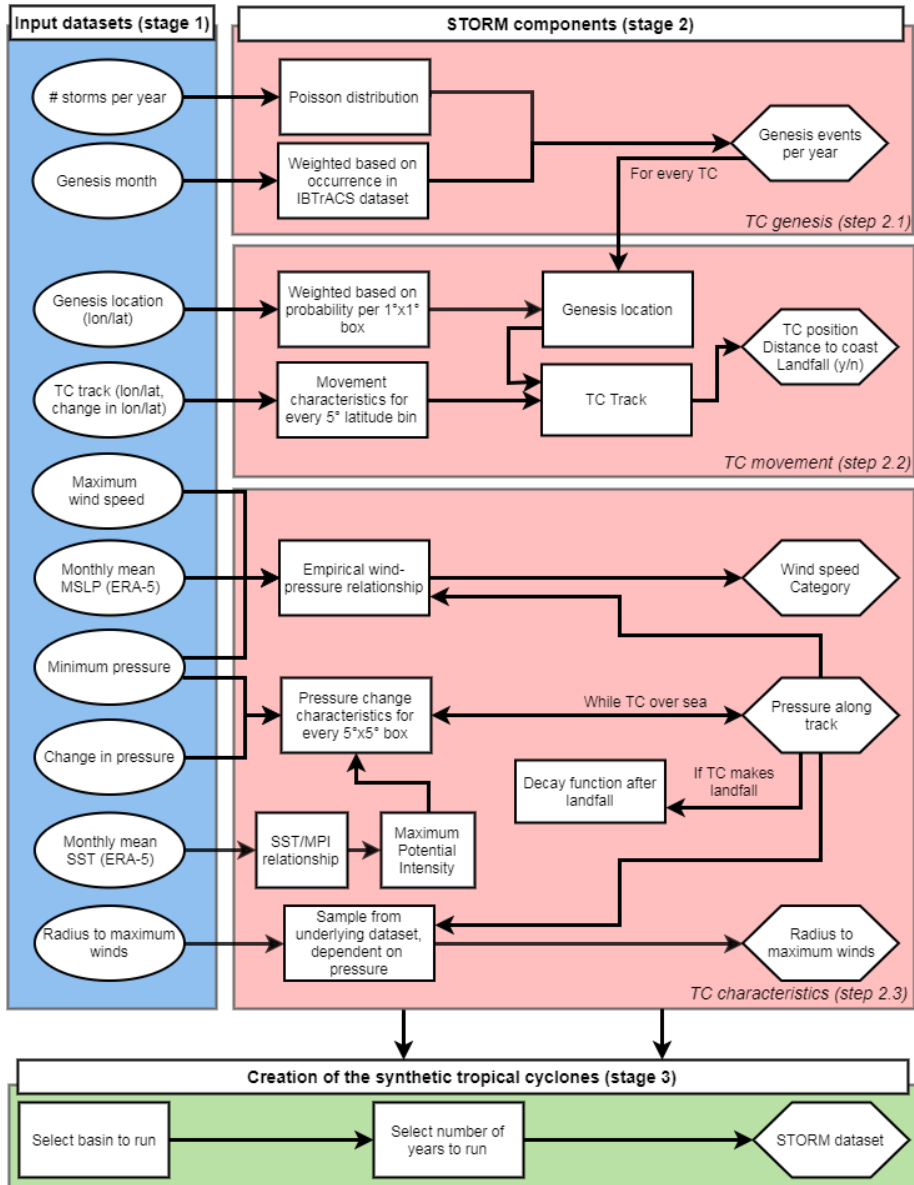


**Figure 3.2** Flowchart with the extracted IBTrACS tropical cyclone (TC) characteristics (stage 1; in blue), the STORM components (stage 2; in red), and the creation of the synthetic tropical cyclones (stage 3; in green). Round boxes represent input data, square boxes represent the methodological steps taken to process this input data, and hexagonal boxes represent the output data.

### 3.2.2 STORM components

In the second stage, the extracted TC tracks and characteristics from IBTrACS along with the environmental conditions from ERA-5 are used as input to our synthetic resampling algorithm called Synthetic Tropical cyclone geneRation Model (STORM). The STORM model follows three main steps that are visualized in Figure 3.2 in the red column. In step 2.1, STORM samples the number of genesis events, and their corresponding genesis month, for every simulated year. In step 2.2, for each of these genesis events, a genesis location is determined, and, by adding consecutive changes in longitude and latitude, a synthetic track is formed. In step 2.3, TC characteristics such as minimum pressure, maximum wind speed, and radius to maximum winds are assigned along each of these tracks. These three steps are described in detail below

#### *Tropical cyclone genesis*

In step 2.1, we simulate the number of genesis events per year using a Poisson distribution, where the Poisson parameter  $\lambda$  is defined as the average number of TC formations a year in the input dataset. For the IBTrACS dataset, values of  $\lambda$  amount to 14.5 for the EP, 10.8 for the NA, 2.0 for the NI, 12.3 for the SI, 9.3 for the SP, and 22.5 for the WP. For each genesis event, we randomly assign it a genesis month, weighted by the genesis months per basin observed in the IBTrACS dataset.

#### *Tropical cyclone movement*

In step 2.2, after determining the number of TC events in a year and assigning each a genesis month, we derive corresponding genesis locations for each TC event. This is based on weighted genesis locations per month from IBTrACS. For this, genesis locations are counted in  $5^\circ \times 5^\circ$  boxes and assigned to the box center point. Analogously, these points are interpolated (using cubic interpolation) to a  $1^\circ \times 1^\circ$  grid. The value these grid boxes is then used as weighting when sampling genesis locations. Lastly, the genesis location of the TC is sampled by selecting a random location (at  $0.1^\circ$  resolution) inside the  $1^\circ \times 1^\circ$  grid cell.

We then extract the changes ( $\Delta$ ) in the longitudinal ( $\xi$ ) and latitudinal ( $\varphi$ ) position of the TC eye at every time step  $t$  for every basin from IBTrACS. These  $\Delta\xi_t$  and  $\Delta\varphi_t$  are then grouped in  $5^\circ$  latitude sections per basin. For every bin, and using non-linear least squares, we fit a set of regression formulas following James and Mason (2005):

$$\Delta\xi_t = a_0 + a_1\Delta\xi_{t-1} \quad (3.1a)$$

$$\xi_t = \xi_{t-1} + \Delta\xi_t + \varepsilon_\xi, \quad \varepsilon_\xi \sim N(\mu_{\varepsilon_\xi}, \sigma_{\varepsilon_\xi}) \quad (3.2b)$$

$$\Delta\varphi_t = b_0 + b_1\Delta\varphi_{t-1} + \frac{b_2}{\varphi_t} \quad (3.2a)$$

$$\varphi_t = \varphi_{t-1} + \Delta\varphi_t + \varepsilon_\varphi, \quad \varepsilon_\varphi \sim N(\mu_{\varepsilon_\varphi}, \sigma_{\varepsilon_\varphi}) \quad (3.2b)$$

The residual term  $\varepsilon$  is drawn from a normal distribution of  $\varepsilon$ -values in IBTrACS. These  $\varepsilon$ -values are calculated as the difference between the fitted values of  $\Delta\xi_t$  and  $\Delta\varphi_t$  (Equations 3.1 and 3.2) and the actual values of  $\Delta\xi_t$  and  $\Delta\varphi_t$  in IBTrACS.



### *Tropical cyclone characteristics*

In step 2.3, TC characteristics such as minimum pressure, maximum wind speed, and radius to maximum winds are assigned along each of the TC tracks. First, the conversion between the maximum U10 and minimum MSLP in a TC is modeled using the empirical wind-pressure relationship (WPR) (Atkinson and Holliday, 1977; Harper, 2002):

$$V_t = a(P_{env} - P_t)^b \quad (3.3)$$

Where  $V_t$  and  $P_t$  are the maximum U10 and minimum MSLP at time step  $t$ , respectively. To estimate the variables  $a$  and  $b$  for every month in every basin, we extract maximum U10 and minimum MSLP from IBTrACS at every time step. The corresponding environmental pressure  $P_{env}$  is taken from the monthly mean MSLP fields from ERA-5. Equation 3.3 is then fitted to this data using non-linear least squares.

Second, we model the TC intensity along each synthetic track. A crucial feature in modeling this TC intensity is inhibiting TCs from growing too intense. In the STORM model, the TC intensity is constrained based on the maximum potential intensity (MPI) (Emanuel, 1987; Holland, 1997), which is a measure of the theoretical maximum TC intensity possible at a location, dependent on environmental factors and atmospheric conditions. This implementation also captures the tendency of TCs to start weakening when they approach the MPI, as well as the tendency of TCs to weaken faster at higher latitudes (James and Mason, 2005). The MPI is computed per month and per basin. First, we calculate the difference between the environmental pressure  $P_{env}$  and the TC's central pressure  $P$  from the IBTrACS data. This value is also known as the TC pressure drop ( $P_{env} - P$ , in hPa). Together with the pressure drop, we store the monthly mean SST (in °C) corresponding to the location of the TC eye. Subsequently, we group these monthly mean SSTs in 0.1°C bins together with their corresponding pressure drop values. We then fit the mean SST and maximum pressure drop per bin to Equation 3.4 (DeMaria and Kaplan, 1994) :

$$P_{env} - P = A + B e^{C(SST - T_0)}, \quad T_0 = 30.0^\circ\text{C} \quad (3.4)$$

The coefficients  $A$ ,  $B$  and  $C$  are estimated using non-linear least-squares. Using this formula, we can calculate the maximum pressure drop at every  $0.25^\circ \times 0.25^\circ$  SST grid point. In the final step, we subtract this maximum pressure drop from the  $P_{env}$  fields to derive the MPI. To inhibit unrealistically low MPI values, the MPI values are bounded by the lowest MPI value per basin and per month derived by Bister and Emanuel (2002).

After calculating the MPI at every  $0.25^\circ \times 0.25^\circ$  grid point for every month, we model changes in  $P$  using an autoregressive formula similar to James and Mason (2005) (Equation 3.5a). For this, we first extract changes in central pressure at every time

step ( $\Delta P_t$ ) from IBTrACS and fit this to Equation 3.5a. The values of the coefficients  $c_0$ ,  $c_1$  and  $c_2$  are deduced per month for every  $5^\circ \times 5^\circ$  box within a basin. The residual term  $\varepsilon_p$  is calculated as the difference between the fitted value of  $\Delta P_t$  (Equation 3.5a) and the actual value of  $\Delta P_t$  in IBTrACS.  $\Delta P_{.01}$  and  $\Delta P_{.99}$  represent the 1th- and 99th-percentile values of  $\Delta P_t$ , respectively.

$$\Delta P_t = c_0 + c_1 \Delta P_{t-1} + c_2 e^{-c_3 X}, \quad c_2 > 0, X = \max\{0, P_t - MPI\} \quad (3.5a)$$

$$\Delta P_{.01} \leq \Delta P_t + \varepsilon_p \leq \Delta P_{.99}, \varepsilon_p \sim N(\mu_{\varepsilon_p}, \sigma_{\varepsilon_p}) \quad (3.5b)$$

$$P_t = P_{t-1} + \Delta P_t + \varepsilon_p \quad (3.5c)$$

At genesis, we set  $U10 = 18$  m/s, and calculate the corresponding genesis pressure  $P_0$  using the WPR (Equation 3.3). The first-step change in  $P$ ,  $\Delta P_0$ , is drawn from a normal distribution fitted around the  $\Delta P_0$  in IBTrACS. To inhibit the synthetic TC to dissipate directly after TC genesis, we force the synthetic TC to intensify ( $\Delta P_0 < 0$ ) for the first 2 to 5 time steps. This amount of time steps is used to calibrate the average lifetime of a TC per basin.

A TC generally starts decaying after making landfall. In order to derive landfall (and distance to coast) for each time step of the TC in the STORM model, a land mask is created for each basin at  $0.1^\circ$  resolution using the Python 2.7 Basemap module. This module uses the GSHHS dataset (Wessel and Smith, 1996) for the coastline data (Whitaker, 2011). When the TC eye is over land for at least three time steps (totaling 9 hours), the decay in TC wind speed in the STORM model is modelled following Kaplan and DeMaria (1995), who assume that the TC intensity decreases as a function of the time and distance the TC has covered whilst being over land:

$$V(t_L) = V_b + (RV_0 - V_b)e^{-\alpha t} - C, \quad R = 0.9, V_b = 26.7 \text{ kt}, \alpha = 0.095 \text{ h}^{-1} \quad (3.6a)$$

$$C = m \left[ \ln \left( \frac{D}{D_0} \right) \right] + b, \quad D \gg 1, D_0 = 1 \quad (3.6b)$$

$$m = \tilde{c}_1 t_L (t_{0,L} - t_L), \tilde{c}_1 = 0.0109 \text{ kth}^{-2}, t_{0,L} = 150 \text{ h} \quad (3.6c)$$

$$b = d_1 t_L (t_{0,L} - t_L), d_1 = -0.0503 \text{ kth}^{-2} \quad (3.6d)$$

Here,  $V$  is the maximum sustained wind speed (in kt) of the TC at any time step  $t_L$  after landfall.  $V_0$  is the wind speed at landfall.  $D$  represents the distance from the landfall location (in km). When the TC moves back over ocean or if the TC is over land for less than three time steps (9 hours), changes in intensity are modeled according to the set of Equations 3.5.

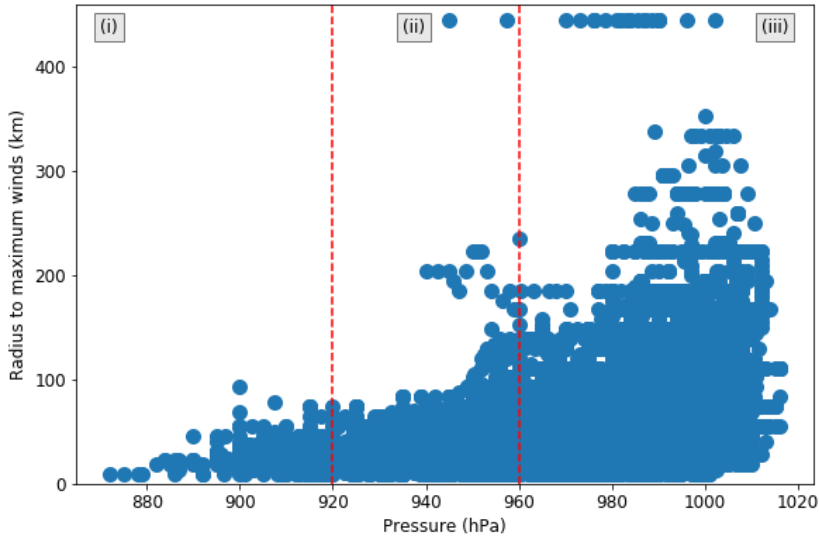


**Figure 3.3** Scatterplot of the tropical cyclone’s minimum pressure (in hPa) against the radius to maximum winds (in km). The data are taken from the IBTrACS dataset. The red lines indicate the selected subsections.

Finally we derive values for  $R_{\max}$ . From IBTrACS we extract the  $R_{\max}$  (in km) and  $P$  for every time step whenever available, and group this together in one global dataset. This is done because for some basins, such dataset would be too small to adequately draw a new set of values from. In Figure 3.3, we see that the relatively intense TCs tend to have a smaller  $R_{\max}$ , which is consistent with Shen (2006). For relatively weak TCs, we observe a much wider range of  $R_{\max}$  in IBTrACS. There is, however, no specific relationship between  $R_{\max}$  and  $P$ .

To calculate  $R_{\max}$  in STORM, we therefore split the dataset in three subsets:

- i)  $R_{\max}$  for  $P < 920$  hPa (relatively small radii);
- ii)  $R_{\max}$  for  $920 \text{ hPa} < P < 960$  hPa (transition), and
- iii)  $R_{\max}$  for  $P > 960$  hPa (wide range of  $R_{\max}$ ).

Sampling of  $R_{\max}$  at every time step can result in large sudden changes in  $R_{\max}$ . To avoid this, we sample values for  $R_{\max}$  at three distinct moments: at genesis ( $R_{\max_{\text{gen}}}$ ), at the moment of peak intensity (minimum  $P$ ) ( $R_{\max_{\text{peak}}}$ ), and at dissipation ( $R_{\max_{\text{dis}}}$ ).  $R_{\max}$  values for the intermediate time steps is interpolated from these values (see the set of Equations 3.7). If  $R_{\max_{\text{peak}}} < R_{\max_{\text{gen}}}$ , this meets the observations that  $R_{\max}$  tends to decrease as intensity increases, and we let  $R_{\max}$  linearly decrease between  $R_{\max_{\text{gen}}}$  and  $R_{\max_{\text{peak}}}$  (Equation 3.7a). If  $R_{\max_{\text{peak}}} \geq R_{\max_{\text{gen}}}$ , we set  $R_{\max_{\text{peak}}} = R_{\max_{\text{gen}}}$ , as otherwise the  $R_{\max}$  and TC intensity would both increase at the same time which is generally not the case (Shen, 2006). In a similar manner, we

let  $R_{max}$  linearly increase if  $R_{max_{dis}} > R_{max_{peak}}$ , and we set  $R_{max_{dis}} = R_{max_{peak}}$ , if  $R_{max_{dis}} \leq R_{max_{peak}}$ . This way, the  $R_{max}$  does not decrease while the TC is weakening, a property usually attributed to intensifying TCs (Shen, 2006). This results in the following set of equations:

$$R_{max}(t) = \frac{(R_{max_{peak}} - R_{max_{gen}}) * t}{t_{peak}} + R_{max_{gen}} \quad t \leq t_{int} \quad (3.7a)$$

$$R_{max}(t) = \frac{(R_{max_{dis}} - R_{max_{peak}}) * (t - t_{dis})}{t_{dis} - t_{peak}} + R_{max_{dis}} \quad t > t_{int} \quad (3.7b)$$

### 3.2.3 Creation of the synthetic tropical cyclones

In the third stage (Figure 3.2, green column), we create 10,000 years of synthetic TCs based on the present climate-conditions from the IBTrACS dataset. This is done by running the STORM model, consisting of a series of Python programs for each of the components described above, on the Lisa Computer Cluster ([www.surf.nl](http://www.surf.nl)). We split the 10,000 years in 10 separate runs of 1,000 years each, for each basin. Model runs of 1,000 years take on average a few hours to run, but specific run times depend on the selected basin. For time periods in the order of decades, it is also possible to run the STORM model on a regular desktop computer or laptop. Figure 3.4 shows the 38 years of TC activity in the input dataset IBTrACS (Figure 3.4a) versus the synthetic TC tracks from such a random 1,000 year STORM model run (Figure 3.4b). The STORM dataset provides a high global coverage of TCs compared to the original IBTrACS dataset, hereby ensuring that all coastal segments in TC-prone regions see multiple landfalling events in the STORM dataset. The STORM model outcomes are further discussed in Section 3.3.

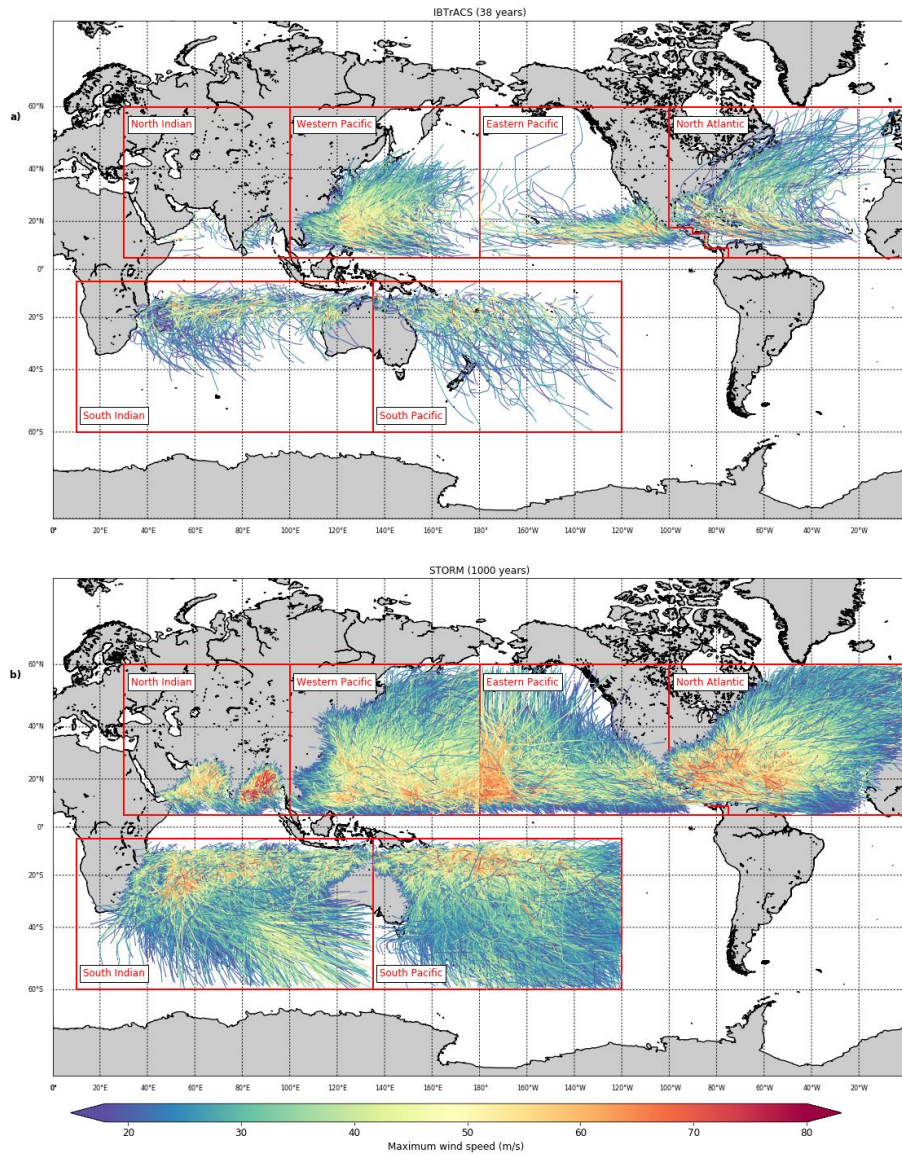


**Figure 3.4** Overview of tropical cyclone tracks in IBTrACS and the STORM dataset. The top panel represents 38 years (1980-2017) of tracks in the IBTrACS dataset (a), the bottom panel represents a random period of 1,000 years of tropical cyclone tracks in the STORM dataset (b). Colors indicate the maximum wind speed of the tropical cyclone.

### 3.3 Technical validation

#### 3.3.1 Tropical cyclone characteristics

To assess the performance of the STORM algorithm, we compare the TC characteristics from the IBTrACS dataset (which serve as input for STORM) to those in STORM. The resulting statistics are listed in Table 3.2 and plotted in Figure 3.5. Because the IBTrACS dataset serves as input for the generation of the STORM dataset, there exists a certain dependency between the two datasets. For this reason, we do not test for significant differences. Instead, we evaluate the performance of the STORM model by demonstrating that the mean values of various TC characteristics are within one standard deviation from those found in the IBTrACS dataset.

In general, there is good agreement between the two datasets. In most basins, the genesis pressure is lower in the STORM dataset compared to IBTrACS (Figure 3.5b). This is likely due to the combination of setting the genesis wind speed at 18 m/s and the use of the wind-pressure relationship (see Section 3.2) to convert this wind speed to a pressure-equivalent. Despite these differences, we see that for all basins, the average pressure along the track in the STORM dataset closely corresponds to the average pressure in the IBTrACS dataset (Figure 3.5c). More importantly, for the calculation of return periods of the peak intensity of a TC, we evaluate the minimum pressure and maximum wind speed along a track in both the STORM and IBTrACS datasets (Figure 3.5d and e). We observe that, for all basins, these values correspond closely to those found in IBTrACS. The largest deviations in wind speed between the two datasets are found for the South Indian and the Western Pacific, with an underestimation of 2.1 m/s and an overestimation of 1.9 m/s in maximum wind speed, respectively. This demonstrates that the STORM model, embedded with the MPI constraint and the wind-pressure relationship (see Section 3.23.2), succeeds in reproducing the intensities found in IBTrACS. For the calculation of TC risk along the global coastline, it is important that STORM reflects the landfall counts per basin as well as the landfall pressure (Figure 3.5f and g). In both datasets, we observe a relatively large standard deviation, indicating that there is a substantial year-to-year difference in landfall counts. This is also mirrored by STORM. However, on average, the average landfall counts of the two datasets fall within one standard deviation of each other.

Considering  $R_{max}$ , there is a small deviation between observed and modelled values (Figure 3.5h). The largest deviations are seen for the North Atlantic basin, with an observed average  $R_{max}$  of 69.7 km versus 50.3 km in the STORM model. This large deviation is likely caused by the sampling process used in the STORM model to calculate  $R_{max}$  (see Section 3.2). All observed  $R_{max}$  values were grouped in one global dataset, and from that dataset  $R_{max}$  values were drawn corresponding to the TCs intensity. This grouping was done to overcome data scarcity in the smaller basins. Although procedure seems to work well for the other basins (i.e. small deviations from

IBTrACS data), the larger Rmax values in the North Atlantic basin are diminished when grouping them together with the lower Rmax values in other basins. One way to overcome this would be to group and consecutively sample Rmax values per basin, however the Rmax dataset needs to be sufficiently large per basin.

Based on this comparison, we conclude that the STORM dataset performs sufficiently to be used for TC risk assessments and TC hazard analyses. Values of peak intensities and landfall pressures in the STORM dataset closely correspond to those found in the original IBTrACS data. The landfall counts also closely correspond to the ones in the IBTrACS dataset. However, there is a large year-to-year difference in annual landfall counts in both datasets, driving the large standard deviations found in both datasets.

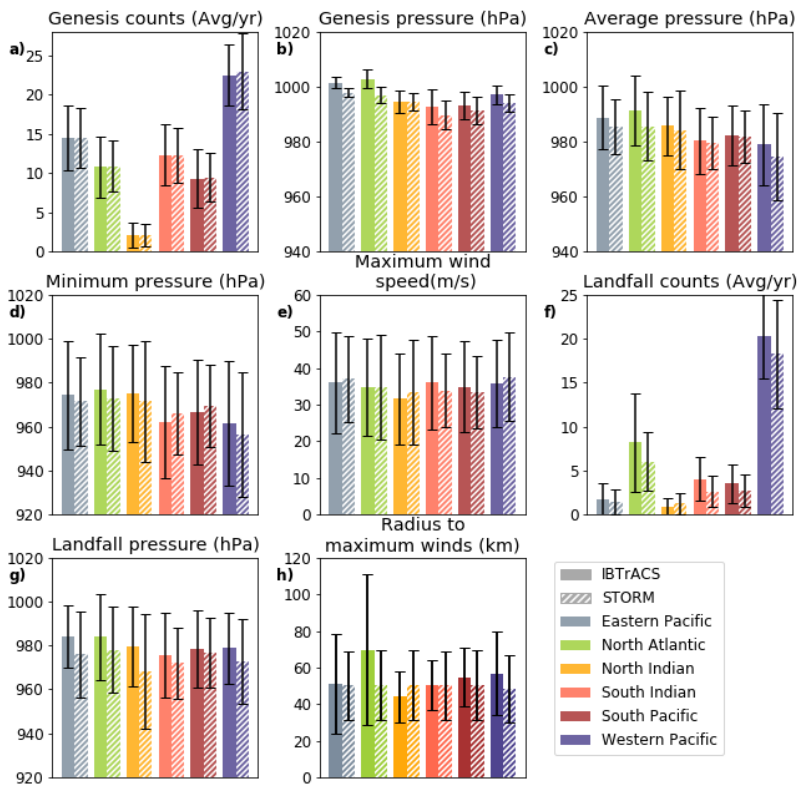


**Figure 3.5** Bar charts showing the mean value of each of the different tropical cyclone characteristics, as listed in Table 3.2. Black lines represent the error bar, given as one standard deviation from the mean. Each of the colors represents a different basin. Solid bars represent IBTrACS data, dashed bars represent STORM data

**Table 3.2** (next page) Distributions of tropical cyclone characteristics in the IBTrACS and STORM datasets per basin. The time period 1980-2017 is used for the IBTrACS dataset (38 years of data). For the STORM dataset, we calculated the mean and standard deviation (between brackets) for a random selection of 1,000 times 38 years of data. The n-value is given as the second number between brackets

		Eastern Pacific	North Atlantic	North Indian	South Indian	South Pacific	Western Pacific	Global
Genesis events (Avg/yr)	IBTrACS	14.5 (4.1; 38)	10.8 (3.9; 38)	2.0 (1.6; 38)	12.3 (3.9; 38)	9.3 (3.8; 38)	22.5 (3.9; 38)	71.3 (8.4; 38)
	STORM	14.5 (3.8; 38000)	10.9 (3.3; 38000)	2.1 (1.4; 38000)	12.3 (3.5; 38000)	9.4 (3.1; 38000)	23.0 (4.9; 38000)	72.3 (8.6; 38000)
Genesis pressure (hPa)	IBTrACS	1001.6 (2.0; 418)	1003.0 (3.5; 410)	994.5 (4.1; 75)	992.7 (6.3; 449)	993.3 (4.9; 351)	997.2 (3.4; 853)	997.4 (5.6; 2556)
	STORM	998.0 (1.8; 551839)	997.0 (2.9; 413801)	994.5 (3.1; 76107)	989.8 (5.4; 468103)	991.3 (5.1; 355663)	994.2 (3.1; 874377)	994.3 (4.7; 2739890)
Average pressure along track (hPa)	IBTrACS	988.9 (11.6; 424)	991.5 (12.8; 410)	985.8 (10.6; 75)	980.4 (12.1; 465)	982.3 (11.0; 352)	978.9 (14.9; 854)	983.5 (13.9; 2580)
	STORM	985.6 (10.1; 551839)	985.6 (12.6; 413801)	984.2 (14.5; 76107)	979.5 (9.6; 468103)	982.0 (9.5; 355663)	974.6 (16.0; 874377)	980.5 (13.5; 2739890)
Minimum pressure along track (hPa)	IBTrACS	974.3 (24.6; 424)	977.0 (25.3; 410)	975.1 (22.0; 75)	962.1 (25.6; 465)	966.6 (24.0; 352)	961.6 (28.4; 854)	967.3 (26.8; 2580)
	STORM	971.5 (20.2; 551839)	972.7 (24.0; 413801)	971.5 (27.8; 76107)	966.0 (18.7; 468103)	969.4 (18.6; 355663)	956.4 (28.4; 874377)	965.6 (24.4; 2739890)
Maximum wind speed along track (m/s)	IBTrACS	36.0 (13.8; 424)	34.8 (13.4; 410)	31.6 (12.4; 75)	36.0 (12.9; 465)	34.9 (12.5; 352)	35.7 (12.0; 854)	35.4 (12.8; 2580)
	STORM	37.0 (11.9; 551839)	34.7 (14.3; 413801)	33.4 (14.3; 76107)	33.9 (10.2; 468103)	33.4 (9.9; 355663)	37.6 (12.1; 874377)	35.7 (12.1; 2739890)
Total landfall counts (Avg/yr)	IBTrACS	1.7 (1.8; 38)	8.2 (5.6; 38)	0.8 (1.0; 38)	4.0 (2.5; 38)	3.5 (2.2; 38)	20.3 (4.8; 38)	38.6 (8.1; 38)
	STORM	1.4 (1.4; 38000)	6.0 (3.3; 38000)	1.2 (1.2; 38000)	2.6 (1.8; 38000)	2.7 (1.9; 38000)	18.3 (6.2; 38000)	32.2 (7.7; 38000)
Landfall pressure (hPa)	IBTrACS	984.1 (14.3; 64)	984.0 (19.7; 312)	979.7 (18.2; 32)	975.7 (19.4; 153)	978.6 (17.5; 134)	979.0 (16.2; 772)	979.9 (17.6; 1467)
	STORM	976.0 (19.7; 54247)	978.1 (19.5; 227302)	968.2 (26.3; 44041)	972.2 (16.2; 99244)	977.0 (15.9; 101171)	972.8 (19.3; 874377)	974.1 (19.3; 1221083)
Radius to maximum winds (km)	IBTrACS	51.1 (27.0; 218)	69.7 (41.4; 133)	43.9 (41.2; 36)	50.4 (13.7; 105)	54.6 (16.1; 49)	56.7 (22.9; 184)	55.7 (27.9; 725)
	STORM	50.2 (18.9; 551839)	50.3 (19.0; 413801)	50.6 (19.2; 76107)	50.2 (18.7; 468103)	50.4 (19.0; 355663)	48.5 (18.4; 874377)	49.7 (18.8; 2739890)



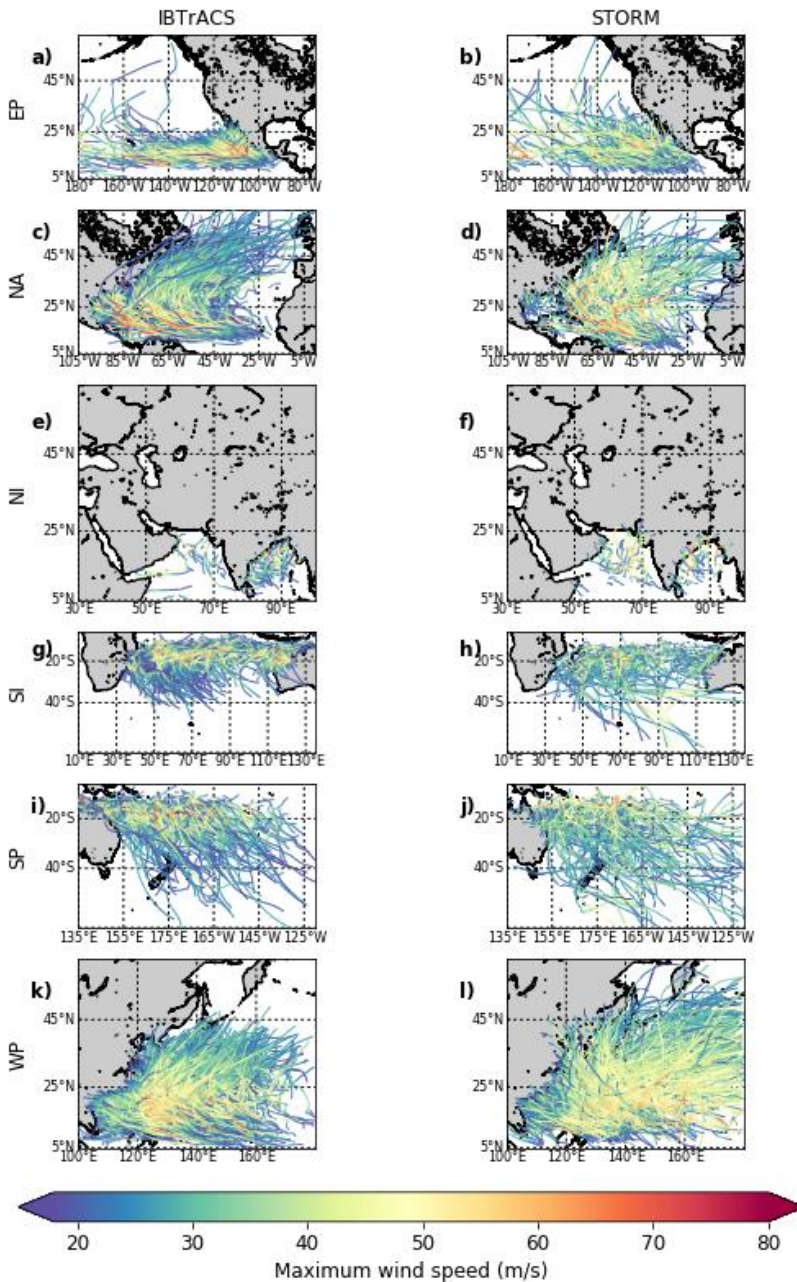


**Figure 3.6** Overview of 38 years of tropical cyclone tracks in the IBTrACS and STORM dataset per basin. The left column represent 38 years (1980-2017) of tropical cyclone tracks in the IBTrACS dataset, the right column represents a random 38-year period in the STORM dataset. Colors indicate the maximum wind speed of the tropical cyclone.

### 3.3.2 Spatial distribution of tropical cyclone tracks

Figure 3.6 shows the spatial distribution of the 38 years of TC tracks in the IBTrACS dataset (Figure 3.6a) against a random selection of 38 years from the STORM dataset (Figure 3.6b), per basin. In general, the location of peak intensity is captured well in the STORM dataset. These locations are more distinguishable when considering the 1,000 years of synthetic TC tracks in Figure 3.4b. In Figure 3.4b, we notice that these locations of peak intensity closely correspond with regions of highest SST per basin, such as the Caribbean Sea and the Gulf of Mexico in the North Atlantic or the Bay of Bengal in the North Indian. In the latter case, however, the intense maximum wind speeds are around 80 m/s in the 1,000-year dataset. These high wind speeds are the result of low MPIs in this basin, driven by high SSTs (see Section 3.2). These low MPIs, in turn, drive TC intensifications. The high wind speeds, however, do not point towards a significant overestimation of maximum wind speeds in this basin, as the average maximum wind speed along the track (see Table 3.2 and Figure 3.5) closely corresponds to the ones found in the IBTrACS dataset.

In addition, Figure 3.6 shows that the general patterns of TC tracks in the STORM dataset closely corresponds to those in the IBTrACS dataset. However, as the STORM model does not distinguish between tropical and extratropical systems, those longer-lived TCs in e.g. the South Indian (Figure 3.6h) or the Western Pacific (Figure 3.6l) are likely of extratropical nature once they reach higher latitudes, and should therefore be omitted from any TC-related analysis at such latitudes.

From Figure 3.4 and Figure 3.6, we can also observe the influence of basin boundary selection. We selected the basin boundaries such that they comply with the basin boundaries used in the IBTrACS dataset (see Section 3.2). The effect of the boundary selection is most prominent in the northern pacific basins (Western Pacific and Eastern Pacific): we observe that on the west side of the Eastern Pacific (between 180°W and 160°W; see Figure 3.6b), TCs tend to grow more intense while moving westward. However they are cut off once they surpass 180°W. As there is little landmass in these regions, such TCs do not affect TC risk assessments, and as such we decided to leave the basin boundaries as is.

## 3.4 Usage notes

We have written the STORM algorithm in a modular and flexible way, so that it could be used to generate a large number of years of TC activity using any meteorological dataset as the input dataset. The resulting dataset with 10,000 years of TC activity can be used by anyone interested in researching TCs and TC risk over the open ocean and in coastal areas. Different aspects of TC hazards can be studied with this dataset, including wind and storm surge hazards. To this end, this dataset is applicable in various fields of study, including coastal modeling, flood risk assessments, and wind damage assessments. Because of its global coverage and the large number of TCs, there are also enough TCs to perform a risk assessment in regions rarely hit by TCs,

such as small islands. The STORM dataset is also particularly beneficial for the calculation of TC wind speed return periods, as is demonstrated in Chapter 4.

Here we have used IBTrACS and ERA-5 as input datasets for the STORM model, but one could also use, for example, high resolution global climate models. Such meteorological dataset should be a realistic representation of TC characteristics such as forward speed and direction, U10 and MSLP fields, and the radius to maximum winds. In addition, realistic monthly mean MSLP and SST fields are necessary for the modeling of environmental effects.

It is, however, important to note that the presented STORM dataset is based on the average climate conditions of the last 38 years and does not capture (multi)-decadal variability on longer time scales. In addition, the STORM model statistically resamples the same climate conditions as the input dataset. To this end, the STORM dataset as presented here cannot be used to assess climate change impacts over longer time scales. We recommend end-users interested in modeling synthetic TCs under future climate scenarios to either (i) re-run the STORM model with a future climate-dataset; or (ii) to use such dataset to estimate changes in TC characteristics under climate change compared to present climate, and to add this difference to a present climate-dataset such as IBTrACS (the delta method). We plan to do this in future work (see Chapter 5).

## Acknowledgments

We thank SURFsara ([www.surf.nl](http://www.surf.nl)) for the support in using the Lisa Computer Cluster. NB and JCJHA are funded by a VICI grant from the Netherlands Organization for Scientific Research (NWO) (Grant Number 453-13-006). IDH was funded by NERC Grant CompFlood (Grant Number NE/S003150/1). SM received funding from the research programme MOSAIC with project number ASDI.2018.036, which is financed by the Dutch Research Council (NWO).





## 4 Low-probability tropical cyclone events in the present climate

**This chapter is published as**

Bloemendaal, N., de Moel, H., Muis, S., Haigh, I.D. & Aerts, J.C.J.H. Estimation of global tropical cyclone wind speed probabilities using the STORM dataset. *Nature Scientific Data* **7**, 377 (2020). <https://doi.org/10.1038/s41597-020-00720-x>

## Abstract

Tropical cyclones (TC) are one of the deadliest and costliest natural disasters. To mitigate the impact of such disasters, it is essential to know extreme exceedance probabilities, also known as return periods, of TC hazards. In this chapter, we demonstrate the use of the STORM dataset, containing synthetic TCs equivalent of 10,000 years under present-day climate conditions, for the calculation of TC wind speed return periods. The temporal length of the STORM dataset allows us to empirically calculate return periods up to 10,000 years without fitting an extreme value distribution. We show that fitting a distribution typically results in higher wind speeds compared to their empirically derived counterparts, especially for return periods exceeding 100-yr. By applying a parametric wind model to the TC tracks, we derive return periods at 10 km resolution in TC-prone regions. The return periods are validated against observations and previous studies, and show a good agreement. The accompanying global-scale wind speed return period dataset is publicly available and can be used for high-resolution TC risk assessments.

## 4.1 Introduction

Tropical cyclones (TCs) are amongst the deadliest and costliest natural disasters, affecting people, economies and the environment in coastal areas around the globe. In 2019, Cyclone Idai caused over 1,000 fatalities and displacing 3 million people upon landfall in Mozambique (The Guardian, 2019). In 2017, Hurricanes Harvey, Irma and Maria entered the top-5 costliest Atlantic hurricanes ever, with combined losses estimated at US\$ 220 billion (NOAA, 2020a). To minimize future loss of life and property, it is crucial to perform accurate TC risk assessments and identify high-risk locations so that appropriate protection measures can be designed.

Wind is one of the major hazards associated with TCs and can do substantial damage to housing, infrastructure and ecosystems both in coastal regions and far inland (Kruk et al., 2010). Moreover, wind correlates with the intensity of other TC-induced hazards, such as storm surges, waves and precipitation (Bloemendaal et al., 2019; Cervený and Newman, 2000; Phadke et al., 2003). To enhance our understanding of TC risk at the global scale, it is therefore essential to analyze wind speed probabilities in coastal zones. Risk is commonly calculated as the integrated value of expected damages over all exceedance probabilities –the inverse of which being return periods (RPs) (Ward et al., 2011). As such, accurately calculating risk requires information on a wide range of RPs. Simpson and Lawrence (1971) empirically estimated TC RPs along 80 km-long coastal segments of the US coastline based on historical TCs. However, RPs could not be calculated for those coastal segments that were not hit by a TC in the 85 years of observations. This shows that, due to the short length of the observational record, data often needs to be aggregated over larger spatial regions to perform a RP analysis, hereby omitting the spatial heterogeneity. Moreover, estimating RPs comes with large uncertainties, especially for RPs exceeding the length of the observational record. To overcome these limitations, the methodology

of synthetic TC track generation has been developed over the past few decades (Bloemendaal et al., 2020c; Emanuel et al., 2006; James and Mason, 2005; Vickery et al., 2000). In this approach, TCs, extracted from either historical data (Emanuel et al., 2006; Haigh et al., 2014) or climate model simulations (Lin et al., 2012), are statistically resampled and modeled to generate synthetic, but realistic, TCs. Using a Monte Carlo approach, this procedure is repeated recurrently to construct a TC dataset having the same statistical characteristics as the input dataset, but spanning hundreds to thousands of years.

Using synthetic data enables the analysis of higher RPs and at higher spatial resolution than previously possible. In an accompanying paper we have presented the global synthetic model STORM (Synthetic Tropical cyclOne geneRation Model) (Bloemendaal et al., 2020c). The STORM dataset spans 10,000 years of global TC activity under present-day climate conditions, based on observed TC tracks. Here, we demonstrate usage of the STORM dataset by creating wind speed RPs at three different spatial scales: i) basin level; ii) within 100 km for 18 selected coastal cities and 63 islands; iii) at 10 km resolution in TC-prone regions. This dataset is unique in presenting (high) RPs at a global scale for all TC-prone regions. More importantly, it represents an important step forward to calculating global TC damages and risk.

## 4.2 Methods

Our approach is based on estimating the empirical RPs on basis of the synthetic TCs derived from the STORM dataset (Bloemendaal et al., 2020c). This dataset is created using historical data from the International Best Track Archive for Climate Stewardship (IBTRACS; Knapp et al., 2010) as input dataset for the Synthetic Tropical cyclOne geneRation Model (STORM). The development of this dataset has been described in detail in Bloemendaal et al. (2020c). Here, we provide a brief description of the STORM dataset, but for more details on the methodology and validation we direct readers to Bloemendaal et al. (2020c).

### 4.2.1 Data

The STORM dataset, a global synthetic dataset comprised of 10,000 years of synthetic TCs under present-climate conditions, is used for the calculation of the return periods (RPs). The STORM dataset was generated using STORM. This model takes the following IBTrACS data as input: the latitudinal and longitudinal position of the TC, maximum 10-meter 10-minute average sustained wind speeds (max U10), mean sea-level pressure (MSLP), and the size of the TC eye (Radius to maximum winds; Rmax). Averaged environmental conditions are modeled using monthly-mean sea-surface temperatures (SST) and MSLP fields from ERA5 (Hersbach and Dee, 2016). From this, autoregressive formulas model consecutive changes in the longitudinal/latitudinal position of the TC (in  $^{\circ}$ ), the minimum pressure (in hPa) and the maximum wind speed (in m/s) at every time step during a TC's lifetime. In addition, STORM also simulates the size of the TC eye, represented via the radius to



maximum winds (in km). STORM is validated in Bloemendaal et al. (2020c). Results show that STORM preserves the TC statistics as found in the IBTrACS input dataset, which indicates a good model performance. The average number of both genesis and landfalling events in the STORM dataset, as well as landfall intensity was found to closely correspond (within one standard deviation) to those in the IBTrACS dataset. The largest deviations in max U10 along a TC track were found to be approximately 2 m/s in the STORM dataset compared to the IBTrACS dataset.

## 4.2.2 Estimation of return periods and 2D wind field parameterization

Using the 10,000 years of TC activity in the STORM dataset, we empirically calculate the max U10 for different RPs using Weibull's plotting formula (Weibull, 1939), see Equation 4.1. The Weibull plotting formula has been demonstrated to be the best performing empirical formula for the estimation of return periods (Makkonen, 2006).

$$P_{exc}(\vec{v}) = \frac{i}{n+1} \cdot \frac{n}{m} \quad (4.1a)$$

$$T(\vec{v}) = 1/P_{exc}(\vec{v}) \quad (4.1b)$$

Here,  $P_{exc}(\vec{v})$  represents the exceedance probability  $P_{exc}$  for a given maximum wind speed  $\vec{v}$  at rank  $i$ .  $n$  is the total number of events in the set, and  $m$  the total length of the dataset (in years; here,  $m = 10,000$ ). The return period  $T(\vec{v})$  is then given as the inverse of  $P_{exc}$ . Because the STORM dataset represents 10,000 years of TC activity, we empirically calculate RPs up to 10,000 years.

To demonstrate the performance of the empirical distribution compared to extreme value distributions (see Section 0), we fit five continuous extreme value distributions to the STORM dataset. These distributions include the Generalized Extreme Value, Exponential, Gumbel, Weibull, and Pareto distribution. Estimation of the optimal parameters for each of the distributions was done using Python's *lmoments* package (Python Software Foundation, 2020) at 0.1-year intervals, up to 1,000 years. For the estimations of RPs at basin scale and within a 100 km radius, we apply Equation 4.1 directly to max U10 values in the STORM dataset. However, for assessing RPs of wind speeds at 10 km resolution, we need to convert the TC tracks, that includes the longitudinal/latitudinal position of the TC eye, maximum wind speed, and radius to maximum winds, to 2D-wind fields. For this, we follow the parametric approach of Holland (1980). We follow the same approach as was suggested by Lin and Chavas (2012) and Muis et al. (2019). The Holland B parameter is calculated following Lin and Chavas (2012). The surface wind is converted to a gradient wind using a wind speed reduction factor of 1/0.85 (Powell et al., 2005). The asymmetry in the surface wind is accounted for by adding the surface background winds to the wind field (Lin

and Chavas, 2012), which is approximated by the translational speed of the TC. We compute the 2D-wind field using a mesh with 10 km resolution. To optimize computational costs, this calculation is done in parallel using a separate mesh per basin. For each synthetic TC, we store the max U10 at each grid cell whenever max U10  $\geq$  20 m/s. Lastly, we apply Equation 4.1 to the max U10 values at every grid cell to estimate the RPs.

### 4.2.3 Basin definitions

The basin definitions used in this chapter are adapted from Bloemendaal et al. (2020c), see Table 4.1.

**Table 4.1** Basin definitions, as adapted from Bloemendaal et al. (2020c)

Basin name	Basin domain
Eastern Pacific	5°-60°N 180°-coastline of North America on the North Atlantic
North Atlantic	5°-60°N coastline of North America on the Eastern Pacific - 360°
North Indian	5°-60°N 30°-100°E
South Indian	5-60°S 10°-135°E
South Pacific	5-60°S 135°-240°E
Western Pacific	5-60°N 100°-180°E

### 4.2.4 The Saffir-Simpson Scale

We use the Saffir-Simpson Scale (Simpson and Saffir, 1974) as an additional metric to communicate about wind speeds. The categorization on this scale, however, is done using 1-minute average sustained wind speeds, whereas the STORM wind data is given as a 10-minute average value. For this reason, we convert the 1-minute threshold values on the Saffir-Simpson scale to a 10-minute equivalent using a conversion factor of 0.88 (Harper et al., 2008), see Table 4.2.

**Table 4.2** Tropical cyclone wind speed categorization on the Saffir-Simpson Scale. Conversion between 1-minute average sustained wind speeds in knots and in m/s is done using a factor of 0.5144, conversion between 1-minute and 10-minute average sustained wind speeds (in m/s) is done using a conversion factor of 0.88 (Harper et al., 2008)

Category	Wind speed threshold	
	1-minute average sustained	10-minute average sustained
Category 1	64-82 kt 32.9-42.2 m/s	29.0-37.1 m/s
Category 2	83-95 kt 42.7-48.9 m/s	37.6-43.0 m/s
Category 3	96-112 kt 49.3-57.6 m/s	43.4-50.7 m/s
Category 4	113-136 kt 58.1-70 m/s	51.1-61.6 m/s
Category 5	$\geq$ 137 kt, $\geq$ 70 m/s	$\geq$ 61.6 m/s

## 4.3 Results and discussion

### 4.3.1 Deriving return periods from the STORM dataset

Calculating RPs of (extreme) wind speeds in the STORM dataset can be done either empirically or statistically. When using an empirical approach, RPs are directly calculated from wind speeds ranked in order of magnitude using formulas like Hazen's or Weibull's plotting formula (Hazen, 1930; Weibull, 1939). A benefit of this approach is that no specific shape of the RP-curve is assumed; RPs are calculated per given wind speed without interpolation or smoothing of the data. However, the highest RP is limited by the temporal length of the data as this method does not allow for extrapolation beyond this timespan. TC risk assessments typically require information on extreme events that have not been observed yet. Therefore RPs are often determined by fitting extreme value (EV) distributions (Kotz and Nadarajah, 2000) to historical data. This way any RP can be estimated, even those beyond the range of observations. To ensure there is enough data for a good fit, this approach is generally carried out in ocean basins or relatively large coastal sections. Such fitted RPs are strongly influenced by the selected EV distribution, especially for higher RPs (Esteves, 2013). Furthermore, short records have large uncertainties, and typically multi-decadal records are needed for reliable estimates of the tail (high RPs) (Wahl et al., 2017).

Here we compare these two approaches to estimate basin-scale RPs using the synthetic TCs from STORM. We apply Weibull's plotting formula to the maximum 10-meter 10-minute average sustained wind speeds (max U10) in the full STORM dataset (10,000 years). We use max U10 because this is globally the most commonly reported value of wind speeds (Knapp et al., 2010), but other averaging periods can easily be obtained using conversion factors (Harper et al., 2008). Next, we fit five EV distributions (the generalized extreme value, exponential, Gumbel, Weibull and Pareto distribution) to 1,000 random realizations of 38 years of data sampled from the STORM dataset. This 38-year length was chosen as the STORM dataset was created using 38 years of historical data (1980-2017) from the International Best Track dataset for Climate Stewardship (IBTrACS; Knapp et al., 2010).

At basin-level, the empirically derived STORM-RPs agree with the observed RPs (Figure 4.1). In the North Atlantic, North Indian, and Western Pacific, STORM-RPs compare well with observations. In the Eastern Pacific and the Southern Hemisphere basins, max U10 in STORM are lower than the highest observed counterparts. Additionally, for four out of five EV distributions the max U10 values are substantially higher than the empirically derived values, particularly at RPs exceeding 100-yr. Compared to the empirical curve, the worst-performing EV distributions are the exponential, generalized extreme value (GEV) and Gumbel distributions, which deviate from the empirical curve above the 10-yr RP. The EV distributions cannot capture the asymptotic behavior of the TC intensity, caused by environmental constraints such as the Maximum Potential Intensity (Emanuel, 1987; Holland, 1997).

Consequently, at high RPs, max U10 from EV distributions are higher than their empirically derived counterparts, with a maximum difference of 117 m/s for the GEV in the North Atlantic at the 1,000-yr RP. For the North Indian, we observe a kink in the empirical curve around the 20-yr RP: this is likely caused by an absence of certain max U10 in the dataset, which are then excluded from the RP calculation. This absence is driven by a limited spatial distribution of sea-surface temperatures (SSTs), causing a more frequent occurrence of higher max U10. Figure 4.1 shows that the Pareto distribution is the best-performing EV distribution compared to the empirical approach. However, for the North Indian, also the Pareto distribution shows substantially higher RPs compared to the empirical curve. Overall, the empirical probabilities of the observations are well in line with the estimates from the STORM dataset, and are considerably lower than using EV fits at RPs exceeding 100-yr.

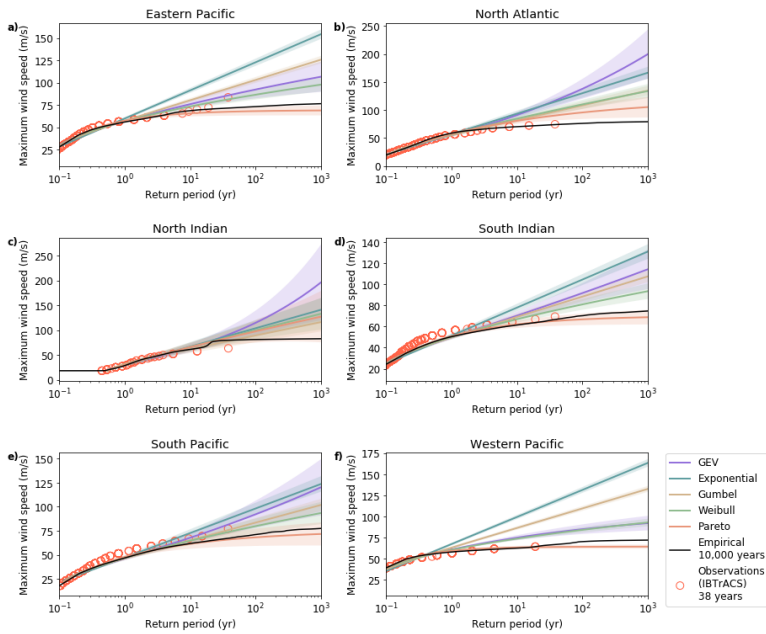


**Figure 4.1** Comparison of the wind speed return periods based on fitting five different extreme value distributions to 1,000 random realizations of 38 years and applying an empirical distribution (the Weibull plotting formula) to the full 10,000 years of data. Data is aggregated at basin level for each of the 6 ocean basins (a-f). The extreme value distributions are the generalized extreme value distribution (purple), the exponential distribution (blue), the Gumbel distribution (also known as the Generalized Extreme Value Distribution Type-I; yellow), the Weibull distribution (also known as the Generalized Extreme Value Distribution Type-II; green), and the Pareto distribution (red). Shaded areas indicate the 95% -confidence interval based on the bootstrap with 1,000 realizations. Empirically derived return periods from observations (IBTrACS) are given as red scatter points. See Section 4.2 for a full description of the basin domains

### 4.3.2 Tropical cyclone return periods for coastal cities

Besides basin-scale RPs, we derive RPs for specific coastal locations using a 100 km radius to capture those TCs that have a substantial impact. We demonstrate this here for 18 coastal cities, but a similar dataset is available for 63 islands (Bloemendaal et al., 2020b). The RP-curves (subplots in Figure 4.2; see Table 4.3) show that probabilities of a TC event occurring within 100 km differ strongly per city. Cities that are not regularly hit by a TC include San Diego (USA), Mumbai (India), and Muscat (Oman) with RPs for a Category-1 exceeding 100-yr. These relatively high RPs are driven by multiple TC characteristics. Firstly, TCs are generally deflected from San Diego and Mumbai (Sobel et al., 2019) and instead move out over the open ocean. This is caused by TCs being embedded within the prevailing easterly (westward) flow at these latitudes. Secondly, TCs dissipate when they make landfall. As Muscat is located in the relatively narrow Gulf of Oman, most TCs in this region will likely have passed land upon approaching Muscat. Lastly, both Mumbai and Muscat lie in the North Indian, where approximately 2 TCs form per year (Bloemendaal et al., 2020c), hereby further decreasing the chances of being hit by a TC in any given year. Of the cities considered here, Taipei (Taiwan) and Tokyo (Japan) experience TCs most often, with RPs for a Category-1 lower than 4-yr. Both cities are located in the Western Pacific, the most active basin with 22.5 TC formations

**Table 4.3** Return periods (yr) of Category 1-5 wind speeds occurring within 100 km for 18 coastal cities. Return periods are derived from the STORM dataset. Wind speeds are given as 10-meter 10-minute sustained average values, see Table 4.2 for more information.

City	Country	Cat 1 (29 m/s)	Cat 2 (37.6 m/s)	Cat 3 (43.4 m/s)	Cat 4 (51.1 m/s)	Cat 5 (61.6 m/s)
Honolulu	Hawaii (USA)	11	17	25	54	442
San Diego	USA	247	1870	5034	>10,000	>10,000
Acapulco	Mexico	22	35	62	156	1684
San Juan	Puerto Rico	5	8	12	22	131
Houston	USA	23	52	92	205	1230
Miami	USA	12	20	28	48	155
Mumbai	India	101	140	199	285	2403
Chittagong	Bangladesh	30	44	59	83	131
Muscat	Oman	151	235	315	768	>10,000
Beira	Mozambique	64	238	1179	6817	>10,000
Saint-Denis	Réunion	6	13	28	87	347
Toamasina	Madagascar	10	19	31	101	616
Brisbane	Australia	28	111	466	9013	>10,000
Nadi	Fiji	7	14	27	87	1093
Noumea	New-Caledonia	8	20	51	263	4755
Ho Chi Minh	Vietnam	33	225	970	9673	>10,000
Taipei	Taiwan	2	4	8	36	2200
Tokyo	Japan	4	7	23	556	>10,000

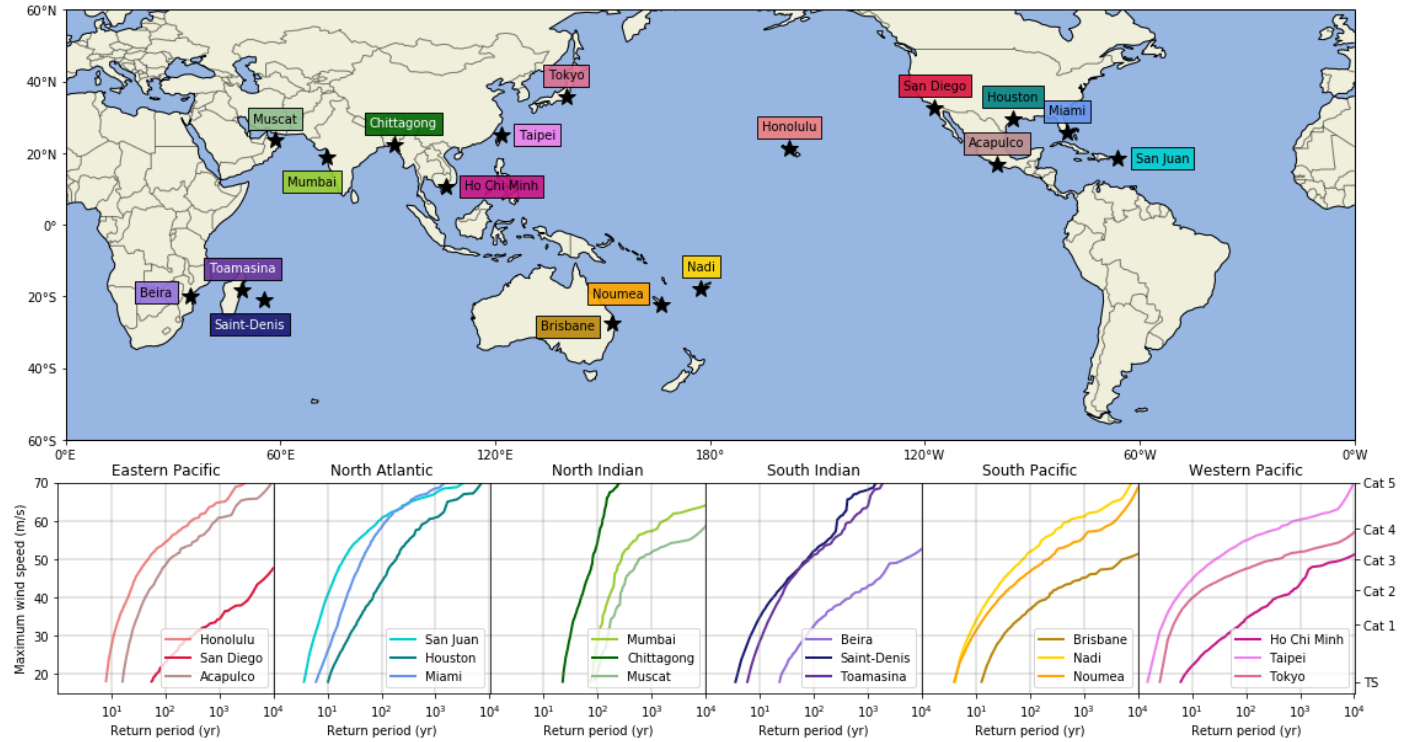


**Figure 4.2** Return periods of maximum 10-minute average wind speeds within a radius of 100 km for a selection of coastal cities. Color tones correspond to the different basins: North Atlantic (blue), Eastern Pacific (red), Western Pacific (pink), North Indian (green), South Indian (purple), and South Pacific (yellow). Graphs show the return period on the x-axis versus the corresponding maximum wind speed (in m/s) on the y-axis. Tropical Storm (TS) and Category-classifications are based on the Saffir-Simpson scale.

per year (Bloemendaal et al., 2020c). Of the cities considered, San Juan (Puerto Rico) and Chittagong (Bangladesh) are most often affected by strong TCs, with Category-5 TCs having a 131-yr RP for both cities. San Juan's central position in the tropical Atlantic Ocean combined with frequent Category-5 TC formations (approximately 1-in-6-years; see Figure 4.1) likely drives these relatively low RPs. Chittagong's relatively low RP is likely due to the high SSTs in the Bay of Bengal, enhancing TC intensification and thus generating strong TCs.

### 4.3.3 Spatial distribution of extreme wind speeds

Using STORM, we can also derive RPs at high (10 km) spatial resolution. While a single extreme event might be captured well in historical datasets (e.g. Hurricane Irma in IBTrACS), there are not enough events in such datasets to robustly calculate high RPs. To calculate max U10 at 10 km resolution, we fit a 2D-parametric wind model

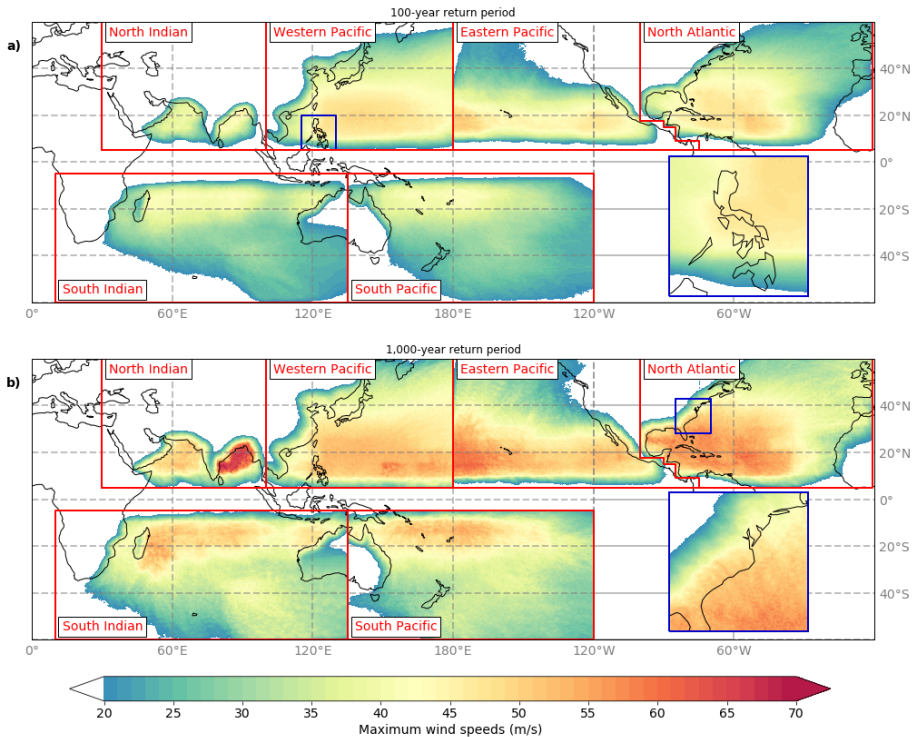


**Figure 4.3** Spatial distribution of 10-meter 10-minute sustained maximum wind speeds (m/s) at 10 km resolution, derived from applying a 2D-wind parametrization to the synthetic tropical cyclone tracks in STORM. The wind speeds are the average value of 1,000 random realizations of 10,000 years of data (sampled with replacement) and determining RPs using Weibull's plotting formula to each realization, performed at each coordinate at the 1-in-100-year (a) and 1-in-1,000 year (b) return period, respectively. The return period-analysis is carried out at the basin scale: as such, there is often no smooth transition of wind speed values at the basin boundaries. Inset figures show the distribution of wind speeds around the Philippines (a) and the United States East Coast (b) at the given return period.

to each synthetic TC (see Section 4.2.2). Note that RPs inherently depend on the spatial scale they are computed at. At basin-scale, multiple TCs form every year, each one potentially reaching a given max U10. At a high-resolution grid cell, a TC passage can be rare. Hence, for equal max U10, RPs are lower when computed at higher resolution.

Figure 4.3 shows that max U10 increases between the 100-yr and 1,000-yr RP level, with largest increases in the Bay of Bengal, the North Atlantic, and west of Hawaii in the Eastern Pacific, and less profound in the mid-latitudes and over land. There is distinct spatial variation within basins driven by the strong relationship between SSTs and TC activity. This is for instant evident in the Bay of Bengal, where SSTs (Hersbach et al., 2019) of approximately 29°C drive TC intensification, resulting locally in max U10 exceeding 65 m/s for a 1,000-yr RP. Aside from basin-scale variability in max U10, the two insets in Figure 4.3 display the variability in max U10 at smaller scales. Distinct differences in max U10 are visible around the Philippines (inset Figure 4.3a), with lower max U10 on the east side caused by the (westward) passage of TCs over the archipelago. Along the US coastline (inset Figure 4.3b), stronger TCs make landfall more frequently on the Florida-North Carolina coastline than around New York City (NYC). This is driven by two factors: (i) TCs generally move north-westward near the Florida-North Carolina regions (onshore direction), whereas TCs are deflected eastward near NYC (offshore direction); and (ii) SSTs are higher along the southern coastline, supporting intense TCs, whilst the lower SSTs around NYC drive a weakening of TCs. The apparent re-intensification of TCs near 40°S is partly caused by relatively high SSTs of 17-22°C. Another cause is that these mid-latitude regions are mostly dominated by extratropical cyclones, which follow a different intensification process than TCs. STORM, however, does not model the extratropical transition of TCs and as such may underestimate RPs in these regions. Another feature visible in predominantly the mid-latitudes is the dotted patterns (e.g. North of Hawaii, Figure 4.3). These patterns are caused by the passage of few TCs, combined with a higher translational speed at these latitudes. As we use 3-hourly intervals, the max U10 values appear as dots.

#### 4.3.4 Spatial distribution of return periods of tropical cyclones

Besides calculating max U10 for specific RPs, we can also reverse the procedure and compute the RP for given TC-categories. Figure 4.4 illustrates the RPs of a Category-1 (max U10  $\geq$  29 m/s) and a Category-3 TC (max U10  $\geq$  43.4 m/s) on the converted Saffir-Simpson Scale (Simpson and Saffir, 1974), see Section 4.2.4. There are large spatial variations, but for all basins RPs are lowest for a Category-1 or Category-3 event in the tropical regions. For large parts of the Western Pacific and the eastern part of the Eastern Pacific, Category-1 TCs have an approximate 2-yr RP. In the other basins, these RPs lie between 5 and 20-yr. Category-3 TCs, however, occur less



frequent, ranging between 10-yr RP for the Western Pacific to 90-yr RP for the North Indian.

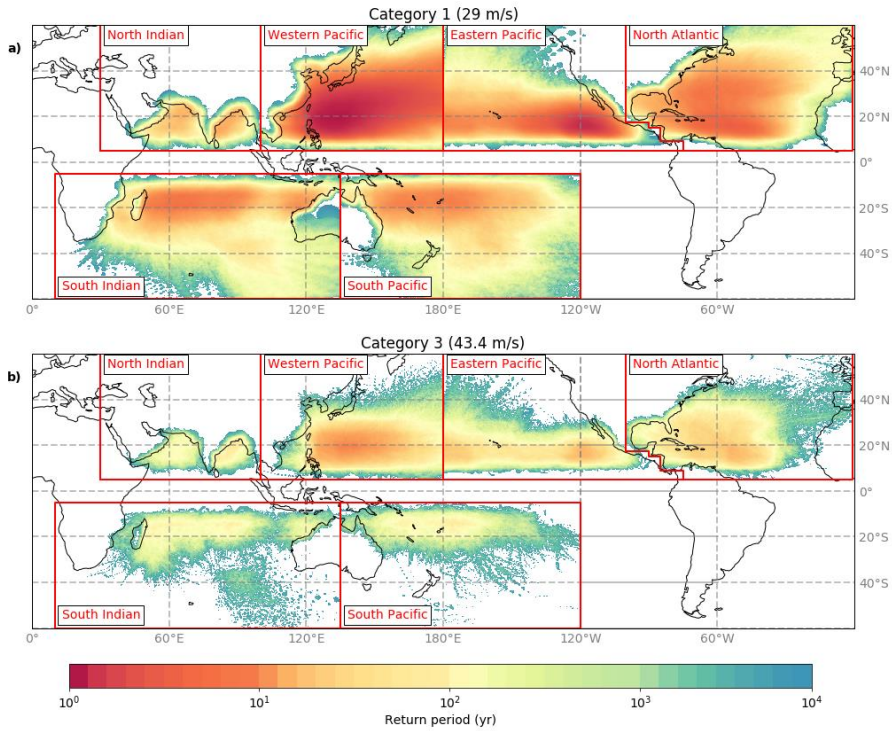


**Figure 4.4** Spatial distribution of return periods (yr) at 10 km resolution, derived from applying a 2D-wind parameterization to the synthetic tropical cyclone tracks in STORM. The return periods are the average value of 1,000 random realizations of 10,000 years of data (sampled with replacement) and determining RPs using Weibull's plotting formula to each realization at each coordinate at Category 1 (wind speeds  $\geq 29$  m/s) (a), and Category 3 tropical cyclone strength (wind speeds  $\geq 43.4$  m/s) (b), respectively.

### 4.3.5 Discussion

#### *Comparison to other synthetic datasets*

At basin-level, we have shown that the STORM-RPs compare well with observations (Figure 4.1). At local scale, however, data can be scarce. Additionally, the observational dataset used here only spans 38 years, making it unfit for RP analysis past this timespan. Hence, here we compare our results to other studies that derived RPs based on thousands of years of synthetic TC tracks. We first compare model outcomes at the local scale, after which we discuss global-scale patterns in RPs.

For 18 cases we compare max U10 for given RPs with STORM, and for Mumbai we compare the RPs for given categories (see Table 4.4). Sobel et al. (2019) reported a 49 to 97-yr RP for a Category-1 TC within 150 km from Mumbai, agreeing well with the STORM-RP of 66-yr. Similarly, they estimate Category-3 RPs around 500-yr,

while STORM-RPs are around 138-yr. For a Category-1 TC occurring in Mumbai, Sobel et al. (2019) list a 224 to 236-yr RP; compared to a STORM-RP of 95-yr. For the city itself, RPs vary between 3,000 to 10,000-yr, compared to 550-yr in STORM. STORM-RPs are predominantly lower than those in Sobel et al. (2019). Sobel et al. (2019), however, speculate that they underestimates the TC hazard. Further differences are likely driven by the use of different track modeling methods, wind field parameterization schemes (including different resolutions) and RP estimation techniques.

STORM performs well for given RPs: for 13 out of 18 cases, absolute differences between max U10 in STORM and other models lie within 5 m/s. The largest difference is 18 m/s for Darwin, Australia (Cook and Nicholls, 2009). This relatively large difference (-38.3%) is likely caused by the fact that Darwin is located near the South Indian-South Pacific basin border, and is hit by TCs originating in both basins. STORM, however, models TCs per basin, cutting off South Pacific TCs at the basin boundary. Townsville and Port Hedland are located further away from the basin boundary and max U10 are in better agreement. Additionally, we observe relative differences of -35.9% and -25.1% for the Federated States of Micronesia (FSM) and Palau, respectively. In STORM, the lower basin boundary in the Western Pacific is set at 5°N. As these island countries lie at around 7°N, and modelled TCs generally deflect away from the Equator, this means most TCs in STORM pass north of the island countries. Conversely, the AIR Tropical Cyclone Model (Commonwealth of Australia, 2013) models the Pacific region as a whole, and thus TCs have a higher probability of affecting FSM and Palau.

At the global scale, Lee et al. (2018) calculated RPs for Category-1 and 3 TCs using the CHAZ model. The general spatial patterns in the CHAZ model (Figure 12-13 in Lee et al., 2018) and STORM (Figure 4.4) agree well, particularly in the Western and Eastern Pacific, including low RPs (around 1 to 10-yr for Category-1 and in the order of 10-yr for Category 3) in the Western and Eastern Pacific. For the North Atlantic and North Indian, STORM-RPs are lower than CHAZ-RPs. However, Lee et al. (2018) illustrate that their RPs are higher in the North Atlantic than observations. In parts of the Southern basins, STORM-RPs are around 90-yr while CHAZ-RPs are approximately 10 to 50-yr for a Category-3.

In conclusion, the STORM-RPs show good agreement with other studies, with differences in max U10 for a given RP often being less than 5 m/s. At the global scale, we observe similar spatial patterns of RPs for a Category-1 TC, but deviations at smaller scales occur when assessing Category-3 RPs.

**Table 4.4** Comparison of maximum 10-meter 10-minute average sustained wind speeds (max U10) at different locations and for different return periods (RPs) between STORM and the models used in other literature.

Location	Spatial scale	Max U10 reference (m/s)	Max U10 STORM (m/s)	RP reference (yr)	RP STORM (yr)	Abs. diff. in max U10 (m/s)	Rel. diff. in max U10 (%)	Evaluation of RP	Research setup, Reference
Mumbai, India	150 km radius <sup>1</sup>	Category 1		49-97	66	-	-	Within range	CHAZ model (Lee et al., 2018) and MIT model (Emanuel et al., 2006), Sobel et al. (2019)
		Category 3		~500	138	-	-	Lower than literature	
	10 km grid cell	Category 1		224-236	95	-	-		
		Category 3		~3000 - >10.000	550	-	-		
Honaira, Solomon Isl.	10 km grid cell	27.2 <sup>2</sup>	31.4	100		4.2	15.4	-	AIR South Pacific Risk Model, Commonwealth of Australia (2013)
Suva, Fiji		41.2 <sup>2</sup>	40.8			0.4	-1.0		
Palikir, Federal States of Micronesia		36.5 <sup>2</sup>	23.4			13.1	-35.9		
Port Vila, Vanuatu		46.8 <sup>2</sup>	40.5			6.3	-12.8		
Port Moresby, P.N.G.		26.7 <sup>2</sup>	23.7			3.0	-11.2		
Dili, Timor-Leste		16.6 <sup>2</sup>	18.4			1.8	10.8		
Koror, Palau		37.9 <sup>2</sup>	28.4			9.5	-25.1		
Tongatapu, Tonga		42.2 <sup>2</sup>	38.7			3.5	-8.3		
Alofi, Niue		40.3 <sup>2</sup>	39.8			0.5	-1.2		
Atiu, Cook Islands		43.1 <sup>2</sup>	35.5			7.8	-17.6		
Apia, Samoa		40.5 <sup>2</sup>	43.2			2.7	6.7		
Vaiaku, Tuvalu		27.3 <sup>2</sup>	28.4			1.1	4.0		

Low-probability tropical cyclone events in the present climate

Charleston (NC), USA	100 km radius	51.8	53.8	100	2	3.9	-	Hurricane Risk Calculator (Malmstadt et al., 2010), Ellis et al. (2016)
The Battery (NY), USA	10 km grid cell	27.3 <sup>2</sup>	30	100	2.7	9.9	-	MIT model (Emanuel et al., 2006), Garner et al. (2017)
		36.1 <sup>2</sup>	40	1,000	3.9	10.8	-	
Darwin, Australia	100 km radius	65 <sup>3</sup>	47	500	18	-38.3	-	MIT model (Emanuel et al., 2006), Cook and Nicholls (2009)
Townsville, Australia		52 <sup>3</sup>	49		3	-5.8		
Port Hedland, Australia		54 <sup>3</sup>	54		0	0		

<sup>1</sup> In this specific case, the STORM return period analysis has been re-run at 150 km radius instead of the regular 100 km used in the other cases.

<sup>2</sup> Converted from 1-min sustained wind speeds to 10-min average maximum wind speeds using a conversion factor of 0.88 (Harper et al., 2008)

<sup>3</sup> Converted from 3-sec wind gusts to 10-min average maximum wind speeds using a conversion factor of 0.66 (Harper et al., 2008)

### *Limitations and directions for future research*

In previous sections, we have demonstrated that the STORM-RPs for max U10 perform well. There are, however, some limitations regarding the usage of this dataset, which we will briefly reflect upon here, as well as giving directions for future research.

First, the STORM dataset is based on average present-day climate conditions (1980-2017), and as such does not capture climate variability. The climatology represented by STORM may be biased by the phases of multi-decadal variability contained in the 38-year period of record that was used to generate the dataset, which may not be representative for longer timescales. Moreover, the STORM dataset cannot be used to assess climate trends on decadal timescales or the effects of climate oscillations on TCs (e.g., the El Niño Southern Oscillation or the Madden-Julian Oscillation; Camargo et al., 2008). Future research could study these aspects by for instance using ensemble runs, or by generating synthetic TCs per oscillation phase.

Second, we used an easily applicable empirical inland decay function (Kaplan and DeMaria, 1995) to model the decay of TC wind speeds after landfall, and combine this with a 2D-parametric wind field model (Holland, 1980; Lin and Chavas, 2012). This decay function was derived using USA landfalling events, and as such may perform less well elsewhere. Moreover, the function assumes that a TC starts to decay after the TC eye crosses land. In reality, the inland surface winds will decay prior to landfall in response to enhanced surface friction caused by the land mass (Done et al., 2020). The 2D-parametric model does not include the influence of land, and therefore inland wind speeds may be overestimated. The use of numerical boundary layer model which includes the effects of terrain on the wind field would result in a better representation of the temporal evolution of the TC wind field over land (Done et al., 2020).

Last, the 2D-parametric wind field model used here assumes the asymmetry in the TC wind field arises from background flow. In extratropical regions, however, enhanced wind shear, caused by large-scale background flows or nearby troughs (Ritchie and Elsberry, 2001), may also induce asymmetry. Furthermore, STORM does not model the extratropical transition of TCs, so systems in these regions may be represented incorrectly and end-users should therefore pay attention when using this regional data.

## 4.4 Concluding remarks

We have demonstrated the application of the STORM dataset to generate a novel, open-access dataset of wind speed RPs for all TC basins. We empirically derived RPs at three spatial levels: at basin-level, within 100 km of selected coastal locations, and at 10 km resolution. First, we demonstrated the benefit of using such large synthetic dataset, composed of 10,000 years of TC activity for present-day climate conditions, over using a climatological dataset of 38 years for the calculation of RPs. Compared

to the empirically derived RPs, fitting a continuous EV distribution to 38 years of data typically leads to higher max U10, especially for RPs exceeding 100-yr. Second, we calculated RPs for TCs within 100 km of 18 coastal cities, and found that RP-curves differ substantially between locations. Finally, we estimated RPs at 10 km resolution by applying a 2D-wind field model to the synthetic TCs. This dataset is applicable for high-resolution TC wind risk assessments, particularly at the local scale such as Pacific island countries or the Caribbean.

To assess our model performance, we compared the STORM-RPs against those derived from other synthetic models across different spatial scales, and found that results generally agree well. Near basin boundaries, however, RPs can be lower compared to other literature. This is because STORM is run at the basin-scale, and TCs are cut off at the basin boundaries. For regional-scale studies, this issue can be solved by applying STORM using adjusted basin boundaries. On the global scale, we observe similar spatial RP patterns for a Category-1 event compared to literature, but larger spatial differences arise when looking at the distribution of Category-3 RPs in the Southern basins (Camargo et al., 2008).

In conclusion, this study is unique in that it is the first to estimate (high) RPs at 10 km resolution on a global scale. It represents an important step forward in global TC wind risk assessments, particularly for island countries and TC-scarce regions. Furthermore, this research can contribute to an improved quantification of other TC-induced hazards such as storm surge and precipitation (Bloemendaal et al., 2019; Cerveny and Newman, 2000; Phadke et al., 2003). To estimate the RPs of TC-induced storm surges, the 2D-wind fields can be used to force a hydrodynamic model (Muis et al., 2016). TC precipitation fields are closely related to max U10 fields (Cerveny and Newman, 2000) and the distance from the eye (Yu and Wang, 2018). These properties can be used to construct a parametric 2D-precipitation field model similar to the parametric wind field model, to assess TC precipitation risk.

## Acknowledgments

We thank Job Dullaart and Anaïs Couasnon for their help in the development and verification of the methodology used in this study. We also acknowledge SURFsara ([www.surf.nl](http://www.surf.nl)) for the support in using the Lisa Computer Cluster. NB and JCJHA are funded by a VICI grant from the Netherlands Organization for Scientific Research (NWO) (Grant Number 453-13-006) and the ERC Advanced Grant COASTMOVE #884442. IDH was funded by NERC Grant CompFlood (Grant Number NE/S003150/1). SM received funding from the research programme MOSAIC with project number ASDI.2018.036, which is financed by the NWO.



EVACUATION  
ROUTE



# 5 Low-probability tropical cyclone events under climate change

**This chapter is based on**

Bloemendaal, N., de Moel, H., Martinez, A.B., Muis, S., Haigh, I.D., van der Wiel, K., Haarsma, R.J., Ward, P.J., Roberts, M.J., Dullaart, J.C.M., & Aerts, J.C.J.H. Low-probability tropical cyclone events under climate change. Submitted to *Nature Communications*



## Abstract

Tropical cyclones (TCs) are among the deadliest and costliest natural hazards, and are projected to become more intense with climate change, increasing their threat to coastal communities. However, there is considerable uncertainty surrounding future changes in TC frequency and intensity, particularly at regional scales. Here we use the Synthetic Tropical cyclOne geneRation Model (STORM) to simulate changes in the frequency and intensity of future TCs, using input from four global climate models (GCMs). Our novel approach generates 10,000 years of synthetic tracks under past (1980–2017) and future climate (2015–2050) conditions. We derive high-resolution (10 km) wind speed return period maps up to 1,000-yr. While the GCM simulations do not show an increase in TC intensity, our results indicate that the probability for the most intense TCs increases in all regions, up to a factor 21, except the Bay of Bengal and the Gulf of Mexico.

## 5.1 Introduction

TCs are responsible for the highest insured losses of any natural hazard, exceeding US\$ 480 billion in the U.S. alone over the last decade (NOAA National Centers for Environmental Information, 2021). TCs are projected to become more intense in a warming climate (Knutson et al., 2020), enhancing the risks associated with their wind speeds, precipitation, storm surges and waves (Lin et al., 2012; Patricola and Wehner, 2018). TC losses have shown to rise steeply and nonlinearly with increasing intensity (Emanuel, 2021; Gettelman et al., 2018; Martinez, 2020; Pielke Jr. et al., 2008; Weinkle et al., 2018). Hence, understanding and accurately mapping TC hazards, their associated risk, and their future changes, is vital in protecting coastal communities.

Future-climate TC impact assessments often rely on projections from GCMs. However, GCMs provide limited information on how climate extremes such as TCs may change (Fiedler et al., 2021; Roberts et al., 2020b), primarily because the spatial resolution of past-generation GCMs ( $\pm 1.0^\circ$ ) is insufficient to adequately resolve TC intensity, size, and track (Murakami and Sugi, 2010). Consequently, there is no consensus on the projected change in TC frequency and characteristics under various climate change scenarios (Knutson et al., 2020). Recently, substantial progress has been made with the development of high-resolution GCMs ( $\pm 0.25^\circ$ ) (Haarsma et al., 2016). However, these GCMs still struggle to capture the most intense TCs (Roberts et al., 2020b), both through continued limitations in resolution and numerical precision (Davis, 2018) and from parameterizations of convective processes that do not hold for intense TCs, such as the assumption of hydrostatic balance. Additionally, such simulations typically only cover 30–100 year periods of historical and future climate (Haarsma et al., 2016), resulting in a small sample of TCs. This is an important constraint that further limits the accurate estimation of (changes in) the probability of extreme events.

Recently, several studies have sought to overcome the issues of poor TC representation and short simulations. One approach is to downscale TCs from GCMs (Emanuel, 2021; Lee et al., 2020). Here, atmospheric variables from GCMs are used to create a large-scale environment in a coupled TC model in which TCs are randomly seeded. This downscaling approach, however, requires a substantial number of inputs, and the simulated effects of climate change on TCs are only caused by processes in the large-scale environment (e.g., changes in wind shear or enhanced atmospheric stability), rather than changes in genesis frequency. Another approach is synthetic modelling (Bloemendaal et al., 2020c; Emanuel et al., 2006; Lee et al., 2018). Here, TC characteristics are extracted from either historical data (Emanuel et al., 2006; Haigh et al., 2014) or GCM simulations (Lin et al., 2012), and are statistically resampled and modeled to generate a new synthetic TC dataset, spanning thousands of years. This supports return period (RP) estimations exceeding the temporal length of the input data.

Here, we use the Synthetic Tropical cyclOne geneRation Model (STORM) (Bloemendaal et al., 2020c) to simulate future-climate TC wind hazard. We design a novel framework to generate future-climate synthetic TCs, combining the benefits of high-resolution GCMs and synthetic modeling (see Section 5.2). We extract information on changes in TC variables (1979-2014 vs 2015-2050) from four high-resolution GCM simulations, based on RCP8.5. Next, we project these changes onto the same TC variables from historical data (Knapp et al., 2010), which served as input for the STORM baseline climate dataset (Bloemendaal et al., 2020c) (STORM-B). We thereby create new input variables related to the future climate for each GCM. Next, we use this as input for STORM to simulate 10,000 years of future TC activity under climate change (STORM-C). Finally, we convert the synthetic tracks to a 2D-wind field using a parametric model (Holland, 1980), and calculate the wind speed RPs at 10 km resolution.

## 5.2 Methods

In this study, we present a novel method to construct a synthetic TC dataset representative of future-climate conditions. In general, such a dataset can be created in two ways: 1) extract future-climate TC statistics for each GCM of the multi-model ensemble and run each set through STORM; or 2) calculate the difference (i.e., delta) between these present- and future-climate TC statistics and add this delta to a baseline dataset (e.g., observed TC statistics). While the first approach is directly applicable to GCM simulation output and therefore does not require the design of additional methodological steps, this approach does not resolve first-order biases of GCMs (such as an underestimation in TC intensity or genesis frequency); rather, it propagates these biases into the synthetic data. Thus, any misrepresentation of TC characteristics in the GCM will be statistically resampled in STORM, and can potentially have a substantial effect on the outcomes. On the other hand, the second approach eliminates the effects of the first-order model bias, making it computationally more efficient because the

same baseline dataset is used for all GCMs. In this section, we first demonstrate why using GCMs in STORM directly results in a poor TC representation; next, we present and validate the so-called delta approach.

### 5.2.1 STORM and global climate models

The STORM model takes information on TC track, characteristics, and environmental variables as input variables and statistically resamples these to an equivalent of 10,000 years of TC activity under the same climate conditions. In Bloemendaal et al. (2020c), the 1980–2017 (38 years) period of IBTrACS (Knapp et al., 2010) was used as input to construct a baseline climate synthetic TC dataset (STORM-B) based on observed TC statistics. TC wind speeds were first converted to 10-minute 10-meter average maximum sustained wind speeds (m/s), and all data was linearly interpolated to three-hourly values. The STORM model only considers TCs that form within a TC basin domain and in a TC season (see Table 1 in Bloemendaal et al. (2020c)). In the current study, we used these observed TC statistics derived from the IBTrACS dataset (Knapp et al., 2010) as the baseline dataset, on which we applied the delta approach.

We use four high-resolution GCM simulations as inputs for STORM. These four GCMs are: CMCC-CM2-VHR4 (Scoccimarro et al., 2017), CNRM-CM6-1-HR (Voldoire, 2019), EC-Earth3P-HR (EC-Earth Consortium, 2018), and HadGEM3-GC31-HM (Roberts, 2017). CMCC-CM2-VHR4 has a spatial resolution of 25 km x 25 km in the atmosphere, while the other GCMs have a spatial resolution of 50 km x 50 km. We direct readers to Roberts et al. (2020b) for further information on these GCMs. The four GCMs are part of the PRIMAVERA-HighResMIP multi-model ensemble (Roberts et al., 2020a), which in turn is part of the Coupled Model Intercomparison Project Phase 6 (CMIP6) (Eyring et al., 2016). From each of the four GCMs, we use the publicly available (Roberts, 2019) TC tracks and characteristics extracted by Roberts et al. (2020b) using the TRACK algorithm (Hodges et al., 2017). We use the high-resolution coupled ocean-atmosphere runs for the periods 1979–2014 (henceforth “present climate”) and 2015–2050 (henceforth “future climate”), based on the high-emission SSP585 scenario (O’Neill et al., 2016; van Vuuren et al., 2011). These time periods were chosen to: 1) ensure maximum overlap with the IBTrACS dataset; and 2) have an equal temporal length of both the present and future period.

The GCMs have a six-hour temporal resolution, which we linearly interpolate to three-hourly values. Following Bloemendaal et al. (2020c), we only use TCs that form within the TC basins and within the TC season. However, we do not apply a wind speed threshold of 18 m/s, instead we use all TCs. This selection is due to GCMs generally underestimating TC intensity; applying a threshold can therefore exclude too many TCs. From each of the four GCMs, we extract information on TC genesis frequency (average per year), TC track (longitudinal and latitudinal position of the eye), TC intensity (minimum pressure in hPa), and environmental information on SSTs and mean sea-level pressure (MSLP).

To motivate our use of the delta approach, we first demonstrate the direct use of the GCMs in STORM. For four GCM-basin combinations, we compare present-climate statistics against historical data from the IBTrACS dataset (Table B.2 and Figure B.2). In all cases, TCs are substantially weaker in the GCMs than in IBTrACS. We then generate 1,000 years of synthetic data using STORM for both the present- and future-climate GCM datasets and observe that the poor representation of TC intensity is carried through the STORM model. For all GCM-basin combinations and for both the present- and future-climate GCM input, the average maximum wind speed along the track is below 30 m/s, whereas this value is around 35 m/s for historical TCs. In addition, the synthetic datasets do not show a (profound) increase in TC intensity under climate change. This shows that the poor representation of TC intensity is propagated through STORM and that it is unadvisable to use TC data from GCM simulations directly as inputs for understanding the impacts of climate change.

## 5.2.2 Designing and applying the delta approach

We first give an overview of the different (generalized) mathematical equations that form the body of the delta approach. These equations are applied to the following GCM TC statistics (see Figure 5.1 for more information): annual frequency, the corresponding genesis months and genesis locations, and changes in track and intensity.

Variables from the present- and future-climate GCM datasets are denoted as  $(\cdot)_{Present}$  and  $(\cdot)_{Future}$ , respectively. The variable from the observational TC dataset (IBTrACS; this dataset served as input for STORM-B) is denoted as  $(\cdot)_{IBTrACS}$ , and the variables resulting from adding the delta to the IBTrACS data is denoted as  $(\cdot)_{IBTrACS,\Delta}$ .

**Relative changes** Relative changes are calculated and applied to the historical TC statistics from IBTrACS as follows:

$$(\cdot)_{IBTrACS,\Delta} = (\cdot)_{IBTrACS} \cdot \frac{(\cdot)_{Future} - (\cdot)_{Present}}{(\cdot)_{Present}} + (\cdot)_{IBTrACS} \quad (5.1)$$

**Absolute changes** Absolute changes are calculated and applied to the historical TC statistics from IBTrACS as follows:

$$(\cdot)_{IBTrACS,\Delta} = (\cdot)_{IBTrACS} + ((\cdot)_{Future} - (\cdot)_{Present}) \quad (5.2)$$

**Shifting the normal distribution** The normal distributions from which variables are drawn, are shifted as follows:

$$\begin{aligned} N(\mu_{IBTrACS,\Delta}, \sigma_{IBTrACS,\Delta}^2) \\ = N\left(\mu_{IBTrACS} + (\mu_{Future} - \mu_{Present}), \sigma_{IBTrACS}^2 \cdot \frac{\sigma_{Future}^2}{\sigma_{Present}^2}\right) \end{aligned} \quad (5.3)$$

Where  $\mu$  denotes the mean and  $\sigma^2$  denotes the variance.

Next, we describe how the delta approach is applied to the different components of STORM (Figure 5.1). We highlight the most relevant aspects of the approach. The STORM components and equations discussed below are described in detail in Bloemendaal et al. (2020c). Rather than repeating the equations and explanations here, we refer the readers to this companion paper.

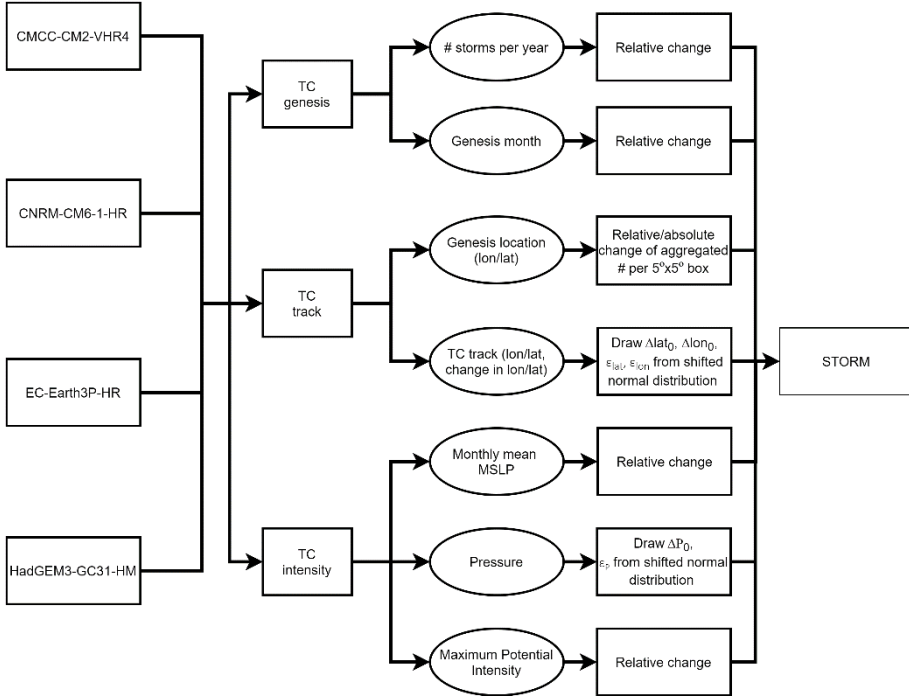


**Figure 5.1** Overview of the propagation of the delta into the STORM model

**Tropical cyclone genesis** We model the change in genesis frequency  $\lambda$  (avg/yr) as a relative change, following Equation 5.1. To ensure that the number of genesis occurrences aggregated over all months equals the genesis frequency, the shift in genesis frequency per genesis month  $\psi$  (avg/month) is modeled relative to the total genesis occurrences. As such, for every month, we calculate the change in genesis frequency relative to IBTrACS ( $\psi_{IBTrACS,\Delta}$ ) as follows:

$$\psi_{IBTrACS,\Delta} = \psi_{IBTrACS} \cdot \frac{\#TCS_{Future(month)} - \#TCS_{Present(month)}}{\#TCS_{Present(total)}} + \psi_{IBTrACS} \quad (5.4)$$

**Tropical cyclone movement** We model the change in genesis locations by first aggregating the number of genesis occurrences in  $5^\circ \times 5^\circ$  boxes and then calculating the changes in genesis counts per box. Next, we apply the relative change following

Equation 1. If there are no genesis counts in the present-climate GCM dataset, we calculated and add the absolute change following Equation 5.2 instead.

Consecutively, the TC track is simulated following the set of regression formulas from James and Mason (2005), see Bloemendaal et al. (2020c). The coefficients in the set of equations are derived directly from the observed TC statistics in IBTrACS. We extract the change in the first-step changes (i.e., the first change after genesis) in longitude and latitude,  $\Delta\xi_0$  and  $\Delta\varphi_0$ , and the longitudinal and latitudinal residual terms,  $\varepsilon_\xi$  and  $\varepsilon_\varphi$ , from the GCMs. The change in these variables is then applied to the ones derived from IBTrACS using Equation 5.3.

**Tropical cyclone characteristics** TC intensification and weakening are modeled following the set of equations 5 in Bloemendaal et al. (2020c). The coefficients in these equations are derived directly from the observed TC statistics. The first-step change in pressure,  $\Delta P_0$ , and the pressure residual term,  $\varepsilon_p$ , are extracted from the GCMs. The change in these variables is then applied to the ones derived from IBTrACS following Equation 5.3.

The Maximum Potential Intensity (MPI; in hPa) serves as an environmental constraint to the maximum TC intensity at a location, and is dependent on the SST at that location. To calculate changes in MPI, we derive the MPI for the GCMs using the SST fields from these GCMs in combination with the coefficients derived from the IBTrACS dataset. Next, we derive the relative changes in MPI per  $5^\circ \times 5^\circ$  box and apply this relative change to those in the IBTrACS dataset.

We do not extract information on maximum TC wind speeds from the GCMs due to their biases. Instead, we apply the wind-pressure relationship from Harper (2002), using the corresponding coefficients that were derived from the observational TC statistics. We do not consider any changes in the radius to maximum winds (Rmax) because it is not possible to derive an accurate Rmax value from the GCMs due to the Rmax values being constrained by the 25-km grid resolution of the GCM.

Lastly, we perform a perfect model run to validate the delta approach. In a perfect model run, we assume the model itself is “perfect”, i.e., we do not focus on intrinsic model errors but rather assess the influence of the input dataset on the outcomes. As such, by setting up this perfect model run, we can test whether the delta approach does not lead to anomalies in the output dataset. For the same four GCM-basin combinations used previously, we generate 1,000 years of synthetic tracks in two setups: 1) using the present-climate GCM dataset as baseline and adding the delta, and 2) directly using the future-climate GCM dataset. When comparing the two approaches, Table B.3 and Figure B.3 show that the mean and standard deviations across all TC variables considered here are almost identical to one another. The TC intensity, measured through the average maximum wind speed along the track, has a maximum deviation of 0.1 m/s for the four GCM-basin combinations. This result implies that the delta approach does not create any anomalies and can be used to

generate synthetic TCs for future climate conditions. Note that the delta approach does not overcome intrinsic model biases in the input dataset: it follows from the intensity statistics in Table B.3 and Figure B.4 that the low TC intensity present in the GCMs is still propagated through STORM.

To we quantify the individual influence of the input variables (that are part of the delta approach) on TC intensity, we conduct a sensitivity analysis for one GCM (HadGEM3-GC31-HM) in the Western Pacific. Table B.4 and Figure B.4 show that the largest influence is seen for the MPI. As this variable serves as an upper bound of TC intensity, it strongly influences the maximum intensity a TC can reach in its lifetime. Figure B.4 shows that keeping the MPI constant in a future-climate STORM run strongly decreases the frequency of the most intense (Category-5) TCs, reducing them to approximately 1% of all TCs compared to approximately 10% in the STORM-C dataset.

### 5.2.3 Calculating return periods

To calculate the wind speed RPs for each of the STORM-C datasets, we follow the same approach as in Bloemendaal et al. (2020a). To calculate RPs at 10 km resolution, we apply the 2D-parametric wind field model of Holland (1980), which has been further refined by Lin and Chavas (2012), to the future-climate synthetic TC tracks. At each cell of the 10-km grid, we store the maximum wind speed of each TC whenever this wind speed exceeds 18 m/s. Next, the RPs up to 1,000-yr are calculated empirically using the Weibull plotting formula (Bloemendaal et al., 2020a; Makkonen, 2006):

$$P_{exc}(\vec{v}) = \frac{i}{n+1} \cdot \frac{n}{m} \quad (5.5a)$$

$$T(\vec{v}) = 1/P_{exc}(\vec{v}) \quad (5.5b)$$

It also follows from the set of Equations 5.5 that if the length of the set of events  $n$  is large ( $n > 100$ ),  $\frac{n}{n+1} \approx 1$  and the value of  $P_{exc}(\vec{v})$  is dominated by the rank  $i$ . This implies that, for large  $n$ , changes in  $P_{exc}(\vec{v})$  for a given event are not due to changes in the total frequency of events  $n$  but are rather driven by changes in the frequency of exceedance of the respective event, which is represented by its rank  $i$ .

### 5.2.4 Exposure analysis

We assess the impacts of climate change on exposed population by combining the RP maps with global population data (Jones and O'Neill, 2020). The population dataset has a  $0.125^\circ \times 0.125^\circ$  resolution and is issued for the year 2000 (called the Base Year) and for five SSP-scenarios, given at decadal intervals between 2010 and 2100. To distinguish between different countries, we overlay the population data with country borders from Natural Earth ([www.naturalearthdata.com](http://www.naturalearthdata.com)). We include countries that

are considered to be prone to TCs; these countries are generally found between 30°N and 30°S (Walsh et al., 2007). To study the sole effect of the future change in TC characteristics on exposure, we aggregate the number of people exposed to Category-1 RPs below 100-yr, and Category-3 RPs below 500-yr per country. We keep the population data constant at the Base Year to solely assess the effects of a change in TC wind speed hazard.

Finally, we study the maximum wind speed weighted by population per basin. This variable represents the average maximum wind speed at a given RP experienced by an individual living in that basin. To ensure that we are only considering individuals who can potentially face such wind speeds, we include all individuals who are exposed to such wind speeds at a RP level below 1,000 yr. This way, societies living far inland and not prone to TCs are not included, thereby not skewing the results. We again keep the population data constant at the Base Year so that emerging differences can solely be attributed to changes in TC wind speeds.

## 5.3 Results and discussion

### 5.3.1 Generation of synthetic tropical cyclones under climate change

Our results show a global-scale increase in the frequency of occurrence of intense TCs (i.e., exceeding Category 3 on the Saffir-Simpson Hurricane Wind Scale, Simpson and Saffir, 1974), and a decrease in the frequency of weaker systems such as tropical storms (Figure 5.2). We find similar results for the different basins except the Bay of Bengal (North Indian), where the frequency of intense TCs decreases under climate change. This is in line with results from other studies using high-resolution (finer than 28 km x 28 km) GCMs (Knutson et al., 2020).

The results also indicate an increase in the magnitude of TC intensity, here assessed through the average maximum wind speed (m/s) across all four STORM-C datasets (Table B.1). On a global scale, maximum wind speeds increase from  $35.0 \pm 1.9$  m/s in the baseline to an average of  $39.9 \pm 3.0$  m/s across the future-climate STORM-C datasets, with all GCMs agreeing on the direction of change. In line with results obtained in other studies (Bhatia et al., 2018; Knutson et al., 2020; Walsh et al., 2019), our results also show a robust change on a basin scale. The largest differences in average maximum wind speeds are found in the Eastern Pacific with an increase of 6.7 m/s compared to the baseline. Relative increases in maximum wind speeds between the baseline and future climate datasets for the different basins lie between 7.5% - 23%. While the sign of change is the same, our range is higher than Knutson et al. (2020), who report a range of 1% - 10% derived from synthesizing the results from many GCM-based studies. Possible reasons for these differences in range include: (1) the strong dependency of TC intensity on sea-surface temperatures (SSTs) in STORM. We calculate the Maximum Potential Intensity (MPI; in hPa) from these SSTs, which serves as an environmental constraint on the maximum TC intensity.



Regions with lower SSTs are therefore more susceptible to TC weakening. In reality, TC weakening is also governed by (amongst other factors) enhanced (vertical) wind shear, the entrainment of dry air, and the influence of nearby land masses (Done et al., 2020; Emanuel, 2007). STORM does not simulate these processes, and therefore TC weakening may be better represented in GCMs; (2) Another potential cause for the difference in estimated intensity changes is the fact that STORM uses a lower bound for the maximum wind speed, set at 18 m/s. It is plausible that previous studies (Knutson et al., 2020) did not contain such threshold, and that the intensity increases under climate change are therefore somewhat tempered by these weaker storms.

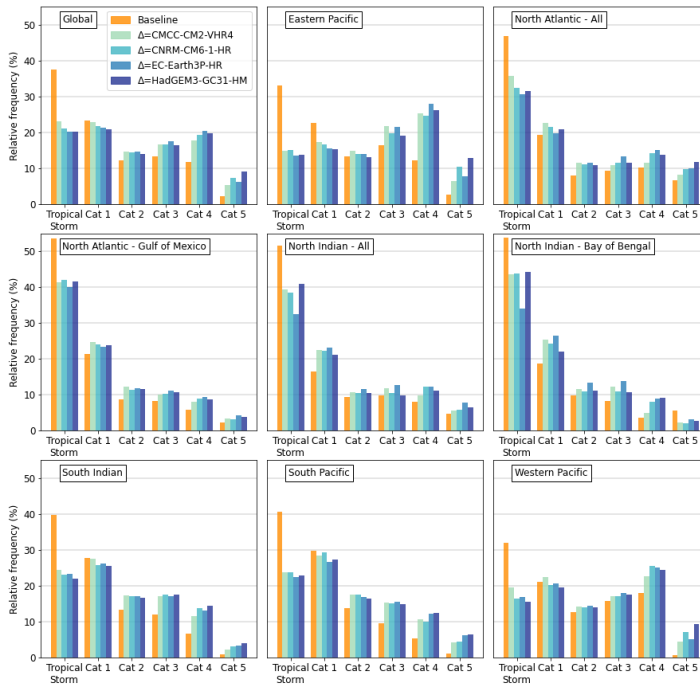


**Figure 5.2** Relative frequency of different tropical cyclone categories (Tropical Storm, Category 1-5) for 1,000 years of baseline climate STORM-B data and 1,000 years of future-climate STORM-C data for each of the four global climate models. We plot the global statistics, the six basins originally modelled by STORM (Eastern Pacific, North Atlantic, North Indian, South Indian, South Pacific, Western Pacific), as well as two sub-regions, the Gulf of Mexico and the Bay of Bengal.

In agreement with literature (Knutson et al., 2020), all four STORM-C datasets indicate a global decrease in annual TC genesis frequency compared to the baseline STORM-B dataset (Table B.1), amounting to  $72.4 \pm 1.4$  in the baseline climate to an average of  $69.6 \pm 3.1$  across the four future-climate datasets. For two out of four GCMs (CMCC and HadGEM3), the decrease is within one standard deviation of the baseline ( $72.0 \pm 1.5$  and  $72.2 \pm 1.5$ , respectively), and we therefore do not consider it to be statistically significant. At the basin level, however, the four STORM-C datasets

only agree on the sign of change in the South Indian basin, whilst in the others they do not.

The STORM-C datasets show a future poleward expansion of the location of maximum intensity in the Northern Hemisphere, particularly in the Western Pacific and the North Atlantic (Figure B.1). This poleward shift is driven by an increase in SSTs at higher latitudes, supporting TC tracks further northward, and is consistent with previous studies (Kossin et al., 2016; Kossin et al., 2014b).

### 5.3.2 Changes in low-probability events

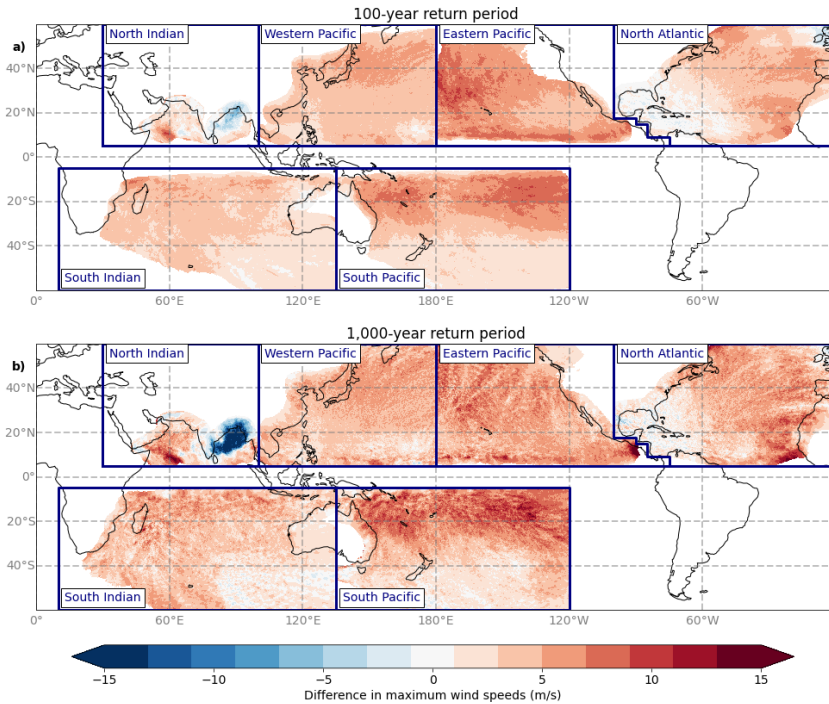


**Figure 5.3** Change in 10-minute 10-meter average maximum wind speed between STORM-B (corresponding to the average climate conditions of 1980-2017) and the ensemble median of the STORM-C datasets (corresponding to the average climate conditions of 2015-2050) for the 100-yr (a) and 1,000-yr (b) return period. Red tones indicate a positive change (i.e. an increase in wind speed), blue tones indicate a negative change.

The main advantage of our approach is that the large sample of synthetic TC tracks allows for a more robust assessment of changes in low-probability events. For this, we assess wind speed RPs at high spatial resolution (10km) by coupling the STORM-B and C datasets to a 2D-wind parametric wind field (see Section 5.2). For the ensemble median of the STORM-C datasets, we observe an increase in maximum wind speeds compared to STORM-B at most locations for the 100- and 1,000-yr RP (Figure 5.3). The largest increases are found in regions in the Eastern Pacific, North

Atlantic, and South Pacific, amounting to approximately 35 m/s for the 1,000-yr RP. There are also regions for which our results show a decrease in maximum wind speeds such as the Bay of Bengal, where maximum wind speeds decrease up to 15 m/s for the 1,000-yr RP. This decrease is primarily driven by a shift in simulated TC genesis locations closer to the Indian/Sri Lankan land masses, associated with a northward shift in the Intertropical Convergence Zone (Mamalakis et al., 2021). This shift increases the chances of a TC making landfall prior to intensifying further, predominantly reducing the formation chances of Category-5 TCs (see also Figure 5.2).

There is only a minor change in maximum wind speeds for both RPs in the Gulf of Mexico and the Caribbean, although our results do show an increase in the relative frequency of intense TCs in this region (Figure 5.2). In this region, the absolute frequency of high-intensity TCs does not change much towards the future (2,767 TCs in the baseline versus an ensemble median of 2,624 across the future-climate datasets). However, as the total frequency of TCs decreases (seen in three out of four GCMs; see Table B.1), the relative frequency of intense TCs also decreases slightly, resulting in similar RP for these events. These findings are consistent with other literature (Bruyère et al., 2017). Note that STORM does not model extratropical transition of TCs; as such, maximum wind speeds and corresponding RP analyses in extratropical regions (poleward of 40°N/S) should be disregarded as they may be represented incorrectly. Furthermore, this RP analysis is carried out at the basin scale; as such, there is often no smooth transition of maximum wind speeds near the basin boundaries – this is for instance visible at the Eastern/Western Pacific basin boundary.

Next, we assess how RPs of maximum wind speeds change for 18 coastal megacities located in TC-prone regions (Figure 5.4). For 14 cities, the simulations show an increase in maximum wind speeds across the range of RPs, indicating an increase in TC hazard. For Noumea (New Caledonia), the maximum wind speed at the 100-yr RP increases from 46.8 m/s in the baseline climate to 53.0 – 59.0 m/s under climate change, which is the largest increase across the 18 cities. At the 1,000-yr RP, the largest increase in maximum wind speed is found for San Diego (USA), increasing from 34.3 m/s to 42.9 – 48.2 m/s. The cities in the North Atlantic basin all lie within the Gulf of Mexico and Caribbean region, where the STORM-C dataset show a very minor change in wind speed RPs. Hence, the STORM-C RP curves for these cities (Houston, Miami, and San Juan) deviate little from the STORM-B RP curve. To illustrate: the largest absolute change in the 100-yr wind speed across these three cities is only 2.5 m/s for San Juan. For Chittagong (Bangladesh), located in the Bay of Bengal, the STORM-C RP curve is substantially lower than the baseline, especially for RPs ranging from 100 to 10,000-yr.

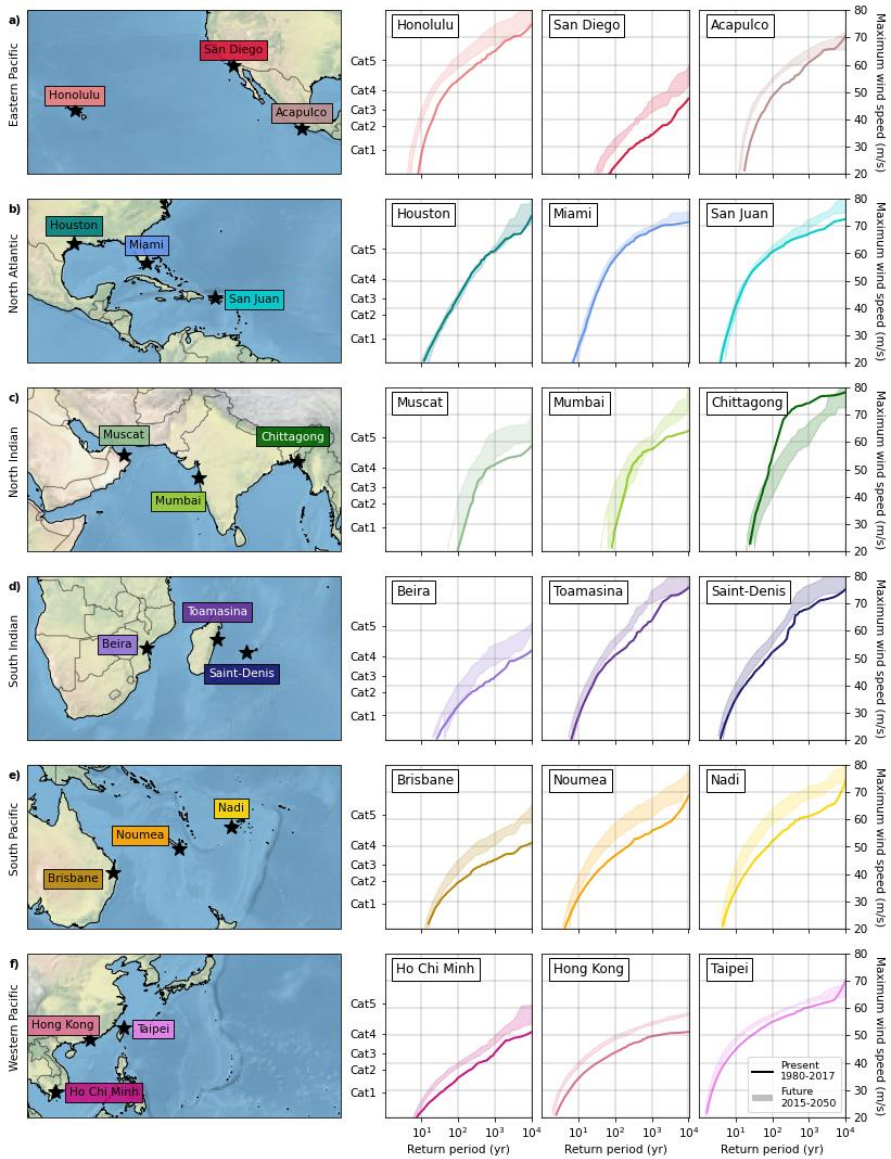


**Figure 5.4** Empirically derived return periods of maximum 10-minute 10-meter average wind speed within a radius of 100 km for a selection of 18 coastal cities, evenly distributed over the six ocean basins. The solid line represents the STORM present climate return periods (corresponding to the average climate conditions of 1980-2017). The shaded areas indicate the range of return periods of the four STORM future climate datasets (corresponding to the average climate conditions of 2015-2050).

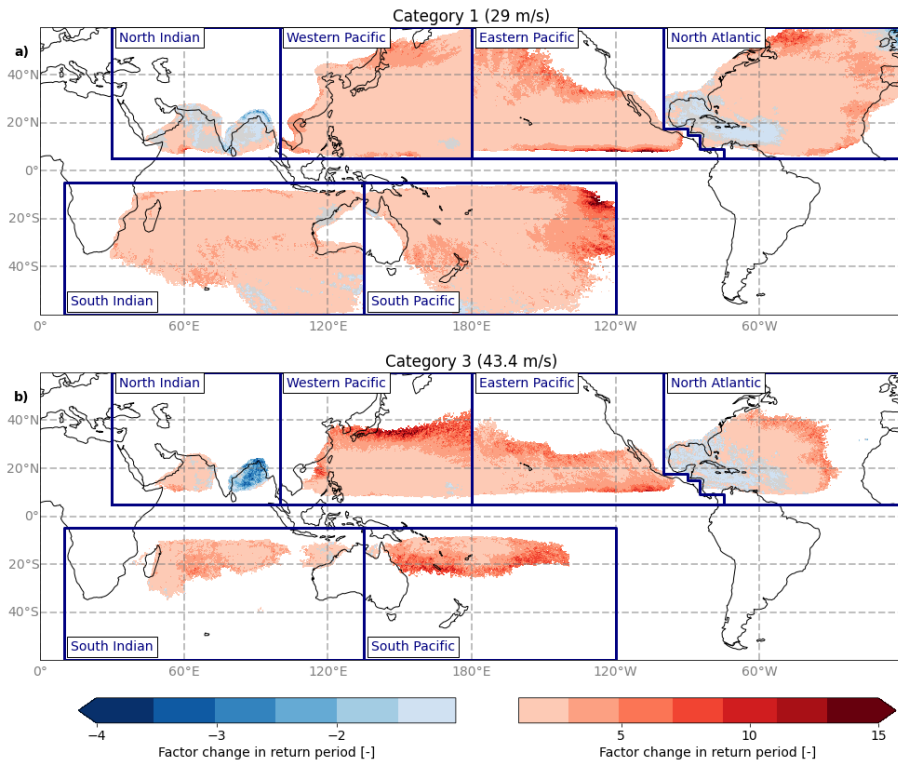


**Figure 5.5** Ensemble median of the factor change in return period between the STORM-B (corresponding to the average climate conditions of 1980-2017) and STORM-C (corresponding to the average climate conditions of 2015-2050) datasets for 10-minute 10-meter wind speeds equivalent to a Category 1 (a; 29 m/s) and Category 3 (b; 43.4 m/s) tropical cyclone. Grey colors indicate regions with no change.

We also calculate the change in RPs for given wind speed thresholds. The probability of Category-1 and Category-3 TC wind speeds increases everywhere, except the Bay of Bengal and the Gulf of Mexico (Figure 5.5). In the Pacific and North Atlantic basins, the highest positive factor changes for Category-3 TCs are generally found toward the boundaries of the regions prone to these wind speeds (between 20°-40° N/S), amounting to a factor 21 in the Western Pacific. These changes are likely driven by the increase in SSTs in the future-climate GCMs, supporting the poleward extension of intense TCs. However, we also note that TCs in these regions, particularly near 40°N/S, may be prone to extratropical transition and since this process is not included in STORM, the intensities of TCs in these areas may be poorly represented. Furthermore, we point out that in these regions, the probabilities of a Category-3 TC are generally lower, and consequently a very minor increase in probabilities will result in a large factor change, in contrast to areas that experience such Category-3 TCs more frequently. Other TC-prone regions showing a more than five-to-tenfold increase in the probability of a Category-3 strike include Japan, Hong

Kong, the Comoros (near Mozambique), and the South Pacific region between 20–30°S. In these areas, the increase in probability is similar across the GCMs (Figure B.7). On the other hand, there is a decrease in probability in the Bay of Bengal (Figure 5.5); this follows from the shift in genesis locations as discussed above. Similarly, results show little change for the Gulf of Mexico and Caribbean, which is also discussed above.

### 5.3.3 Changes in exposed population

Next, we assess changes in exposed population. We find the largest relative increase in population exposed to Category-1 RPs below 100-yr in Cambodia, with a relative increase of 12,550% compared to the baseline (Table 5.1). This change is driven by a shift in exposed areas; in the baseline climate, mostly smaller villages along the Cambodian coastline are affected with RPs of Category-1 wind speeds below 100-yr (total population of around 40,000), whereas under climate change, a much larger area, including the capital city of Phnom Penh (total population exceeding 1 million), is exposed. Note that we deliberately keep the population constant over time, allowing us to solely assess the impact of climate change on exposed populations (see Section 5.2). Australia faces the largest relative increase in exposed population to Category-3 RPs below 500-yr, amounting to 9,375% (Table 5.2). Moreover, five of the top 10 countries are located in the South Pacific, the other four countries being Papua New Guinea, New Caledonia, the Solomon Islands, and Tonga. Note that these four countries are all small island developing states, which are typically characterized by high vulnerability to climate impacts, scarce financial resources, and small economies to scale to overcome such impacts (United Nations, 2021). In fact, 18 out of the 21 countries listed in Tables 5.1 and 5.2 that are facing an increase (relative and/or absolute) in exposed population are considered developing countries (United Nations, 2020).

**Table 5.1** Top-10 countries experiencing the largest relative and absolute change in people exposed to Category-1 wind speed return periods below 100-yr.

	Country	Relative change (%)	Country	Absolute change (M)
1	Cambodia	12,550	China	153.0
2	Laos	1,514	Vietnam	36.7
3	Mozambique	466	Bangladesh	-23.5
4	Iran	373	United States	18.8
5	Papua New Guinea	237	India	-16.3
6	Palau	116	Somalia	-16.3
7	Vietnam	42	Mexico	7.5
8	Yemen	39	Mozambique	6.5
9	Honduras	-26	Philippines	6.4
10	Myanmar	-26	Cambodia	5.6

**Table 5.2** Top-10 countries experiencing the largest relative and absolute change in people exposed to Category-3 wind speed return periods below 500-yr.

	Country	Relative change (%)	Country	Absolute change (M)
1	Australia	9,375	China	250.0
2	Yemen	2,916	Japan	133.0
3	Papua New Guinea	1,442	South Korea	59.4
4	South Korea	935	Bangladesh	-62.4
5	New Caledonia	292	India	-59.3
6	Japan	279	United States	9.9
7	China	161	Mexico	7.1
8	Solomon Islands	135	Madagascar	6.9
9	Venezuela	94	Pakistan	5.0
10	Tonga	92	Myanmar	-5.0

### 5.3.4 Coastal regions at risk

To get a basin-wide view of changes in population, we weighted the RP curves by population (combining the information from Figures 5.4 and 5.5), hereby deriving the average maximum wind speed experienced by a person living near the coast in that basin per RP (Figure 5.6). In the Western and Eastern Pacific basins, the future-climate RP curve is visibly higher than the baseline climate curve, indicating that chances of an individual experiencing a stronger TC increase under climate change in all STORM-C datasets. In the other basins, the baseline climate RP curve overlaps with the future-climate range, indicating that climate change will not lead to substantial changes.

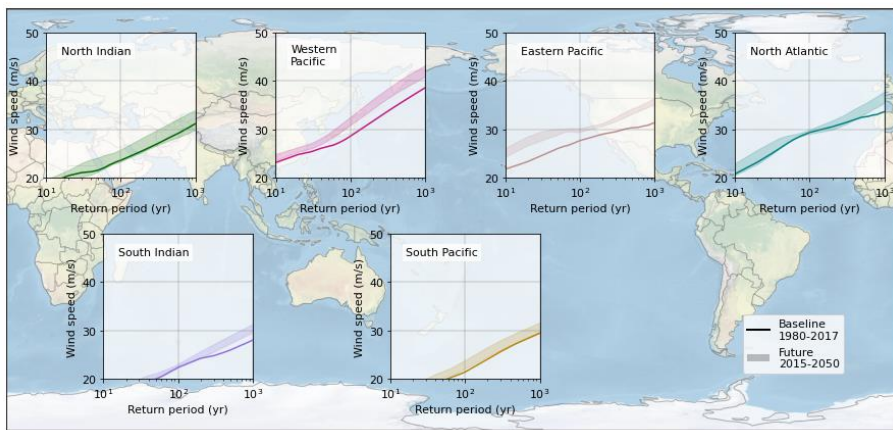


**Figure 5.6** Empirically derived return periods (x-axis) of 10-minute 10-meter average wind speeds (y-axis), weighted by population. The graph represents the average wind speed at a given return period experienced by an individual living in that basin and exposed to such wind speed probabilities.



## 5.4 Concluding remarks

We have presented a novel method to analyze low-probability TC events under climate change, combining the benefits of high-resolution GCMs with synthetic TC modelling. By statistically extending baseline and future TC datasets from 36 to 10,000 years, this method overcomes sampling and resolution issues that have affected previous studies, allowing future changes to be more clearly discerned, quantified and assessed. This has allowed us to identify hotspot regions facing the largest changes in the probability of being hit by a TC. Our results indicate that the Hong Kong region and the South Pacific are prone to the largest increase in probability for a Category-3 TC event. At the same time, there is little change in probabilities in the Gulf of Mexico and a decrease in probabilities for the Bay of Bengal. By combining the RP data with population data, we showed that primarily developing countries, such as Cambodia and Yemen, are prone to large increases in populations exposed to Category-1 and Category-3 TCs, respectively. To isolate the climate signal, our results were derived by keeping the population data constant. However, population growth and migration toward TC-prone areas are expected to further increase future population exposure (Neumann et al., 2015a; Tellman et al., 2021).

This research represents an important step forward in global TC wind risk assessments by determining the changes in frequency and intensity of TC events under climate change at the basin and local scale. Furthermore, this research can contribute to an improved quantification of other TC-induced hazards, such as storm surge and precipitation. The future-climate STORM datasets can also be used as a hazard input dataset in catastrophe and risk models, such as those used by, for example, the (re)insurance industry. The procedure presented here is easily applicable to other GCMs and for other RCP scenarios, thereby allowing for analyses of TC risk under different climate scenarios and time periods.

## Acknowledgments

NB and JCJA are funded by a VICI grant from the Netherlands Organization for Scientific Research (NWO) (Grant Number 453-13-006) and the ERC Advanced Grant COASTMOVE #884442. IDH was funded by NERC Grant CompFlood (Grant Number NE/S003150/1). ABM received funding from Climate Econometrics and the Robertson Foundation (Grant Number 9907422). SM received funding from the research programme MOSAIC with project number ASDI.2018.036, which is financed by the NWO. MJR was funded by the the Joint UK BEIS/Defra Met Office Hadley Centre Climate Programme (grant no. GA01101), and we thank H2020 PRIMAVERA (grant no. 641727) for supplying the model datasets. PJW received funding from the NWO VIDI research grant 016.161.324 This research is part of the IS-ENES3 project that has received funding from the European Union's Horizon 2020 research and innovation programme under grant agreement No 824084. The views presented in this research are solely those of the authors and do not necessarily represent those of the Treasury Department or the U.S. Government.



We thank Anaïs Couasnon and René van Westen for their thoughtful comments and suggestions. We also acknowledge SURFsara ([www.surf.nl](http://www.surf.nl)) for the support in using the Lisa and Cartesius Computer Cluster, and the JASMIN data analysis facility for support in retrieving the HighResMIP datasets. We thank 4TU.ResearchData for their support in the storage and maintenance of the STORM datasets.





BIKE  
SHOP  
WE ARE  
OPEN

BE  
NICE  
HARVEY



## 6 The Tropical Cyclone Severity Scale

**This chapter is published as**

Bloemendaal, N., de Moel, H., Mol, J.M., Bosma, P.R.M., Polen, A.N. & Collins, J.M. Adequately reflecting the severity of tropical cyclones using the new Tropical Cyclone Severity Scale. *Environmental Research Letters* **16**, 1 (2021).

<https://doi.org/10.1088/1748-9326/abd131>

## Abstract

For decades, meteorologists and governments have been warning communities in coastal areas for an imminent tropical cyclone (TC) using the Saffir-Simpson Hurricane Wind Scale (SSHWS). The SSHWS categorizes a TC based on its maximum wind speed, and is used in defining evacuation strategies and humanitarian response. However, the SSHWS considers only the wind hazard of a TC, whereas a TC can also cause severe conditions through its high storm surges and extreme rainfall, triggering coastal and inland flooding. Consequently, the SSHWS fails to mirror the TC's total severity. This becomes evident when looking at past events such as Hurricane Harvey (2017), which was classified as a Tropical Storm while it caused widespread flooding in the Houston (TX) area, with precipitation totals exceeding 1.5 m. Without including storm surge and rainfall information, adequate risk communication with the SSHWS can be challenging, as the public can (mistakenly) perceive a low-category TC as a low-risk TC. To overcome this, we propose the new Tropical Cyclone Severity Scale (TCSS) that includes all three major TC hazards in its classification. The new scale preserves the categorization as used in the SSHWS, to maintain familiarity amongst the general public. In addition, we extend the scale with a Category 6, to support communication about the most extreme TCs with multiple hazards. The TCSS is designed to be applied on a local-scale, hereby supporting local-scale risk communication efforts and evacuation strategies prior to a TC landfall. The scale can be used for risk communication on both the total TC risk and on the categories of the separate hazards, which can be valuable especially in cases when one hazard is the predominant risk factor, such as excess rainfall triggering flooding.

## 6.1 Introduction

Over the past decades, tropical cyclones (TCs) have greatly impacted the North Atlantic region, causing large economic damage and loss of life through their high wind speeds, storm surges, and precipitation. Some examples are Hurricane Sandy (2012), with over US\$ 70 billion in damage, and the 2017 Hurricanes Harvey, Irma and Maria, with total damages exceeding \$260 billion (NOAA, 2020b). To communicate about the potential threat of the TC, meteorologists commonly classify its maximum wind speeds following the Saffir-Simpson Hurricane Wind Scale (SSHWS; Simpson and Saffir (1974)). The SSHWS categorizes a TC's wind speed on a scale of 1 to 5 for wind speeds exceeding 33 m/s, i.e. of at least hurricane strength, and uses the classifications "tropical storm" and "tropical depression" for weaker storm systems. However, recent research has shown that most TC-related fatalities in the U.S. are not caused by wind (8%), but by storm surge (49%) and rainfall (27%) (Rappaport, 2014). For instance, Hurricane Katrina (2005) was classified as a Category 3 at landfall with wind speeds of around 55 m/s, but its 8.6 m storm surge caused widespread levee failure around New Orleans (LA), resulting in over 1,800 casualties and US\$ 125 billion in damage, making it the costliest U.S.

TC to date (NOAA, 2020b). Another example is Hurricane Harvey (2017), which weakened to a tropical storm after landfall in Texas, but became the highest precipitation event in recorded history with precipitation totals exceeding 1.5 m in the greater Houston area (Blake and Zelinsky, 2018). These examples demonstrate that a classification method solely based on wind speed, such as the SSHWS, fails to capture the full severity of a TC. In recent years, various alternative methods of TC classification and indexation have been proposed to overcome this weakness (see Table 6.1). Almost all methods are applied on a pre-event basis, in that they use forecast information to classify a TC hazard, which is important given its function to warn and prepare. However, most classification methods assess either the wind or storm surge hazard, but rarely combine them. Moreover, most of the methods leave out precipitation altogether. The Hurricane Classification System by Senkbeil and Sheridan (2006) is the only method that includes all three TC hazards. However, their Hurricane Classification System is computed post-landfall, meaning that it is limited in use related to warning and preparation.

TC classification methods are an important component of TC risk communication. Past research from psychology and economics shows that people generally have difficulty understanding low probabilities, and that responses to risk communication can be mediated by emotions such as worry (Petrova et al., 2014), and presentation mode (Goldstein and Rothschild, 2014; Okan et al., 2018). Besides communicating risk, TC hazard warnings should explain uncertainty of predictions, adding another layer of complexity to the interpretation (see e.g. van der Bles et al. (2019) for an interdisciplinary review on communicating uncertainty to the general public). Several attempts to improve TC risk communication have been documented, including proposals for and implementations of alternative forecast graphics (Broad et al., 2007; NHC, 2017, n.d.; Radford et al., 2013) and interactive visualization tools (Lindner et al., 2018).

Naturally, TC classification categories are used by residents for disaster-related decision-making, such as evacuation behavior and preparedness measures. Individuals have to consider many factors when making protective action decisions (such as evacuating or sheltering in place). These factors can include prior TC experiences, social connections and networks, environmental cues, warning messages, and the sources and channels of information they are exposed to (Collins et al., 2017; Collins et al., 2018; Kasperson and Kasperson, 1996; Lindell and Perry, 2012; Mase et al., 2015). When confronted with incomplete or inaccurate information, individuals are likely to spend more time gathering additional information before making a decision; this can cost valuable time during the window before a TC impacts (Bean et al., 2016; Perry and Lindell, 2006). Lazo et al. (2010) show that the intention to evacuate seems to be linearly related to SSHWS Category. Recent studies on evacuation behavior in light of hurricanes impacting Puerto Rico, the U.S. Virgin Islands, and Texas show that residents rely heavily on SSHWS Category in evacuation decisions (FEMA, 2014a, 2014b; Morss and Hayden, 2010).

Improving the classification method to better reflect the TC severity could therefore improve residents' preparedness and evacuation decisions aiding a rapid response.

A novel field of disaster research stems from the desire to understand how the public's perceptions of natural hazards are influenced by different risk communication methods (Bourque et al., 2012). Studies show that concepts of return periods are difficult to grasp and there is a clear preference for concrete descriptions (Bell and Tobin, 2007) and that mobile warning messages are often deemed confusing (Bean et al., 2016). Another difficulty in lay understanding of hazard scales is the type of scale. People often apply linear logic to all scales encountered, including logarithmic scales. This may anchor or bias perceptions and leads to problems in risk communication, for example with regards to the logarithmic Richter scale of earthquake magnitude (Celsi et al., 2005; Jones and Richardson, 2007). Risk communication efforts in various domains have shown that categorization, for example with color coding or traffic light schemes, may be helpful to bring the most important information to attention (Jones and Richardson, 2007). Table 6.2 gives an overview of hazard classification methods for several types of hazards. Note that most classifications are discrete and based on a continuous index. Interestingly, the Pandemic Severity Index (PSI) was specifically modelled to mimic the discrete hurricane categorization of the SSHWS (Caduff, 2010).

To overcome the aforementioned weaknesses of the SSHWS and building on past TC classification methods, we argue that an improved classification method should follow the following criteria:

1. The scale should include all major hazards, being wind, storm surge, and precipitation;
2. The scale should be applicable for pre-event hazard communication;
3. The scale should be discrete.

Here, we propose the new Tropical Cyclone Severity Scale (TCSS) following these criteria. Although a discrete scale might impose saturation at high intensities (Kantha, 2006), a continuous scale can be more difficult to apply in risk communication to the lay public, as they have been familiar with discrete TC classification for decades. As such, we preserve the 1 to 5 categorization in the TCSS. Moreover, we extend the scale by an additional Category 6 to communicate the additional risk from multiple extreme hazards that may become more frequently encountered due to the effects of climate change. Even though a Category 6 is not necessary in the current SSHWS as Category 5 already represents total devastation, we believe that an additional category would be useful to communicate the ultimate severity of combined extreme hazards of wind, precipitation and storm surge. Finally, the scale should be applicable for pre-event communication, which can only be achieved if the scale solely consists of variables also used in forecasting. While the SSHWS is commonly applied to communicate on an event-scale basis, a major benefit of the TCSS is that it can be

**Table 6.1** Overview of past tropical cyclone classification methods. Scale characteristics that meet our set of criteria are presented in bold. These criteria are: 1) inclusion of wind, storm surge, and precipitation, 2) applicability for pre-landfall hazard assessment, and 3) discrete nature.

Tropical Cyclone Classification Method	Tropical cyclone hazard(s) reflected by scale			Applicability	Continuous/ Discrete	Reference
	Wind	Storm surge	Precipitation			
<b>Saffir-Simpson Hurricane Wind Scale*</b>	<b>Yes</b>	No	No	<b>Pre-landfall</b>	<b>Discrete</b>	Simpson and Saffir (1974)
<b>Hurricane Severity Index</b>	<b>Yes</b>	No	No	<b>Pre-landfall</b>	<b>Discrete</b>	Hebert et al. (2010)
<b>Hurricane Hazard Index</b>	<b>Yes</b>	No	No	<b>Pre-landfall</b>	Continuous	Kantha (2006)
<b>Hurricane Intensity Index</b>	<b>Yes</b>	No	No	<b>Pre-landfall</b>	Continuous	Kantha (2006)
<b>Integrated Kinetic Energy</b>	<b>Yes</b>	No	No	<b>Pre-landfall</b>	Continuous	Powell and Reinhold (2007)
<b>Hurricane Classification System</b>	<b>Yes</b>	<b>Yes</b>	<b>Yes</b>	Post-landfall	<b>Discrete</b>	Senkbeil and Sheridan (2006)
<b>Surge scale</b>	No	<b>Yes</b>	No	<b>Pre-landfall</b>	Continuous	Irish and Resio (2010)
<b>Hurricane Surge Index</b>	No	<b>Yes</b>	No	Pre-landfall	Continuous	Kantha (2008)
<b>Multihazard Hurricane Index</b>	<b>Yes</b>	No	<b>Yes</b>	Pre-landfall	Continuous	Song et al. (2020)

\*From 1971 till 2009, the NHC used the Saffir-Simpson Hurricane Scale (SSHS), which utilized pressure, storm surge, and wind measurements (Kantha, 2013; NHC, 2019b). After Hurricanes Katrina (2005) and Ike (2008) demonstrated that storm surge potential based solely on wind categorization was misleading, the NHC dropped all requirements except wind. In 2012, the SSHS was modified to include only the wind component, and has been named the Saffir-Simpson Hurricane Wind Scale since.



**Table 6.2** Overview of hazard classification methods

Hazard	Scale name	Nature	Categories	Categories in words
Tropical cyclone wind speed	Saffir-Simpson Hurricane Wind Scale	Discrete	5	Very dangerous winds will produce some damage, Extremely dangerous winds will cause extensive damage, Devastating damage will occur, Catastrophic damage will occur, Catastrophic damage will occur
Earthquake (magnitude)	Richter	Logarithmic	-	-
Earthquake (intensity)	Modified Mercalli Intensity	Discrete	10	Not felt, Weak, Weak, Light, Moderate, Strong, Very strong, Severe, Violent, Extreme, Extreme, Extreme
Forest fire	McArthur Forest Fire Index	Discrete, based on continuous index	6	Low-moderate, High, Very high, Severe, Extreme, Catastrophic
Snowfall	Northeast Snowfall Impact Scale	Discrete, based on continuous index	5	Notable, Significant, Major, Crippling, Extreme
Tornado	Enhanced Fujita	Discrete, based on continuous index	6	Light, Moderate, Considerable, Severe, Devastating, Incredible
Pollution	Air Quality Index	Discrete, based on continuous index	6	Good, Moderate, Unhealthy for sensitive groups, Unhealthy, Very Unhealthy, Hazardous
Epidemic	Pandemic Severity Index	Discrete, based on continuous index (case-fatality ratio)	5	Category 1 to category 5, designed to mimic hurricane classifications
Heatwave	Heat Index	Discrete, based on two continuous variables (temperature and relative humidity)	4	Caution, Extreme Caution, Danger, Extreme Danger
Volcano	Alert-Notification System for Volcanic Activity	Discrete	4	Normal, Advisory, Watch, Warning

applied on a local scale to warn communities about their imminent danger. This way, people can receive tailored information on the TC's severity for their location, and prepare accordingly.

## 6.2 Methods

### 6.2.1 Tropical cyclone event dataset

To design and construct the new TCSS, we first extract all North Atlantic landfalling historical TCs between 1996 and 2018 from the National Hurricane Center (NHC) TC reports (NHC, 2020b). Subsequently, we exclude those landfall events without casualty or damage statistics. A landfall event (as stated in the “best track” table in the report) is included when there is either observational or estimated data on the maximum wind speed, storm surge and accumulated precipitation within 100 km from the landfall location. This yields a dataset of 90 TC events, including multiple landfall events from individual TCs. The maximum accumulated precipitation is taken as the highest total amount of rainfall that has been measured at a station within this 100 km of the landfall location. We assume that each of these observations within 100 km from the landfall location provide a good indication of the conditions at the precise landfall location. Local topographical effects, however, might influence each of these variables, but it is difficult to account for these effects when using data from a limited number of measurement stations. Reported wind data in the TC reports are gathered from, amongst others, satellite data, U.S. Airforce Reserve aircraft reconnaissance flights (the so-called “Hurricane Hunters”), ship reports, radars, automated weather stations, and ocean buoys (NHC, 2020b). Storm surge estimates are commonly collected from National Oceanographic Service tide gauge stations and high water-mark surveys conducted by the U.S. Army Corps of Engineers and U.S. Geological Survey. Rainfall data is retrieved from rainfall measurements stations.

Whilst the data from the TC reports used in this study have been acquired post-landfall to test the scale for past storms, the TCSS is designed for pre-landfall usage. In this case, hazard data will be retrieved from TC forecasts. For wind and precipitation, forecast information is collected from numerical weather models (NHC, 2019a; NOAA, 2009). Such models are generally run at 6-hourly intervals, with a forecast range of 120-240 hours. For every model run, its initial conditions are derived from combining model information with observational data from satellites, a procedure also known as data assimilation (see e.g. ECMWF (2020) or NOAA (2020c) for more information on data assimilation in the ECMWF IFS and GFS models, respectively). Storm surges are modeled using the Sea, Lake and Overland Surges from Hurricanes (SLOSH) model (Jelesnianski et al., 1984; NHC, 2020a). This hydro-dynamical model simulates storm surge heights by using forecast data on atmospheric pressure, TC size, and TC forward speed as input data, and combining this with bathymetry and coastline data.

As with any scale, the performance of the TCSS is inherently dependent on the quality of the input data. Because of possible differences between pre- and post-landfall data, it is important to address forecast errors here. At the end of every TC season, the NHC releases its Forecast Verification Report, the latest one available being the 2018 report at the time of writing (Cangialosi, 2019). For the 2018 season, the NHC reported mean forecast errors of 2.6 m/s at 12h forecast time, and 6.7 m/s at 72h and 96h, both being lower than the 5-year averages. Besides accurate TC intensity forecasts, TC track forecasts also play an important role in storm surge modeling, as storm surge heights are strongly influenced by the location and timing of landfall (NHC, 2020a). The NHC Forecast Verification Report lists mean track errors ranging from 44 km at 12 h forecast time, to 344 km at 120 h, which is lower than the 5-year average. Aside from TC track errors, the NHC Forecast Verification Report does not list storm surge and rainfall forecast errors. Luitel et al. (2018) found that TC rainfall forecasts provide good skill, especially for lead-times up to 48h. Various studies have also found good agreement between modeled (using SLOSH) and observed storm surges for different historical TCs (Forbes et al., 2014; Glahn et al., 2009). As such, we consider the forecast errors to be small enough for any difference between pre- and post-landfall data to not be of substantial impact. Hence, we use the post-landfall data here to design and demonstrate the TCSS.

## 6.2.2 Design of the Tropical Cyclone Severity Scale

Next, we define a categorization for wind speed, storm surge, and accumulated rainfall respectively (see Table 6.3). This categorization is based on the severity (potential to damage), similar to the philosophy of the SSHWS. To facilitate interpretation and familiarity amongst risk communicators, the wind speed categorization is directly taken from the SSHWS. For storm surge and accumulated precipitation, there is currently no categorization in place. Choosing thresholds for categories is inherently subjective and, from a mathematical point of view, non-unique. In order to incorporate the SSHWS as the wind-categorization in our TCSS, we therefore follow the design of the SSHWS also for the other hazards. This means that a Category 1 represents moderate damage and a Category 5 catastrophic damage (Simpson and Saffir, 1974). However, for the SSHWS, extensive research was done to determine the threshold values for each of the intermediate category thresholds (Thomas, 2001). As there is no equivalent study for rainfall and storm surge, we evenly distribute the other thresholds amongst the other categories. The highest threshold for storm surge (4 m) is determined based on observations from TCs with known high-impact storm surges in the historical dataset, including Hurricane Michael (4.26 m) and Hurricane Rita (4.57 m). The TC reports show that historical TCs with storm surges lower than 0.75 m generally had very little impact from this hazard. Therefore, 0.75 m is set as the lowest threshold.

The highest threshold for accumulated rainfall is chosen based on the notice of “catastrophic” rainfall impacts in the NHC TC reports. As such, past events like 2017

Hurricane Harvey (1538 mm), 2018 Hurricane Florence (912 mm) and 2001 Tropical Storm Allison (908 mm near the Texas landfall location, 758 mm near the Louisiana landfall location) would have been classified as a Category 5 when considering precipitation. Following these examples, we set the Category 5-threshold for precipitation totals above 750 mm. The lowest threshold should represent accumulated rainfall totals that can have an impact in urbanized regions, albeit temporarily. Such a value, however, cannot be uniformly set for the U.S., as this depends on a city’s infrastructure and sewage system. Instead, we use the American Meteorological Society’s definitions of rainfall events, and choose the lowest threshold such that moderate rainfall events (between 26-76 mm h<sup>-1</sup>) lasting for 2-4 hours, or heavy rainfall events (more than 76 mm h<sup>-1</sup>) lasting for more than one hour will be categorized on the TCSS (AMS, 2020). Please note that the classification thresholds set here are based on the criteria outlined above, and these could be further improved by including more well-documented historical events and studies on damage of TCs by each of the three hazards (wind, storm surge, and rainfall).

**Table 6.3** Category thresholds for each hazard

Category	Wind speed (m/s)	Storm surge (m)	Accumulated rainfall (mm)
5	≥70	≥4.00	≥750
4	59-69	3.15-3.99	589-749
3	50-58	2.35-3.14	426-588
2	43-49	1.55-2.34	263-425
1	33-42	0.75-1.54	100-262
0	<33	<0.75	<100

The separate categories in Table 6.3 can already be used in risk communication, especially for TCs where one hazard is the main driver of the TC risk, such as extreme rainfall driving inland flooding. As flooding risk requires different storm preparation strategies than for instance wind risk, risk communicators may wish to convey this distinct TC risk by communicating the separate categories (e.g. a Category-5 rain event) rather than the final category, as is presented next.

After defining the categorization for each separate hazard, these categories are combined into one final category that will be used for risk communication to the general public. This final category needs to adequately reflect the severity of the TC in one location. Therefore, we define a set of constraints that the final categorization should meet:

1. The final category can never be lower than the highest hazard-based category;

2. The TCSS should adequately reflect the case of high potential risk of two or more hazards. We consider a hazard of high risk when its respective category is classified as 3 or higher (equal to the definition for a Major Hurricane on the SSHWS). Whenever (at least) two high risk hazards have the same category value and the third hazard has a lower category value, the final category should increment the highest hazard-based category. This implies that a TC scoring a Category 3 on both wind and storm surge, and a Category 1 on rainfall, will be classified as a Category 4.
3. To warn the general public for an event with multiple extreme hazards, a high-risk TC can be classified as a Category 6 when either (i) at least two of the hazard-based categories are of Category 5; or (ii) two categories are of Category 4, and one of Category 5.

To end up at the final category, we first rescale each of the hazard categories using rescaling values (see Table 6.4). These rescaling values have been chosen such that the set of constraints for the final category are maintained. The reason we implement these rescaling values is twofold. First, it is not possible to sum the hazard-based categories as is; a TC scoring a Category 5 and two Category-0s as hazard-based categories would end up as a final Category 5, while a TC scoring a Category 2 on all three hazards would end up as a final Category 6. This would thus violate the above set of constraints. Second, these rescaling values enhance implementation in data post-processing algorithms, as this is a mathematical procedure that can easily be carried out by any programming language. The alternative, i.e. a decision tree based on the set of constraints outlined above, is a more complicated procedure to both implement and execute. The final category is now determined from the sum of these rescaling values, see Table 6.5.

**Table 6.4** Rescaling values for each of the hazard categories

Category of hazard	Rescaling value
5	40
4	20
3	9
2	2.5
1	0.5
0	0

**Table 6.5** Determination of the final category of the tropical cyclone, with the rescaling values resulting from Table 6.4.

Final Category	Sum of rescaling values
6	≥80
5	40-80
4	18-39
3	9-17
2	2.5-8
1	0.5-2.4
0	<0.5

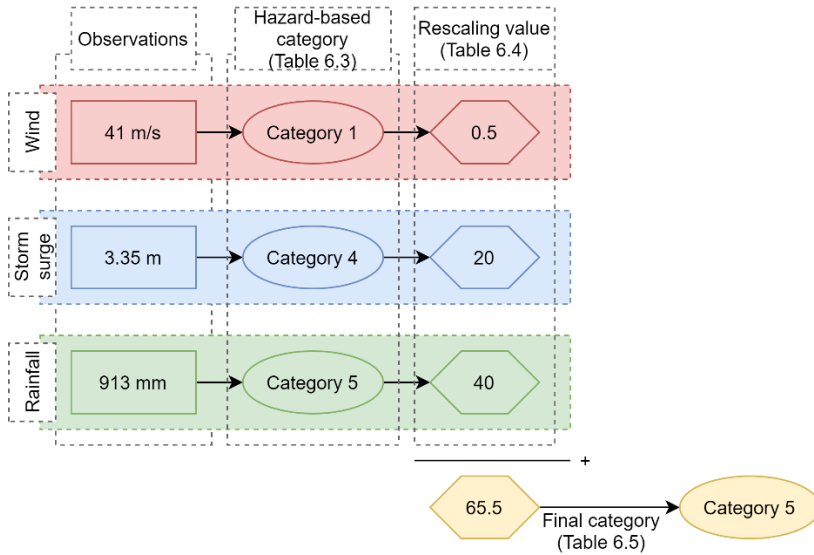


**Figure 6.1** Flowchart demonstrating the application of the Tropical Cyclone Severity Scale to Hurricane Florence (2018)

To demonstrate the use of the TCSS, Figure 6.1 shows the application to Hurricane Florence (2018). Upon landfall in North Carolina, Hurricane Florence had a maximum wind speed of 41 m/s, a maximum storm surge height of 3.35 m, and maximum precipitation total of approximately 913 mm. Based on Table 6.3, we categorize the wind as a Category 1, the storm surge as a Category 4, and the precipitation totals as a Category 5. Using Table 6.4, these categories would receive a rescaling value of 0.5, 20, and 40, respectively, summing up to a total of 65.5 points. Hence, based on Table 6.5, Hurricane Florence is categorized as a Category 5 on the TCSS.

Hurricane Florence is a typical case where risk communicators could benefit from the individual as well as the combined nature of the TCSS. Florence’s Category-5 ranking is mainly driven by its extreme storm surge and rainfall, which would require

different preparation strategies as opposed to a wind event. Here, risk communicators can clearly convey the imminent flooding threat by expressing that Hurricane Florence is a Category-4 for storm surge and a Category-5 for rainfall. Opting for such communication strategies, however, should be evaluated on a case-to-case basis. As such, the results presented in the next section are based on the final categories, but we will clarify the separate hazards wherever appropriate.

## 6.3 Results and discussion

### 6.3.1 Classification of past tropical cyclones on the Tropical Cyclone Severity Scale

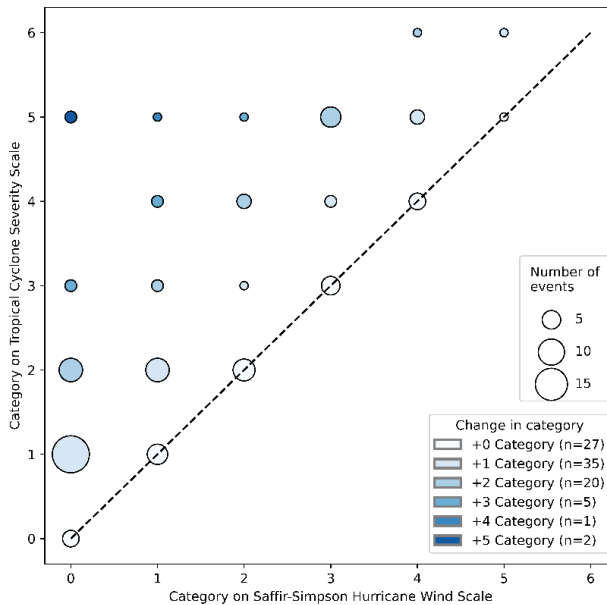


**Figure 6.2** Change in tropical cyclone categorization between the Saffir-Simpson Hurricane Wind Scale and the Tropical Cyclone Severity Scale. Numbers between brackets indicate the total number of landfalling events shifting in categorization

Figure 6.2 shows a comparison of the categories of all landfalling TCs between the SSHWS and the TCSS. Note that every individual landfall event is included, hence individual storms can be included multiple times. Overall, we see that many TCs increase in category with the TCSS compared to the SSHWS, which is expected given that we use the same thresholds for the wind hazard and give a rating equal to at least the highest hazard category. Of the total 90 landfalling TCs considered, 27 events have the same category using our proposed scale compared to the current SSHWS. The majority, however, is classified as a higher category: 55 TCs are classified one or two categories higher upon landfall, five TCs are three categories higher and one TC is four categories higher. There are also two TC landfall events that are classified

five categories higher (i.e. from tropical storm to Category 5: Tropical Storm Allison upon landfall in Texas and Louisiana). We find that the new Category 6 is only given to two TCs that were classified as Category 4 or 5 on the SSHWS, namely Hurricanes Wilma (2005; landfall in Mexico) and Michael (2018; landfall in Florida) respectively.

Next, Table 6.6 lists the 14 unique TCs that are now classified as a Category 5 or 6 on the TCSS. On the TCSS, the aforementioned Hurricanes Michael and Wilma are classified as a Category 6 due to the combination of high winds and storm surge (Michael) and precipitation (Wilma). Michael made landfall near Panama City, FL, and its wind and storm surge caused “devastating to catastrophic damage in Bay County, Florida” (Beven II et al., 2019), resulting in five direct deaths and an estimated 18.4 billion US\$ in damage in Florida alone. Wilma hit Yucatan, Mexico, and despite official information on damage not being available, some reports state that conditions were very severe in portions of the peninsula (Pasch et al., 2006). Aside from these two Category-6 TCs, 12 TCs are classified as a Category-5 on the TCSS, of which one was also classified as a Category-5 on the SSHWS, namely 2017 Hurricane Irma. This implies that the remainder of the TCs are upgraded in classification using the TCSS, with seven out of twelve classifying as a Category-5 on storm surge, and three as a Category-5 on precipitation. 2016 Hurricane Matthew is the only TC in this list with lower hazard-based categories, but which combination ends up at a final Category-5.

**Table 6.6** Overview of Category 5 and 6 tropical cyclones on the Tropical Cyclone Severity Scale (TCSS), and how this categorization compares to the Saffir-Simpson Hurricane Wind Scale (SSHWS) at the location of maximum severity

Name	Year	Landfall location of maximum severity	SSHWS	TCSS	Composition of TCSS (wind-surge-rain)
Michael	2018	Tyndall Air Force Base, Florida	5	6	5-5-2
Wilma	2005	Cozumel, Mexico	4	6	4-5-5
Florence	2018	Wrightsville Beach, North Carolina	1	5	1-4-5
Irma	2017	Cayo Romano, Cuba	5	5	5-4-1
Maria	2017	Yabucoa, Puerto Rico	4	5	4-3-5
Matthew	2017	Jauco, Cuba	4	5	4-4-4
Joaquin*	2015	Rum Cay, Bahamas	3	5	3-5-1
Ike	2008	Galveston Island, Texas	2	5	2-5-3
Emily	2005	Tulum, Mexico	4	5	4-5-1
Katrina	2005	Louisiana/Mississippi border	3	5	3-5-2
Rita	2005	Johnson’s Bayou, Louisiana	3	5	3-5-1
Charley	2004	Playa del Cajío, Cuba	3	5	3-5-1
Ivan	2004	Pine Beach, Alabama	3	5	3-5-1
Allison <sup>1</sup>	2001	Freeport, Texas	0	5	0-1-5

<sup>1</sup> Hurricane Joaquin and Tropical Storm Allison made a second landfall, also as a Category 5 on the TCSS, close to the landfall location given in this table. To avoid repetition, these events have been excluded.



### 6.3.2 Local-scale application of the Tropical Cyclone Severity Scale

To demonstrate the applicability of the TCSS in local-scale warnings, Figure 6.3 shows the categorization on the SSHWS (left) and the TCSS (right) for Hurricane Harvey based on observational data (Blake and Zelinsky, 2018). Whilst conditions in the majority of the affected region would have been classified as a Tropical Storm on the SSHWS, the TCSS shows a clear spatial distribution of categories, ranging from Category 0 in the outer regions to Category 5 around the Houston-Port Arthur area. These higher categories are driven by Harvey's high accumulated precipitation totals, up to 1.5 m near Port Arthur. By using the TCSS, official warning channels can warn citizens at the local scale for imminent severe conditions from either wind, storm surge, or rainfall, or a combination of these hazards.

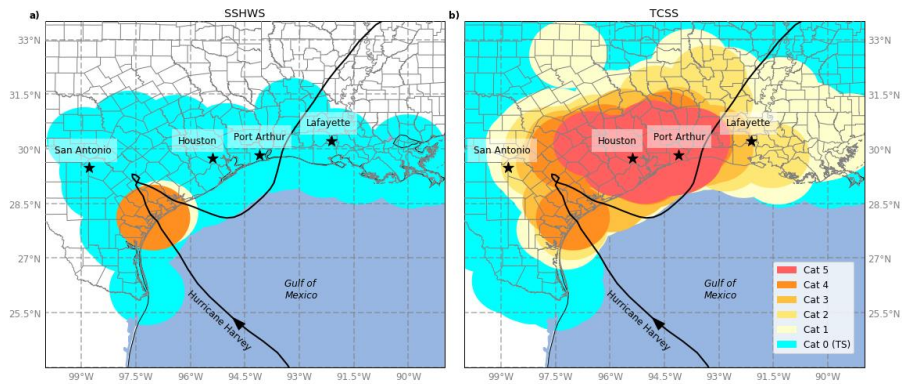


**Figure 6.3** Spatial distribution of Hurricane Harvey's (2017) category based on (a) the Saffir-Simpson Hurricane Wind Scale (SSHWS) and (b) the Tropical Cyclone Severity Scale (TCSS). Categorization is based on available observational data

### 6.3.3 Categorizing the costliest U.S. tropical cyclones

To further illustrate the use of the TCSS, Figure 6.4 shows the costliest TCs between 1996-2018 (NOAA, 2020a). As actual impact also depends on exposure, we do not expect a perfect match, but given that the TCSS reflects the severity of a storm, and arguing that a severe storm can cause more damage, we do anticipate that TCs that caused extensive damage will also score high on the TCSS. Note that the SSHWS categories for the top-20 of the costliest TCs since 1996 vary considerably, including a Tropical Storm (Allison) and four Category-1 TCs at landfall. On the TCSS, 16 out of 20 TCs are classified as a major hurricane (Category 3 or higher), nine of these being in the top-10. The only exception in this top-10 is Hurricane Sandy (ranked the 4<sup>th</sup> costliest hurricane), which is categorized as a Category-1 on the SSHWS and a Category-2 on the TCSS. Although not being a very intense storm, Sandy was an exceptionally large storm, affecting a large portion of the U.S. East Coast through its storm surge and rainfall. Most of the damage occurred approximately 150 km north

of the landfall location, around New York City. Here, the shape of the New York Bight region caused exceptionally high storm surges (>4 m) (Brandon et al., 2014), which would have been classified as a Category 5 for that location. This combined with the high population and asset density of that area resulted in the high aggregated damages associated with Sandy. Overall, the effects of high storm surges and rainfall totals are clearly visible in Figure 6.4 by the transition in category: TCs with a higher category on the TCSS obtained this category through a higher categorization on storm surge/precipitation than on wind speed. These results therefore underline earlier findings that storm surge and precipitation considerably add to TC damages (Bakkensen et al., 2018; Neumann et al., 2015b).

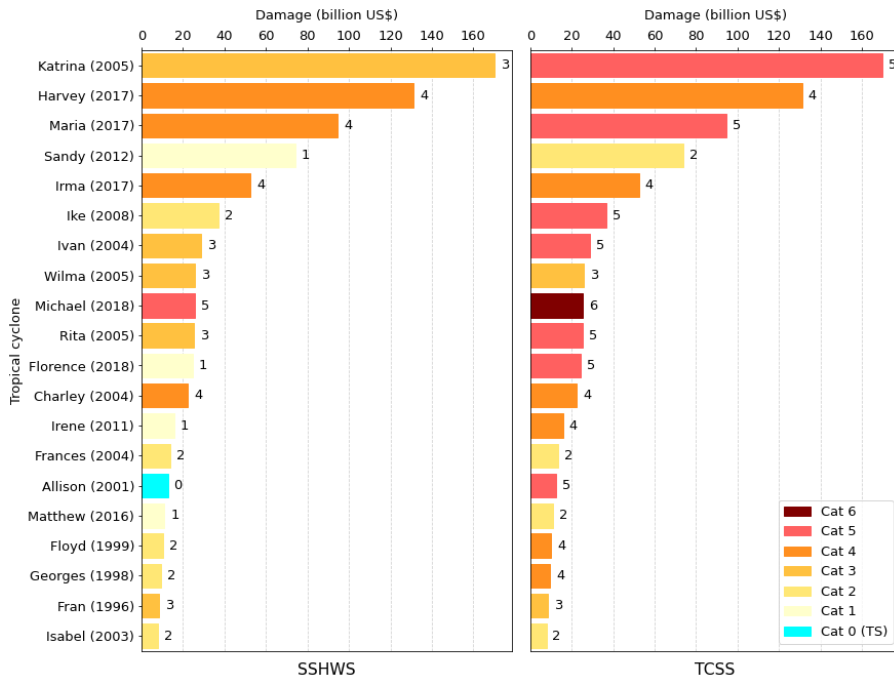


**Figure 6.4** Overview of the top-20 costliest U.S. tropical cyclones between 1996-2018 and their categorization based on (a) the Saffir-Simpson Hurricane Wind Scale (SSHWS) and (b) the Tropical Cyclone Severity Scale (TCSS). These damages are totals over the U.S. per event and are adjusted for inflation to 2020 US\$ using the Consumer Price Index adjusted cost. Note that Hurricane Jeanne (2004; 17<sup>th</sup> costliest between 1996-2018) is excluded as no observed storm surge height within 100 km from the landfall location was given in the official tropical cyclone report.

### 6.3.4 Limitations and directions for future research

In the previous sections, we demonstrated that the TCSS performs well in reflecting the TC’s major hazards in terms of potential impacts. As with any system of categorization, there are, however, some limitations to the usage of this scale; these are briefly reflected upon in this section.

First, the classification thresholds of the scale could be further improved by including more (well-documented) historical events and studies on damage of TCs. Moreover, studies on risk perception and behavior could provide valuable input on how the public perceives the scale with the method of combining categories, as well as the practicality of use of the TCSS. Future research on the comprehension of the use of a single category (i.e. our proposed final category) versus using individual hazard categories (which underlie our proposed final category), and the use of Category 6 events, in communication to the public should be considered as they are novel and have not been investigated before.

Second, the current scale is developed for the North Atlantic basin but can theoretically also be used for TCs in other basins. The thresholds of the underlying hazard categories likely have to be revised per basin, as the potential to cause damage and fatalities may be different in other basins. For instance, the rainfall categorization thresholds used in the current version of the TCSS (for the North Atlantic) may not necessarily cause as much problems in areas that have e.g. seasonal monsoons, thus being more used to such rainfall amounts.

Third, the TCSS does not explicitly account for the compound effects of multiple hazards, as the hazards are not interlinked. An example of such compound effect is rainfall water accumulating inland because the rivers cannot discharge into the sea due to high storm surges, even though these hazards by themselves would have had limited impact (e.g. van den Hurk et al. (2015)). While the current generation of numerical weather models are capable of providing accumulated rainfall forecasts days prior to a landfall event, and the hydro-dynamical model SLOSH is currently used to estimate storm surge heights along the coasts, the combined effect of these hazards is yet to be represented in models. Such compound effects can be analyzed by coupling hydraulic models (fluvial/pluvial flooding) with hydro-dynamical models (storm surges). Once such a model setup is in place and used in the forecasting of storm surges, the TCSS would then reflect such compound effects as well.

Finally, the design of the TCSS allows for categorization of those TCs that affect land through wind, storm surge, and rainfall. This also implies that risk communication for TCs that either remain over sea, or at time steps where the TC is over open waters, is not possible using the full TCSS, since storm surge and precipitation data are generally absent at these locations. As this can play a role in e.g. risk communication for marine traffic, we suggest using solely the wind categorization of the TCSS (the SSHWS) for these specific situations.

## 6.4 Concluding remarks

We have presented a new method of categorizing TCs based on wind speed, storm surge, and precipitation totals. Our Tropical Cyclone Severity Scale (TCSS) first categorizes each of these three hazards separately, and subsequently derives a final category based on the combination of hazard categories. This final category is a

number between 0 and 5, following the discrete nature of the current Saffir-Simpson Hurricane Wind Scale (SSHWS), and is extended by a Category 6 for storms that are extremely severe on several fronts. By first assessing each of the hazards separately and then combining them into one holistic scoring, the TCSS adequately reflects the true TC severity, which will result in better risk communication, evacuation strategies, and humanitarian response. Examples of TCs that score substantially higher on the TCSS compared to the SSHWS are Tropical Storm Allison (2001; Tropical Storm on SSHWS versus Category 5 on TCSS), and Hurricane Ike (2008; Category 2 on SSHWS versus Category 5 on the TCSS). Overall, two TCs that occurred between 1996 and 2018 would have been classified as a Category 6 upon landfall, namely Hurricanes Michael (2018) and Wilma (2005). We showed that the top-20 costliest U.S. hurricanes score higher categories on the TCSS as opposed to the current SSHWS, hereby better reflecting the relationship between TC severity and potential impact on society.

The TCSS is set up to be used pre-landfall, using data available from meteorological and hydrological forecasts. As such, it can be used to create a spatially varying scale, to define different categories for different locations (see Figure 6.3 for a demonstration). This way, the TCSS can assist in more localized risk communication and evacuation strategies. Moreover, the specific hazards of an approaching storm can be communicated easier to the public by referring to the individual hazard categories (e.g. Category 5 for rainfall, but Category 1 for wind and surge). This opens up more possibilities of understanding and communicating the TC's severity, hereby improving information communication to the general public and allowing for enhanced storm preparations and, ultimately, saving more lives.

## Acknowledgments

This research has been funded by a VICI grant from the Netherlands Organization for Scientific Research (NWO) (Grant Number 453-13-006).



## 7 Synthesis

## 7.1 Introduction

With tropical cyclones (TCs) posing a significant risk to coastal communities under present-climate conditions, it is crucial to enhance our understanding of changes in TC risk under climate change so that adequate risk mitigation strategies can be designed and implemented. Therefore, the research goal of this thesis was set as follows:

To improve our understanding of TC risk by developing a global-statistical synthetic model to assess return periods of TCs in the current and future climate, including low-probability events, and by improving risk communication strategies.

This goal was addressed through the five research questions defined in Chapter 1. This final chapter revisits these research questions and summarizes the main findings (Section 7.2). It then discusses the remaining challenges in improving our understanding of global-scale TC risk under climate change (Section 7.3) and ways forward for research and management (Section 7.4).

## 7.2 Overview of the main findings

### 7.2.1 Which model resolution is sufficient to adequately represent tropical cyclones in climate datasets?

In Chapter 2, we used the ECMWF Integrated Forecasting System (IFS) at 0.225° (T799) horizontal resolution as meteorological forcing for the storm surge modeling of eight historical TCs, using the Global Tide and Surge Model (GTSM). Comparing the modeled maximum surge heights of Hurricanes Irma (2017) and Sandy (2012) with tide gauge stations resulted in  $R^2$ -values of 0.86 and 0.74, respectively. For the other six TCs, we found that modeled maximum surge heights are generally lower than reported heights. For most TCs, the difference between the observed and modeled maximum surge heights is less than 0.5 m. On the basis of that difference, we concluded that the IFS-GTSM model setup at T799-resolution framework is capable of capturing the large-scale spatial patterns of the maximum surge heights.

Next, we analyzed the effects of different horizontal resolutions of meteorological forcing data on the simulated maximum surge heights by upscaling the meteorological forcing of the eight historical TCs to various coarser resolutions, between 0.25° to 1.0°. Simulated TC storm surges are lower using coarser resolution datasets compared to using the T799-resolution forcing, with differences varying between 0.01 m for Hurricane Patricia (2015) and 1.02 m for Irma. We observed that the effect of coarser resolution was largest for TCs with the highest surge heights. Hence, TCs with high storm surges require high-resolution meteorological forcing for accurate storm surge and impact modeling.

Furthermore, we examined the relationship between storm surge heights and several geographical characteristics known to influence them: intensity, TC size, coastal

complexity, and coastal slope. In the eight TCs examined in this study, the geographical characteristics have a larger effect than the TC characteristics, with the highest storm surges found in regions with high coastal complexity and, in general, a small slope.

Our findings show that the use of high-resolution meteorological forcing is particularly beneficial for areas prone to high (several meters) TC storm surges, such as areas with low slopes and high coastal complexity. We also concluded that coarser-resolution datasets can be used in areas generally experiencing limited surge heights (i.e., smaller than 0.5 m) as the reduction of these surges was limited compared to observations.

### 7.2.2 Can we build a global-scale, fully statistical synthetic tropical cyclone model, to simulate tropical cyclone activity over longer temporal time scales?

Synthetic models are useful tools to overcome the short temporal time scale of historical observations and meteorological data from global climate models (GCMs). Previously developed global-scale synthetic models were, however, set up as coupled statistical-dynamical models using information on a wide range of (environmental) variables as input (Emanuel et al., 2006; Lee et al., 2018). Fully statistical models requiring fewer variables have thus far only been developed for the local scale (e.g. Haigh et al., 2014; James and Mason, 2005; Vickery et al., 2000).

To apply the benefits of statistical modelling on the global scale, we presented the Synthetic Tropical cyclOne geneRation Model (STORM) in Chapter 3. STORM is a fully statistical model that can be applied to any meteorological dataset to statistically resample and model TC tracks and intensities. We applied STORM to 38 years (1980–2017) of historical TC data from IBTrACS (Knapp et al., 2010) to statistically extend this dataset to 10,000 years of TC activity. For each historical TC, we extracted its genesis month, longitudinal and latitudinal position of the eye, the maximum wind speed, minimum pressure, and radius to maximum winds. Furthermore, we extracted information on environmental conditions, such as the mean of monthly mean sea-level pressure and sea-surface temperatures from the ECMWF’s fifth-generation climate reanalysis dataset ERA5 (Hersbach et al., 2019). As output, the resulting STORM dataset contains the following information for every synthetic TC track at three-hourly resolution: longitudinal and latitudinal position of the eye, minimum pressure, maximum wind, radius to maximum winds, category on Saffir-Simpson Hurricane Wind Scale, landfall flag (0 = no landfall, 1 = landfall), and distance to land.

STORM is validated by comparing TC statistics, such as frequency and intensity against IBTrACS. The mean values of all TC variables were all found to be within one standard deviation of the values in IBTrACS. The largest deviations between STORM and IBTrACS in average maximum wind speed along the TC track on a



basin scale were approximately 2 m/s, with an equal number of basins having higher and lower wind speeds compared to IBTrACS. As such, we concluded that STORM mimics the TC statistics from the input dataset well and that the STORM model is capable of simulating long(er) periods of TC activity while preserving the characteristics found in the shorter input dataset. It is, however, important to note that the presented STORM dataset is based on the average climate conditions from 1980 to 2017 and does not capture climate variability. In addition, the STORM model statistically resamples the TC statistics in the input dataset; therefore, the performance of STORM inherently depends on how well the TC characteristics are captured in the input dataset.

### 7.2.3 What is the global distribution of tropical cyclone wind speeds for extreme (low-probability) events, and how do these compare to observed tropical cyclone activity?

In Chapter 4, we demonstrated the application of the STORM dataset to generate a novel, open-access dataset of wind speed RPs for all TC basins. Using this dataset, we empirically derived RPs at three spatial levels: 1) at a basin-level, 2) within 100 km of selected coastal locations, and 3) at a 10 km resolution grid. First, we demonstrated the benefit of using such a large synthetic dataset, composed of 10,000 years of TC activity for present-day climate conditions, over using only 38 years of observed TCs for the calculation of RPs. Compared to the empirically derived RPs, fitting a continuous extreme value (EV) distribution to 38 years of data typically leads to considerably higher wind speeds (max U10), especially for RPs exceeding 100-yr. Second, we calculated RPs for TCs within 100 km of 18 coastal cities spread out across all basins, illustrating the geographic differentiation of TC hazard within and between basins. Finally, we estimated RPs at 10 km resolution by applying a 2D-wind-field model to the synthetic TCs. This dataset is applicable for high-resolution TC wind risk assessments, including local-scale assessments—for example, for Pacific or Caribbean island countries.

To assess our model performance, we compared the RPs from STORM against those derived from other synthetic models and found that wind speeds for specific RPs generally agree well. In 13 out of 18 cases, wind speeds were within 5 m/s of each other. Near basin boundaries, RPs are often lower compared to other models; this is because STORM is run at the basin scale and because TCs are cut off at the basin boundaries. For regional-scale studies, this issue can be solved by applying STORM with adjusted basin boundaries. On the global scale, we observed spatial RP patterns for a Category-1 event that were similar to the literature. However, larger deviations arose when looking at the distribution of Category-3 RPs, particularly in the Southern basins (Lee et al., 2018).

#### 7.2.4 What is the influence of climate change on the spatial distribution of tropical cyclone wind speed possibilities, especially for low-probability events?

In Chapter 5, we applied the STORM model to generate 10,000 years of synthetic tracks under climate change for 2015–2050. To do so, we used information from four GCMs. TC characteristics such as intensity, however, are often poorly captured in these GCMs (Roberts et al., 2020a). Combined with the fact that STORM amplifies the input data to longer time scales, this poor representation would have propagated through the STORM model and could have significantly affected the outcomes.

To address these issues, we present a novel methodology that maintains the benefits of using STORM and GCMs but that circumvents the potential propagation of the poor TC representation. This methodology is based on the delta approach and follows three steps, applied to each of the GCMs separately: First, we extract the change in TC variables that are part of STORM, calculated as the difference between present and future climate GCM data – referred to as the delta. Second, we apply the delta to the IBTrACS data that was used for the derivation of the present-climate STORM dataset. This step creates a future-climate version of the historical TC statistics but omits the first-order model biases (e.g., too low TC intensity) present in the GCMs. Third, we use these TC statistics as input for STORM and generate 10,000 years of synthetic tracks and high-resolution wind speed maps for different RPs. Results show that most TC-prone regions will face an increase in TC wind speed hazard under near-future climate change, with the largest increases found in the South Pacific and Hong Kong region. Furthermore, by overlaying the hazard maps with population maps, we found that predominantly developing countries, such as Cambodia and Yemen, will face the largest changes in exposed population under near-future climate change.

#### 7.2.5 Can the Saffir-Simpson Hurricane Wind Scale be improved by accounting for the combination of wind, storm surge, and precipitation?

The widely used Saffir-Simpson Hurricane Wind Scale (SSHWS) classifies a TC based on its maximum 1-minute sustained wind speeds (increasing in severity from Category 1 to 5). Historical storms, such as Hurricane Katrina (Category 3) and Tropical Storm Harvey, however, caused widespread havoc not because of strong winds but predominantly through their storm surge and rainfall. This reality demonstrates the fallibility of the SSHWS in reflecting the severity of a TC. To overcome this limitation of the SSHWS and to enhance risk communication for such TCs, we presented a new method of categorizing TCs based on wind speed, storm surge, and precipitation totals. Our Tropical Cyclone Severity Scale (TCSS) first categorizes each of these three hazards separately and subsequently derives a final severity rating based on the combination of hazard categories. This final category is a number between 0 and 5, following the discrete nature of the current SSHWS. It

also includes a Category 6 rating for storms that have multiple very severe hazards. We found that the top-20 costliest US hurricanes scored higher categories on the TCSS (mostly Category 4 and 5) as opposed to the current SSHWS. Thus, the TCSS better reflects the relationship between TC severity and potential impact on society.

The TCSS is designed to be used pre-landfall and uses data available from meteorological and hydrological forecasts. As such, it can be used to create location-specific forecasts of TC severity using information already available in these current forecasts. As a result, the TCSS can assist in increased risk communication at the local level. Moreover, by first assessing each of the hazards separately and then combining them into one aggregate score, the TCSS better reflects the TC severity, contributing to improved risk communication, evacuation strategies, and humanitarian response. The specific hazards of an approaching storm can be communicated more easily to the public by referring to the individual hazard categories (e.g., Category 5 for rainfall, but Category 1 for wind and surge). This precision opens up more possibilities to understand and communicate a TC's severity, thereby improving information communication to the general public, allowing for enhanced storm preparations and, ultimately, saving more lives.

### 7.3 Directions for future research

Global-scale synthetic TC models, such as the STORM, CHAZ (Lee et al., 2018), and the MIT model (Emanuel et al., 2006) greatly advance our understanding of the distribution of TC events, and particularly of the low-probability, high-impact events. It is not surprising to see such models are at the heart of TC risk assessments, both in academia and the industry (e.g., Commonwealth of Australia, 2013; Lin and Emanuel, 2016; Sobel et al., 2019). There are opportunities for research to further improve and exploit such models, as discussed below.

#### 7.3.1 Studying tropical cyclone hazards

The current generation of global-scale synthetic TC models primarily model a TC's wind speeds. These synthetic tracks are then translated to a 2D wind field either by using nested models (e.g. Emanuel et al., 2006), or by applying a 2D-parametric wind field model. In this research, we applied the Holland parametric wind field model (Holland, 1980). This model is widely used and requires few parameters (i.e., forward speed, minimum pressure, and maximum wind speed) compared to more complex models. The Holland model, however, is relatively simple in the representation of the wind field in that it assumes the asymmetry in the TC wind field to arise from background flow. Enhanced wind shear (e.g., in extratropical regions), however, may also induce asymmetry. In addition, the Holland model does not take into account surface friction, which can have a substantial effect on the representation of inland winds. Other more complex wind field models, such as the Done et al. (2020) model, do take surface friction into account, hereby better representing the TC wind field. These models, however, also require information on variables currently not part of

most synthetic model output. In addition, they are computationally more intensive, complicating the application of these models to large synthetic databases such as STORM. Nonetheless, when future generations of synthetic models include all variables necessary for wind field models like the Done et al. (2020) model, they will likely become very valuable for studying extreme events in regions of interest.

The total hazard emerging from a TC, however, is not solely composed of wind speed but also consists of storm surge and precipitation (see Chapter 6). TC storm surges can be simulated by using the synthetic model output as input for a hydrodynamic model. The MIT model, for instance, has been used to simulate TC storm surges at both local and continental scales (e.g. Garner et al., 2017; Lin and Emanuel, 2016; Marsooli and Lin, 2020; Meza-Padilla et al., 2015). Global-scale modeling of storm surges based on synthetic tracks is computationally intensive, but it is feasible given the recent advances in high-performance computing and numerical modeling. Dullaart et al. (2021) are the first to conduct such a study on the global-scale, coupling the present-climate synthetic tracks from STORM with the hydrodynamic model GTSM. However, when assessing changes in probabilities of TC-induced storm surges for a wide range of climate models, the computational costs of the hydrodynamic model rapidly escalate. One potential way to overcome this hurdle is to use statistical and machine-learning techniques, which can be used to build data-driven models that can predict water levels with good performance and at low computational costs (Tadesse et al., 2020; Tadesse and Wahl, 2021). In previous research, data-driven models were trained with wind speed, mean sea-level pressure, and water level data from tide gauges to predict water levels for other atmospheric conditions. A way forward would be to train such data-driven models with atmospheric and hydrodynamical data from synthetic models such as STORM (Dullaart et al., 2021). Next, the data-driven model can be run with for instance future-climate synthetic tracks to derive the corresponding future-climate storm surge heights. In so doing, we can identify hotspot regions prone to large changes in TC storm surge risk under climate change.

Precipitation also plays an important role in determining the severity of a TC. Global-scale synthetic models are currently not capable of generating rainfall probabilities. On a case study basis, Emanuel (2017) expanded the MIT model with a numerical rainfall model to simulate Hurricane Harvey's rainfall probabilities. However, the integration of a numerical rainfall model with synthetic models is computationally intensive and therefore infeasible for application to global-scale synthetic models spanning thousands of years. An alternative direction would be to develop a parametric 2D-precipitation field model similar to the parametric 2D-wind field model. Such a parametric model could build on existing knowledge on the relationship between TC characteristics and precipitation patterns: for example, the precipitation totals being closely related to maximum wind speeds (Cerveny and Newman, 2000) and the spatial precipitation pattern depending on the distance from the eye (Yu and Wang, 2018). Developing such a parametric model therefore requires

adequate understanding of the (inter)dependencies of various TC characteristics and deriving governing equations for the parametric model from these dependencies. Synthetic tracks can then be coupled to this model to derive rainfall RPs, similar to how wind speed RPs were derived in this thesis. This approach will yield a novel dataset composed of all major TC hazards, which can be used to assess the full scope of TC impacts in coastal regions, including inland and compound flooding hazards.

### 7.3.2 From hazard to risk

STORM paves the way to a better understanding of global-scale TC risk. Enhancing our understanding of TC risk, however, also requires enhancing our understanding of how the synthetic model's output influences TC risk calculations. First of all, besides STORM, there exist various global- and local-scale synthetic models, developed within academia or as part of a catastrophe model used in the insurance industry. To evaluate a model's performance, one can design a model intercomparison study, as, for instance, done by Sobel et al. (2019), who used two models to investigate one location. Such intercomparison studies are a powerful approach for enhancing our collective understanding of TC risk distributions (creating insights into the (dis)agreements between models) and for learning from other approaches and improving weaknesses in own models therefrom. Including more models and more locations in such intercomparison studies can improve our collective understanding of model strengths, weaknesses, and further development opportunities.

A similar model intercomparison study can be executed on TC risk. TC damages emerging from these synthetic TCs can be calculated, for instance, by coupling the synthetic tracks to a statistical model (e.g., Martinez, 2020) or to regional impact functions (Eberenz et al., 2021). By using a plethora of synthetic datasets as input for such models, we can improve our understanding of potential (expected annual) damages in TC-prone regions.

### 7.3.3 Limitations imposed by global climate models

The overarching limitation in analyzing TCs using meteorological data is often the model resolution or the temporal extent of the dataset. TCs are characterized by strong wind and pressure gradients, which are typically poorly captured by (coarse resolution) GCMs. This limitation was discussed at length in Chapter 2 and was the main reason to design the climate change methodology outlined in Chapter 5. While model resolution and TC representation are continuously improving (Bauer et al., 2015; Dullaart et al., 2020; Roberts et al., 2020a), the most intense TCs are still poorly captured by GCMs. This poor representation significantly affects TC risk assessments in coastal areas, where the most intense TCs often result in the most damaging events, thereby substantially contributing to TC risk (Emanuel, 2021). To circumvent this limitation, risk assessments are now often confined to the application of alternative methods, such as the delta approach (Chapter 5) or a downscaling method (Emanuel, 2021; Knutson et al., 2013; Lee et al., 2020). In the downscaling approach, variables

from GCMs are used as environmental conditions in a coupled TC model. TCs are then randomly seeded within the large-scale environment, governing the TC motion and evolution from genesis to dissipation. This method allows for the simulation of large sets of TCs within the same climate conditions, overcoming the limitations imposed by the GCMs themselves. In this approach, however, the impact of climate change on (the frequency of) TCs only follows from processes in the large-scale environment rather than from changes in the seed disturbances. Thus, this approach provides little information on changes in TC frequency under climate change.

STORM and other synthetic models overcome the short temporal extent of GCMs by statistically resampling the TC characteristics. There do currently exist GCM-derived datasets that are run for longer time scales than a few decades, such as the Community Earth System Model (Kay et al., 2015) or the Database for Policy Decision Making for Future Climate Change (Mizuta et al., 2017), both spanning thousands of years. These models, however, come with a coarse model resolution ( $0.5^{\circ}$ – $1^{\circ}$  globally), and as such, they likely will not adequately capture a TC's characteristics (Strachan et al., 2013). This clearly illustrates the trade-off between temporal length and model resolution: to overcome computational limitations, GCMs at longer time scales are generally run on spatial resolutions too coarse for adequate TC representation, while GCM experiments tailored toward good TC representation are run on time scales too short for adequate TC risk assessments. A straightforward solution would therefore be to increase computational power; this solution, though, unfortunately depends on technological advances that lie outside the scope of this research field. A workaround could therefore be to apply deep learning methods (Reichstein et al., 2019). These methods use information on linkages between large-scale atmospheric patterns and high-resolution processes, such as tropical convection from high-resolution GCMs, to train the data-driven model. Thereafter, these derived relationships could be applied to atmospheric patterns in coarse-resolution GCMs, run over longer time scales, so that these higher-resolution processes could still be identified and analyzed. This approach would allow us to look at relevant TC information over longer timescales and to assess changes in these TC characteristics for different variations in the climate and under various forcing scenarios.

### 7.3.4 Tropical Cyclone Severity Scale

TC classification categories are used by residents for disaster-related decision-making, such as evacuation behavior and preparedness measures. In the process of making such decisions, individuals often consider factors such as prior TC experiences or warning messages (Collins et al., 2017). When confronted with incomplete or inaccurate information, individuals are likely to spend more time gathering additional information before making a decision; this can cost valuable time during the window before a TC impacts (Bean et al., 2016; Perry and Lindell, 2006). Furthermore, residents have shown to rely heavily on the SSHWS category in their

decision-making processes (FEMA, 2014a, 2014b; Lazo et al., 2010; Morss and Hayden, 2010).

However, the SSHWS fails to capture the full severity of a TC. To overcome this limitation, we designed the TCSS and demonstrated that the severity of historical hurricanes is often better captured by using this new classification method. However, one important question that remains unanswered is whether the TCSS improves the public's decision-making processes and risk perception during an imminent storm compared to their response based on the SSHWS. In the context of this question, controlled experiments (e.g. Mol et al., 2021) could provide insight into whether people alter their decision-making process based on the additional hazard information provided by the TCSS. In addition, the TCSS currently does not take the influence of adaptation measures into account. Including such measures might change the TCSS category in a specific region, as (for instance) predicted storm surge heights might be lower due to effective measures.

## 7.4 Implications for tropical cyclone risk research and mitigation strategies

The results presented in this thesis contribute to the ongoing efforts of academia, the risk management community, and the insurance industry to better understand and mitigate TC risk. In this section, we outline potential applications of the results in this thesis to advance our collective efforts to better protect people and assets from these violent storms.

First, the STORM datasets and model follow the FAIR Guiding Principles (Wilkinson et al., 2016), allowing researchers to directly apply the data in their own work. STORM is currently being used in various TC risk assessment projects and catastrophe models, both within academia and at large (re)insurance and consultancy companies. Additionally, model comparison studies such as Meiler et al. (2021) provide a valuable tool to better understand the strengths and weaknesses of the different synthetic TC datasets.

Second, STORM has been designed to reproduce basin-scale TC characteristics and statistics, and has been shown to perform well on mimicking these basin-scale properties. The TC statistics in the future climate STORM datasets contain valuable information on the sign and magnitude of change in TC risk for TC-prone regions. This way, it becomes possible to identify which regions in the world are most vulnerable to changes in TC risk under the climate change scenarios assessed in this thesis. These regions can then be assessed in more detail by for example running local-scale high-resolution models. This assessment, in turn, can help improve or design risk mitigation strategies in these regions, such as improving forecasting capabilities and availability of insurance or designing building regulations for houses or storm shelters.

Lastly, the Tropical Cyclone Severity Scale (TCSS) strengthens the argument for a new and improved hurricane classification system. Over the past few decades, numerous studies have revived the discussion regarding the fallibility of the SSHWS (e.g. Holland et al., 2019; Irish and Resio, 2010; Kantha, 2006). Insights gained from categorizing either one, two, or all three TC hazards show that the currently used SSHWS has disadvantages when wind is not the main threat emerging from an imminent TC. As such, risk mitigation strategies in the form of preparing and evacuating societies in the path of a TC can benefit greatly from the use of a new hurricane classification system.





# Appendices

# Appendix A

## Supplementary Figures A

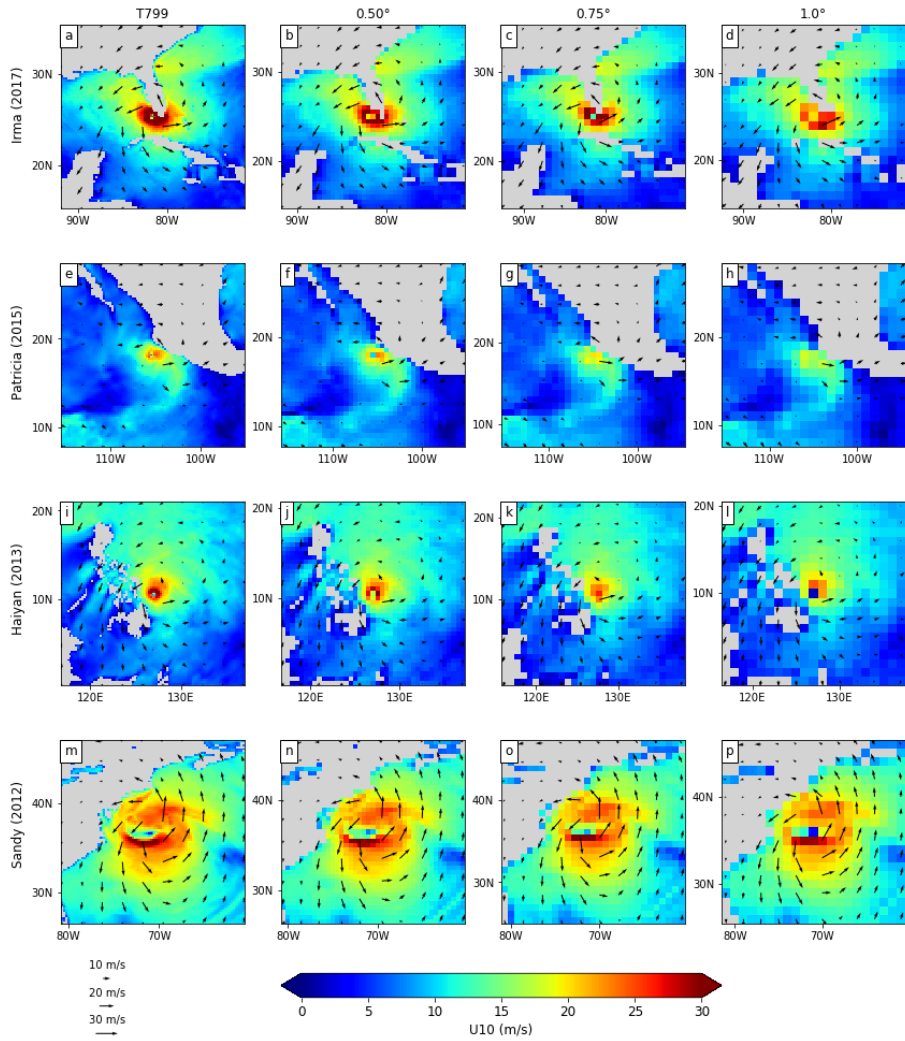


**Figure A.1** Spatial map of U10 for (a-d) Irma, (e-h) Patricia, (i-l) Haiyan and (m-p) Sandy. From left to right: T799, 0.50°, 0.75° and 1.0° resolution

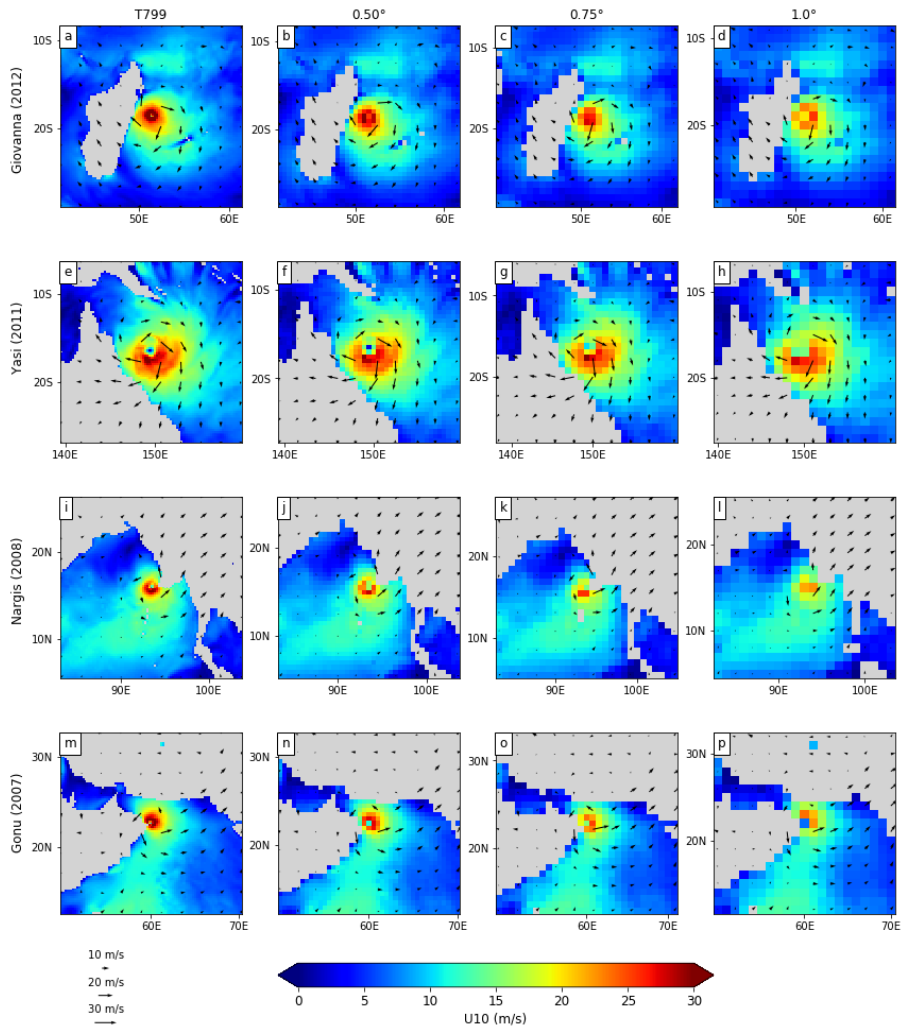


**Figure A.2** Spatial map of U10 for (a-d) Giovanna, (e-h) Yasi, (i-l) Nargis and (m-p) Gonu. From left to right: T799, 0.50°, 0.75° and 1.0° resolution

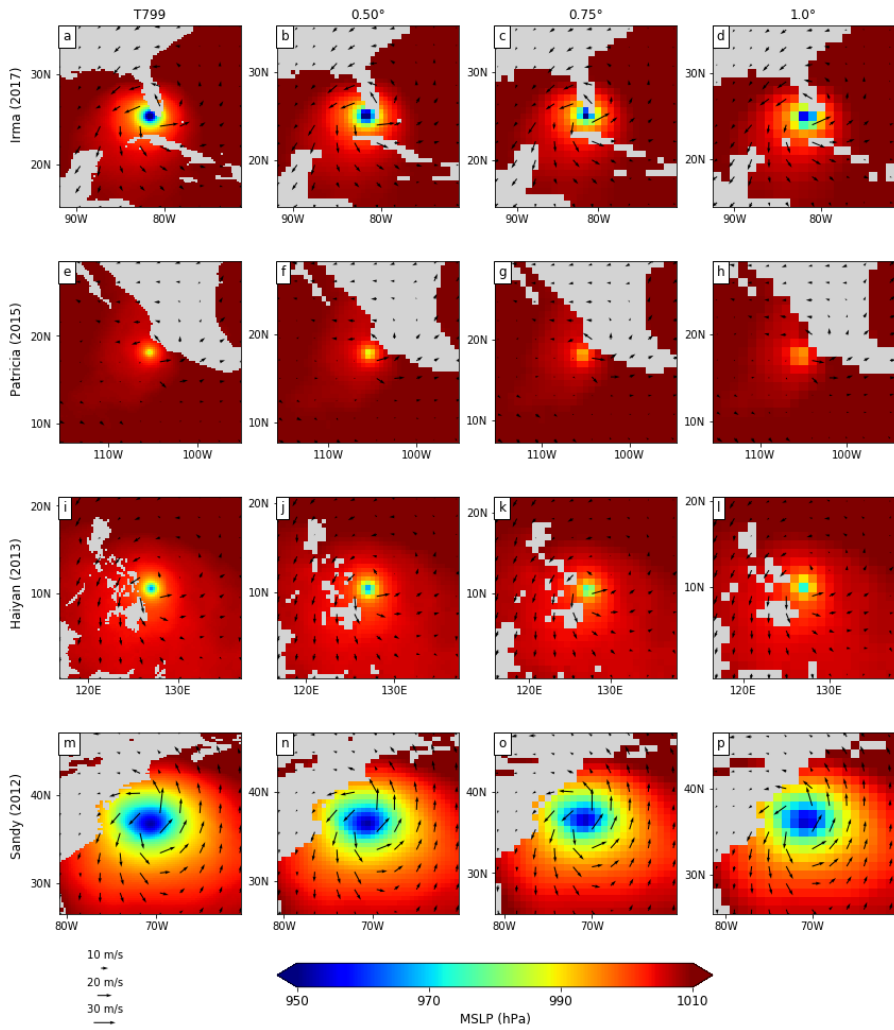


**Figure A.3** Spatial map of MSLP for (a-d) Irma, (e-h) Patricia, (i-l) Haiyan and (m-p) Sandy. From left to right: T799, 0.50°, 0.75° and 1.0° resolution

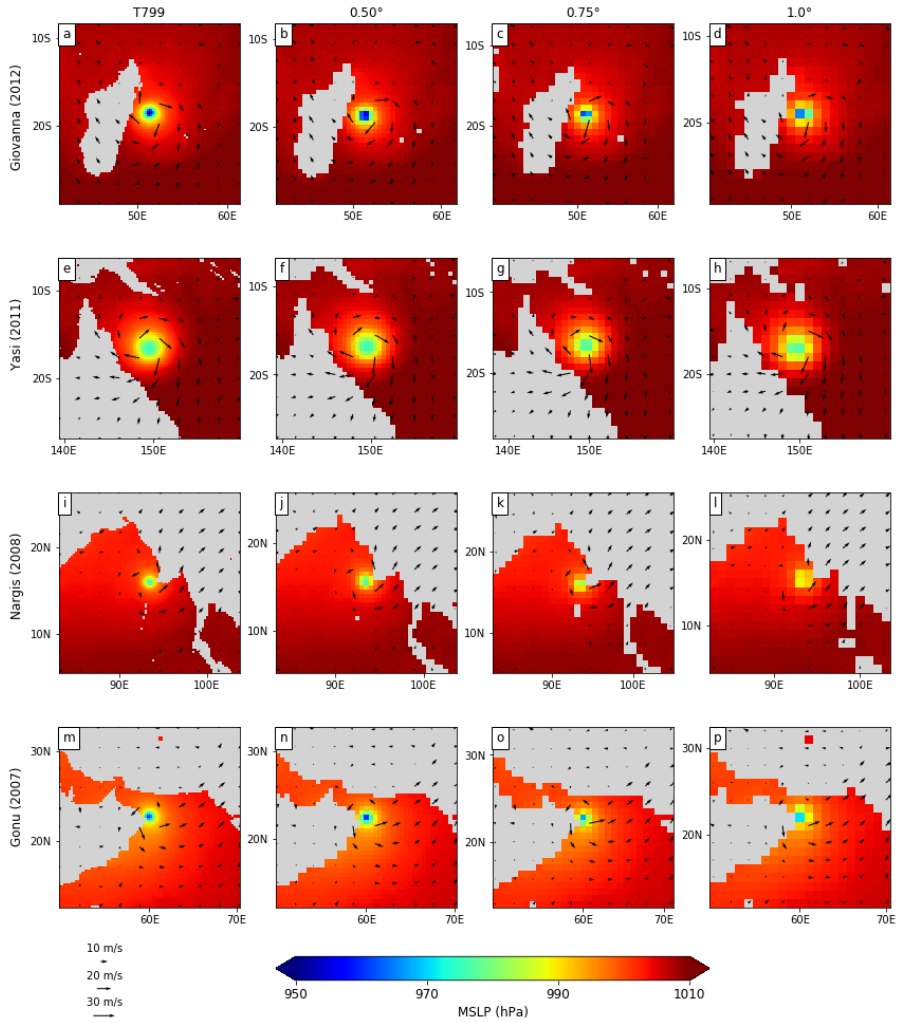


**Figure A.4** Spatial map of MSLP for (a-d) Giovanna, (e-h) Yasi, (i-l) Nargis and (m-p) Gonu. From left to right: T799, 0.50°, 0.75° and 1.0° resolution

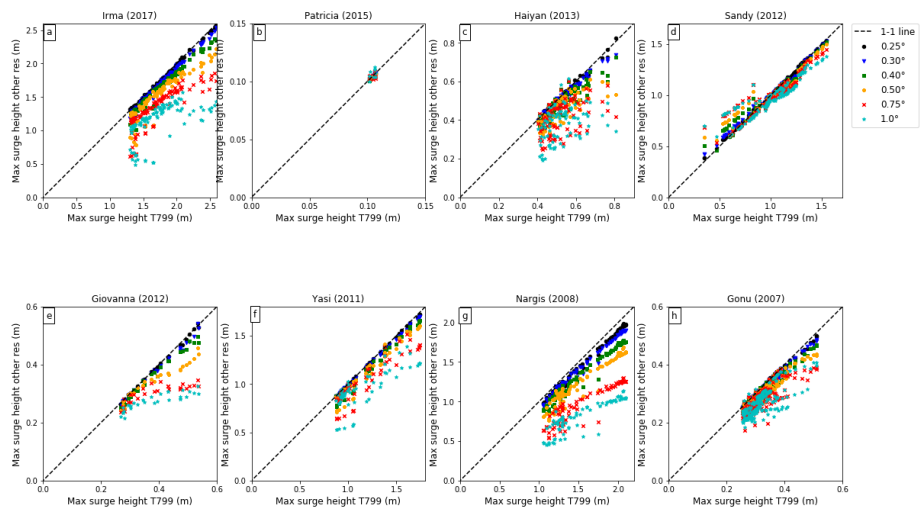


**Figure A.5** Scatterplot of maximum surge height at T799-resolution forcing vs. other resolutions for (a) Hurricane Irma (Florida), (b) Cyclone Giovanna (Madagascar), (c) Cyclone Yasi (Australia) and (d) Cyclone Nargis (Myanmar)

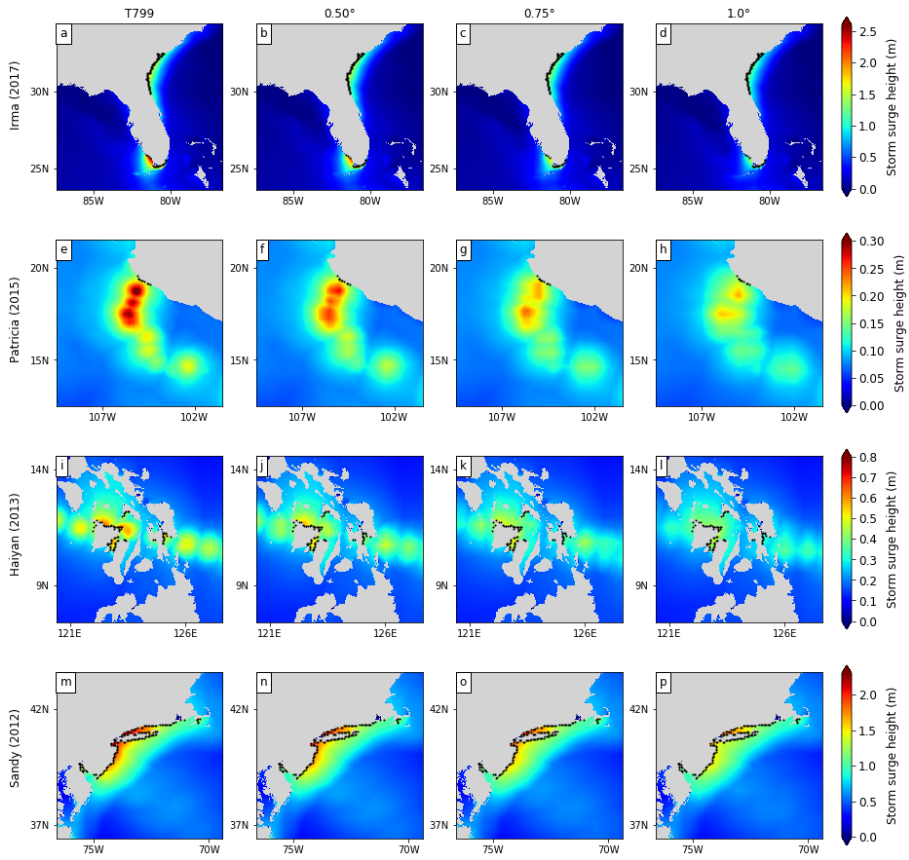


**Figure A.6** Spatial map of maximum storm surge heights for (a-d) Irma, (e-h) Patricia, (i-l) Haiyan and (m-p) Sandy. From left to right: T799, 0.50°, 0.75° and 1.0° resolution. Black dots represent GTSM coastal grid points used in the statistical analysis



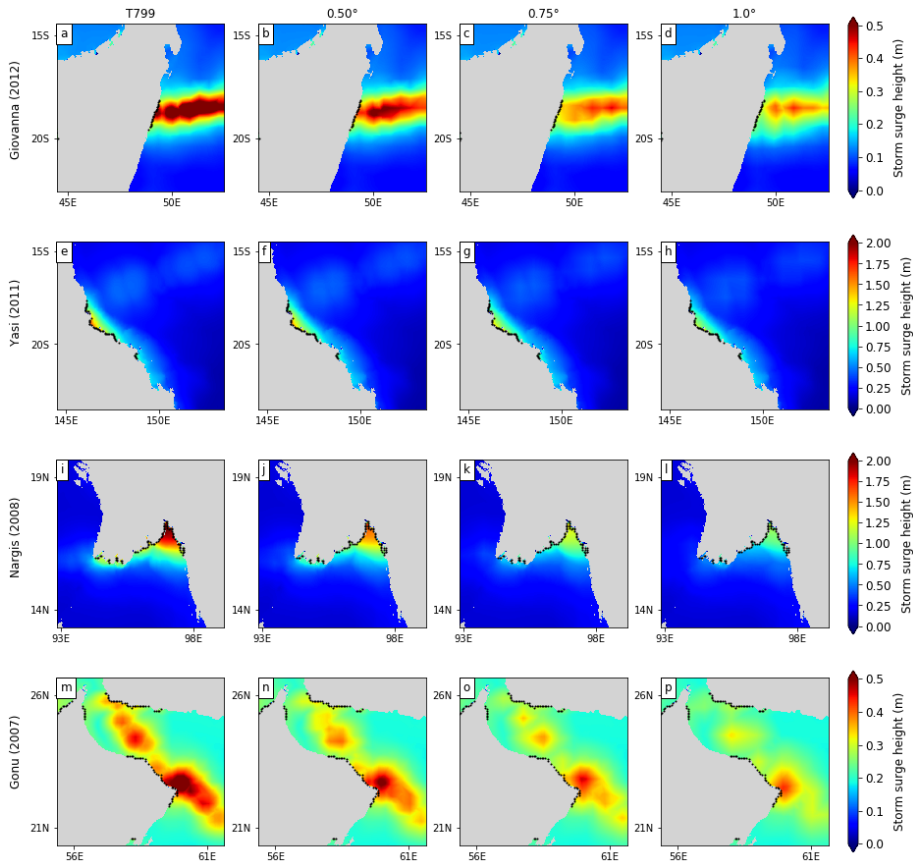


**Figure A.7** Spatial map of maximum storm surge heights for (a-d) Irma, (e-h) Patricia, (i-l) Haiyan and (m-p) Sandy. From left to right: T799, 0.50°, 0.75° and 1.0° resolution. Black dots represent GTSM coastal points used in the statistical analysis

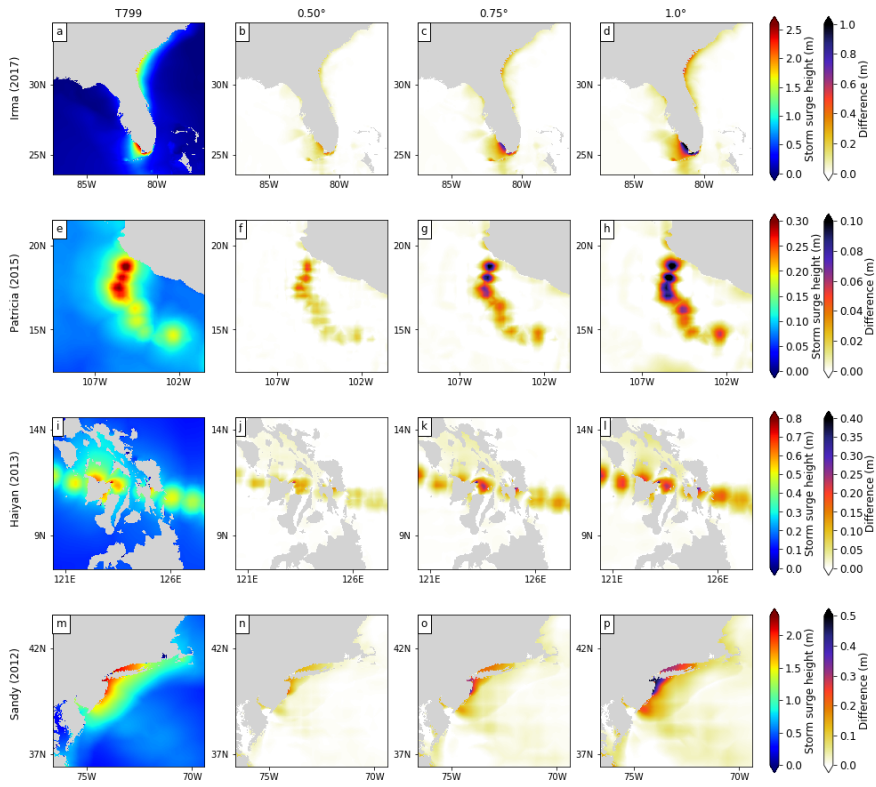


**Figure A.8** Spatial map of maximum storm surge heights and difference in maximum storm surge heights for (a-d) Irma, (e-h) Patricia, (i-l) Haiyan and (m-p) Sandy. From left to right: maximum storm surge height in T799 resolution forcing, difference between T799 resolution forcing and 0.50°, 0.75° and 1.0° resolution forcing

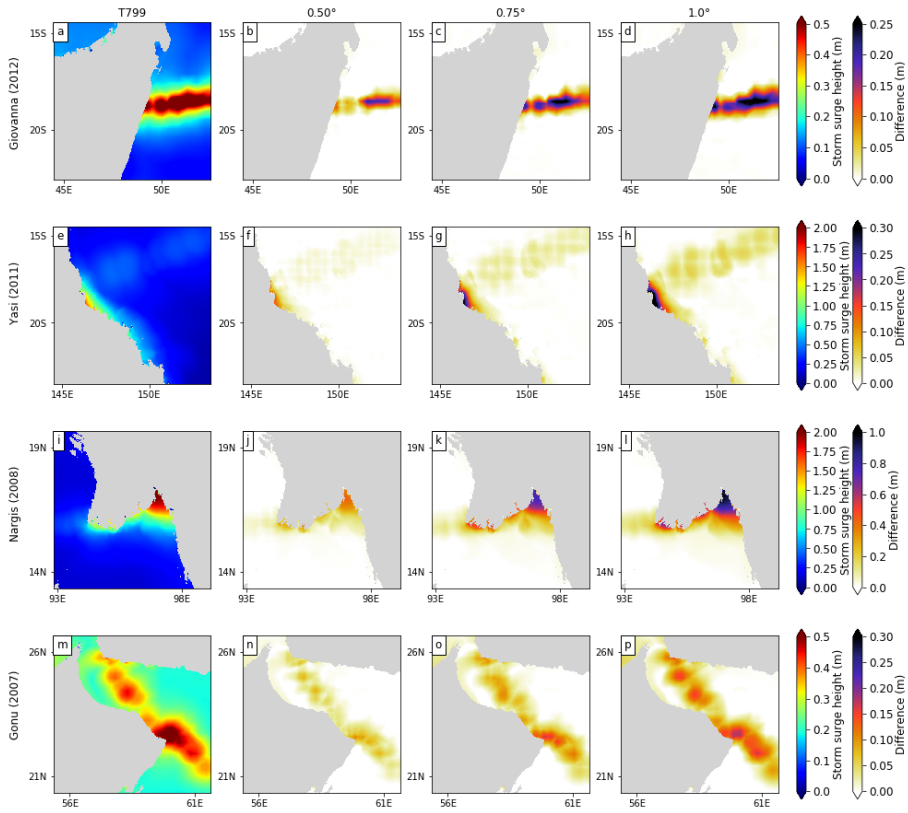


**Figure A.9** Spatial map of maximum storm surge heights and difference in maximum storm surge heights for (a-d) Giovanna, (e-h) Yasi, (i-l) Nargis and (m-p) Gonu. From left to right: maximum storm surge height in T799 resolution forcing, difference between T799 resolution forcing and 0.50°, 0.75° and 1.0° resolution forcing

## Supplementary Tables A

**Table A.1** Maximum wind speeds (m/s) around landfall

	<b>Irma</b>	<b>Sandy</b>	<b>Nargis</b>	<b>Yasi</b>	<b>Haiyan</b>	<b>Giovanna</b>	<b>Gonu</b>	<b>Patricia</b>
<b>T799</b>	40.0	31.0	32.6	29.6	34.1	40.1	30.6	25.2
<b>0.25°</b>	40.3	35.3	30.0	31.9	34.5	39.0	29.2	24.9
<b>0.30°</b>	39.2	35.1	30.6	32.1	33.7	38.1	28.9	25.1
<b>0.40°</b>	38.2	33.4	29.2	31.9	31.5	34.0	28.3	24.1
<b>0.50°</b>	36.1	32.1	28.2	30.1	30.3	34.0	27.5	23.4
<b>0.75°</b>	31.6	29.4	25.8	29.8	26.3	27.7	25.2	20.1
<b>1.0°</b>	28.9	30.4	22.6	25.8	24.4	25.6	23.8	18.1

**Table A.2** Minimum MSLP (hPa) around landfall

	<b>Irma</b>	<b>Sandy</b>	<b>Nargis</b>	<b>Yasi</b>	<b>Haiyan</b>	<b>Giovanna</b>	<b>Gonu</b>	<b>Patricia</b>
<b>T799</b>	942.3	956.3	973.0	972.4	965.9	937.8	955.1	984.2
<b>0.25°</b>	942.5	945.4	975.3	975.0	965.5	937.5	958.5	984.5
<b>0.30°</b>	942.8	945.6	976.1	975.0	966.1	939.4	957.2	984.8
<b>0.40°</b>	943.3	946.2	977.6	975.0	967.5	945.6	959.6	987.2
<b>0.50°</b>	946.7	946.0	977.2	975.3	968.0	955.6	960.6	987.9
<b>0.75°</b>	949.4	948.4	983.2	977.3	976.0	961.7	967.3	993.7
<b>1.0°</b>	956.1	948.0	988.9	973.4	973.7	965.5	971.0	995.5

**Table A.3** Average maximum storm surge heights at the GTSM output stations for the different TCs. Values between brackets indicate the maximum storm surge height (in m)

	<b>Irma</b>	<b>Sandy</b>	<b>Nargis</b>	<b>Yasi</b>	<b>Haiyan</b>	<b>Giovanna</b>	<b>Gonu</b>	<b>Patricia</b>
<b>#stations</b>	106	155	82	58	86	30	244	10
<b>T799</b>	1.72 (2.59)	1.62 (2.22)	1.54 (2.10)	1.17 (1.74)	0.52 (0.81)	0.38 (0.54)	0.31 (0.51)	0.17 (0.18)
<b>0.25°</b>	1.70 (2.57)	1.61 (2.20)	1.46 (1.99)	1.16 (1.72)	0.52 (0.83)	0.38 (0.54)	0.31 (0.50)	0.17 (0.18)
<b>0.30°</b>	1.66 (2.54)	1.59 (2.15)	1.42 (1.90)	1.16 (1.70)	0.51 (0.74)	0.38 (0.54)	0.31 (0.49)	0.17 (0.18)
<b>0.40°</b>	1.59 (2.37)	1.55 (2.09)	1.33 (1.77)	1.12 (1.66)	0.48 (0.73)	0.36 (0.50)	0.30 (0.47)	0.17 (0.18)
<b>0.50°</b>	1.49 (2.22)	1.53 (2.09)	1.24 (1.69)	1.10 (1.60)	0.46 (0.61)	0.34 (0.46)	0.29 (0.44)	0.17 (0.18)
<b>0.75°</b>	1.33 (1.86)	1.46 (2.01)	0.96 (1.30)	1.03 (1.51)	0.42 (0.60)	0.30 (0.35)	0.28 (0.39)	0.17 (0.19)
<b>1.0°</b>	1.15 (1.57)	1.37 (1.90)	0.81 (1.14)	0.95 (1.39)	0.38 (0.61)	0.27 (0.33)	0.26 (0.41)	0.16 (0.17)

**Table A.4** Relative difference in maximum storm surge height (%) compared to the T799 resolution forcing

	<b>Irma</b>	<b>Sandy</b>	<b>Nargis</b>	<b>Yasi</b>	<b>Haiyan</b>	<b>Giovanna</b>	<b>Gonu</b>	<b>Patricia</b>
<b>0.25°</b>	0.83	1.06	5.31	1.22	-2.51	-0.92	2.14	0.73
<b>0.30°</b>	2.17	3.42	9.35	2.29	8.26	-0.94	4.88	0.23
<b>0.40°</b>	8.66	5.89	15.53	4.61	9.81	7.07	8.51	0.64
<b>0.50°</b>	14.5	6.13	19.78	7.86	24.34	14.81	14.69	1.33
<b>0.75°</b>	28.23	9.65	37.99	12.89	25.16	35.41	23.70	-1.07
<b>1.0°</b>	39.62	14.66	45.80	19.90	23.79	39.05	19.99	9.93

**Table A.5** Relative difference in average maximum storm surge height at the GTSM output stations (%) compared to the T799 resolution forcing

	<b>Irma</b>	<b>Sandy</b>	<b>Nargis</b>	<b>Yasi</b>	<b>Haiyan</b>	<b>Giovanna</b>	<b>Gonu</b>	<b>Patricia</b>
<b>0.25°</b>	0.92	0.43	5.29	0.84	1.50	0.51	1.44	0.36
<b>0.30°</b>	3.46	1.83	7.80	1.59	3.15	2.43	2.38	0.37
<b>0.40°</b>	7.42	3.84	13.66	4.20	8.04	5.19	4.23	1.02
<b>0.50°</b>	13.27	5.58	19.65	6.26	12.22	11.31	6.23	1.09
<b>0.75°</b>	22.34	9.96	37.39	12.10	20.42	21.84	12.21	-0.74
<b>1.0°</b>	33.04	15.42	47.58	18.74	28.01	28.75	16.28	8.79

**Table A.6** Absolute difference in maximum storm surge height (m) compared to the T799 resolution forcing

	<b>Irma</b>	<b>Sandy</b>	<b>Nargis</b>	<b>Yasi</b>	<b>Haiyan</b>	<b>Giovanna</b>	<b>Gonu</b>	<b>Patricia</b>
<b>0.25°</b>	0.02	0.02	0.1	0.02	-0.02	0.00	0.01	0.00
<b>0.30°</b>	0.06	0.08	0.20	0.04	0.07	-0.01	0.02	0.00
<b>0.40°</b>	0.22	0.13	0.33	0.08	0.08	0.04	0.04	0.00
<b>0.50°</b>	0.38	0.14	0.42	0.14	0.20	0.08	0.08	0.00
<b>0.75°</b>	0.73	0.21	0.80	0.22	0.20	0.19	0.12	0.00
<b>1.0°</b>	1.03	0.33	0.96	0.35	0.19	0.21	0.10	0.02

**Table A.7** Absolute difference in average maximum storm surge height (m) at the GTSM output stations compared to the T799 resolution forcing

	<b>Irma</b>	<b>Sandy</b>	<b>Nargis</b>	<b>Yasi</b>	<b>Haiyan</b>	<b>Giovanna</b>	<b>Gonu</b>	<b>Patricia</b>
<b>0.25°</b>	0.02	0.01	0.08	0.01	0.01	0.00	0.00	0.00
<b>0.30°</b>	0.06	0.03	0.12	0.02	0.02	0.01	0.01	0.00
<b>0.40°</b>	0.13	0.06	0.21	0.05	0.04	0.02	0.01	0.00
<b>0.50°</b>	0.23	0.09	0.30	0.07	0.06	0.04	0.02	0.00
<b>0.75°</b>	0.38	0.16	0.58	0.14	0.11	0.08	0.04	0.00
<b>1.0°</b>	0.57	0.25	0.73	0.22	0.15	0.11	0.05	0.02

**Table A.8** RMSE (m) compared to the T799 resolution forcing

	<b>Irma</b>	<b>Sandy</b>	<b>Nargis</b>	<b>Yasi</b>	<b>Haiyan</b>	<b>Giovanna</b>	<b>Gonu</b>	<b>Patricia</b>
<b>0.25°</b>	0.03	0.02	0.09	0.01	0.01	0.00	0.00	0.00
<b>0.30°</b>	0.07	0.04	0.13	0.02	0.02	0.01	0.01	0.00
<b>0.40°</b>	0.15	0.07	0.23	0.06	0.06	0.02	0.01	0.00
<b>0.50°</b>	0.27	0.10	0.32	0.10	0.09	0.06	0.02	0.00
<b>0.75°</b>	0.42	0.19	0.60	0.18	0.14	0.11	0.05	0.01
<b>1.0°</b>	0.63	0.29	0.76	0.28	0.18	0.13	0.06	0.02

## Appendix B

### Supplementary Notes B

Here, we provide additional information on the validity of STORM and the STORM+climate change (STORM-C) datasets. We first present the STORM-C statistics for the four GCMs and in all basins. Then, we focus on the validation and justification of our method. We show the STORM model outcomes when directly using the tropical cyclone (TC) data from the global climate models (GCMs). Next, we demonstrate the way the delta approach propagates through STORM, by performing a perfect model run. Subsequently, we test the sensitivity of the model outcomes to various changes in variables by performing a sensitivity analysis.

#### *STORM climate change datasets*

Table B.1 shows the statistics for the TC characteristics (mean and standard deviation) for the STORM-B dataset and each of the four STORM-C datasets. A discussion of the results is given in Section 5.3.1.

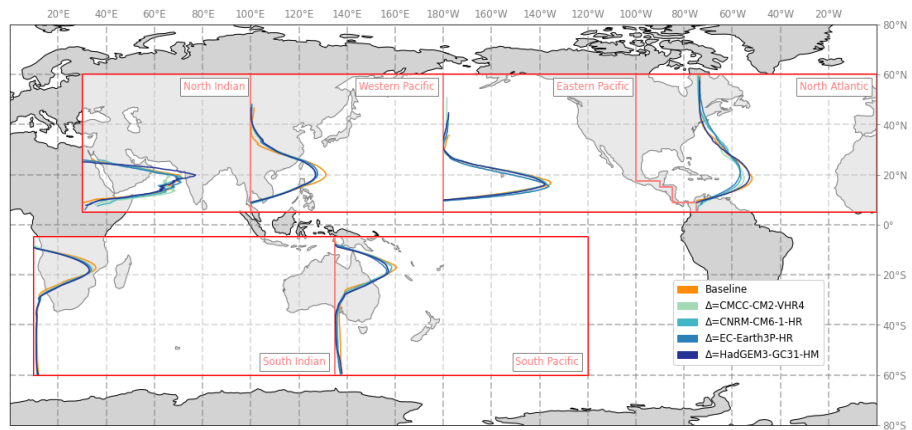


**Figure B.1** Latitudinal distribution per basin of the location of maximum intensity in the STORM-B and STORM-C datasets

**Table B.1** Basin-wide mean and standard deviation (between brackets) of tropical cyclone characteristics of 1,000 36-year samples from the STORM-B and STORM-C datasets. STORM baseline resembles the baseline-climate STORM dataset, generated using IBTrACS and corresponding to the 1980-2017 climate conditions. Similarly, the four “ $\Delta$ =” columns represent the STORM-C dataset for each of the four GCMS. The last column shows the STORM statistics aggregated over all GCM datasets to show the general direction and magnitude of change. For STORM-C, the second number between brackets indicates how many (out of four) GCMs agree on the sign of change

		STORM baseline	$\Delta$ =CMCC	$\Delta$ =CNRM	$\Delta$ =EC-Earth	$\Delta$ =HadGEM	Aggregated over GCMs
Genesis freq. (avg/yr)	EP	14.5 (0.6)	15.6 (0.6)	14.5 (0.7)	14.9 (0.7)	15.2 (0.6)	15.1 (0.8; 3)
	NA	10.9 (0.6)	12.6 (0.6)	9.3 (0.5)	7.5 (0.4)	9.9 (0.6)	9.8 (1.9; 3)
	NI	2.0 (0.2)	1.7 (0.2)	1.6 (0.2)	2.6 (0.3)	1.8 (0.2)	1.9 (0.4; 3)
	SI	12.3 (0.6)	10.5 (0.6)	11.6 (0.6)	11.2 (0.6)	11.4 (0.6)	11.2 (0.7; 4)
	SP	9.4 (0.5)	9.5 (0.5)	8.2 (0.5)	9.5 (0.6)	10.3 (0.6)	9.4 (0.9; 2)
	WP	23.1 (0.8)	21.9 (0.9)	20.2 (0.8)	23.1 (0.8)	23.5 (0.8)	22.2 (1.5; 2)
	Global	72.4 (1.4)	72.0 (1.5)	65.5 (1.4)	68.8 (1.5)	72.2 (1.5)	69.6 (3.1; 4)
Average pressure along track (hPa)	EP	985.6 (0.4)	979.2 (0.5)	978.1 (0.6)	978.1 (0.6)	977.2 (0.6)	978.2 (0.9; 4)
	NA	985.6 (0.6)	982.7 (0.6)	981.6 (0.8)	980.5 (0.9)	981.1 (0.8)	981.5 (1.1; 4)
	NI	984.3 (1.8)	982.8 (1.8)	981.6 (1.7)	979.9 (1.5)	982.0 (1.9)	981.6 2.0; 4)
	SI	979.5 (0.5)	976.7 (0.6)	975.1 (0.6)	974.9 (0.6)	974.9 (0.6)	975.4 (0.9; 4)
	SP	981.9 (0.5)	977.4 (0.7)	977.8 (0.8)	976.2 (0.7)	976.5 (0.7)	977.0 (1.0; 4)
	WP	974.6 (0.6)	968.4 (0.7)	965.4 (0.8)	967.0 (0.6)	964.9 (0.7)	966.4 (1.5; 4)
	Global	981.9 (4.0)	977.8 (4.9)	976.6 (5.6)	976.1 (4.6)	976.1 (5.7)	976.7 (5.3; 4)
Minimum pressure (hPa)	EP	971.5 (0.8)	960.2 (0.9)	958.4 (1.1)	958.1 (1.1)	956.2 (1.0)	958.2 (1.8; 4)
	NA	972.7 (1.2)	968.4 (1.1)	966.1 (1.4)	964.5 (1.6)	965.1 (1.5)	966.1 (2.0; 4)
	NI	971.6 (3.6)	969.0 (3.3)	967.4 (3.3)	964.5 (2.7)	968.0 (3.5)	967.2 (3.6; 4)
	SI	966.0 (0.9)	959.8 (1.1)	957.5 (1.1)	957.6 (1.1)	956.8 (1.1)	957.9 (1.6; 4)
	SP	969.4 (1.0)	961.1 (1.2)	961.5 (1.5)	958.8 (1.4)	959.3 (1.3)	960.2 (1.8; 4)
	WP	956.3 (1.0)	947.7 (1.1)	943.1 (1.2)	945.5 (1.0)	942.1 (1.2)	944.6 (2.5; 4)
	Global	967.9 (5.9)	961.0 (7.2)	959.0 (8.2)	958.2 (6.6)	958.2 (8.7)	959.1 (7.8; 4)



<b>Maximum wind speed (m/s)</b>	<b>EP</b>	37.0 (0.5)	43.6 (0.5)	44.6 (0.6)	44.8 (0.6)	45.8 (0.6)	44.7 (1.0; 4)
	<b>NA</b>	34.7 (0.7)	37.2 (0.7)	38.8 (0.8)	39.6 (0.9)	39.5 (0.9)	38.8 (1.3; 4)
	<b>NI</b>	33.4 (1.8)	35.8 (1.8)	36.2 (1.7)	37.9 (1.4)	35.9 (1.8)	36.5 (1.9; 4)
	<b>SI</b>	33.9 (0.5)	37.8 (0.6)	38.8 (0.6)	38.6 (0.6)	39.2 (0.6)	38.6 (0.8; 4)
	<b>SP</b>	33.4 (0.5)	38.2 (0.6)	38.1 (0.7)	39.4 (0.7)	39.3 (0.6)	38.8 (0.9; 4)
	<b>WP</b>	37.6 (0.4)	41.2 (0.5)	43.1 (0.5)	42.4 (0.4)	43.6 (0.5)	42.6 (1.0; 4)
	<b>Global</b>	35.0 (1.9)	39.0 (2.8)	39.9 (3.1)	40.4 (2.6)	40.4 (3.4)	39.9 (3.0; 4)
<b>Landfall counts (avg/yr)</b>	<b>EP</b>	0.3 (0.1)	0.4 (0.1)	0.6 (0.1)	0.5 (0.1)	0.6 (0.1)	0.5 (0.1; 4)
	<b>NA</b>	1.6 (0.1)	1.7 (0.1)	1.9 (0.1)	2.0 (0.2)	1.9 (0.1)	1.9 (0.2; 4)
	<b>NI</b>	2.8 (0.4)	3.0 (0.3)	3.1 (0.4)	3.2 (0.3)	3.0 (0.4)	3.1 (0.4; 4)
	<b>SI</b>	0.8 (0.1)	0.9 (0.1)	0.9 (0.1)	0.9 (0.1)	0.8 (0.1)	1.1 (0.2; 3)
	<b>SP</b>	0.8 (0.1)	0.9 (0.1)	0.9 (0.1)	0.9 (0.1)	0.8 (0.1)	0.9 (0.1; 3)
	<b>WP</b>	2.2 (0.1)	2.7 (0.1)	2.8 (0.1)	2.6 (0.1)	2.7 (0.1)	2.7 (0.1; 3)
	<b>Global</b>	8.6 (0.4)	9.6 (0.4)	10.3 (0.4)	10.5 (0.4)	10.0 (0.4)	10.1 (0.5; 4)
<b>Landfall pressure (hPa)</b>	<b>EP</b>	983.1 (2.7)	980.6 (2.3)	979.9 (2.4)	981.0 (2.4)	980.6 (2.4)	980.5 (2.4; 4)
	<b>NA</b>	985.8 (1.0)	984.4 (1.0)	984.6 (1.3)	983.2 (1.2)	983.9 (1.0)	9840 (1.3; 4)
	<b>NI</b>	981.6 (2.4)	983.4 (2.1)	982.6 (1.9)	980.5 (1.7)	981.8 (2.0)	982.1 (2.2; 3)
	<b>SI</b>	980.1 (1.2)	978.7 (1.4)	978.3 (1.2)	978.0 (1.1)	977.3 (1.3)	978.1 (1.3; 4)
	<b>SP</b>	981.4 (1.5)	977.4 (1.7)	977.9 (1.9)	975.7 (1.8)	975.8 (2.0)	976.7 (2.1; 4)
	<b>WP</b>	980.9 (0.7)	977.7 (0.7)	975.4 (0.8)	976.9 (0.7)	975.5 (0.7)	976.4 (1.2; 4)
	<b>Global</b>	982.1 (2.5)	980.3 (3.1)	979.7 (3.4)	979.2 (3.0)	978.9 (3.2)	979.5 (3.2; 4)

### *STORM and global climate model simulations*

One of the novel aspects in this study is the methodology of projecting a climate change signal ( $\Delta$ ) onto the historical TC data from IBTrACS. The main reason of using IBTrACS is because TCs, and more particularly TC intensity, is poorly captured by GCMs (Roberts et al., 2020a). To demonstrate this, we first compare the present-climate (1979-2014) statistics of four GCM/basin combinations with statistics from historical data from IBTrACS (1980-2015) (“present climate” column in Table B.2). The latter time period was chosen to have an equal temporal length to, and maximum overlap with, the present-climate GCM data. Secondly, we use the present- and future-climate TC statistics from the same GCM-basin combinations and amplify this to 1,000 years of synthetic data using STORM (“STORM+GCM” column in Table B.2), to assess their statistics.

**Table B.2** Comparison of tropical cyclone characteristics in the global climate models (GCMs). The “baseline climate” column shows the comparison of these characteristics between 36 years of baseline-climate GCM data (1979-2014) and historical data from IBTrACS (1980-2015). The “STORM+GCM” column shows the statistics extracted from 1,000 years of synthetic data, using the baseline (1979-2014) and future (2015-2050) GCM data as input for STORM.

	Basin	GCM	Present climate		STORM + GCM	
			IBTrACS	GCM	Present	Future
Genesis frequency (avg/yr)	EP	CMCC	14.4 (4.1)	30.3 (4.8)	31.7 (5.7)	33.5 (5.3)
	SI	CNRM	12.6 (3.9)	18.1 (3.2)	19.1 (4.1)	18.0 (4.2)
	NA	EC-Earth	10.6 (4.0)	5.9 (2.5)	7.2 (2.6)	5.2 (2.0)
	WP	HadGEM	22.2 (4.0)	35.8 (5.5)	37.4 (6.2)	38.4 (6.1)
Average pressure (hPa)	EP	CMCC	988.6 (11.8)	1003.5 (6.4)	994.9 (5.2)	994.8 (4.6)
	SI	CNRM	980.2 (12.1)	1003.3 (7.0)	985.4 (7.0)	986.0 (6.5)
	NA	EC-Earth	991.6 (12.7)	1007.7 (4.1)	994.3 (3.2)	994.2 (3.8)
	WP	HadGEM	978.7 (14.8)	998.8 (6.2)	984.0 (11.4)	983.4 (14.4)
Minimum pressure (hPa)	EP	CMCC	973.9 (25.0)	989.6 (17.1)	989.2 (11.6)	989.3 (8.8)
	SI	CNRM	961.9 (25.4)	990.4 (16.4)	978.8 (12.9)	979.6 (12.4)
	NA	EC-Earth	977.3 (25.1)	998.3 (10.6)	992.2 (5.5)	992.1 (6.9)
	WP	HadGEM	961.5 (28.2)	985.9 (13.7)	975.2 (20.3)	973.4 (25.9)
Maximum wind speed (m/s)	EP	CMCC	35.9 (13.5)	24.9 (6.9)	26.2 (7.2)	26.5 (6.4)
	SI	CNRM	36.0 (12.7)	23.6 (7.7)	26.4 (7.6)	25.8 (7.1)
	NA	EC-Earth	34.6 (13.1)	18.3 (4.5)	20.7 (3.8)	20.8 (4.9)
	WP	HadGEM	35.7 (11.9)	23.8 (5.5)	28.5 (9.4)	29.3 (11.1)

<b>Landfall counts (avg/yr)</b>	<b>EP</b>	CMCC	1.9 (1.7)	9.2 (4.5)	0.2 (0.8)	0.3 (0.9)
	<b>SI</b>	CNRM	4.4 (2.5)	0.0 (0.0)	1.3 (2.1)	1.3 (2.1)
	<b>NA</b>	EC-Earth	7.8 (5.1)	11.1 (5.9)	0.9 (1.6)	0.9 (1.6)
	<b>WP</b>	HadGEM	18.7 (4.5)	27.5 (22.1)	2.0 (2.7)	1.8 (2.6)
<b>Landfall pressure (hPa)</b>	<b>EP</b>	CMCC	982.6 (14.6)	1003.5 (12.9)	989.7 (16.9)	993.7 (10.4)
	<b>SI</b>	CNRM	976.1 (19.9)	-	985.3 (7.1)	985.8 (6.9)
	<b>NA</b>	EC-Earth	984.0 (19.4)	1008.7 (4.5)	994.0 (4.8)	994.0 (3.9)
	<b>WP</b>	HadGEM	978.9 (15.9)	996.5 (11.0)	983.4 (11.6)	983.2 (13.6)

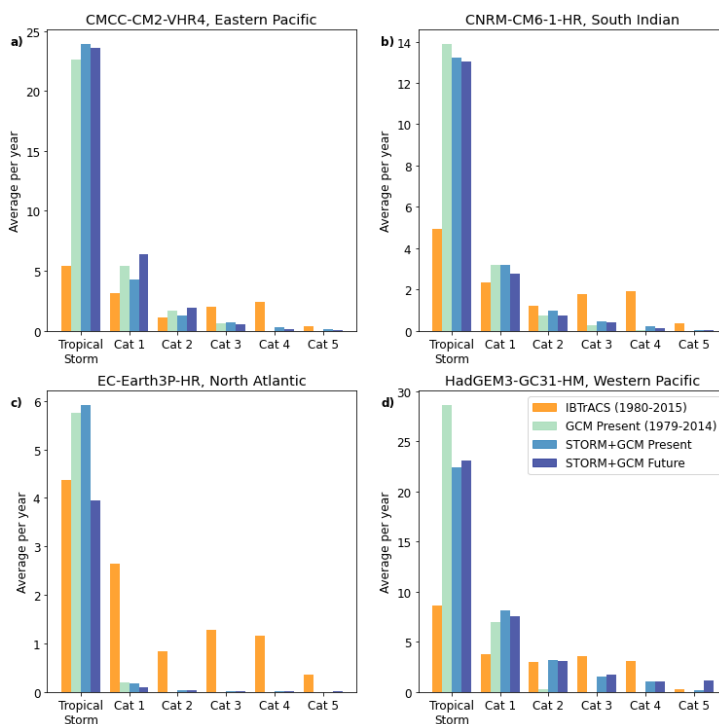


**Figure B.2** Distribution of tropical cyclone categories (on the Saffir-Simpson scale) in each of the four model/basin combinations. Shown are the present-climate dataset comparisons (historical data from IBTrACS versus climate data from the global climate models –GCMs–), and 1,000 years of synthetic data using the present- and future-climate GCM runs as input for STORM.

For the present-climate comparison, we observe that there is little consensus in the specific basins between the GCMs and the historical data: in all cases, TCs are substantially weaker in the GCMs as compared to IBTrACS. Furthermore, there is also little agreement on the genesis frequency: in three out of four GCM/basin

combinations, there is an overestimation of TC occurrences compared to historical data. The largest difference can be seen for the CMCC model, where there are on average twice as much TC formations in the Eastern Pacific than in observations. Contrarily, there are almost twice as little formations in the North Atlantic in the EC-Earth model. In the synthetic datasets (STORM+GCM column) we observe that the weak TC intensities are preserved by STORM, as for instance the average maximum wind speed is well below hurricane strength ( $<29$  m/s), whereas the average TC in IBTrACS reaches wind speeds of around 35 m/s (Category 1 on the Saffir-Simpson scale). By design, STORM statistically resamples the statistics found in original input datasets, and as such the poor representation of TC intensity in the GCMs is propagated through STORM. Hence, using these GCMs as input for STORM will result in a (severe) underestimation of TC intensity, in turn affecting TC wind speed probabilities and risk assessments, especially for stronger storms.

### *Perfect model run*

To overcome the limitations imposed by the GCMs, we need to diverge from directly using the GCM data, and instead create a STORM input dataset based on the observed TC statistics from IBTRACS. This way, we can ensure that we have a realistic number of TC formations, and that the statistics of stronger TCs are also included in STORM. Therefore, in this study, we adjust IBTrACS such to include the delta derived from the four GCMs, this way creating a “future climate” version of the historical statistics. To test if introducing such delta does not instigate anomalies, we perform a perfect model run using a combination of the four GCMs and four basins as input. In a perfect model run, we assume that the model itself is “perfect”, that is, we do not focus on intrinsic model errors, but rather assess the influence of the input dataset on the outcomes.

**Table B.3** Average of 36,000 years, sampled from 1,000 years of synthetic data from each of the models in the indicated basin. In run 1, we extract the present-climate variables and add the climate signal ( $\Delta$ ) onto them to produce a “future-climate version” of this present-climate dataset. In run 2, we directly use the future-climate variables. In both runs, we use the regression formula coefficients from the present-climate datasets.

	Basin	Model	Run 1: Present climate + $\Delta$	Run 2: Future climate
Genesis frequency (avg/yr)	EP	CMCC	33.3 (5.6)	33.7 (5.6)
	SI	CNRM	18.0 (4.3)	18.0 (4.2)
	NA	EC-Earth	5.1 (1.9)	5.2 (2.1)
	WP	HadGEM	38.3 (6.2)	38.1 (6.1)
Average pressure (hPa)	EP	CMCC	994.2 (5.6)	994.2 (5.6)
	SI	CNRM	985.5 (6.7)	985.4 (6.8)
	NA	EC-Earth	994.0 (3.6)	993.9 (4.0)
	WP	HadGEM	985.4 (9.9)	985.3 (10.0)

<b>Minimum pressure (hPa)</b>	<b>EP</b>	CMCC	987.8 (12.2)	987.7 (12.5)
	<b>SI</b>	CNRM	978.7 (12.5)	978.7 (12.6)
	<b>NA</b>	EC-Earth	991.6 (6.1)	991.3 (7.1)
	<b>WP</b>	HadGEM	977.2 (18.0)	977.2 (18.2)
<b>Maximum wind speed (m/s)</b>	<b>EP</b>	CMCC	27.5 (8.0)	27.5 (8.1)
	<b>SI</b>	CNRM	26.6 (7.5)	26.6 (7.5)
	<b>NA</b>	EC-Earth	21.3 (4.6)	21.4 (5.2)
	<b>WP</b>	HadGEM	27.9 (8.7)	27.8 (8.7)
<b>Landfall counts (avg/yr)</b>	<b>EP</b>	CMCC	0.3 (1.1)	0.3 (1.1)
	<b>SI</b>	CNRM	1.5 (2.2)	1.5 (2.2)
	<b>NA</b>	EC-Earth	1.1 (1.8)	1.1 (1.8)
	<b>WP</b>	HadGEM	1.9 (2.7)	2.0 (2.7)
<b>Landfall pressure (hPa)</b>	<b>EP</b>	CMCC	991.3 (15.0)	990.7 (15.9)
	<b>SI</b>	CNRM	985.4 (7.0)	985.4 (6.8)
	<b>NA</b>	EC-Earth	993.4 (4.0)	993.4 (4.1)
	<b>WP</b>	HadGEM	983.6 (11.2)	983.6 (11.4)

In the data preprocessing step in STORM, we extract the various variables and variable distributions, as well as determine the coefficients for the regression formulas; see Figure 5.1 for an overview of all variables, and Bloemendaal et al. (2020c) for a full description of all variables and coefficients. Additionally, we also extract the delta from the four GCMs following the approach set out in Section 5.2. Next, to test whether the delta approach is stable and does not introduce anomalies, we perform two runs in which we use the coefficients from the present-climate GCM dataset, but vary the variables as follows: i) in the first run, we use the TC statistics from the present-climate GCM simulation, but add the delta to create a future-climate version of these present-climate statistics (we call this “present+ $\Delta$ ”). This approach mimics the methodology we apply to the observed TC statistics from the IBTrACS dataset; and ii) in the second run, we directly use the TC statistics from the future-climate GCM simulation. If the present + $\Delta$  run performs well, the outcomes of the first run should compare well to the second one. These two run setups serve as input for STORM, and are used to generate 1,000 of synthetic data for four GCM/basin combinations. Subsequently, we randomly sample 1,000 times 36 years of data (to comply with the temporal length of the original GCM simulations; this totals to 36,000 years of data), and extract the yearly number of genesis and landfall occurrences, as well as the of various TC intensity measures. We then calculate the mean and standard deviation of each of the six characteristics, see Table B.3. We

observe that the means and standard deviations of the two runs are almost identical to one another, which implies that adding the delta does not impose anomalies and thus that the delta approach is stable, mimicking the results that we would obtain if we were to use the TC statistics directly from a future-climate GCM dataset as input (run 2).

Figure B.3 shows the distribution of TC categories for each of the four GCM/basin combinations for the present+ $\Delta$  and future-climate STORM simulations in the perfect model setup. As was the case with the statistics of the various TC characteristics (see Table B.1) we also see that the average annual number of TCs per category is approximately equal in each of the category bins, meaning that the present+ $\Delta$  perfect model run again mimics the results if we had used the future-climate GCM TC statistics instead, and that no anomalies are brought into the synthetic STORM datasets.

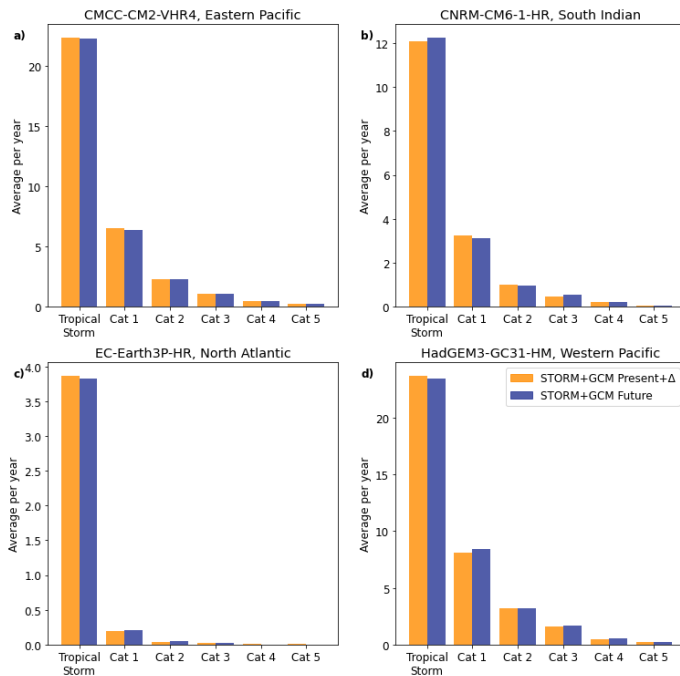


**Figure B.3** Distribution of tropical cyclone categories (average per year) on the Saffir-Simpson scale in 1,000 random realizations of 36 years of data drawn from 1,000 years of synthetic data from STORM for the present (orange) and future climate (turquoise). Results are shown for (a) CMCC-CM2-VHR4 in the Eastern Pacific, (b) CNRM-CM6-1-HR in the South Indian, (c) EC-Earth3P-HR in the North Atlantic, and (d) HadGEM3-GC31-HM in the Western Pacific.

### *Sensitivity analysis*

To analyze the influence of applying the delta approach on the different variables (see Figure 5.1 in Section 5.2) on the overall outcome of the STORM runs, we perform a

sensitivity analysis using the TC statistics from HadGEM in the Western Pacific. The reason we use this GCM in this basin is because it consists of the most TC data of all GCM/basin combinations, and the Western Pacific generally faces some of the strongest TCs of all basins.

The statistics (mean and standard deviation) of six tropical cyclone characteristics for each of the sensitivity test runs are listed in Table B.4. Figure B.4 shows the distribution of TC categories in the STORM-B dataset, the STORM-C dataset, and the ten synthetic runs in which we kept each of the ten input variables constant (that is, we used the baseline-climate value and did not shift it using the delta approach set out in Section 5.2) while shifting the other variables. As such, we can analyze the individual influence of each of the variables on the STORM-C dataset. From Figure B.4, we see that most of the variables on itself do not influence the mean value of each of the characteristics, but the only variable that does is the Maximum Potential Intensity (MPI, in hPa). This variable is a measure of the theoretical maximum TC intensity possible at a location, dependent on environmental factors such as sea-surface temperature (SST) and the environmental pressure. It directly influences TC intensification and weakening, as TCs will weaken as soon as they approach the MPI, and when they reach higher latitudes, where SSTs are lower (Bister and Emanuel, 2002). From Table B.4 we can observe the influence of the MPI on the maximum intensity of a TC; the baseline climate MPI leads to approximately 2.4 m/s lower maximum wind speeds compared to its future-climate counterpart in the STORM-C dataset. This has a direct influence on the distribution of TC categories (Figure B.4), where we observe a substantial drop in Category-5 occurrences, similar to the STORM-B dataset. This means that the MPI predominantly affects the occurrence of the strongest TCs.

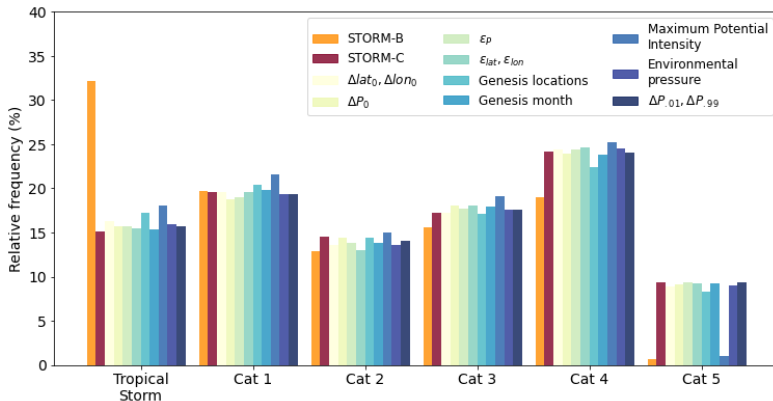


**Figure B.4** Relative frequency of tropical cyclone categories for the STORM baseline climate run (STORM-B), the STORM-climate change run (STORM-C), and the ten synthetic runs in which the named variable was kept constant (i.e. the baseline climate value) and not shifted according to the delta approach.

**Table B.4** Statistics of six key tropical cyclone characteristics for the baseline STORM run (STORM-B), the STORM-climate change run (STORM-C; IBTrACS+ $\Delta$ ), and the ten synthetic runs in which the named variable was kept constant (i.e. the baseline-climate value) and not shifted according to the delta approach. Average values of 1,000 times 36 years of data (36,000 years) are given, standard deviations are listed between brackets.

	Genesis frequency (avg/yr)	Average pressure (hPa)	Minimum pressure (hPa)	Maximum wind speed (m/s)	Landfall counts (avg/yr)	Landfall pressure (hPa)
<b>STORM-B</b>	23.9 (4.9)	974.6 (16.1)	956.4 (28.5)	37.5 (12.1)	2.2 (2.5)	980.9 (13.6)
<b>STORM-C</b>	24.5 (5.0)	965.0 (19.8)	942.4 (31.9)	43.5 (12.7)	2.7 (2.8)	975.5 (15.0)
$\Delta lat_0, \Delta lon_0$	24.4 (5.0)	965.2 (19.8)	942.7 (32.0)	43.4 (12.8)	2.7 (2.8)	975.6 (15.2)
$\Delta P_0$	24.3 (4.9)	965.0 (19.8)	942.3 (32.0)	43.6 (12.8)	2.7 (2.8)	975.3 (15.2)
$\epsilon_P$	24.2 (4.9)	964.8 (19.9)	942.1 (32.0)	43.6 (12.8)	2.7 (2.7)	975.4 (15.3)
$\epsilon_{lat}, \epsilon_{lon}$	24.0 (4.9)	964.7 (20.0)	942.0 (31.9)	43.7 (12.7)	2.7 (2.8)	975.5 (15.3)
<b>Genesis location</b>	24.0 (5.0)	966.2 (19.7)	944.4 (31.7)	42.7 (12.8)	2.8 (2.7)	976.3 (14.8)
<b>Genesis month</b>	24.5 (4.7)	965.1 (19.8)	942.3 (32.0)	43.6 (12.7)	2.7 (2.7)	975.5 (15.1)
<b>Maximum Potential Intensity</b>	24.6 (4.9)	969.4 (16.5)	948.7 (27.7)	41.1 (11.4)	2.4 (2.6)	979.1 (13.3)
<b>Environmental pressure</b>	24.3 (4.8)	964.8 (19.8)	942.2 (32.0)	43.5 (12.8)	2.7 (2.7)	975.4 (15.3)
$\Delta P_{01}, \Delta P_{99}$	24.3 (5.1)	964.9 (19.8)	942.2 (32.0)	43.6 (12.8)	2.8 (2.8)	975.5 (15.0)
<b>Poisson parameter</b>	23.7 (4.9)	964.9 (19.8)	942.1 (32.0)	43.6 (12.8)	2.7 (2.8)	975.1 (15.4)



### Return period analysis – wind speeds for fixed return periods

Figures B.5 and B.6 show the maximum wind speeds for the fixed return periods discussed in Chapter 5 for the individual GCMs. Figure B.7 shows the number of GCMs agreeing on the sign of change for the different return periods – this number provides an indication of the confidence in the sign of change. Figure B.8 shows the largest and smallest differences in maximum wind speed; Figure B.9 portrays to which GCM these largest and smallest changes are attributed to.

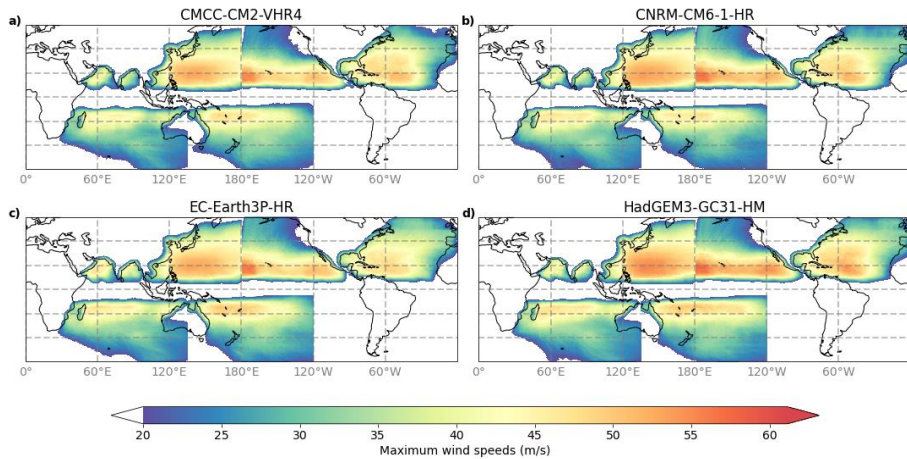


**Figure B.5** Spatial distribution of maximum 10-minute 10-meter wind speeds at the 100-yr return period in each of the four global climate models. The wind speeds are the average value of 1,000 random realizations of 10,000 years of data (sampled with replacement)

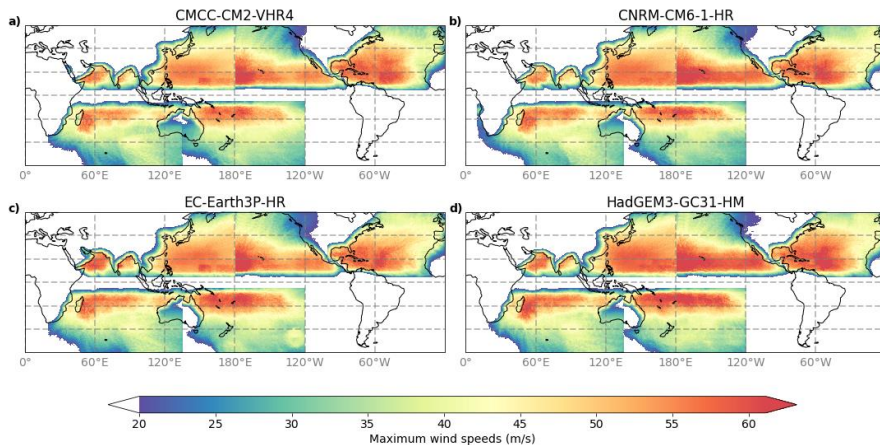


**Figure B.6** Same as Figure B.5, but now for the 1,000-yr return period.

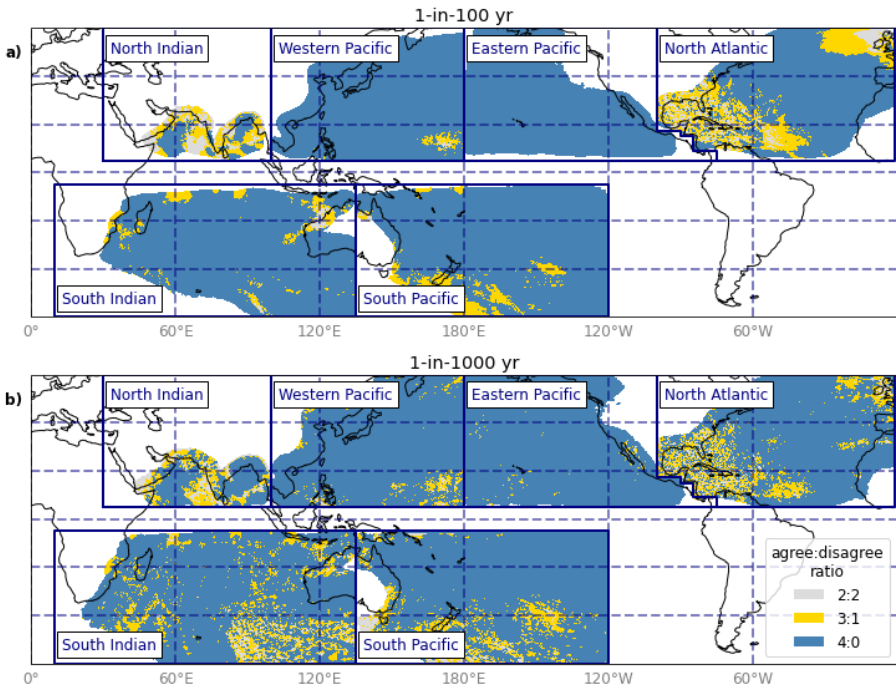


**Figure B.7** Number of global climate models agreeing on the sign of change compared to the STORM baseline climate datasets.

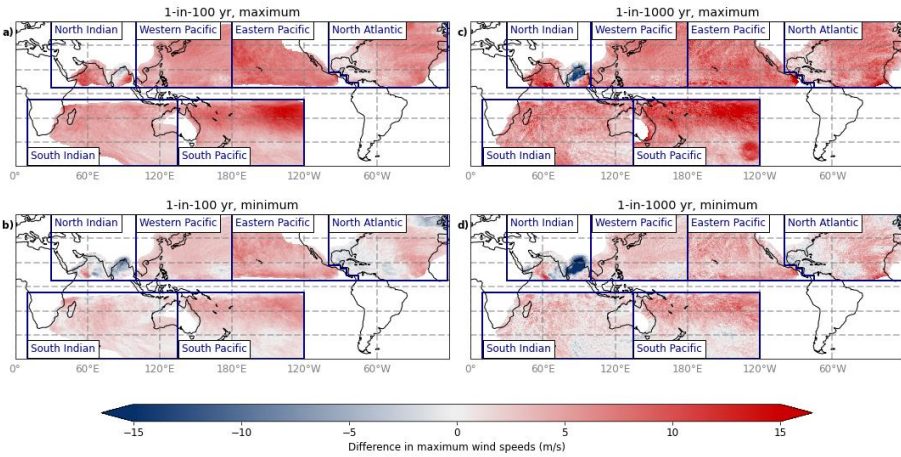


**Figure B.8** Maximum (top row) and minimum (bottom row) value of the difference in maximum wind speeds compared to the STORM baseline climate dataset.

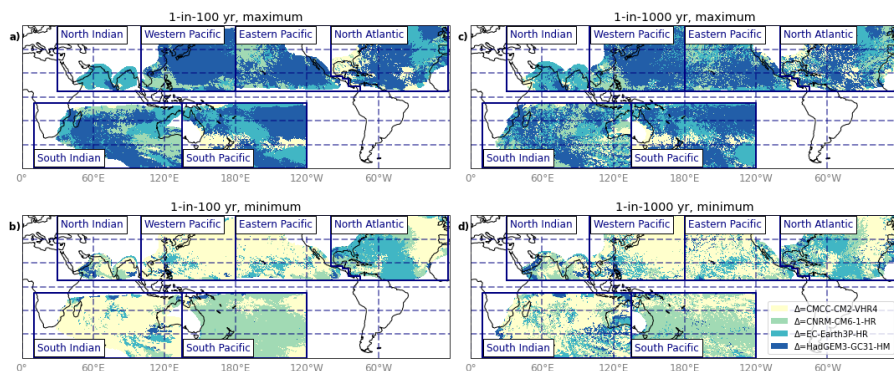


**Figure B.9** Global climate model having the maximum (top) and minimum (bottom) value of the difference in maximum wind speed compared to the STORM baseline climate dataset.

### *Return period analysis – return periods for fixed wind speeds*

Figures B.10 and B.11 show the return periods for the fixed TC categories discussed in Chapter 5 for the individual GCMs. Figure B.12 shows the number of GCMs agreeing on the sign of change for the Category-1 and Category-3 return periods – this number provides an indication of the confidence in the sign of change. Figure B.13 shows the largest and smallest factor change in return periods; Figure B.14 portrays to which GCM these largest and smallest changes are attributed to.

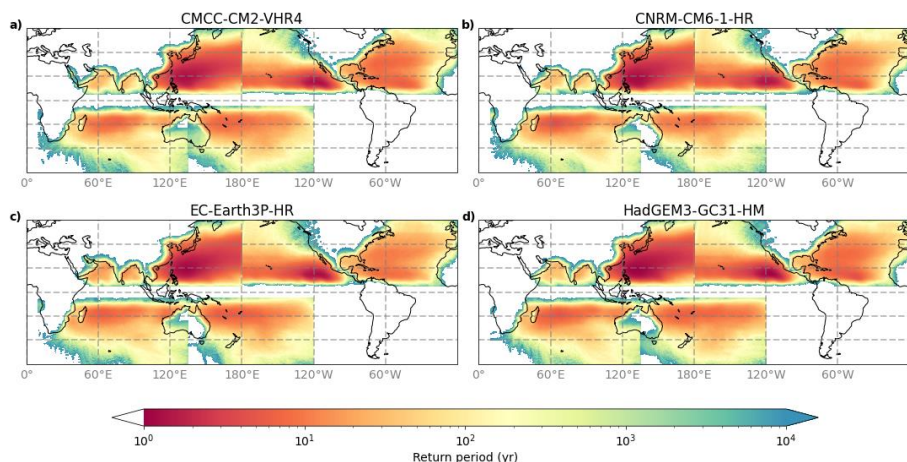


**Figure B.10** Spatial distribution of return periods (yr) at 10 km resolution, derived from applying a 2D-wind parameterization to the synthetic tropical cyclone tracks in the STORM+GCM datasets. The return periods are the average value of 1,000 random realizations of 10,000 years of data (sampled with replacement) and determining RPs using Weibull's plotting formula to each realization at Category 1 (maximum 10-minute 10-meter wind speeds  $\geq 29$  m/s) tropical cyclone strength. Sub-panels show outcomes for each of the four global climate models.

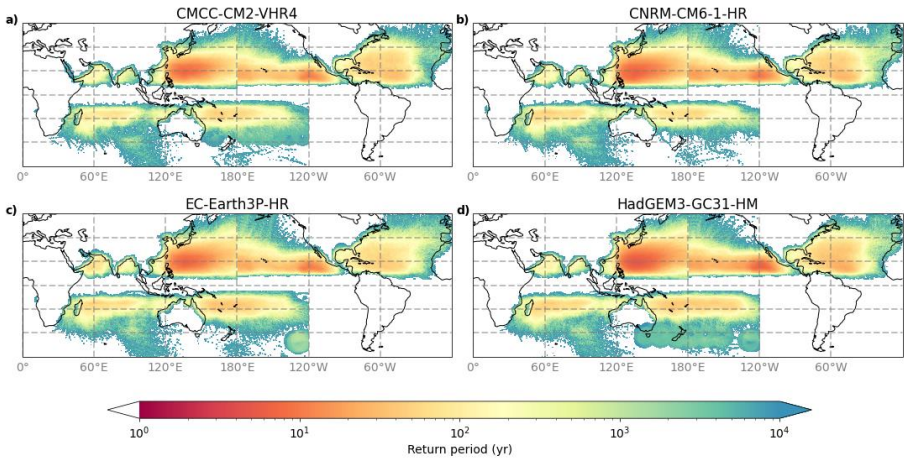


**Figure B.11** Same as Figure B.10, but now for Category-3 (maximum 10-minute 10-meter wind speeds  $\geq 43.4$  m/s) tropical cyclone strength.

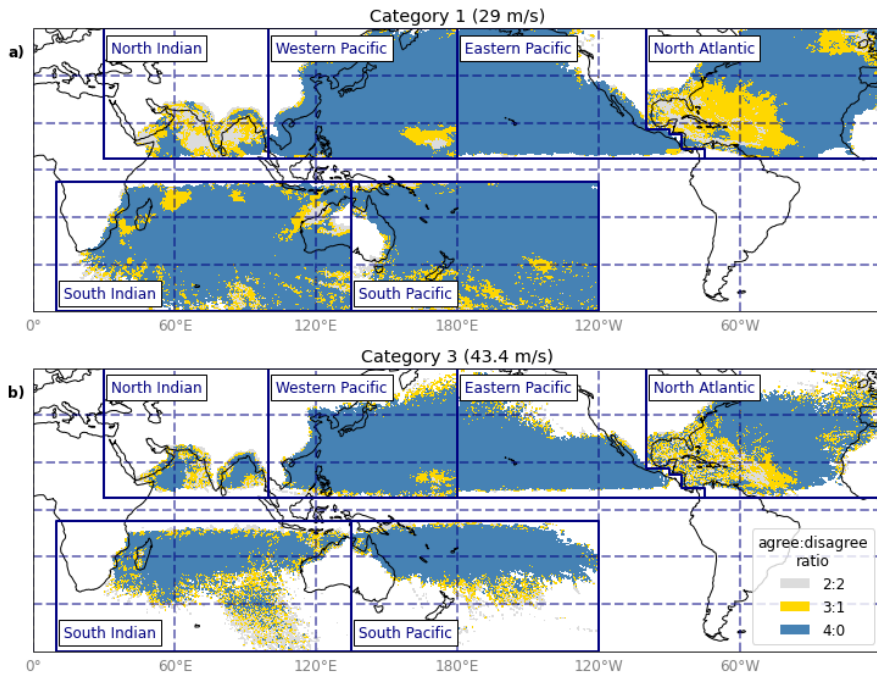


**Figure B.12** Number of models agreeing on the sign of change compared to the STORM baseline climate dataset



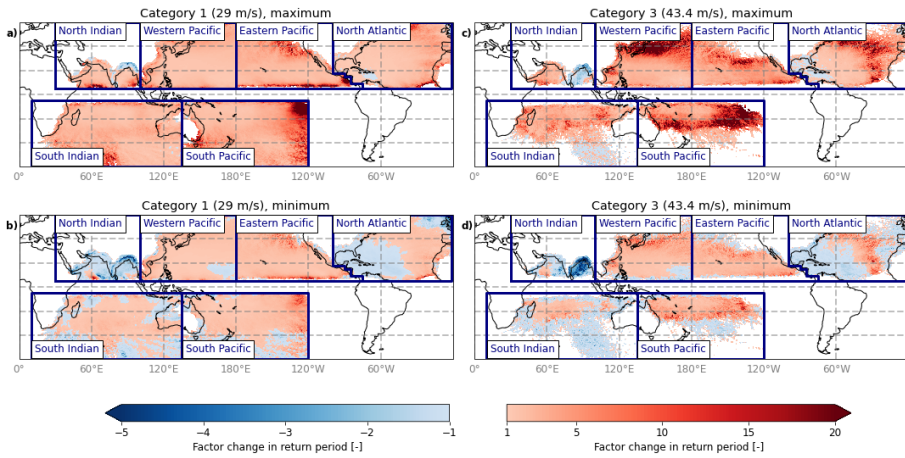


**Figure B.13** Maximum (top row) and minimum (bottom row) factor difference in return periods compared to the STORM baseline climate dataset. A negative factor indicates an increase in return period, equivalent to a decrease in probability. A positive factor indicates a decrease in return period, equivalent to an increase in probability.

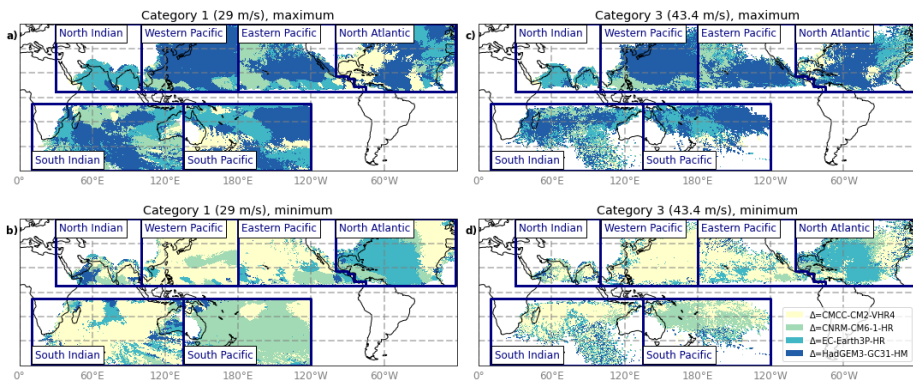


**Figure B.14** Global climate model having the highest (top) and lowest (bottom) difference in return period compared to the STORM baseline climate dataset.





## References

- Aerts, J. C. J. H. (2018). A Review of Cost Estimates for Flood Adaptation. *Water*, 10(11), p 1646.
- Aerts, J. C. J. H., Botzen, W. J. W., Emanuel, K., Lin, N., de Moel, H., & Michel-Kerjan, E. O. (2014). Evaluating Flood Resilience Strategies for Coastal Megacities. *Science*, 344(6183), pp. 473-475. doi:10.1126/science.1248222
- Aerts, J. C. J. H., Lin, N., Botzen, W., Emanuel, K., & de Moel, H. (2013). Low-Probability Flood Risk Modeling for New York City. *Risk Analysis*, 33(5), pp. 772-788. doi:10.1111/risa.12008
- Altman, J., Ukhvatkina, O. N., Omelko, A. M., Macek, M., Plener, T., Pejcha, V., . . . Dolezal, J. (2018). Poleward migration of the destructive effects of tropical cyclones during the 20th century. *Proceedings of the National Academy of Sciences*, 115(45), pp. 11543-11548. doi:10.1073/pnas.1808979115
- AMS. (2020). American Meteorological Society glossary of meteorology: Rain. Retrieved Date Accessed, 2020 from <http://glossary.ametsoc.org/wiki/Rain>.
- Appendini, C., Torres-Freyermuth, A., Oropeza, F., Salles, P., López, J., & Mendoza, E. (2013). *Wave modeling performance in the Gulf of Mexico and Western Caribbean: Wind reanalyses assessment*.
- Atkinson, G. D., & Holliday, C. R. (1977). Tropical Cyclone Minimum Sea Level Pressure/Maximum Sustained Wind Relationship for the Western North Pacific. *Mon. Wea. Rev.*, 105(4), pp. 421-427. doi:[https://doi.org/10.1175/1520-0493\(1977\)105<0421:tcmssp>2.0.co;2](https://doi.org/10.1175/1520-0493(1977)105<0421:tcmssp>2.0.co;2)
- Baatsen, M., Haarsma, R. J., Van Delden, A. J., & de Vries, H. (2015). Severe Autumn storms in future Western Europe with a warmer Atlantic Ocean. [journal article]. *Clim Dynam*, 45(3), pp. 949-964. doi:10.1007/s00382-014-2329-8
- Bacmeister, J. T., Reed, K. A., Hannay, C., Lawrence, P., Bates, S., Truesdale, J. E., . . . Levy, M. (2016). Projected changes in tropical cyclone activity under future warming scenarios using a high-resolution climate model. [journal article]. *Climatic Change*doi:10.1007/s10584-016-1750-x
- Bakkensen, L. A., Park, D.-S. R., & Sarkar, R. S. R. (2018). Climate costs of tropical cyclone losses also depend on rain. *Environmental Research Letters*, 13(7), p 074034. doi:10.1088/1748-9326/aad056
- Bassill, N. P. (2014). Accuracy of early GFS and ECMWF Sandy (2012) track forecasts: Evidence for a dependence on cumulus parameterization. *Geophys Res Lett*, 41(9), pp. 3274-3281. doi:10.1002/2014GL059839
- Bauer, P., Thorpe, A., & Brunet, G. (2015). The quiet revolution of numerical weather prediction. *Nature*, 525(7567), pp. 47-55. doi:10.1038/nature14956
- Bean, H., Liu, B. F., Madden, S., Sutton, J., Wood, M. M., & Mileti, D. S. (2016). Disaster Warnings in Your Pocket: How Audiences Interpret Mobile Alerts for an Unfamiliar Hazard. *Journal of Contingencies and Crisis Management*, 24(3), pp. 136-147. doi:10.1111/1468-5973.12108
- Bell, H. M., & Tobin, G. A. (2007). Efficient and effective? The 100-year flood in the communication and perception of flood risk. *Environmental Hazards*, 7(4), pp. 302-311. doi:10.1016/j.envhaz.2007.08.004
- Beven II, J. L., Berg, R., & Hagen, A. (2019). *Tropical Cyclone Report: Hurricane Michael*.
- Bhatia, K., Vecchi, G., Murakami, H., Underwood, S., & Kossin, J. (2018). Projected response of tropical cyclone intensity and intensification in a global climate model. *Journal of Climate*, 31(20), pp. 8281-8303.
- Bister, M., & Emanuel, K. A. (2002). Low frequency variability of tropical cyclone potential intensity I. Interannual to interdecadal variability. *Journal of Geophysical Research: Atmospheres*, 107(D24), pp. ACL 26-21-ACL 26-15. doi:<https://doi.org/10.1029/2001JD000776>
- Blake, E. S., Kimberlian, T. B., Cangialosi, J. P., & Beven II, J. L. (2013). *Tropical Cyclone Report: Hurricane Sandy*.
- Blake, E. S., & Zelinsky, D. A. (2018). *National Hurricane Center Tropical Cyclone Report: Hurricane Harvey*. [https://www.nhc.noaa.gov/data/tcr/AL092017\\_Harvey.pdf](https://www.nhc.noaa.gov/data/tcr/AL092017_Harvey.pdf)
- Bloemendaal, N., de Moel, H., Muis, S., Haigh, I. D., & Aerts, J. C. J. H. (2020a). Estimation of global tropical cyclone wind speed probabilities using the STORM dataset. *Scientific Data*, 7(1), p 377. doi:10.1038/s41597-020-00720-x



- Bloemendaal, N., De Moel, H., Muis, S., Haigh, I. D., & Aerts, J. C. J. H. (2020b). *STORM tropical cyclone wind speed return periods* [Data set]. doi:<https://doi.org/10.4121/uuid:779b9dfd-b0ff-4531-8833-aaa9c0cf6b5a>
- Bloemendaal, N., Haigh, I. D., de Moel, H., Muis, S., Haarsma, R. J., & Aerts, J. C. J. H. (2020c). Generation of a global synthetic tropical cyclone hazard dataset using STORM. *Sci. Data*, 7(1), p 40. doi:<https://doi.org/10.1038/s41597-020-0381-2>
- Bloemendaal, N., Muis, S., Haarsma, R. J., Verlaan, M., Irazoqui Apecechea, M., de Moel, H., . . . Aerts, J. C. J. H. (2019). Global modeling of tropical cyclone storm surges using high-resolution forecasts. *Climate Dynamics*, 52(7), pp. 5031-5044. doi:10.1007/s00382-018-4430-x
- Boer, G. J., & Denis, B. (1997). Numerical convergence of the dynamics of a GCM. [journal article]. *Clim Dynam*, 13(5), pp. 359-374. doi:10.1007/s003820050171
- Bourque, L. B., Regan, R., Kelley, M. M., Wood, M. M., Kano, M., & Mileti, D. S. (2012). An Examination of the Effect of Perceived Risk on Preparedness Behavior. *Environment and Behavior*, 45(5), pp. 615-649. doi:10.1177/0013916512437596
- Brandon, C. M., Woodruff, J. D., Donnelly, J. P., & Sullivan, R. M. (2014). How Unique was Hurricane Sandy? Sedimentary Reconstructions of Extreme Flooding from New York Harbor. *Scientific Reports*, 4(1), p 7366. doi:10.1038/srep07366
- Broad, K., Leiserowitz, A., Weinkle, J., & Steketee, M. (2007). Misinterpretations of the “Cone of Uncertainty” in Florida during the 2004 Hurricane Season. *Bulletin of the American Meteorological Society*, 88(5), pp. 651-668. doi:10.1175/BAMS-88-5-651
- Bruyère, C., Rasmussen, R., Gutmann, E., Done, J., Tye, M., Jaye, A., . . . Fredrick, S. (2017). Impact of climate change on Gulf of Mexico hurricanes. *NCAR Tech Note. NCAR/TN535*
- Bunya, S., Dietrich, J. C., Westerink, J. J., Ebersole, B. A., Smith, J. M., Atkinson, J. H., . . . Roberts, H. J. (2010). A High-Resolution Coupled Riverine Flow, Tide, Wind, Wind Wave, and Storm Surge Model for Southern Louisiana and Mississippi. Part I: Model Development and Validation. *Mon Weather Rev*, 138(2), pp. 345-377. doi:10.1175/2009MWR2906.1
- Bureau of Meteorology. (2017). Severe Tropical Cyclone Yasi, 30 January - 3 February 2011. Retrieved Date from <http://www.bom.gov.au/cyclone/history/yasi.shtml>.
- Byrne, D., Horsburgh, K., Zachry, B., & Cipollini, P. (2017). Using remotely sensed data to modify wind forcing in operational storm surge forecasting. [journal article]. *Nat Hazards*, 89(1), pp. 275-293. doi:10.1007/s11069-017-2964-6
- Caduff, C. (2010). Public prophylaxis: Pandemic influenza, pharmaceutical prevention and participatory governance. *BioSocieties*, 5(2), pp. 199-218. doi:10.1057/biosoc.2010.1
- Camargo, S. J. (2013). Global and Regional Aspects of Tropical Cyclone Activity in the CMIP5 Models. *Journal of Climate*, 26(24), pp. 9880-9902. doi:10.1175/jcli-d-12-00549.1
- Camargo, S. J., Robertson, A. W., Barnston, A. G., & Ghil, M. (2008). Clustering of eastern North Pacific tropical cyclone tracks: ENSO and MJO effects. *Geochem Geophys*, 9(6)doi:<https://doi.org/10.1029/2007gc001861>
- Cangialosi, J. P. (2019). *National Hurricane Center Forecast Verification Report: 2018 Hurricane Season*. [https://www.nhc.noaa.gov/verification/pdfs/Verification\\_2018.pdf](https://www.nhc.noaa.gov/verification/pdfs/Verification_2018.pdf)
- Cangialosi, J. P., Latto, A. S., & Berg, R. (2018). *Tropical Cyclone Report: Hurricane Irma, 30 August - 12 September 2017*.
- Cardone, V. J., & Cox, A. T. (2009). Tropical cyclone wind field forcing for surge models: critical issues and sensitivities. [journal article]. *Nat Hazards*, 51(1), pp. 29-47. doi:10.1007/s11069-009-9369-0
- Carrère, L., & Lyard, F. (2003). Modeling the barotropic response of the global ocean to atmospheric wind and pressure forcing - comparisons with observations. *Geophys Res Lett*, 30(6), pp. n/a-n/a. doi:10.1029/2002GL016473
- Casson, E., & Coles, S. (2000). Simulation and extremal analysis of hurricane events. *J Royal Stat. Soc.*, 49(3), pp. 227-245. doi:<https://doi.org/10.1111/1467-9876.00189>
- Celsi, R., Wolfenbarger, M., & Wald, D. (2005). The effects of earthquake measurement concepts and magnitude anchoring on individuals' perceptions of earthquake risk. *Earthquake Spectra*, 21(4), pp. 987-1008. doi:10.1193/1.2099047
- Cervený, R. S., Bessemoulin, P., Burt, C. C., Cooper, M. A., Cunjie, Z., Dewan, A., . . . Wahab, M. M. A. (2017). WMO Assessment of Weather and Climate Mortality Extremes: Lightning, Tropical Cyclones, Tornadoes, and Hail. *Weather, Climate, and Society*, 9(3), pp. 487-497. doi:10.1175/WCAS-D-16-0120.1

- Cervený, R. S., & Newman, L. E. (2000). Climatological Relationships between Tropical Cyclones and Rainfall. *Monthly Weather Review*, 128(9), pp. 3329-3336. doi:10.1175/1520-0493(2000)128<3329:crbtca>2.0.co;2
- Chavas, D. R., Lin, N., Dong, W., & Lin, Y. (2016). Observed Tropical Cyclone Size Revisited. *J. Climate*, 29(8), pp. 2923-2939. doi:10.1175/jcli-d-15-0731.1
- Collins, J., Ersing, R., & Polen, A. (2017). Evacuation Decision-Making during Hurricane Matthew: An Assessment of the Effects of Social Connections. *Weather, Climate, and Society*, 9(4), pp. 769-776. doi:10.1175/wcas-d-17-0047.1
- Collins, J., Ersing, R., Polen, A., Saunders, M., & Senkbeil, J. (2018). The Effects of Social Connections on Evacuation Decision Making during Hurricane Irma. *Weather, Climate, and Society*, 10(3), pp. 459-469. doi:10.1175/wcas-d-17-0119.1
- Commonwealth of Australia. (2013). *Current and future tropical cyclone risk in the South Pacific: South Pacific regional risk assessment*. <https://www.pacificclimatechange.net/document/current-and-future-tropical-cyclone-risk-south-pacific-south-pacific-regional-risk>
- Cook, G. D., & Nicholls, M. J. (2009). Estimation of Tropical Cyclone Wind Hazard for Darwin: Comparison with Two Other Locations and the Australian Wind-Loading Code. *J Appl Meteorol Climatol*, 48(11), pp. 2331-2340. doi:https://doi.org/10.1175/2009JAMC2013.1
- Davis, C. A. (2018). Resolving Tropical Cyclone Intensity in Models. *Geophysical Research Letters*, 45(4), pp. 2082-2087. doi:https://doi.org/10.1002/2017GL076966
- De Moel, H., Asselman, N. E. M., & Aerts, J. C. J. H. (2012). Uncertainty and sensitivity analysis of coastal flood damage estimates in the west of the Netherlands. *Nat. Hazards Earth Syst. Sci.*, 12, pp. 1045-1058. doi:10.5194/nhess-12-1045-2012
- Dee, D. P., Uppala, S. M., Simmons, A. J., Berrisford, P., Poli, P., Kobayashi, S., . . . Vitart, F. (2011). The ERA-Interim reanalysis: configuration and performance of the data assimilation system. *Q J R Meteorol Soc*, 137(656), pp. 553-597. doi:10.1002/qj.828
- DeMaria, M., & Kaplan, J. (1994). Sea Surface Temperature and the Maximum Intensity of Atlantic Tropical Cyclones. *J. Climate*, 7(9), pp. 1324-1334. doi:https://doi.org/10.1175/1520-0442(1994)007<1324:ssstatm>2.0.co;2
- Dietrich, J. C., Bunya, S., Westerink, J. J., Ebersole, B. A., Smith, J. M., Atkinson, J. H., . . . Roberts, H. J. (2010). A High-Resolution Coupled Riverine Flow, Tide, Wind, Wind Wave, and Storm Surge Model for Southern Louisiana and Mississippi. Part II: Synoptic Description and Analysis of Hurricanes Katrina and Rita. *Mon Weather Rev*, 138, pp. 378-404.
- Doblas-Reyes, F. J., Navarro, J. C., Batté, L., Volpi, D., Acosta, M., Bellprat, O., . . . Massonet, F. (2018). Using EC-Earth for climate prediction research. <https://www.ecmwf.int/node/18205>
- Done, J. M., Ge, M., Holland, G. J., Dima-West, I., Phibbs, S., Saville, G. R., & Wang, Y. (2020). Modelling global tropical cyclone wind footprints. *Nat. Hazards Earth Syst. Sci.*, 20(2), pp. 567-580. doi:https://doi.org/10.5194/nhess-20-567-2020
- Dullaart, J. C. M., Muis, S., Bloemendaal, N., & Aerts, J. C. J. H. (2020). Advancing global storm surge modelling using the new ERA5 climate reanalysis. *Climate Dynamics*, 54(1), pp. 1007-1021. doi:10.1007/s00382-019-05044-0
- Dullaart, J. C. M., Muis, S., Bloemendaal, N., Chertova, M. V., Couasnon, A., & Aerts, J. C. J. H. (2021). Accounting for tropical cyclones more than doubles the global population exposed to low-probability coastal flooding. *Communications Earth & Environment*, 2(1), p 135. doi:10.1038/s43247-021-00204-9
- Eberenz, S., Lüthi, S., & Bresch, D. N. (2021). Regional tropical cyclone impact functions for globally consistent risk assessments. *Nat. Hazards Earth Syst. Sci.*, 21(1), pp. 393-415. doi:10.5194/nhess-21-393-2021
- EC-Earth Consortium. (2018). *EC-Earth-Consortium EC-Earth3P-HR model output prepared for CMIP6 HighResMIP* [Data set]. doi:10.22033/ESGF/CMIP6.2323
- ECMWF. (2016). ERA-Interim. Retrieved Date Accessed, 2016 from <http://www.ecmwf.int/en/research/climate-reanalysis/era-interim>.
- ECMWF. (2017a). Changes in ECMWF model: evolution of the IFS. Retrieved Date from <http://www.ecmwf.int/en/forecasts/documentation-and-support/changes-ecmwf-model>.
- ECMWF. (2017b). Known IFS forecasting issues. Retrieved Date from <https://software.ecmwf.int/wiki/display/FCST/Known+IFS+forecasting+issues>.
- ECMWF. (2017c). What is ERA5. Retrieved Date from <https://software.ecmwf.int/wiki/display/CKB/What+is+ERA5>.

- ECMWF. (2020). Continuous data assimilation for the IFS. Retrieved Date Accessed, 2020 from <https://www.ecmwf.int/en/newsletter/158/meteorology/continuous-data-assimilation-ifs>.
- Ellis, K. N., Trepanier, J. C., & Hodges, R. E. (2016). Using Synthetic Tropical Cyclones to Characterize Extreme Hurricanes Affecting Charleston, South Carolina. *J Appl Meteorol Climatol*, 55(4), pp. 883-892. doi:<https://doi.org/10.1175/JAMC-D-15-0215.1>
- Emanuel, K. (2007). Environmental Factors Affecting Tropical Cyclone Power Dissipation. *Journal of Climate*, 20(22), pp. 5497-5509. doi:[doi:10.1175/2007JCLI1571.1](https://doi.org/10.1175/2007JCLI1571.1)
- Emanuel, K. (2008). The Hurricane—Climate Connection. *Bull. Amer. Meteor. Soc.*, 89(5), pp. ES10-ES20. doi:<https://doi.org/10.1175/BAMS-89-5-Emanuel>
- Emanuel, K. (2017). Assessing the present and future probability of Hurricane Harvey's rainfall. *Proceedings of the National Academy of Sciences* doi:[10.1073/pnas.1716222114](https://doi.org/10.1073/pnas.1716222114)
- Emanuel, K. (2021). Response of Global Tropical Cyclone Activity to Increasing CO<sub>2</sub>: Results from Downscaling CMIP6 Models. *Journal of Climate*, 34(1), pp. 57-70. doi:[10.1175/JCLI-D-20-0367.1](https://doi.org/10.1175/JCLI-D-20-0367.1)
- Emanuel, K., Ravela, S., Vivant, E., & Risi, C. (2006). A Statistical Deterministic Approach to Hurricane Risk Assessment. *Bull. Am. Meteor. Soc.*, 87(3), pp. 299-314. doi:<https://doi.org/10.1175/BAMS-87-3-299>
- Emanuel, K., Sundararajan, R., & Williams, J. (2008). Hurricanes and Global Warming: Results from Downscaling IPCC AR4 Simulations. *Bulletin of the American Meteorological Society*, 89(3), pp. 347-367. doi:[10.1175/BAMS-89-3-347](https://doi.org/10.1175/BAMS-89-3-347)
- Emanuel, K. A. (1987). The dependence of hurricane intensity on climate. *Nature*, 326, pp. 483-485. doi:<https://doi.org/10.1038/326483a0>
- Esteves, L. S. (2013). Consequences to flood management of using different probability distributions to estimate extreme rainfall. *J. Environ. Manage*, 115, pp. 98-105. doi:<https://doi.org/10.1016/j.jenvman.2012.11.013>
- Eyring, V., Bony, S., Meehl, G. A., Senior, C. A., Stevens, B., Stouffer, R. J., & Taylor, K. E. (2016). Overview of the Coupled Model Intercomparison Project Phase 6 (CMIP6) experimental design and organization. *Geosci. Model Dev.*, 9(5), pp. 1937-1958. doi:[10.5194/gmd-9-1937-2016](https://doi.org/10.5194/gmd-9-1937-2016)
- FEMA. (2014a). *Puerto Rico Hurricane Evacuation Study Behavioral Analysis*.
- FEMA. (2014b). *U. S. Virgin Islands Hurricane Evacuation Study Behavioral Analysis*.
- Fiedler, T., Pitman, A. J., Mackenzie, K., Wood, N., Jakob, C., & Perkins-Kirkpatrick, S. E. (2021). Business risk and the emergence of climate analytics. *Nature Climate Change*, 11(2), pp. 87-94. doi:[10.1038/s41558-020-00984-6](https://doi.org/10.1038/s41558-020-00984-6)
- Fiorino, M. (2008). *Record-setting performance of the ECMWF IFS in medium-range tropical cyclone track prediction*.
- Flato, G., Marotzke, J., Abiodun, B., Braconnot, P., Chou, S. C., Collins, W., . . . Rummukainen, M. (2013). Evaluation of Climate Models. In T. F. Stocker, D. Qin, G.-K. Plattner, M. Tignor, S. K. Allen, J. Boschung, A. Nauels, Y. Xia, V. Bex & P. M. Midgley (Eds.), *Climate Change 2013: The Physical Science Basis. Contribution of Working Group I to the Fifth Assessment Report of the Intergovernmental Panel on Climate Change* (pp. 741-866). Cambridge, United Kingdom and New York, NY, USA: Cambridge University Press.
- Forbes, C., Rhome, J., Mattocks, C., & Taylor, A. (2014). Predicting the Storm Surge Threat of Hurricane Sandy with the National Weather Service SLOSH Model. *Journal of Marine Science and Engineering*, 2(2), p 437.
- Fritz, H. M., Blount, C. D., Albusaidi, F. B., & Al-Harthy, A. H. M. (2010). Cyclone Gonu storm surge in Oman. *Estuar Coast Shelf S*, 86(1), pp. 102-106. doi:[10.1016/j.ecss.2009.10.019](https://doi.org/10.1016/j.ecss.2009.10.019)
- GADM. (2017). GADM database of Global Administrative Areas. Retrieved Date from <http://www.gadm.org/>.
- Garner, A. J., Mann, M. E., Emanuel, K. A., Kopp, R. E., Lin, N., Alley, R. B., . . . Pollard, D. (2017). Impact of climate change on New York City's coastal flood hazard: Increasing flood heights from the preindustrial to 2300 CE. *PNAS*, 114(45), p 11861. doi:<https://doi.org/10.1073/pnas.1703568114>
- Gettelman, A., Bresch, D. N., Chen, C. C., Truesdale, J. E., & Bacmeister, J. T. (2018). Projections of future tropical cyclone damage with a high-resolution global climate model. *Climatic Change*, 146(3), pp. 575-585. doi:[10.1007/s10584-017-1902-7](https://doi.org/10.1007/s10584-017-1902-7)
- Glahn, B., Taylor, A., Kurkowski, N., & Shaffer, W. A. (2009). The role of the SLOSH model in National Weather Service storm surge forecasting. *National Weather Digest*, 33(1), pp. 3-14.

- Goldstein, D. G., & Rothschild, D. (2014). Lay understanding of probability distributions. *Judgment & Decision Making*, 9(1)
- Haarsma, R. J., Hazeleger, W., Severijns, C., de Vries, H., Sterl, A., Bintanja, R., . . . van den Brink, H. W. (2013). More hurricanes to hit western Europe due to global warming. *Geophysical Research Letters*, 40(9), pp. 1783-1788. doi:10.1002/grl.50360
- Haarsma, R. J., Roberts, M., Vidale, P. L., Senior, C. A., Bellucci, A., Bao, Q., . . . von Storch, J. S. (2016). High Resolution Model Intercomparison Project (HighResMIP) for CMIP6. *Geosci. Model Dev.*, 2016, pp. 1-35. doi:10.5194/gmd-2016-66
- Haigh, I. D., MacPherson, L. R., Mason, M. S., Wijeratne, E. M. S., Pattiaratchi, C. B., Crompton, R. P., & George, S. (2014). Estimating present day extreme water level exceedance probabilities around the coastline of Australia: tropical cyclone-induced storm surges. [journal article]. *Clim Dynam*, 42(1), pp. 139-157. doi:https://doi.org/10.1007/s00382-012-1653-0
- Hardy, T. A., McConochie, J. D., & Mason, L. B. (2003). Modeling Tropical Cyclone Wave Population of the Great Barrier Reef. *J Waterw Port C Div*, 129(3), pp. 104-113. doi:https://doi.org/10.1061/(ASCE)0733-950X(2003)129:3(104)
- Harper, B. (2002). *Tropical Cyclone Parameter Estimation in the Australian Region: Wind-Pressure Relationships and Related Issues for Engineering Planning and Design - A Discussion Paper*.
- Harper, B., & Holland, G. (1999). *An updated parametric model of the tropical cyclone*. Proc. 23rd Conf. Hurricanes and Tropical Meteorology.
- Harper, B. A., Kepert, J. D., & Ginger, J. D. (2008). *Guidelines for converting between various wind averaging periods in tropical cyclone conditions*.
- Hazen, A. (1930). Flood flows: a study of frequencies and magnitudes *Flood flows: a study of frequencies and magnitudes*: John Wiley & Sons.
- Hebert, C. G., Weinzapfel, R. A., & Chambers, M. A. (2010) *Hurricane Severity Index: A New Way of Estimating Hurricane Destructive Potential*. Paper presented at the 29th Conference on Hurricanes and Tropical Meteorology, Tucson (AZ), USA.
- Hersbach, H., Bell, B., Berrisford, P., Horányi, A., Muñoz Sabater, J., Nicholas, J., . . . Dee, D. (2019). *Global Reanalysis: goodbye ERA-Interim, hello ERA5*. <https://www.ecmwf.int/node/19027>
- Hersbach, H., & Dee, D. (2016). ERA5 reanalysis is in production. *ECMWF Newsletter*(147)
- Hijmans, R. (2016). 2. The length of a coastline. Retrieved Date from <http://rtpatial.org/cases/rst/2-coastline.html>.
- Hiroaki, I., Yukiko, H., Dai, Y., Sanne, M., J., W. P., C., W. H., . . . Shinjiro, K. (2017). Compound simulation of fluvial floods and storm surges in a global coupled river-coast flood model: Model development and its application to 2007 Cyclone Sidr in Bangladesh. *J Adv Model Earth Sy*, 9(4), pp. 1847-1862. doi:doi:10.1002/2017MS000943
- Hodges, K., Cobb, A., & Vidale, P. L. (2017). How Well Are Tropical Cyclones Represented in Reanalysis Datasets? *J Climate*, 30(14), pp. 5243-5264. doi:10.1175/jcli-d-16-0557.1
- Holland, G. J. (1980). An Analytic Model of the Wind and Pressure Profiles in Hurricanes. *Mon Weather Rev*, 108(8), pp. 1212-1218. doi:https://doi.org/10.1175/1520-0493(1980)108<1212:aamotw>2.0.co;2
- Holland, G. J. (1997). The Maximum Potential Intensity of Tropical Cyclones. *J Atmos. Sci.*, 54(21), pp. 2519-2541. doi:https://doi.org/10.1175/1520-0469(1997)054<2519:tmpiot>2.0.co;2
- Holland, G. J., Done, J. M., Douglas, R., Saville, G. R., & Ge, M. (2019). Global Tropical Cyclone Damage Potential. In J. M. Collins & K. Walsh (Eds.), *Hurricane Risk* (pp. 23-42). Cham: Springer International Publishing.
- Irazoqui Apecechea, M., Verlaan, M., Zijl, F., Le Coz, C., & Kernkamp, H. (2017). Effects of self-attraction and loading at a regional scale: a test case for the Northwest European Shelf. [journal article]. *Ocean Dyn*, 67(6), pp. 729-749. doi:10.1007/s10236-017-1053-4
- Irish, J. L., & Resio, D. T. (2010). A hydrodynamics-based surge scale for hurricanes. *Ocean Engineering*, 37(1), pp. 69-81. doi:https://doi.org/10.1016/j.oceaneng.2009.07.012
- Irish, J. L., Resio, D. T., & Ratcliff, J. J. (2008). The Influence of Storm Size on Hurricane Surge. *J Phys Oceanogr*, 38(9), pp. 2003-2013. doi:10.1175/2008jpo3727.1
- Jagers, B., Rego, J., Verlaan, M., Lalic, A., Genseberger, M., Friocourt, Y., & van der Pijl, S. (2014). *A Global Tide and Storm Surge Model with a Parallel Unstructured-Grid Shallow Water Solver*. AGU Fall Meeting Abstracts.
- Jakobsen, F., & Madsen, H. (2004). Comparison and further development of parametric tropical cyclone models for storm surge modelling. *J Wind Eng Ind Aerod*, 92(5), pp. 375-391. doi:http://dx.doi.org/10.1016/j.jweia.2004.01.003

- James, M. K., & Mason, L. B. (2005). Synthetic Tropical Cyclone Database. *J Waterw Port C Div*, 131(4), pp. 181-192. doi:https://doi.org/10.1061/(ASCE)0733-950X(2005)131:4(181)
- Jelesnianski, C., Jye, C., Shaffer, W., & Gilad, A. (1984, 0-0 Sept. 1984). *SLOSH - A Hurricane Storm Surge Forecast Model*. OCEANS 1984.
- Jones, B., & O'Neill, B. C. (2020). *Global One-Eighth Degree Population Base Year and Projection Grids Based on the Shared Socioeconomic Pathways, Revision 01* [Data set].
- Jones, G., & Richardson, M. (2007). An objective examination of consumer perception of nutrition information based on healthiness ratings and eye movements. *Public Health Nutrition*, 10(3), pp. 238-244. doi:10.1017/S1368980007258513
- Jones, P. W. (1999). First- and Second-Order Conservative Remapping Schemes for Grids in Spherical Coordinates. *Mon Weather Rev*, 127(9), pp. 2204-2210. doi:10.1175/1520-0493(1999)127<2204:fasocr>2.0.co;2
- Jongman, B., Winsemius, H. C., Aerts, J. C. J. H., Coughlan de Perez, E., van Aalst, M. K., Kron, W., & Ward, P. J. (2015). Declining vulnerability to river floods and the global benefits of adaptation. *Proceedings of the National Academy of Sciences*, 112(18), pp. E2271-E2280. doi:10.1073/pnas.1414439112
- Kalnay, E., Kanamitsu, M., Kistler, R., Collins, W., Deaven, D., Gandin, L., . . . Joseph, D. (1996). The NCEP/NCAR 40-Year Reanalysis Project. *B Am Meteorol Soc*, 77(3), pp. 437-471. doi:10.1175/1520-0477(1996)077<0437:tnyrp>2.0.co;2
- Kantha, L. (2006). Time to replace the Saffir-Simpson hurricane scale? *Eos, Transactions American Geophysical Union*, 87(1), pp. 3-6. doi:doi:10.1029/2006EO010003
- Kantha, L. (2008). Tropical Cyclone Destructive Potential by Integrated Kinetic Energy. *Bulletin of the American Meteorological Society*, 89(2), pp. 219-221.
- Kantha, L. (2013). Classification of hurricanes: Lessons from Katrina, Ike, Irene, Isaac and Sandy. *Ocean Engineering*, 70, pp. 124-128. doi:https://doi.org/10.1016/j.oceaneng.2013.06.007
- Kaplan, J., & DeMaria, M. (1995). A Simple Empirical Model for Predicting the Decay of Tropical Cyclone Winds after Landfall. *J. Appl. Meteorol.*, 34(11), pp. 2499-2512. doi:https://doi.org/10.1175/1520-0450(1995)034<2499:ASEMFP>2.0.CO;2
- Kasperson, R. E., & Kasperson, J. X. (1996). The Social Amplification and Attenuation of Risk. *The Annals of the American Academy of Political and Social Science*, 545, pp. 95-105.
- Kay, J. E., Deser, C., Phillips, A., Mai, A., Hannay, C., Strand, G., . . . Vertenstein, M. (2015). The Community Earth System Model (CESM) Large Ensemble Project: A Community Resource for Studying Climate Change in the Presence of Internal Climate Variability. *Bulletin of the American Meteorological Society*, 96(8), pp. 1333-1349. doi:10.1175/bams-d-13-00255.1
- Kernkamp, H. W. J., Van Dam, A., Stelling, G. S., & de Goede, E. D. (2011). Efficient scheme for the shallow water equations on unstructured grids with application to the Continental Shelf. [journal article]. *Ocean Dyn*, 61(8), pp. 1175-1188. doi:10.1007/s10236-011-0423-6
- Kerr, P. C., Martyr, R. C., Donahue, A. S., Hope, M. E., Westerink, J. J., Luettich, R. A., . . . Westerink, H. J. (2013). U.S. IOOS coastal and ocean modeling testbed: Evaluation of tide, wave, and hurricane surge response sensitivities to mesh resolution and friction in the Gulf of Mexico. *Journal of Geophysical Research: Oceans*, 118(9), pp. 4633-4661. doi:doi:10.1002/jgrc.20305
- Kimberlian, T. B., Blake, E. S., & Cangialosi, J. P. (2016). *Tropical Cyclone Report: Hurricane Patricia*.
- Klima, K., Lin, N., Emanuel, K., Morgan, M. G., & Grossmann, I. (2012). Hurricane Modification and Adaptation in Miami-Dade County, Florida. *Environmental Science and Technology*, 46(2), pp. 636-642. doi:10.1021/es202640p
- Knapp, K. R., Kruk, M. C., Levinson, D. H., Diamond, H. J., & Neumann, C. J. (2010). The International Best Track Archive for Climate Stewardship (IBTrACS) Unifying Tropical Cyclone Data. *Bull. Am. Meteor. Soc.*, 91(3), pp. 363-376. doi:https://doi.org/10.1175/2009BAMS2755.1
- Knutson, T., Camargo, S. J., Chan, J. C., Emanuel, K., Ho, C.-H., Kossin, J., . . . Walsh, K. (2020). Tropical cyclones and climate change assessment: Part II: Projected response to anthropogenic warming. *Bulletin of the American Meteorological Society*, 101(3), pp. E303-E322.
- Knutson, T. R., Sirutis, J. J., Vecchi, G. A., Garner, S., Zhao, M., Kim, H.-S., . . . Villarini, G. (2013). Dynamical Downscaling Projections of Twenty-First-Century Atlantic Hurricane Activity: CMIP3 and CMIP5 Model-Based Scenarios. *Journal of Climate*, 26(17), pp. 6591-6617. doi:doi:10.1175/JCLI-D-12-00539.1
- Kolmogorov, A. N. (1937). Markov chains with a countable number of possible states. *Bull. Mosk. Gos. Univ. Math. Mekh*, 1(3), pp. 1-15.

- Kossin, J. P., Emanuel, K. A., & Camargo, S. J. (2016). Past and Projected Changes in Western North Pacific Tropical Cyclone Exposure. *Journal of Climate*, 29(16), pp. 5725-5739. doi:10.1175/jcli-d-16-0076.1
- Kossin, J. P., Emanuel, K. A., & Vecchi, G. A. (2014a). The poleward migration of the location of tropical cyclone maximum intensity. *Nature*, 509, p 349. doi:10.1038/nature13278
- Kossin, J. P., Emanuel, K. A., & Vecchi, G. A. (2014b). The poleward migration of the location of tropical cyclone maximum intensity. *Nature*, 509(7500), pp. 349-352. doi:10.1038/nature13278
- Kotz, S., & Nadarajah, S. (2000). *Extreme Value Distributions: Theory and Applications* London: Imperial College Press.
- Kruk, M. C., Gibney, E. J., Levinson, D. H., & Squires, M. (2010). A Climatology of Inland Winds from Tropical Cyclones for the Eastern United States. *J Appl Meteorol Climatol*, 49(7), pp. 1538-1547. doi:https://doi.org/10.1175/2010jamc2389.1
- Lazo, J. K., Waldman, D. M., Morrow, B. H., & Thacher, J. A. (2010). Household Evacuation Decision Making and the Benefits of Improved Hurricane Forecasting: Developing a Framework for Assessment. *Weather and Forecasting*, 25(1), pp. 207-219. doi:10.1175/2009WAF2222310.1
- Lee, C.-Y., Camargo, S. J., Sobel, A. H., & Tippett, M. K. (2020). Statistical-Dynamical Downscaling Projections of Tropical Cyclone Activity in a Warming Climate: Two Diverging Genesis Scenarios. *Journal of Climate*, 33(11), pp. 4815-4834. doi:10.1175/jcli-d-19-0452.1
- Lee, C.-Y., Tippett, M. K., Sobel, A. H., & Camargo, S. J. (2018). An Environmentally Forced Tropical Cyclone Hazard Model. *JAMES*, 10(1), pp. 223-241. doi:https://doi.org/10.1002/2017MS001186
- Lin, N., & Chavas, D. (2012). On hurricane parametric wind and applications in storm surge modeling. *J Geophys Res - Atmos*, 117(D9), pp. n/a-n/a. doi:https://doi.org/10.1029/2011JD017126
- Lin, N., & Emanuel, K. (2016). Grey swan tropical cyclones. *Nature Climate Change*, 6, pp. 106-111. doi:10.1038/nclimate2777
- Lin, N., Emanuel, K., Oppenheimer, M., & Vanmarcke, E. (2012). Physically based assessment of hurricane surge threat under climate change. [10.1038/nclimate1389]. *Nat. Clim. Change*, 2(6), pp. 462-467. doi:https://doi.org/10.1038/nclimate1389
- Lin, N., Emanuel, K. A., Smith, J. A., & Vanmarcke, E. (2010). Risk assessment of hurricane storm surge for New York City. *J Geophys Res*, 115doi:10.1029/2009JD013630
- Lin, N., Kopp, R. E., Horton, B. P., & Donnelly, J. P. (2016). Hurricane Sandy's flood frequency increasing from year 1800 to 2100. *Proceedings of the National Academy of Sciences*doi:10.1073/pnas.1604386113
- Lin, N., Lane, P., Emanuel, K. A., Sullivan, R. M., & Donnelly, J. P. (2014). Heightened hurricane surge risk in northwest Florida revealed from climatological-hydrodynamic modeling and paleorecord reconstruction. *J. Geophys. Res Atmos.*, 119(14), pp. 8606-8623. doi:https://doi.org/10.1002/2014JD021584
- Lindell, M. K., & Perry, R. W. (2012). The Protective Action Decision Model: Theoretical Modifications and Additional Evidence. *Risk Analysis*, 32(4), pp. 616-632. doi:10.1111/j.1539-6924.2011.01647.x
- Lindner, B. L., Alsheimer, F., & Johnson, J. (2018). Assessing Improvement in the Public's Understanding of Hurricane Storm Tides Through Interactive Visualization Models. *Journal of Coastal Research*, pp. 130-142. doi:10.2112/JCOASTRES-D-17-00223.1
- Luitel, B., Villarini, G., & Vecchi, G. A. (2018). Verification of the skill of numerical weather prediction models in forecasting rainfall from U.S. landfalling tropical cyclones. *Journal of Hydrology*, 556, pp. 1026-1037. doi:https://doi.org/10.1016/j.jhydrol.2016.09.019
- Magnusson, L., Bidlot, J.-R., Lang, S. T. K., Thorpe, A., Wedi, N., & Yamaguchi, M. (2014). Evaluation of Medium-Range Forecasts for Hurricane Sandy. *Mon Weather Rev*, 142(5), pp. 1962-1981. doi:10.1175/mwr-d-13-00228.1
- Makkonen, L. (2006). Plotting positions in extreme value analysis. *J Appl Meteorol Climatol*, 45(2), pp. 334-340.
- Malmstadt, J. C., Elsner, J. B., & Jagger, T. H. (2010). Risk of Strong Hurricane Winds to Florida Cities. *J Appl Meteorol Climatol*, 49(10), pp. 2121-2132. doi:https://doi.org/10.1175/2010JAMC2420.1
- Mamalakis, A., Randerson, J. T., Yu, J.-Y., Pritchard, M. S., Magnusdottir, G., Smyth, P., . . . Fofoula-Georgiou, E. (2021). Zonally contrasting shifts of the tropical rain belt in response to climate change. *Nature Climate Change*, 11(2), pp. 143-151. doi:10.1038/s41558-020-00963-x

- Mandelbrot, B. (1967). How Long Is the Coast of Britain? Statistical Self-Similarity and Fractional Dimension. *Science*, 156(3775), pp. 636-638. doi:10.1126/science.156.3775.636
- Marsooli, R., & Lin, N. (2020). Impacts of climate change on hurricane flood hazards in Jamaica Bay, New York. *Climatic Change*, 163(4), pp. 2153-2171. doi:10.1007/s10584-020-02932-x
- Martinez, A. B. (2020). Forecast Accuracy Matters for Hurricane Damage. *Econometrics*, 8(2), p 18.
- Mase, A. S., Cho, H., & Prokopy, L. S. (2015). Enhancing the Social Amplification of Risk Framework (SARF) by exploring trust, the availability heuristic, and agricultural advisors' belief in climate change. *Journal of Environmental Psychology*, 41, pp. 166-176. doi:https://doi.org/10.1016/j.jenvp.2014.12.004
- Meiler, S., Emanuel, K., & Bresch, D. N. (2021) *How much do modeled tropical cyclone impacts depend on the hazard set choice?* Paper presented at the EGU General Assembly 2021, online.
- Meza-Padilla, R., Appendini, C. M., & Pedrozo-Acuña, A. (2015). Hurricane-induced waves and storm surge modeling for the Mexican coast. *Ocean Dynamics*, 65(8), pp. 1199-1211. doi:10.1007/s10236-015-0861-7
- Mizuta, R., Murata, A., Ishii, M., Shiogama, H., Hibino, K., Mori, N., . . . Aoyagi, T. (2017). Over 5,000 years of ensemble future climate simulations by 60-km global and 20-km regional atmospheric models. *Bulletin of the American Meteorological Society*, 98(7), pp. 1383-1398.
- Mizuta, R., Yoshimura, H., Murakami, H., Matsueda, M., Endo, H., Ose, T., . . . Kitoh, A. (2012). Climate Simulations Using MRI-AGCM3.2 with 20-km Grid. *J Meteorol Soc Jap*, 90A, pp. 233-258. doi:10.2151/jmsj.2012-A12
- Mol, J. M., Botzen, W. J. W., Blasch, J. E., Kranzler, E. C., & Kunreuther, H. C. (2021). All by myself? Testing descriptive social norm-nudges to increase flood preparedness among homeowners. *Behavioural Public Policy*, pp. 1-33. doi:10.1017/bpp.2021.17
- Mori, N., Kato, M., Kim, S., Mase, H., Shibutani, Y., Takemi, T., . . . Yasuda, T. (2014). Local amplification of storm surge by Super Typhoon Haiyan in Leyte Gulf. *Geophys Res Lett*, 41(14), pp. 5106-5113. doi:10.1002/2014GL060689
- Morss, R. E., & Hayden, M. H. (2010). Storm Surge and "Certain Death": Interviews with Texas Coastal Residents following Hurricane Ike. *Weather, Climate, and Society*, 2(3), pp. 174-189. doi:10.1175/2010WCAS1041.1
- Muis, S., Lin, N., Verlaan, M., Winsemius, H. C., Ward, P. J., & Aerts, J. C. J. H. (2019). Spatiotemporal patterns of extreme sea levels along the western North-Atlantic coasts. *Sci Rep* doi:https://doi.org/10.1038/s41598-019-40157-w
- Muis, S., Verlaan, M., Nicholls, R. J., Brown, S., Hinkel, J., Lincke, D., . . . Ward, P. J. (2017). A comparison of two global datasets of extreme sea levels and resulting flood exposure. *Earth's Future*, pp. n/a-n/a. doi:10.1002/2016EF000430
- Muis, S., Verlaan, M., Winsemius, H. C., Aerts, J. C. J. H., & Ward, P. J. (2016). A global reanalysis of storm surges and extreme sea levels. *Nat Comm*, 7doi:https://doi.org/10.1038/ncomms11969
- Munich Re. (2017). *TOPICS GEO Natural Catastrophes 2017*. https://www.munichre.com/content/dam/assets/munichre/content-pieces/documents/pdf/302-09092\_en.pdf
- Murakami, H. (2014). Tropical cyclones in reanalysis data sets. *Geophys Res Lett*, 41(6), pp. 2133-2141. doi:10.1002/2014GL059519
- Murakami, H., & Sugi, M. (2010). Effect of Model Resolution on Tropical Cyclone Climate Projections. *SOLA*, 6, pp. 73-76. doi:10.2151/sola.2010-019
- Neumann, B., Vafeidis, A. T., Zimmermann, J., & Nicholls, R. J. (2015a). Future Coastal Population Growth and Exposure to Sea-Level Rise and Coastal Flooding - A Global Assessment. *PLOS ONE*, 10(3), p e0118571. doi:10.1371/journal.pone.0118571
- Neumann, J. E., Emanuel, K., Ravela, S., Ludwig, L., Kirshen, P., Bosma, K., & Martinich, J. (2015b). Joint effects of storm surge and sea-level rise on US Coasts: new economic estimates of impacts, adaptation, and benefits of mitigation policy. *Climatic Change*, 129(1), pp. 337-349. doi:10.1007/s10584-014-1304-z
- NHC. (2017). Proposed changes to the NHC tropical cyclone forecast graphics for 2017. Retrieved Date from https://www.nhc.noaa.gov/new-tc-graphics/.
- NHC. (2019a). NHC Track and Intensity Models. Retrieved Date Accessed, 2020 from https://www.nhc.noaa.gov/modelsummary.shtml.
- NHC. (2019b). *The Saffir-Simpson Hurricane Wind Scale*. https://www.nhc.noaa.gov/pdf/sshws.pdf
- NHC. (2020a). Sea, Lake, and Overland Surges from Hurricanes (SLOSH). Retrieved Date Accessed, 2020 from https://www.nhc.noaa.gov/surge/slosh.php.

- NHC. (2020b). Tropical Cyclone Reports. Retrieved Date from <https://www.nhc.noaa.gov/data/tcr/>.
- NHC. (n.d.). NHC Tropical cyclone graphical product descriptions. Retrieved Date from <https://www.nhc.noaa.gov/aboutnhcgraphics.shtml>.
- Nikulin, G., Jones, C., Giorgi, F., Asrar, G., Büchner, M., Cerezo-Mota, R., . . . Sushama, L. (2012). Precipitation Climatology in an Ensemble of CORDEX-Africa Regional Climate Simulations. *J. Climate*, 25(18), pp. 6057-6078. doi:10.1175/jcli-d-11-00375.1
- NOAA. (2009). *Technical Summary of the National Hurricane Center Track and Intensity Models*.
- NOAA. (2017). Tides & Great Lakes Water Levels. Retrieved Date from <https://tidesandcurrents.noaa.gov/>.
- NOAA. (2020a). Costliest U.S. Tropical Cyclones. Retrieved Date Accessed, 2020 from <https://www.ncdc.noaa.gov/billions/demi.pdf>.
- NOAA. (2020b). Costliest U.S. Tropical Cyclones. Retrieved Date from <https://www.ncdc.noaa.gov/billions/demi.pdf>.
- NOAA. (2020c). Global Data Assimilation System (GDAS). Retrieved Date Accessed, 2020 from <https://www.ncdc.noaa.gov/data-access/model-data/model-datasets/global-data-assimilation-system-gdas>.
- NOAA National Centers for Environmental Information. (2021). U.S. Billion-Dollar Weather and Climate Disasters. Retrieved Date from <https://www.ncdc.noaa.gov/billions/>.
- Nott, J., & Hayne, M. (2001). High frequency of super-cyclones along the Great Barrier Reef over the past 5,000 years. *Nature*, 413, p 508. doi:<https://doi.org/10.1038/35097055>
- O'Neill, B. C., Tebaldi, C., van Vuuren, D. P., Eyring, V., Friedlingstein, P., Hurtt, G., . . . Sanderson, B. M. (2016). The Scenario Model Intercomparison Project (ScenarioMIP) for CMIP6. *Geosci. Model Dev.*, 9(9), pp. 3461-3482. doi:10.5194/gmd-9-3461-2016
- OCHA. (2019). Cyclones Idai and Kenneth. Retrieved Date from <https://www.unocha.org/southern-and-eastern-africa-rosea/cyclones-idai-and-kenneth>.
- Okan, Y., Stone, E. R., & Bruine de Bruin, W. (2018). Designing Graphs that Promote Both Risk Understanding and Behavior Change. *Risk Analysis*, 38(5), pp. 929-946. doi:10.1111/risa.12895
- Pasch, R. J., Blake, E. S., Cobb III, H. D., & Roberts, D. P. (2006). *Tropical Cyclone Report: Hurricane Wilma*.
- Patricola, C. M., & Wehner, M. F. (2018). Anthropogenic influences on major tropical cyclone events. *Nature*, 563(7731), pp. 339-346. doi:10.1038/s41586-018-0673-2
- Peduzzi, P., Chatenoux, B., Dao, H., De Bono, A., Herold, C., Kossin, J., . . . Nordbeck, O. (2012). Global trends in tropical cyclone risk. [10.1038/nclimate1410]. *Nature Clim. Change*, 2(4), pp. 289-294. doi:<http://www.nature.com/nclimate/journal/v2/n4/abs/nclimate1410.html#supplementary-information>
- Perry, R. W., & Lindell, M. K. (2006). *Wiley Pathways Emergency Planning*: John Wiley & Sons.
- Persson, A., & Grazzini, F. (2005). *User guide to ECMWF forecast products*.
- Petrova, D. G., van der Pligt, J., & Garcia-Retamero, R. (2014). Feeling the Numbers: On the Interplay Between Risk, Affect, and Numeracy. *Journal of Behavioral Decision Making*, 27(3), pp. 191-199. doi:10.1002/bdm.1803
- Phadke, A. C., Martino, C. D., Cheung, K. F., & Houston, S. H. (2003). Modeling of tropical cyclone winds and waves for emergency management. *Ocean Eng*, 30(4), pp. 553-578. doi:[https://doi.org/10.1016/S0029-8018\(02\)00033-1](https://doi.org/10.1016/S0029-8018(02)00033-1)
- Pielke Jr., R. A., Gratz, J., Landsea, C. W., Collins, D., Saunders, M. A., & Musulin, R. (2008). Normalized Hurricane Damage in the United States: 1900-2005. *Natural Hazards Review*, 9(1), pp. 29-42. doi:10.1061/(ASCE)1527-6988(2008)9:1(29)
- Powell, M., Soukup, G., Cocke, S., Gulati, S., Morisseau-Leroy, N., Hamid, S., . . . Axe, L. (2005). State of Florida hurricane loss projection model: Atmospheric science component. *J Wind Eng Ind Aerod*, 93(8), pp. 651-674. doi:<https://doi.org/10.1016/j.jweia.2005.05.008>
- Powell, M. D., & Reinhold, T. A. (2007). Tropical Cyclone Destructive Potential by Integrated Kinetic Energy. *Bulletin of the American Meteorological Society*, 88(4), pp. 513-526. doi:10.1175/bams-88-4-513
- Probst, P., Franchelo, G., Annunziato, A., De Groeve, T., Vernaccini, L., Himer, A., & Andredakis, I. (2012). *Tropical Cyclone GIOVANNA Madagascar, February 2012* (EUR - Scientific and Technical Research Reports No. Luxembourg: P. O. o. t. E. Union.



- 
- Pugh, D., & Woodworth, P. (2014). *Sea-Level Science: Understanding Tides, Surges, Tsunamis and Mean Sea-Level Changes*: Cambridge University Press.
- Python Software Foundation. (2020). Imoments 0.2.3. Retrieved Date from <https://pypi.org/project/Imoments/>.
- Raderschall, N., Lehning, M., & Schär, C. (2008). Fine-scale modeling of the boundary layer wind field over steep topography. *Water Resour. Res.*, *44*(9)doi:10.1029/2007WR006544
- Radford, L., Senkbeil, J. C., & Rockman, M. (2013). Suggestions for alternative tropical cyclone warning graphics in the USA. *Disaster Prevention and Management: An International Journal*, *22*(3), pp. 192-209. doi:10.1108/DPM-06-2012-0064
- Rappaport, E. N. (2014). Fatalities in the United States from Atlantic Tropical Cyclones: New Data and Interpretation. *Bulletin of the American Meteorological Society*, *95*(3), pp. 341-346. doi:10.1175/bams-d-12-00074.1
- Reichstein, M., Camps-Valls, G., Stevens, B., Jung, M., Denzler, J., Carvalhais, N., & Prabhat. (2019). Deep learning and process understanding for data-driven Earth system science. *Nature*, *566*(7743), pp. 195-204. doi:10.1038/s41586-019-0912-1
- Ritchie, E. A., & Elsberry, R. L. (2001). Simulations of the Transformation Stage of the Extratropical Transition of Tropical Cyclones. *Mon Weather Rev*, *129*(6), pp. 1462-1480. doi:[https://doi.org/10.1175/1520-0493\(2001\)129<1462:Sottso>2.0.Co;2](https://doi.org/10.1175/1520-0493(2001)129<1462:Sottso>2.0.Co;2)
- Roberts, M. (2017). *MOHC HadGEM3-GC31-HM model output prepared for CMIP6 HighResMIP* [Data set]. doi:10.22033/ESGF/CMIP6.446
- Roberts, M. J. (2019). *CMIP6 HighResMIP: Tropical storm tracks as calculated by the TRACK algorithm* [Data set].
- Roberts, M. J., Camp, J., Seddon, J., Vidale, P. L., Hodges, K., Vanniere, B., . . . Ullrich, P. (2020a). Impact of Model Resolution on Tropical Cyclone Simulation Using the HighResMIP-PRIMAVERA Multimodel Ensemble. *Journal of Climate*, *33*(7), pp. 2557-2583. doi:10.1175/JCLI-D-19-0639.1
- Roberts, M. J., Camp, J., Seddon, J., Vidale, P. L., Hodges, K., Vannière, B., . . . Wu, L. (2020b). Projected Future Changes in Tropical Cyclones Using the CMIP6 HighResMIP Multimodel Ensemble. [<https://doi.org/10.1029/2020GL088662>]. *Geophysical Research Letters*, *47*(14), p e2020GL088662. doi:<https://doi.org/10.1029/2020GL088662>
- Ross, J. C. (1854). On the effect of the pressure of the atmosphere on the mean level of the ocean. *Philos Tr R Soc*, *144*, pp. 285-296.
- Saha, S., Nadiga, S., Thiaw, C., Wang, J., Wang, W., Zhang, Q., . . . Xie, P. (2006). The NCEP Climate Forecast System. *J. Climate*, *19*(15), pp. 3483-3517. doi:10.1175/jcli3812.1
- Schenkel, B. A., & Hart, R. E. (2012). An examination of tropical cyclone position, intensity, and intensity life cycle within atmospheric reanalysis datasets. *J. Climate*, *25*(10), pp. 3453-3475. doi:10.1175/2011JCLI4208.1
- Scoccimarro, E., Bellucci, A., & Peano, D. (2017). *CMCC CMCC-CM2-VHR4 model output prepared for CMIP6 HighResMIP* [Data set]. doi:10.22033/ESGF/CMIP6.1367
- Senkbeil, J., & Sheridan, S. (2006). *A Postlandfall Hurricane Classification System for the United States*.
- Shen, W. (2006). Does the size of hurricane eye matter with its intensity? *Geophys Res Lett*, *33*(18)doi:<https://doi.org/10.1029/2006GL027313>
- Simpson, R. H., & Lawrence, M. B. (1971). *Atlantic hurricane frequencies along the US coastline*.
- Simpson, R. H., & Saffir, H. (1974). The hurricane disaster-potential scale. *Weatherwise*, *27*(4), pp. 169-186. doi:<https://doi.org/10.1080/00431672.1974.9931702>
- Sobel, A. H., Lee, C.-Y., Camargo, S. J., Mandli, K. T., Emanuel, K. A., Mukhopadhyay, P., & Mahakur, M. (2019). Tropical cyclone hazard to Mumbai in the recent historical climate. *Mon Weather Rev*, *147*(7), pp. 2355-2366. doi:<https://doi.org/10.1175/mwr-d-18-0419.1>
- Song, J. Y., Alipour, A., Moftakhari, H., & Moradkhani, H. (2020). Toward a more effective hurricane hazard communication. *Environmental Research Letters*
- Strachan, J., Vidale, P. L., Hodges, K., Roberts, M., & Demory, M.-E. (2013). Investigating Global Tropical Cyclone Activity with a Hierarchy of AGCMs: The Role of Model Resolution. *J. Climate*, *26*(1), pp. 133-152. doi:10.1175/JCLI-D-12-00012.1
- Tadesse, M., Wahl, T., & Cid, A. (2020). Data-Driven Modeling of Global Storm Surges. [Original Research]. *Frontiers in Marine Science*, *7*(260)doi:10.3389/fmars.2020.00260
- Tadesse, M. G., & Wahl, T. (2021). A database of global storm surge reconstructions. *Scientific Data*, *8*(1), p 125. doi:10.1038/s41597-021-00906-x

- Tasnim, K. M., Shibayama, T., Esteban, M., Takagi, H., Ohira, K., & Nakamura, R. (2015). Field observation and numerical simulation of past and future storm surges in the Bay of Bengal: case study of cyclone Nargis. *Nat Hazards*, 75(2), pp. 1619-1647.
- Tellman, B., Sullivan, J. A., Kuhn, C., Kettner, A. J., Doyle, C. S., Brakenridge, G. R., . . . Slayback, D. A. (2021). Satellite imaging reveals increased proportion of population exposed to floods. *Nature*, 596(7870), pp. 80-86. doi:10.1038/s41586-021-03695-w
- The Guardian. (2019, 13 April 2019). Cyclone Idai caused \$2bn of damage and affected millions, says World Bank. *The Guardian*.
- Thomas, K. (2001). Hurricanes have shaped life of scale inventor. *Ellensburg Daily Record*.
- United Nations. (2020). *World Economic Situation and Prospects*. New York
- United Nations. (2021). About Small Island Developing States. Retrieved Date Accessed, 2021 from <https://www.un.org/ohrrls/content/about-small-island-developing-states>.
- van den Hurk, B., van Meijgaard, E., de Valk, P., van Heeringen, K.-J., & Gooijer, J. (2015). Analysis of a compounding surge and precipitation event in the Netherlands. *Environmental Research Letters*, 10(3), p 035001. doi:10.1088/1748-9326/10/3/035001
- van der Bles, A. M., van der Linden, S., Freeman, A. L. J., Mitchell, J., Galvao, A. B., Zaval, L., & Spiegelhalter, D. J. (2019). Communicating uncertainty about facts, numbers and science. *Royal Society Open Science*, 6(5), p 181870. doi:10.1098/rsos.181870
- van Vuuren, D. P., Edmonds, J., Kainuma, M., Riahi, K., Thomson, A., Hibbard, K., . . . Rose, S. K. (2011). The representative concentration pathways: an overview. [journal article]. *Climatic Change*, 109(1), p 5. doi:10.1007/s10584-011-0148-z
- Verlaan, M., De Kleermaeker, S., & Buckman, L. (2015) *GLOSSIS: Global storm surge forecasting and information system*. Paper presented at the Australasian Coasts & Ports Conference 2015: 22nd Australasian Coastal and Ocean Engineering Conference and the 15th Australasian Port and Harbour Conference, Auckland, New Zealand.
- Vickery, P. J., Skerlj, P. F., & Twisdale, L. A. (2000). Simulation of Hurricane Risk in the U.S. Using Empirical Track Model. *J. Struct. Eng.*, 126(10), pp. 1222-1237. doi:[https://doi.org/10.1061/\(ASCE\)0733-9445\(2000\)126:10\(1222\)](https://doi.org/10.1061/(ASCE)0733-9445(2000)126:10(1222))
- Vitousek, S., Barnard, P. L., Fletcher, C. H., Frazer, N., Erikson, L., & Storlazzi, C. D. (2017). Doubling of coastal flooding frequency within decades due to sea-level rise. *Sci Rep*, 7(1), p 1399. doi:10.1038/s41598-017-01362-7
- Voldoire, A. (2019). *CNRM-CERFACS CNRM-CM6-1-HR model output prepared for CMIP6 HighResMIP* [Data set]. doi:10.22033/ESGF/CMIP6.1387
- Vousdoukas, M. I., Mentaschi, L., Voukouvalas, E., Verlaan, M., Jevrejeva, S., Jackson, L. P., & Feyen, L. (2018). Global probabilistic projections of extreme sea levels show intensification of coastal flood hazard. *Nat Comm*, 9(1), p 2360. doi:10.1038/s41467-018-04692-w
- Wahl, T., Haigh, I. D., Nicholls, R. J., Arns, A., Dangendorf, S., Hinkel, J., & Slagen, A. B. A. (2017). Understanding extreme sea levels for broad-scale coastal impact and adaptation analysis. *Nat Comm*, 8(1), p 16075. doi:<https://doi.org/10.1038/ncomms16075>
- Wakelin, S. L., & Proctor, R. (2002). The impact of meteorology on modelling storm surges in the Adriatic Sea. *Glob Planet Change*, 34, pp. 97-119. doi:10.1016/S0921-8181(02)00108-X
- Walsh, K. J. E., Camargo, S. J., Knutson, T. R., Kossin, J., Lee, T. C., Murakami, H., & Patricola, C. (2019). Tropical cyclones and climate change. *Tropical Cyclone Research and Review*, 8(4), pp. 240-250. doi:<https://doi.org/10.1016/j.terr.2020.01.004>
- Walsh, K. J. E., Fiorino, M., Landsea, C., & McInnes, K. L. (2007). Objectively Determined Resolution-Dependent Threshold Criteria for the Detection of Tropical Cyclones in Climate Models and Reanalyses. *J. Climate*, 20(10), pp. 2307-2314. doi:10.1175/jcli4074.1
- Walsh, K. J. E., McBride, J. L., Klotzbach, P. J., Balachandran, S., Camargo, S. J., Holland, G., . . . Sugi, M. (2016). Tropical cyclones and climate change. *WIREs Climate Change*, 7(1), pp. 65-89. doi:<https://doi.org/10.1002/wcc.371>
- Ward, P. J., De Moel, H., & Aerts, J. C. J. H. (2011). How are flood risk estimates affected by the choice of return-periods? *Nat. Hazards Earth Syst. Sci.*, 11, pp. 3181-3195. doi:<https://doi.org/10.5194/nhess-11-3181-2011>
- Weenink, M. P. H. (1958). *A Theory and method of calculation of wind effects on sea levels in a partly-enclosed sea, with special application to the Southern coast of the North Sea.* (University of California.
- Weibull, W. (1939). *A statistical theory of the strength of materials*: Generalstabens litografiska anstalts förlag.

- 
- Weinkle, J., Landsea, C., Collins, D., Musulin, R., Crompton, R. P., Klotzbach, P. J., & Pielke, R. (2018). Normalized hurricane damage in the continental United States 1900–2017. *Nature Sustainability*, 1(12), pp. 808-813. doi:10.1038/s41893-018-0165-2
- Weinkle, J., Maue, R., & Jr, R. P. (2012). Historical Global Tropical Cyclone Landfalls. *J. Climate*, 25(13), pp. 4729-4735. doi:<https://doi.org/10.1175/jcli-d-11-00719.1>
- Wessel, P., & Smith, W. H. F. (1996). A global, self-consistent, hierarchical, high-resolution shoreline database. *J Geophys Res Solid Earth*, 101(B4), pp. 8741-8743. doi:<https://doi.org/10.1029/96JB00104>
- Whitaker, J. S. (2011). Matplotlib basemap toolkit. Retrieved Date Accessed, 2019 from [https://matplotlib.org/basemap/api/basemap\\_api.html](https://matplotlib.org/basemap/api/basemap_api.html).
- Wilkinson, M. D., Dumontier, M., Aalbersberg, I. J., Appleton, G., Axton, M., Baak, A., . . . Mons, B. (2016). The FAIR Guiding Principles for scientific data management and stewardship. *Scientific Data*, 3(1), p 160018. doi:10.1038/sdata.2016.18
- Williams, J., Irazoqui Apecechea, M., Saulter, A., & Horsburgh, K. J. (2018). Storm surge forecasting: quantifying errors arising from the double-counting of radiational tides. *Ocean Sci. Discuss.*, 2018, pp. 1-21. doi:10.5194/os-2018-63
- Yu, Z., & Wang, Y. (2018). Rainfall Distribution in Landfalling Tropical Cyclones *Extreme Weather*: IntechOpen.
- Yukimoto, S., Noda, A., Kitoh, A., Hosaka, M., Yoshimura, H., Uchiyama, T., . . . Kusunoki, S. (2006). Present-Day Climate and Climate Sensitivity in the Meteorological Research Institute Coupled GCM Version 2.3 (MRI-CGCM2.3). *Journal of the Meteorological Society of Japan. Ser. II*, 84(2), pp. 333-363. doi:10.2151/jmsj.84.333

## About the author



Nadia Bloemendaal was born in Arnhem, the Netherlands, on 24 November 1992. She obtained a BSc degree in Applied Mathematics at the University of Twente and a MSc degree in Meteorology, Physical Oceanography, and Climate at Utrecht University. She conducted her Master thesis at the Royal Netherlands Meteorological Institute, where she focused on improving the representation of surface turbulent fluxes in the HARMONIE numerical weather prediction model.

In September 2016, Nadia joined the Institute for Environmental Studies (IVM) at the Vrije Universiteit Amsterdam as a PhD researcher working on tropical cyclone risk under climate change. The project was funded by an NWO-VICI grant that was awarded to prof. dr. Jeroen C.J.H. Aerts. During her PhD, Nadia visited the School of Ocean and Earth Science at the University of Southampton as a visiting researcher.

Over the course of her PhD, Nadia (co-)authored over eleven publications in national and international peer-reviewed journals. She collaborated with researchers from various universities and institutes, and presented her work at international scientific conferences, including a keynote presentation at the AGU Fall Meeting in 2018. Nadia received international recognition for her PhD research, both from academia and the insurance industry. She received the poster and travel award at the 6<sup>th</sup> International Summit on Hurricanes and Climate Change, and the STORM dataset won the 2020 RDNL Dutch Data Prize for best dataset published following the FAIR Guiding Principles. The accompanying paper on the STORM model was awarded second place in the Lloyd's Science of Risk competition, and Nadia won third place in the 2020 Allianz Climate Risk Research Award competition, both prizes acknowledging the contributions of her work to better understand risk from an insurance perspective.

In her current position as postdoctoral researcher at the IVM, Nadia continues her work on STORM and quantifying tropical cyclone risk under climate change. She temporarily joined the catastrophe modelling team at Allianz Re, supporting the development of tropical cyclone hazard maps for various climate change scenarios.



# List of publications

## Publications on which this thesis is based

**Bloemendaal, N.**, Muis, S., Haarsma, R.J., Verlaan, M., Irazoqui Apecechea, M., de Moel, H., Ward, P.J. & Aerts, J.C.J.H. Global modeling of tropical cyclone storm surges using high-resolution forecasts. *Climate Dynamics* **52**, 5031-5044 (2019). <https://doi.org/10.1007/s00382-018-4430-x>

**Bloemendaal, N.**, Haigh, I.D., de Moel, H., Muis, S., Haarsma, R.J. & Aerts, J.C.J.H. Generation of a global synthetic tropical cyclone hazard dataset using STORM. *Nature Scientific Data* **7**, 40 (2020). <https://doi.org/10.1038/s41597-020-0381-2>

**Bloemendaal, N.**, de Moel, H., Muis, S., Haigh, I.D. & Aerts, J.C.J.H. Estimation of global tropical cyclone wind speed probabilities using the STORM dataset. *Nature Scientific Data* **7**, 377 (2020). <https://doi.org/10.1038/s41597-020-00720-x>

**Bloemendaal, N.**, de Moel, H., Mol, J.M., Bosma, P.R.M., Polen, A.N. & Collins, J.M. Adequately reflecting the severity of tropical cyclones using the new Tropical Cyclone Severity Scale. *Environmental Research Letters* **16**, 1 (2021). <https://doi.org/10.1088/1748-9326/abd131>

**Bloemendaal, N.**, de Moel, H., Dullaart, J.C.M., Haarsma, R.J., Haigh, I.D., Martinez, A.B., Muis, S., Roberts, M.J., Ward, P.J., van der Wiel, K. & Aerts, J.C.J.H. Low-probability tropical cyclone events under climate change. *Submitted to Nature Communications*

## Other publications

**Bloemendaal, N.**, & Tijn, A.B.C. Extreme temperatuurverwachtingen in HARMONIE vanwege een verkeerd gemodelleerd groeiseizoen *Meteorologica* **25**, 4 (2016)

**Bloemendaal, N.**, van 't Veen, B., Huirne, J., van den Born, R. & Baatsen, M.L.J. Tornado's en zware windstoten in Oost-Nederland op 4 juni 2019 *Meteorologica* **29**, 1 (2020)

**Bloemendaal, N.**, & Koks, E.E. Current and future tropical cyclone wind risk in the Small Island Developing States *In review with J.M. Collins & J.M. Done (Eds) Hurricane Risk in a Changing Climate*

De Bruijn, J.A., Daniell, J.E., Pomonis, A., Gunasekera, R., Macabuag, J., de Ruiter, M.C., Koopman, S.J., **Bloemendaal, N.**, de Moel, H., & Aerts, J.C.J.H. Using rapid damage observations from social media for Bayesian updating of hurricane

vulnerability functions: A case study of Hurricane Dorian *Natural Hazards and Earth System Sciences [preprint]*, <https://doi.org/10.5194/nhess-2020-282>, in review, 2020.

Dullaart, J.C.M., Muis, S., **Bloemendaal, N.**, & Aerts, J.C.J.H. Advancing global storm surge modelling using the new ERA5 climate reanalysis *Climate Dynamics* **54** 1-2 (2020) <https://doi.org/10.1007/s00382-019-05044-0>

Dullaart, J.C.M., Muis, S., **Bloemendaal, N.**, Chertova, M., Couasnon, A., & Aerts, J.C.J.H. Accounting for tropical cyclones more than doubles the global population exposed to low-probability coastal flooding *Nature Communications Earth & Environment* **2** 135 (2021) <https://doi.org/10.1038/s43247-021-00204-9>

Ebrey, R., de Ruiter, M.C., Botzen, W., Koks, E., Aerts, J.C.J.H., Wens, M., **Bloemendaal, N.**, Wouters, L., Robinson, P.J., Mol, J.M., Nirandjan, S., Tesselaar, M., Bosello, F., Mysiak, J., Scoccimarro, E., & Mercogliano, P. STUDY ON ADAPTATION MODELLING: comprehensive desk review: climate adaptation models and tools (2021) <https://doi.org/10.2834/280156>

Ward, P.J., Blauhut, V., **Bloemendaal, N.**, Daniell, J.E., De Ruiter, M.C., Duncan, M.J., Emberson, R., Jenkins, S.F., Kirschbaum, D., Kunz, M., Mohr, S., Muis, S., Riddell, G.A., Schäfer, A., Stanley, T., Veldkamp, T.I.E. & Winsemius, H.C. Natural hazard risk assessments at the global scale *Natural Hazards and Earth System Sciences* **20** 4 (2020) <https://doi.org/10.5194/nhess-20-1069-2020>

# Acknowledgments

I would like to welcome you to the (undoubtedly) most-read part of this thesis, the only part that has not been proof-read by others, and therefore the most Nadia-esque part of all: the acknowledgment-section! There are many people that I would like to thank for being a part of my PhD thesis trajectory, either because they have managed to stay by my side from start to finish, or because I met them along the way and they added a lot of joy to the journey.

First and foremost, I would like to thank my promotor Prof. Dr. Jeroen Aerts for giving me the opportunity to conduct this PhD research. I vividly remember picking up my phone on a late afternoon in May 2016, expecting a different voice (namely Philip's) on the other end of the line, but instead hearing you telling me I got the PhD position on tropical cyclone risk (and yes, I screamed after hanging up). I have enjoyed my PhD research from the day I first stepped into my office until the last day of my contract and I will always cherish this time in my life. I would also like to thank you for being the best employer after my diagnosis. I wish everyone could have a professor telling them that “even if you can only work 1% of the time, together we will make sure you finish your PhD research” in response to unexpectedly being diagnosed with multiple sclerosis one year into their PhD. Thank you for standing up for me and protecting me when I needed it most.

I also want to thank my copromotors and daily supervisors Dr. Sanne Muis and Dr. Hans de Moel. Sanne, thank you for your supervision, support, and wise words whenever I needed it. Your extensive feedback on whatever piece of text I would send your way has tremendously increased my writing skills (by xx%) and finding that random apple or orange in my text always put a smile on my face. Hans, I first want to apologize to you for all the horrific visualizations, color maps, and flowcharts I have ever sent your way. The fact that you are using one of my flowcharts as an example for students on how *not* to make a flowchart should say enough to the other readers .. I also want to thank you for your supervision and support, for letting me storm into your office (but not after giving me a thumbs up so I knew I could actually come in) to talk about whatever it was I needed to talk about, and for giving me the confidence I needed to stand in front of that math classroom.

I want to thank the members of my reading committee for taking the time and effort to read my thesis and providing very valuable feedback: Prof. Dr. Suzana Camargo, Prof. Dr. James Done, Prof. Dr. Bart van den Hurk, Prof. Dr. Roshanka Ranasinghe, and Dr. Ir. Kees Boersma. I would also like to thank Prof. Dr. Pieter van Beukering for chairing my defense.

A huge thanks goes out to my amazing paranymphs. Jantsje, Dr. Mol(!), I have always been extremely impressed by the structure you bring into anything (exhibit A: that whiteboard in your old office with the status of your papers) and dedication you put



into any research. It was an absolute joy to coauthor that hurricane risk perception paper with you! Thank you for keeping me motivated and focused during the last phase of my PhD, criticizing my terrible figures, letting me spam you with GIFjes on Slack, and playing an endless amount of Azul with me. Elizabeth, our friendship surely is the best thing that came out of those failed relationships with our exes ☺ It has been amazing seeing our friendship evolve over the years, from Hema ontbijtjes to (takeaway) sushi and from rollerskating around my block in Enschede to supping in 't Twiske (and walking the goats!). Having you by my side throughout my academic career has been the best support I could ever wish for and I am very happy you'll be standing next to me when I defend my thesis.

I have been very fortunate to spend the majority of my time at the IVM in *the best office ever!*, W&N C-553. Timothy, our office hero, lord and savior, thank you for being our shepherd and leader (and taking my jokes). Gabi, thank you for all your good advice during the early stages of my academic adventure. I also owe you (and Sanne) quite a bit for carrying me all the way to the workshop room when I fell down those stairs in Portugal. Kostis, ευχαριστώ που μου έμαθες ελληνικά, every now and then I still randomly shout κλείσε την πόρτα or χριστουγεννιάτικο δέντρο. I enjoyed your enthusiasm regarding my stamp collection and you hysterically pointing at my country list whenever someone would announce they'd be going to a conference in some remote country (p.s.: I am getting close to finishing my one-stamp-from-every-country-goal!). Rhian, *my lovely*, from the minute you stepped into our office I knew we would become really good friends. I miss not having your bubbly character around in the office anymore, but I am very much enjoying our substitute-WhatsApp calls. I look forward to going on a puffin-sightseeing trip with you! Bianca, Kris, Douwe, and Petra, thank you for all the joy you brought into the office. Together with my office mates we created the perfect balance between ridicule and seriousness: we held office dances, built a wall and tore it down again, turned the office into a living room .. but my office mates were also the greatest support when I needed it most.

Apart from my C-553 *best office ever!* office mates, I also want to thank a lot of other colleagues for the joy and support they brought throughout my PhD, and share some fond memories I have of them. FRÄULEIN JOHANNAAAA, I don't think I have laughed so much in my life as whenever I was with you. We should definitely record an advertisement for STORM with the *Naabecker*-voiceover. Elco, thank you for playing the 'where-is-the-helicopter-going' game with me during those two months we got to spend in the new office, and sending me an endless supply of photos and videos of your beautiful baby Jonathan to cheer me up whenever I needed it. Job, ever since that little disappointment in that restaurant in Vienna I have learned to always explicitly ask for *pommes* with my Wiener schnitzel ☺. Lars, thank you for our paper bets, our casual rants about the flaws of academia, for eating all my chocolate: for being a part of this PhD adventure. Eric, *my island in the stream*, thank you for your endless enthusiasm, love, and shared passion for extreme weather and RuPaul's Drag Race gifs. My dear *haakbuddy* Marjolijn, thank you for becoming my friend in the

office, for listening to all my stories, and trusting me with the honorable task of the masterkey holder. I enjoy our mutual love for crochet and sharing our finished projects or new project ideas (why finish something when you can also start something new?) with each other. I hope we can soon attend the Kreadoe again! Marleen, going to that Zuccherò concert in the Verona Arena with you was definitely one of the highlights of my PhD. I enjoy having your enthusiastic character around and doing mini-cheer dances with you (but please don't walk so fast, my little legs can't keep up with you!). Tommy *the office dog*, my furry friend, thank you for all the joy and love you (used to, looking at you security staff) spread around the office and in the dog park. Elvia, I am very proud that I get to call myself your PhD buddy. I hope you will enjoy your PhD as much as I did! Anaïs, *ma petite croissant*, perhaps I should apologize for all those years of me shouting random French words your way (and perhaps also sorry Johanna for doing this but then in German) ☺. Giorgia, I was always looking forward to when you would be visiting our department again, and it was an absolute honor to be your paranymp in Potsdam! "*In bocca al lupo*" "*crepi!*" will stay with me forever! I also want to thank Philip, Dirk, Jens, Max, Erick, Pete, Pedja, Tadzio, Fei, Sem (V and D), Sadhana, Marthe, Hanna, Lies, Lisa, Toon, Ted, Efi, Eline, Pieter, Mehmet, Kate, Marije, Niels, Henrique, Ileen, Paolo, Dim, Teun, Michelle, Anna, Claudia, Katharina, Cecilia, Alex, Rebecca, Jonas, Anne, Raed, Tim, Oscar, Rosa, and all my other (former) colleagues for the fun they brought to the (home)office.

I want to thank all my coauthors for their valuable contributions to my research. Ivan, *cyclone brother*, thank you for being a cornerstone in my PhD research. I still giggle over the time you told me you thought I was crazy for trying to expand your Australian synthetic tropical cyclone research to the global scale, but hey, we did it! I had the most amazing time with you and your group in Southampton and I look forward to conducting a lot more research with you. Rein, I admire your inexhaustible enthusiasm for climate research. Thank you for being my go-to person for climate modelling-related questions these past five years.

The foundation for my PhD research was laid during my MSc in Meteorology, Physical Oceanography, and Climate at Utrecht University. There I became a member of the prestigious *Players van Boundary Layers*-group, a group whose members would later all happen to pursue a PhD degree at different universities (coincidence? I think not). The WhatsApp group name that emerged from this is unfortunately not sharable with the wider audience ☺. Eef, René, and Pleun, it was amazing to go on this adventure together, and I am extremely proud that we all successfully finished our PhD research within the last year!

Conducting research on tropical cyclones while living in a not-so-prone-to-tropical-cyclones-country like the Netherlands and thereby being practically the only one in your country researching tropical cyclones on a full-time basis can be a bit "lonely" at times. However, I encountered some amazing fellow hurricane researchers at

conferences that I am very fortunate to call my friends now. Amy, the fact that I had to literally push and drag you through the Netherlands when you came to visit in June 2018 really strengthened our hurricane-twin-sister bond (and my arm muscles). It was amazing to work with you on the TCSS paper and to present our results at the RISK-KAN conference! Andrew, thank you for letting me share my everyday research frustrations with you, and spamming you with whatever tropical cyclone-fun fact I can think of (or whatever gif I can find). I look forward to combining our research to build the ultimate synthetic-tropical-cyclone-damage-model!

I also want to thank my (already former) colleagues at Allianz Re for letting me be a part of your ACCRIS team in the months after my PhD contract ended. It was an amazing experience to work with you and apply my academic knowledge in an industry setting. Bastian, thank you for guiding me a bit through the wonderful world of cat modelling and reinsurances. I truly enjoyed working with you and I hope we can continue to bridge the gap between academia and the insurance industry in the future.

Team Arnhem (& Breda & Munich): you are the absolute best. To put it in some hurricane terminology: our *vriendenweekenden* and countless meet-ups over the years provided the calmness of the eye in my otherwise eyewall-like PhD life. Emma, thank you for being by my side practically from the day we first met at *Dikkertje Dap* (almost 26 years ago! I checked with my mum ☺). We truly put the “forever” in bff ☺. Inge, thank you for your shared passion for games, and dragging me into the wonderful world of *Wie is de Mol?* If I ever find myself stuck in an escape room: I have your number on speed dial. Sandrike, I bet it must have been hilarious for you to see me emerge into the world of metal during my PhD (for anyone reading this, programming is so much better with Rammstein). I’m looking forward to becoming your neighbor! Rianne, I never knew I would fear for my life playing Kubbs ☺ Thank you for joining me on the Southampton adventure, you were a great support during that period. Simone, thank you for the shared Eurovision Song Contest-passion and your constant mood-for-karaoke. And also thanks for that big jar of *kipkruiden* ☺ I also want to thank the *aanhang* Bernd, Jan-Willem, en Jeroen for all the fun they bring to the table!

I also want to thank the *Escape room gang* (+all the cute little ones that have joined the party these past few years!) for their continuous support throughout my PhD. Julieta, a more-than-massive (humongous! Gargantuan!) thanks goes out to you for designing the artwork of my thesis. I am in love with the final result!! Eline and Ruth, thank you for our numerous sushi dates (live/on zoom) over the past few years. *When in doubt, eat sushi.*

Due to a certain pandemic, I spent the last year of my PhD contract working mostly from home. The Dutch saying *beter een goede buur dan een verre vriend* couldn’t have been more applicable in this situation. I want to thank my neighbor Kirsten for

our countless chats during spontaneous (and planned) encounters, and my friend Anne for going on little cycling trips with me to get me out of the house.

As I already briefly mentioned in the beginning, I (quite unexpectedly) was diagnosed with multiple sclerosis almost one year into my PhD. The first few months after my diagnosis were terrifying, as I was trying to come to terms with my diagnosis with my MS symptoms worsening at the same time. Thinking about how the tremendous love and support I received from my family, friends, and colleagues got me through it still makes me tear up till this day. Thank you all for everything, we *weathered the storm* together. I am forever grateful for the team of neurologists, researchers and hospital staff at the Amsterdam UMC MS Centrum that are part of the ENSEMBLE medical trial. I particularly want to mention my team of doctors Prof. Dr. Joep Killestein, Floor Loonstra, Eline Coerver, and Gianina Eissens here. As a result of their efforts, support, and research, I can now say that MS does not play a role in my everyday life, and words cannot express my gratitude towards that.

Lieve papa en mama, zonder jullie onvoorwaardelijke liefde en steun zou ik niet zijn waar ik nu ben. Bedankt dat jullie altijd in mij en mijn dromen geloofd hebben en mij altijd aangemoedigd hebben om mijn passie voor extreem weer te volgen. Lieve Yara, ook al kunnen we soms nog zo verschillen in dingen, ik ben trots om je mijn zus te mogen noemen. Bedankt voor alle idiote (WhatsApp) gesprekken en stomme grappen die we samen hebben ☺ Lieve Magnus, Nino, en wijlen Odin en Elli, bedankt voor de eindeloze toevoer van oxytocine en vreugde die jullie brengen in mijn leven. Lieve opa's en oma's, overige familieleden en schoonfamilie, bedankt voor jullie liefde en interesse in mijn onderzoek deze jaren, ook al heb ik mijn werk misschien soms wat moeilijk uitgelegd (sorryyyy). Caren, bedankt dat je me hebt laten inzien dat een promotieonderzoek "misschien toch wel" wat voor mij zou zijn. De rest is inmiddels geschiedenis! Jolanda, je bent een *topper*. Bedankt voor alles.

I dedicate the last words in this thesis to my love Frank. After seeing you stressing out in the last few months of your own PhD thesis, I vividly remember saying I never wanted to pursue a PhD. Oh the irony ☺ Thank you for letting me pave my own PhD path (haha see what I did there), but also being there whenever I needed to vent or needed a bit of advice. Thank you for being by my side throughout everything, supporting and taking care of me when I needed it most, and keeping our focus on the bright side of life. To quote you: "*wat hebben wij toch een goed leven*". I love you!!

